



Skolkovo Institute of Science and Technology

Skolkovo Institute of Science and Technology

EXPERIMENTAL MODELING OF GAS HYDRATES INTERACTION WITH A SALT
SOLUTION IN PERMAFROST

Doctoral Thesis

by

VALENTINA EKIMOVA

DOCTORAL PROGRAM IN PETROLEUM ENGINEERING

Supervisor

Leading Research Scientist Dr. Evgeny Chuvilin

Moscow 2022

© Ekimova Valentina 2022

I hereby declare that the work presented in this thesis was carried out by myself at Skolkovo Institute of Science and Technology, Moscow, except where due acknowledgement is made, and has not been submitted for any other degree.

Candidate (Valentina Ekimova)

Supervisor (Leading Research Scientist Dr.
Evgeny Chuvilin)

Abstract

Today, one of the most promising area for oil and gas production is the Arctic region. Though, the hydrocarbon production in this region is frequently associated with many complications, among them is the existence of sensitive permafrost component – gas hydrates. Gas hydrates destabilization may occur when thermobaric conditions of their stability change or as a result of inhibition by various chemical compounds, in particular by salts. Consequently, intensive methane emission can happen.

To date, issues related to the influence of geochemical conditions on methane hydrate stability (particularly migration of salt solutions) in the sediments pore space at negative temperatures have turned out to be poorly understood. This research is dedicated to experimental study of the mechanism and regularities of the interaction of methane hydrates (as most widespread hydrate in nature) with salt solutions in the pore space of hydrate-saturated sediments under various thermobaric conditions. The object of the study was sandy sediments, as well as the ones obtained during drilling in the area of permafrost distribution, where the existence of gas hydrates is assumed by a number of indirect signs.

During the experiments, it was found that the migration of salts in frozen sediments, containing gas hydrates stimulates the hydrate decomposition in pore space of sediments, and can accelerates ice thawing. As a result, a dissociation front of gas hydrates in sediment porous media was observed.

It has been found that salt migration proceeds more intensively in frozen hydrate-saturated sediment than in frozen non-hydrate-saturated ones. At the same time, a significant decrease in the temperature of a frozen hydrate-containing sample was recorded during the migration and accumulation of salts, while a less significant decrease in temperature was observed in frozen sediment. It is shown that the most important factor determining the intensity of salt ions migration in

frozen sandy sediment, containing gas hydrates, is gas pressure, in contrast to frozen hydrate-free sediments, where the influence of pressure was not so significant.

It was revealed that during salt migration in frozen hydrate-saturated sediments, the intensity of methane hydrate dissociation rises with an increase in ambient temperature, salt solution concentration, and with a decrease in the amount of clay particles. Moreover, the intensity of hydrate dissociation decreases in the series of salt solution composition: MgCl_2 - NaCl - CaCl_2 - KCl - Na_2SO_4 . On the basis of experimental data, the salt ion flux was calculated, and the critical concentration of complete dissociation of pore gas hydrate was obtained.

A scheme of phase transformations and temperature changes in the pore space of frozen hydrate-saturated sediment during their interaction with salt solutions at gas pressures above and below equilibrium is proposed. A schematic model of the contact of natural and technogenic salt solutions with frozen hydrate-saturated strata in continental conditions and on the shelf is also given.

Publications

Journal publications:

1. Chuvilin E., **Ekimova V.**, Davletshina D., Krivokhat E., Shilenkov V., Bukhanov B. Pressure factor Influence on the Salt Migration in frozen hydrate-saturated sediments. *Experimental Modeling. Energy & Fuels*. 2022 Jul; 38 (18), 10519–10528. <https://doi.org/10.1021/acs.energyfuels.2c01282>, WoS/Scopus indexed journal. Impact Factor: 3.605.
2. Chuvilin E., **Ekimova V.**, Davletshina D., Krivokhat E., Shilenkov V., Bukhanov B. Migration of Salt Ions in Frozen Hydrate-Saturated Sediments: Temperature and Chemistry Constraints. *Geosciences*. 2022 Jul; 12 (7), 276. <https://doi.org/10.3390/geosciences12070276>, WoS/Scopus indexed journal. Impact Factor: 2.076.
3. Chuvilin E., **Ekimova V.**, Davletshina D., Krivokhat E., Shilenkov V., Bukhanov B. Temperature Variation during Salt Migration in Frozen Hydrate-Bearing Sediments: Experimental Modeling. *Geosciences*. 2022 Jun; 12 (7), 261. <https://doi.org/10.3390/geosciences12070261>, WoS/Scopus indexed journal. Impact Factor: 2.076.
4. Chuvilin E, **Ekimova V.**, Davletshina D, Sokolova N, Bukhanov B. Evidence of Gas Emissions from Permafrost in the Russian Arctic. *Geosciences*. 2020 Sept: 10 (10), 383. <https://doi.org/10.3390/geosciences10100383>, WoS/Scopus indexed journal. Impact Factor: 2.076.
5. Chuvilin E, Davletshina D, **Ekimova V.**, Bukhanov B, Shakhova N, Semiletov I. Role of Warming in Destabilization of Intrapermafrost Gas Hydrates in the Arctic Shelf: Experimental Modeling. *Geosciences*. 2019 Sept; 9: 407. <https://doi.org/10.3390/geosciences9100407>, WoS/Scopus indexed journal. Impact Factor: 2.076.
6. Chuvilin E, **Ekimova V.**, Bukhanov B, Grebenkin S, Shakhova N, Semiletov I. Role of salt migration in destabilization of intra permafrost hydrates in the Arctic Shelf: Experimental modeling.

Geosciences. 2019 Apr; 9(4), 188. <https://doi.org/10.3390/geosciences9040188>, WoS/Scopus indexed journal. Impact Factor: 2.076.

Conference proceedings:

1. **Ekimova V.**, Chuvilin E., Davletshina D., Bukhanov B., Krivokhat E., Shilenkov V. Salt transfer in frozen hydrate-containing sediments during their interaction with salt solutions. In the Proceeding of IV Conference of Geocryologists of Russia "Monitoring in permafrost", Moscow, Russia, June 14 - 17, 2022, pp. (published in Russian).

2. **Ekimova V.**, Chuvilin E, Bukhanov B, Grebenkin S, Shakhova N, Semiletov I. Evaluation of the role of salt migration in the destabilization of intrapermafrost gas-hydrate formations on the Arctic shelf on the basis of the experimental modeling. In Proceedings of the IX International Scientific and Practical Conference "Marine Research and Education (MARESEDU-2020)", Moscow, Russia, 2020, pp. 59-62 (published in Russian).

3. **Ekimova V.**, Chuvilin E, Bukhanov B, Grebenkin S, Shakhova N, Semiletov I. Experimental modeling of dissociation of intrapermafrost gas hydrates caused by salt transfer. In Proceeding of the Conference "Global Issues in the Arctic and Antarctic", Archangelsk, Russia, 2020, pp. 101-104 (published in Russian).

4. Chuvilin E., Bukhanov B., **Ekimova V.** Experimental modeling of interaction between salt solutions and frozen sediments containing gas hydrates // The 8th International Conference on Gas Hydrates. Beijing, China, 2014.

Acknowledgements

This work would be impossible without my Research Supervisor Leading Research Scientist of Skoltech Dr. Evgeny Chuvilin. I am grateful for guidelines, and all valuable recommendations.

I would like to extend my sincere thanks to my Ph.D. committee members – Prof. Mikhail Spasennykh, and Dr. Vladimir Istomin for their suggestions and insightful comments during my study and research.

I am deeply grateful to my colleagues, who were ready to assist at every stage of the research work and helped in conducting the experiments: Senior Research Scientist Boris Bukhanov, Engineers Natalia Sokolova, Dinara Davletshina, Sergei Grebenkin, Daria Sergeeva, Vladimir Shilenkov, Ms student Ekaterina Krivokhat, Ms student Elena Pankratova from Skoltech University, Gleb Berloff from Warwick University.

I want to give my deepest appreciation to the Skolkovo Institute of Science and Technology for amazing 4 years of advanced research, innovations, enjoyable lectures, and extracurricular activity.

I would like to thank all Jury committee members – for their time, recommendations and comments for the work perfection.

Finally, a special appreciations to my family and friends for their belief in me, unwavering support, and inspiration in conducting research work.

The research was supported by the Russian Science Foundation (grants No. 22-17-00112, 21-77-10074).

Table of Contents

Abstract	3
Publications	5
Acknowledgements	7
Table of Contents	8
List of Figures	10
List of Tables.....	17
Chapter 1. Introduction	18
1.1. Relevance. Statement of the problem	18
1.2. Goal.....	20
1.3. Objectives	20
1.4. Novelty.....	21
1.5. Outline of the Thesis.....	22
Chapter 2. Research background and literature survey	23
2.1. Arctic permafrost and problems of hydrocarbon fields development in the Arctic.....	23
2.1.1. Permafrost-geological structure of the Russian Arctic region.....	23
2.1.2. Peculiarities of hydrocarbon deposits development in areas of permafrost distribution	30
2.2. Conditions for gas hydrate existence and formation in permafrost	35
2.2.1. Characteristics of gas hydrate as a substance	35
2.2.2. Conditions for the existence of permafrost associated gas hydrate and possible causes of their destabilization.....	45
2.3. The study of salt migration processes in frozen sediments.....	56
2.3.1. Experimental research of salt migration processes in ice-containing sediments.....	59
2.3.2. Existing physico – chemical models of salt transfer processes in sediment media	65
Chapter 3. Method of experimental study of salt ions migration in hydrate-bearing sediments.....	72
3.1. Experimental setup and preparation technology of hydrate-bearing sediments	73
3.2. Sediment characteristics used in experimental simulation.....	77
3.3. Technique for studying the interaction of frozen hydrate-containing sediments with saline solutions in non-equilibrium and equilibrium conditions	80
3.4. Method of the temperature field change investigation during the contact of frozen hydrate-bearing sediment with salt solution.....	84
3.5. Method for assessing the salt content in sediment samples	87
3.6. Processing of the experimental data	93
Chapter 4. Mechanism and dynamics of salt transfer processes in hydrate-bearing sediments.....	97
4.1. Influence of hydrate presence on the salt migration in frozen sediments	98
4.2. The interaction of frozen hydrate-bearing sediments with salt solutions in time	101
4.3. Temperature changes as a result of salt migration in frozen hydrate-bearing sediments.....	106

4.4. Mechanisms of salt migration in frozen hydrate-containing sediments.....	116
Chapter 5. Influence of the different factors on the process of salt migration in frozen hydrate-bearing sediments	123
5.1. Salt and mass transfer in sediment containing gas hydrate as a function of pressure.....	123
5.2. Temperature influence on the process of hydrate-bearing sediment interaction with saline solutions	131
5.3. Influence of salt solution concentration on the intensity of salt migration and hydrate dissociation in hydrate-bearing sediments	136
5.4. The process of interaction of hydrate-containing sediments with salt solutions of various chemical compositions	145
5.5. Sediment grain size influences the process of salt migration in hydrate-bearing sediments	151
Chapter 6. Concept models of hydrate interaction with natural and technical salt solution in hydrate-bearing collectors in permafrost	165
Chapter 7. Conclusion	169
Bibliography	175
Appendix 1. Table of the conducted experiments on the interaction of frozen-hydrate bearing sediments with salt solution.....	218

List of Figures

Figure 1. Sediment's temperature profile in the area of permafrost distribution [69].....	26
Figure 2. Map of the permafrost distribution on land [73].....	27
Figure 3. Simulation of the zero isotherm propagation on the Arctic shelf [82].....	29
Figure 4. Structure of gas hydrates [141].	36
Figure 5. Different crystalline arrangement of hydrates: a – structure I, b – structure II, c – structure H and d – host cages of water. Dense line is the hydrate unit-cell [147].	37
Figure 6. Gas hydrate burning (photo by Dinara Davletshina).	38
Figure 7. Schematic stability curve for CH ₄ hydrate (build in “HydraFlash” software [153]): GH – gas hydrate; liq – liquid water; red dot – quatroupole point (four-phase equilibrium "gas – water – ice – hydrate"); red line – line of ice-liquid water phase equilibrium.	39
Figure 8. Shift of gas hydrate equilibrium by different methods of methane extraction [146].....	40
Figure 9. Scheme of bulk hydrate self-preservation at the negative temperature (picture obtained and analyzed through extensive cryo-FE-SEM imaging [171].	41
Figure 10. Different hydrate inhibitors and scheme of their work principle [147].	42
Figure 11. Hydrate decomposition in water by NaCl ions migration in time by mathematical modeling (red – methane, green – Na ⁺ , yellow – Cl ⁻) [204].	43
Figure 12. Existence of methane hydrate in natural permafrost conditions (modified from [17,226]).	45
Figure 13. Schematic map of registered gas emanations in the Russian Arctic [239].	52
Figure 14. Scheme of solvation of ice due to the action of NaCl ions [301].	57
Figure 15. Phase diagram of NaCl aqueous solution (modified after [308]).	58
Figure 16. Equipment (pressure cell) for artificial formation of hydrate in sediment samples.....	74
Figure 17. The appearance of frozen sand filled with pore hydrate after extraction from the pressure cell.	76

Figure 18. Distribution of water content, porosity, and hydrate coefficient by the length of frozen hydrate-bearing sediment samples.....	77
Figure 19. Scheme of the installation for the interaction of frozen hydrate-bearing and non-hydrate-bearing sediments with salt solutions under pressure.....	82
Figure 20. Scheme of Kriolab Tbf system for temperature field change investigation (a) and picture of the frozen hydrate-bearing sand sample with temperature sensors (b). 1 - frozen hydrate-bearing sediment; 2 - solution container; 3 - frozen NaCl solution; 4 - temperature sensors; 5 - thermistor streamer; 6 - multiplexer module; 7 - fan; 8 - USB cable; 9 - PC with Kriolab Tbf software; 10 - cooling chamber. Modified after [310].....	85
Figure 21. The water activity of non-saline sand at the various water content.	88
Figure 22. Distribution of water activity from sand salinity.	89
Figure 23. The water activity from NaCl concentration in pore water solution.....	90
Figure 24. Comparison of the measurement results of the Na ⁺ concentration by a flame photometer and a conductometer.	90
Figure 25. Pore water activity versus Na ⁺ ion concentration.	91
Figure 26. Effect of gas pressure on the accumulation of salt ions (Na ⁺) in frozen sand (fine sand -1) samples (W=12%) containing (solid line) and not containing (dashed line) gas hydrates 4 hours after interaction with 0.2 N NaCl solution (t=-6 °C).	99
Figure 27. Accumulation of Na ⁺ ions (A) and changes in the hydrate coefficient (B) in samples of frozen hydrate-containing sand-1 (K _h ⁱⁿ = 0.6, W=12%) at different times after interaction with NaCl solution 0.1 N (P=0.1 MPa, t=-6 °C).....	101
Figure 28. Experimental evaluation of the decomposition front of porous gas hydrates and the thawing front in frozen hydrate-containing sand samples (sand-1, W = 12%) when interacting with 0.1 N NaCl salt solution at a temperature -6°C and pressure 0.1MPa.....	103
Figure 29. The appearance of frozen sand samples (fine sand 4, W=12%) before (A) and after interaction (B) with 0.1 NaCl solution at -6°C.....	104
Figure 30. Average Na ⁺ flux change in time during interaction of frozen hydrate-bearing sediment (fine sand-1) with NaCl solution of 0.1N at -6 °C and 0.1 MPa.	105

Figure 31. Dynamics of temperature change in time in the near-contact area (2.5 cm from the contact) in frozen sand samples (fine sand-2) interacting with 0.4 N saline solution at atmospheric pressure: 1 – non-hydrate-containing frozen sample (dotted line); 2 - hydrate-containing (solid line); 3 - initial temperature (t_{in}) -6.5 °C (dashed line).	107
Figure 32. Temperature distribution along the length of a frozen sample (fine sand-2), not containing (1) and containing gas hydrate (2) after 0.6 h of interaction with 0.4 N. NaCl solution at atmospheric pressure. The dotted line - 3 shows the initial temperature $t_{in} = -6.5^{\circ}\text{C}$	108
Figure 33. Dynamics of temperature change in time in a frozen hydrate-containing samples (fine sand-2, $S_h^{in}=38\%$, $S_i^{in}=15\%$) on the distance 2.5; 3.5; 5.5 and 7.0 cm from the contact zone with 1 N NaCl solution ($t_{in} = -6.5^{\circ}\text{C}$, $P=0.1\text{ MPa}$).	109
Figure 34. Change in the temperature distribution along the length of the frozen hydrate-bearing sample fine sand-2 ($S_h^{in}=41\%$, $S_i^{in}=12\%$) at the stage of cooling in the first hour (time on the legend is in minutes) of interaction with 1 N NaCl solution ($t_{in}=-6.5^{\circ}\text{C}$, $P=0.1\text{ MPa}$).	111
Figure 35. Dynamics of temperature changes in time of frozen hydrate-containing samples (fine sand-2) in the near-contact area (2.5 cm from the contact) interacting with NaCl solution of various concentrations (0.2-1N) ($t_{in} = -6.5^{\circ}\text{C}$, $P=0.1\text{ MPa}$).	112
Figure 36. Influence of the contact solution concentration on the maximum temperature drop ($\Delta t=t_{in}-t_{min}$) in frozen hydrate-bearing fine sand-2 (C_{sol} from 0.1 to 1 N, $t_{in} = -6.5^{\circ}\text{C}$, $P=0.1\text{ MPa}$).	113
Figure 37. Influence of contact solution concentration on the rate of temperature decrease (Vt) of frozen hydrate-bearing fine sand-2 (C_{sol} from 0.1 to 1 N, $t_{in} = -6.5^{\circ}\text{C}$, $P=0.1\text{ MPa}$).	114
Figure 38. Influence of concentration on the time taken for the temperature of the sample to return to the initial value (T_r) after the cooling period caused by the interaction of hydrate-containing frozen sand with saline solution ($t_{in} = -6.5^{\circ}\text{C}$, $P=0.1\text{ MPa}$).	115
Figure 39. Scheme of phase-transformation of frozen hydrate-bearing sediments during salt migration: (a) metastable conditions (experimental pressure $P_{exp} < \text{equilibrium pressure } P_{eq}$); (b) stable conditions ($P_{exp} \geq P_{eq}$).	117
Figure 40. Scheme of temperature changes during the interaction of a frozen hydrate-containing sample with saline solution.	120

Figure 41. Scheme of temperature changes in a frozen hydrate-containing sample in the process of salt transfer, phase transformations, and changes in ice and hydrate saturation along the height of the investigated sample.	121
Figure 42. Modeling P-T conditions of methane hydrate stability in the HydraFlash program [153] and thermobaric conditions for conducting experiments on the migration of salt ions in frozen hydrate-bearing sediments (T1-T6).	124
Figure 43. The effect of pressure on the accumulation of salt ions (Na ⁺) (a) and the decrease in the hydrate coefficient (K _h) (b) in samples of frozen hydrate-bearing fine sand-2 (K _{hin} ~ 0.3, W=12%) at non-equilibrium and equilibrium pressure 4 hours after the start of interaction with a frozen NaCl solution 0.1 N (t= -6°C).	125
Figure 44. Influence of gas pressure on the flux density of Na ⁺ ions through the cross section of a frozen hydrate-containing sample 4 hours after the start of interaction with a frozen salt solution 0.1 N NaCl (t= -6°C).	126
Figure 45. Dependence of the critical concentration (C _{cr}) causing decomposition of pore hydrate in a frozen sand sample on gas pressure (t= -6°C, C _{sol} =0.1 N).	127
Figure 46. Altitude distribution of a frozen hydrate-containing sample (fine sand-2): (A) salt concentrations and hydration coefficient; (B) – critical pressure of dissociation of methane hydrate (concentration of contacting NaCl solution 0.1 N, t= -6°C).	129
Figure 47. Effect of temperature on the accumulation of salt ions (Na ⁺) in frozen hydrate-containing samples (fine sand-2) after 2 hours of interaction with 0.2 N NaCl solution (P=0.1 MPa).	132
Figure 48. The effect of temperature (-3, -6, -20°C) on the decrease in the hydration coefficient (K _h) in samples of frozen hydrate-containing fine sand-2 (K _{hin} ~ 0.4, W=12%) 2 hours after the start of interaction with frozen 0.2 N NaCl salt solution.	133
Figure 49. Effect of temperature on the average Na ⁺ flux into a frozen hydrate-containing sample (fine sand-2) for 4 hours of interaction with a frozen salt solution of 0.1N NaCl (P=0.1 and 0.4 MPa).	134
Figure 50. Effect of temperature on the critical concentration (C _{cr}) causing decomposition of pore hydrate in a frozen sand sample (fine sand-2, P=0.1 and 4MPa, C _{sol} =0.1N).	135

Figure 51. Thermobaric conditions of hydrate stability in the water-NaCl solution of different concentration simulated in “HydraFlash” software [153].	137
Figure 52. Effect of contact solution concentration on the accumulation of salt ions (Na ⁺) in frozen hydrate-containing samples (fine sand-2) after 4 hours of interaction with NaCl solution (t=-6°C, P=0.1 MPa).	138
Figure 53. Influence of NaCl contact solution concentration on the distribution of hydrate coefficient (K _h) along the length of frozen hydrate-containing samples (fine sand-2) (K _h ⁱⁿ ~ 0.4, W=12%) after 4 hours of interaction (t=-6°C, P=0.1 MPa).	139
Figure 54. Influence of the contact solution concentration on the accumulation of salt ions (Na ⁺) in frozen hydrate-containing samples (fine sand-2) interacting for 4 hours under a pressure of 4.0 MPa with a NaCl solution (t=-6°C): A – 0.1N; B – 0.2N.	140
Figure 55. Effect of contact solution concentration on distribution of hydrate coefficient (K _h) along the height of frozen hydrate-containing sample (fine sand-2, K _h ⁱⁿ ~ 0.4, W=12%) after 4 hours of the interaction with frozen NaCl salt solution (t=-6°C, P=4.0 MPa): A – 0.1N; B – 0.2N.	141
Figure 56. Influence of contact solution concentration on the average Na ⁺ flux in frozen hydrate-bearing sample (fine sand-2) after 4 hours of the interaction (t= -6°C, P=0.1 MPa and 4.0 MPa).	142
Figure 57. Influence of a chemical composition of salt solution (Na ₂ SO ₄ , KCl, CaCl ₂ , NaCl, MgCl ₂) with a concentration of 5wt% on the conditions of methane hydrate stability in the range of negative temperatures from 0 to -20°C (calculations were made in the “HydraFlash” software [153]).	146
Figure 58. Accumulation of Na ⁺ ions in samples of frozen hydrate-bearing sand (fine sand-2, W=12%) after 4 hours of contact with 0.1N NaCl solution of different composition (t= -6°C, P=0.1MPa).	147
Figure 59. The influence of the chemical composition of the contact salt solution on the decrease in the hydrate coefficient (K _h) in frozen hydrate-containing samples (fine sand-2, K _h ⁱⁿ ~ 0.5, W=12%) after 4 hours of interaction with the frozen salt solution (t=-6.5°C, Csol=0.1N, P=0.1MPa).	148
Figure 60. The influence of the chemical composition of the salt contact solution on the salt flux into frozen hydrate-containing sample (fine sand-2) after 4 hours of interaction with a frozen salt solution (t=-6°C, Csol=0.1N, P=0.1MPa).	149

Figure 61. Influence of kaolinite content in fine-grained sand (fine sand-2) on the accumulation of Na ⁺ ions in frozen hydrate-bearing samples 3 hours after interaction with 0.1 N NaCl solution at -6 °C and p=0.1 MPa.	152
Figure 62. Effect of kaolinite content in fine sand-2 on hydrate dissociation in a frozen hydrate-bearing sample ($K_h^{in} \sim 0.5$, W=12%) 3 hours after the start of interaction with a frozen salt solution of 0.1 N NaCl at -6 °C.	153
Figure 63. Influence of kaolinite content in sand (fine sand-2) on water accumulation in a frozen hydrate-bearing sample (W=12%) after 3 hours of interaction with frozen salt solution of 0.1 N NaCl at -6 °C.	154
Figure 64. Effect of kaolinite content in sand (fine sand-2) on the average water flux through a frozen hydrate-bearing sample (W=12%) after 4 h of interaction with a frozen salt solution of 0.1 N NaCl at -6 °C.	154
Figure 65. Influence of the mineralogical composition of clay in quartz sand (fine sand-2 with 5% additives) on the accumulation of Na ⁺ ions in frozen hydrate-bearing samples after 4 hours of interaction with 0.1 N NaCl solution at t=-6°C: A – kaolinite; B – montmorillonite.....	155
Figure 66. Influence of the mineralogical composition of clay in quartz sand (fine sand-2) on the decrease in the hydration coefficient (K_h) in frozen hydrate-containing samples ($K_h^{in} \sim 0.4$, W=12%) 4 hours after the start of interaction with frozen salt solution 0.1 N NaCl at t= -6°C: A – kaolinite; B, montmorillonite.	156
Figure 67. Influence of the mineralogical composition of clay in quartz sand (fine sand-1) on the accumulation of water in a frozen hydrate-bearing sample (W=12%) after 4 hours of interaction with a frozen salt solution of 0.1 N NaCl at -6 °C: A - kaolinite; B - montmorillonite.	156
Figure 68. Influence of the content of clay particles of various compositions (kaolinite and montmorillonite) in quartz sand (fine sand-2) on the average flux density of Na ⁺ ions into a frozen hydrate-containing sample over 4 hours of interaction with a frozen salt solution of 0.1N NaCl (p=0.1MPa, t= -6°C): A – kaolinite; B – montmorillonite.....	157
Figure 69. Influence of the content of clay particles of different mineral composition in quartz sand (fine sand-2) on the critical concentration (C_{cr}) causing the decomposition of pore hydrate in a frozen sand sample (t= -6°C, p=0.1MPa, C_{sol} =0.1N): A – kaolinite; B – montmorillonite.	158

Figure 70. Influence of the size of sand particles on the accumulation of salt ions (Na^+) and the decrease in the hydrate coefficient (K_h) in frozen hydrate-containing samples ($K_h^{\text{in}} \sim 0.4$, $W=12\%$, $t=-6^\circ\text{C}$) 4 hours after the start of interaction with frozen salt solution 0.1 N NaCl: A - fine sand-2 (0.1-0.2 mm $\sim 80\%$); B – medium sand (0.2-0.5 mm $\sim 60\%$)..... 159

Figure 71. Influence of silt content on the accumulation of salt ions in frozen hydrate-containing samples 4 hours after interaction with 0.1 N NaCl solution at $t=-6^\circ\text{C}$: A –fine sand-2 (silt $\sim 1\%$); B – fine sand-3 (silt $\sim 5\%$); C – sandy loam (silt $\sim 18\%$). 161

Figure 72. Influence of silt content on the hydrate coefficient (K_h) of frozen hydrate-containing samples ($K_h^{\text{in}} \sim 0.4-0.5$, $W=12\%$) 4 hours after interaction with 0.1 N NaCl solution at $t=-6^\circ\text{C}$: A – fine sand-2 (silt $\sim 1\%$); B – fine sand-3 (silt $\sim 5\%$); C – sandy loam (silt $\sim 18\%$). 161

Figure 73. Influence of silt content on water accumulation in a frozen hydrate-bearing sample ($W=12\%$) after 4 hours of interaction with a frozen salt solution of 0.1 N NaCl at -6°C : A – fine sand-2 (silt $\sim 1\%$); B – fine sand-3 (silt $\sim 5\%$); C – sandy loam (silt $\sim 18\%$)..... 162

Figure 74. Influence of fineness and amount of clay particles (kaolinite) on the average migration flow of Na^+ in frozen hydrate-bearing samples interacting with NaCl solution 0.1 N for 4 hours at $t=-6^\circ\text{C}$: A – fine sand-3; B – fine sand-2 with kaolinite (from 0 to 10%); C – medium sand; D – sandy loam..... 163

Figure 75. Proposed model of interaction between saline horizons and frozen deposits containing gas hydrates: a) initial state; b) start of salt migration from cryopegs due to ambient temperature increase; c) dissociation of metastable hydrates occurs; b) dissociation of stable hydrates occurs. 166

Figure 76. The proposed conceptual model on the interaction between frozen hydrate-containing sediments and sea water: A) preliminary state – sea regression; B. 1) after sea transgression – start of interaction between frozen sediments and sea water; B. 2) migration of salt into permafrost sediments (development of salinity and thawing fronts); B. 3) propagation salt front into sediments, containing intrapermafrost gas hydrate followed by hydrate decomposition and active methane emission..... 168

List of Tables

Table 1. Depth of permafrost bottom on the north of West Siberia gas fields [8].	29
Table 2. Complications, which can be caused during drilling in the permafrost.	33
Table 3. Registered cases of gas emanations in the Russian Arctic [239].	49
Table 4. Particle size distribution, mineral composition, and salinity of investigated sediments.	77
Table 5. Main initial characteristics of frozen hydrate-containing sand samples.	97
Table 6. Average Na ⁺ flux in frozen hydrate-containing and non-hydrate-containing sand (fine sand-1) under the equilibrium (2.5 MPa) and non-equilibrium (0.1 MPa) pressure (4 hours of interaction with 0.2N NaCl solution at -6 °C).	100
Table 7. Frozen non-hydrate-bearing (sample 1) and hydrate-bearing (sample 2) fine sand -2 initial characteristics.	106
Table 8. Initial characteristics of the frozen hydrate-bearing fine sand-2 samples before the contact with NaCl solution of different concentrations.	112
Table 9. Scheme of phase-transformation in the pore space of the frozen hydrate-bearing sediments during increase of salt solution concentration at stable conditions (experimental pressure $P_{exp} \geq$ equilibrium pressure P_{eq}) and metastable conditions ($P_{exp} < P_{eq}$).	143
Table 10. Dependence of the critical concentration (C_{cr}) causing the decomposition of pore hydrate in a frozen fine sand-2 sample on the chemical composition of the contacting solution ($t=-6^{\circ}\text{C}$, $P=0.1\text{MPa}$, $C_{sol}=0.1\text{N}$).	150
Table 11. Properties of hydrate-bearing frozen sand with different amount of kaolinite.	152
Table 12. Properties of hydrate-bearing frozen sand with different composition of clay (5% additives).	155
Table 13. Properties of hydrate-bearing frozen sand with different amount of silt.....	160
Table 14. Dependence of the critical NaCl concentration on the amount of silt in frozen hydrate-bearing sandy sediment at the temperature -6°C	162
Table 15. The list of experiments conducted on the interaction of frozen hydrate-bearing sediments with salt solution.....	218

Chapter 1. Introduction

1.1. Relevance. Statement of the problem

Today, the leading area for oil and gas production remains the Arctic region. Nevertheless, the exploitation of hydrocarbon deposits here is often accompanied by many complexities, mainly related to the spread of permafrost [1–8]. Frozen sediments are a complex multi-component and multi-phase system containing natural salt solutions (cryopegs), underground ice, as well as methane hydrates, which easily affected by different local man-made impacts (mechanical, thermobaric, chemical, etc.) [1,3,9–11].

Gas hydrates (clathrates) are crystalline compounds that look like ice, which are formed from water and a low molecular weight gas at high pressure and low temperatures [12–14]. In the nature, hydrates occur in the deep water and ocean sediments (at the depths of the northern seas from 250-300 meters, and from a depth of 600 meters in the southern seas), along with permafrost areas with satisfactory thermobaric and geochemical conditions in the so-called hydrate stability zone [15–21]. There is variety of gases able to form hydrate, but most widespread in nature is methane hydrates. There are also examples of the methane hydrate existence in the frozen strata above the modern stability zone (metastable gas hydrates) due to the effect of self-preservation [15,22–29]. These shallow, metastable gas hydrates are especially sensitive to the changes in environmental conditions (further pressure decrease, temperature increase, and salt migration) [30–32].

An important characteristic of methane hydrates is their possibility to store a significant gas amount - up to 160 m³ of methane in 1 m³ of hydrate [33]. This allows to consider natural gas hydrate accumulations, on the one hand, as a promising unconventional source of hydrocarbons, and, on the other hand, as a serious geological hazard in the development of traditional oil and gas fields, which, as a rule, are located below the zone of possible hydrate formation [10,12,19,27,33–38].

Gas hydrate formations in the Arctic can be destabilized as a result of permafrost degradation (due to the rise of temperature) [32], and throughout salt migration into the frozen hydrate-containing sediment [31,39,40]. The reasons for the destabilization of gas hydrate accumulations as a result of the impact of salts can be separated into natural and technogenic. Among the natural causes, there are the migration of salt ions into frozen hydrate-bearing sediment from sea water on the Arctic shelf, and from cryopegs or saline sediment horizons in continental conditions. Technogenic causes include the flow of exposed cryopegs and saline sediment horizons from sea water as a result of drilling exploratory and production wells when various salt solutions are used in the drilling process, as well as during the burial of industrial solutions in frozen hydrate-containing sediment [41]. These negative phenomena lead to an increase in the risk of emergencies and negative consequences, leading to an increase in financial costs during the hydrocarbon field development in the Arctic [4,5,10,42].

To date, the issues of salt migration during the interaction of salt solutions with intrapermafrost methane hydrates have been poorly studied, especially from the standpoint of the kinetics and mechanism of the process. Many studies are dedicated to experimental and mathematical research on the interaction between frozen sediments and salt solutions, without taking into account the hydrate component [43–52]; mathematical and experimental modeling of the process of hydrate inhibition in sediments by saline solutions [53–56]. And only recently there have been works on mathematical modeling of the process of dissociation of gas hydrates on the Arctic shelf as a result of the migration of salt ions into hydrate-bearing frozen sediments [57].

In this regard, experimental modeling aimed to study the mechanism and dependences of dissociation of methane hydrates in porous media of frozen sediment as a result of salt migration at various pressures (both equilibrium and below equilibrium) is of certain interest. The result of such research can help to evaluate the role of salt migration in the destabilization of intrapermafrost hydrate and methane emission in the Arctic.

1.2. Goal

Experimental study of the mechanism and dependencies of the interaction of gas hydrates with salt solutions in the pore space of hydrate-bearing sediments under various thermobaric conditions.

1.3. Objectives

1. Development of an experimental method for the interaction of gas hydrate with salt solutions in the pore space of frozen sediments under pressure equal to or above atmospheric and negative temperatures;

2. Development of an experimental method for the temperature field investigation during salt transfer in frozen hydrate-bearing sediments;

3. Experimental study of the mechanism and dynamics of the interaction of gas hydrates with salt solutions in the pore space of frozen sediments;

4. Experimental study of the influence of various factors (temperature, pressure, salt solution concentration and composition, and sediment composition) on the processes of hydrate dissociation during the salt ions penetration into hydrate-bearing frozen sediments;

5. Experimental investigation of the temperature change dependencies in the processes of mass transfer and hydrate dissociation during salt migration in frozen sediments, containing methane hydrates;

6. Creation of schematic model of the interaction of gas hydrates-bearing frozen strata with salt containing natural and technical (i.e.drilling fluids) solutions in hydrate-bearing reservoirs in permafrost.

1.4. Novelty

- A method for determining the content of salt ions (Na^+) in sand was developed based on the measurement of pore moisture activity;
- An experimental method for the interaction of frozen hydrate-bearing frozen sediment with salt solutions under pressure > 0.1 MPa has been developed;
- An experimental method for study of the temperature change in frozen hydrate-bearing sediment interacting with salt solution was developed;
- The effect of salt migration on the dissociation of hydrates in frozen hydrate-bearing sediments was experimentally shown, and compared with the process of salt migration in frozen non-hydrate-bearing sediment;
- Temperature variation during salt migration in frozen hydrate-bearing sediments was investigated;
- The influence of various factors (temperature, pressure, concentration and composition of salts, clay content and dispersity) on the dissociation of hydrates in the pore space of frozen sediment during their contact with salt solutions was revealed;
- The critical concentration of salts for the complete decomposition of the hydrate (C_{cr}) was determined depending on various factors;
- The change in the average salt flux in frozen hydrate-bearing sediments was calculated depending on various factors;
- Conceptual scheme-model of destabilization of intrapermafrost gas hydrates in areas of permafrost distribution in continental conditions and on the Arctic shelf is proposed.

1.5. Outline of the Thesis

Chapter 1 give an introduction to the research, contain goal, objectives, novelty and current outline.

Chapters 2 contains research background and literature review. Chapter 2.1. explores the current understanding of Arctic permafrost from the geological point of view, and possible natural and technogenic geohazards in the area of hydrocarbon production in the continental conditions and on the shelf. Chapter 2.2. provides a literature review for the current state of the knowledge connected with gas and gas hydrates as a component of permafrost, and the dependences of their destabilization, with special emphasis on the salt influence investigation on hydrate dissociation. Chapter 2.3. introduces existing experimental and mathematical research on hydrate-salt solution and frozen sediment-salt solution interaction.

Chapter 3 illustrates the method for artificial hydrate saturation of frozen sediments, their interaction with the salt solution under stable and metastable conditions, and temperature field investigation during the interaction process. Also it contain the characteristic of the object of research (sediments characteristic). In addition, a new method for salt concentration determination in sandy sediments is proposed. And the calculation procedure of the main experimental parameters are given.

Chapter 4 describes the experimental data on the dynamics of hydrate-bearing frozen sediment interaction with salt solution in time. A comparison of salt migration in frozen hydrate-containing and frozen non-hydrate-containing frozen sediments is given. In addition, the temperature change in the process of salt transfer in hydrate-bearing frozen sediments is analyzed. Based on the experimental data the description of the mechanism of phase transitions in frozen sediments, containing gas hydrates in stable and metastable form, is given.

Chapter 5 demonstrates, via experimental modelling, the influence of different factors on the interaction of hydrate-bearing frozen sediments with salt solution, such as pressure (above and below

equilibrium), temperature (from -3 to -20 °C), salt solution concentration (from 0.1 to 0.4N) and composition (NaCl, CaCl₂, NaSO₄, MgCl₂, KCl). In addition the influence of clay content of different mineralogical composition (kaolinite and montmorillonite) and dispersity on the intensity of salt migration and hydrate dissociation in frozen sediments is provided.

Chapter 6 cover concept schematic models of the process of hydrate destabilization by natural and technogenic solutions on the Arctic shelf and in continental conditions.

Chapter 7 summarize and conclude the work, as well as contains future direction of the research on gas hydrates interaction with a salt solution in permafrost.

Chapter 2. Research background and literature survey

2.1. Arctic permafrost and problems of hydrocarbon fields development in the Arctic

Large number of hydrocarbon deposits in Russia are concentrated in the Arctic, where more than 83% of natural gas and 12% of oil are produced [7,8,58,59]. However, the largest part of the Arctic territory of Russia is occupied by permafrost, reaching thicknesses from hundreds of meters to 1 km [60,61]. In this regard, in order to plan safe economic development, including the development of energy resources, it is first of all necessary to understand the geological structure and main parameters of frozen sediments (temperature conditions, ice content, sediment composition, frozen sediment thickness, etc.).

2.1.1. Permafrost-geological structure of the Russian Arctic region

Basic information on the permafrost distribution patterns and the main components of permafrost is described in the classical Russian textbooks of geocryology [60,62]. Permafrost is defined as a layer of the ground, which exists at the temperatures below zero for more than 2 years in

the row. It includes as frozen sediments, as well as frosty (cryotic) and cooled sediments. Frozen sediments refers to sediments whose ground particles are cemented by ice. Sediments without ice content, that have a negative temperature are divided into frosty sediments (not containing any water at all) and cooled sediments. The peculiarity of the cooled sediments is that they are saline or containing cryohaline waters (cryopegs) with a concentration of 1 to 300 g/l. At the same time, salts from cryopegs can migrate into the frozen stratum, and thus changing its thickness [60,62]. In the frame of this research only frozen sediments (ice-containing) is under the consideration.

Chuvilin E.M. with co-authors in 2005 gave a detailed description of the main structural elements of frozen sediment, such as the organomineral skeleton and components that fill the sediment pore space: ice, unfrozen water and gas [63]. Each of those components is important for the investigation of salt migration.

Ice, mainly hexagonal in structure, is the main cementing component of frozen sediment. In addition, water films on the surface of the ice crystals is the main transport medium for chemicals in permafrost [48]. The main characteristic of the ice content in the sediment is the coefficient ice content (i , u.f) - the ratio of the mass (volume) of ice contained in pore space to the entire mass (volume) of the sediment. Frozen sediments are subdivided into icy ($i = 0-0.2$), medium icy ($i = 0.2-0.4$), and heavily icy ($i > 0.4$) [58,60].

Unfrozen water is a part of bound water, which has not been frozen. The content of unfrozen water decreases with reducing of the ambient temperature. In this case, ice and unfrozen water are in constant dynamic equilibrium. Also, the amount of unfrozen water increases with an increase in the salinity of sediments and with a decrease in gas pressure [60,64–67].

Compared to ice and unfrozen water, the gas component of frozen sediment has been studied much less. According to [63], gas in permafrost by the genesis is divided into biochemical, deep

(catagen), and coal gas. The gas might migrate to the permeable zone and then gather under the impermeable layer in permafrost creating an area of high pressure [63,68].

According to the phase state, three main classes (forms) of gas are distinguished - sorbed, including adsorbed and absorbed forms, free and dissolved [63]. The sorbed class includes mineral surface gas present in frosty sediment; a gas that exists as a gas hydrate in frozen (stable and metastable form, discussed in detail in Chapter 2.2) or cooled sediment (stable form); coal gas that can exist in both frozen and cooled sediment. Dissolved gas is subdivided into free and bound water gas. Free gas - pinched and movable type [63]. Compositionally heterogeneous cryogenic strata with different filtration properties can accumulate gas, which can be converted into a solid gas hydrate form, or partially accumulate in lenticular bodies and remain sealed both in the gas phase and in the form of hydrates.

In general, permafrost strata along the vertical section can be divided into three layers [60] (Figure 1):

1. A seasonal thawing and refreezing (active) layer with thickness < 5 meters, characterized by temperature changes;
2. Seasonally active strata (transition zone), where the annual temperature fluctuation happens within thickness < 30 meters - with high ice content and permanent temperatures below zero in the bottom part of the strata;
3. Perennially frozen sediments with persistent sub-zero temperatures. In terms of thickness, this sequence makes up the main and most part of the permafrost section.

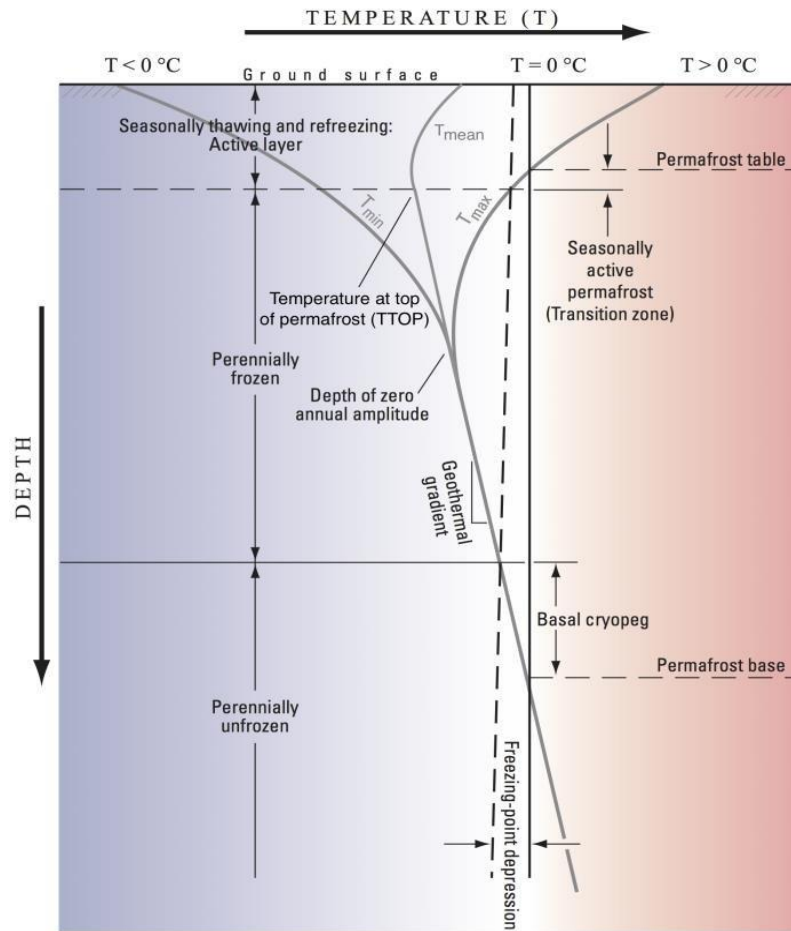


Figure 1. Sediment's temperature profile in the area of permafrost distribution [69].

Frozen strata can be merging with a layer of seasonal thawing and non-merging, separated from it by a thawed layer of sediment [60–62]. Depending on the distribution of permafrost, there are: continuous (more than 90% of the area, up to 1400 m thick), discontinuous (50% -90%) and sporadic (isolated patches) (10% -50%, up to 10-20 m thick) , between which it is possible to draw conditional boundaries [60,70].

In terms of composition, permafrost strata can be composed of loose sediments of various genesis from Paleogene to modern Quaternary time of formation, as well as sediments and rocks of sedimentary, intrusive, effusive and metamorphic origin from Proterozoic to Mesozoic time [8].

Permafrost is constantly evolving depending on long-term climate fluctuations or changes in annual and sediment temperatures. Its thickness can increase (aggrandize) or decrease (degrade) [60,61,71]. In this regard, there are also modern permafrost and relict. Modern strata of permafrost is formed from the surface under a layer of seasonal thawing, and relict ones occur below modern strata at a certain depth [8].

Previously, it was found that in Russia, the thickness of permafrost reaches an average of 600-700 m, and the average temperature varies within $-2.5\text{ }^{\circ}\text{C}$ to -10°C). At the same time, the maximum depth of permafrost (1400 m) was recorded during drilling in the northwestern part of Yakutia [60].

Figure 2 shows a map of the spreading of the permafrost zone on land, indicating the type of distribution [72].



Figure 2. Map of the permafrost distribution on land [73].

In Russia the continuous distribution of permafrost is characteristic of the northern regions. However, under large natural water reservoirs (rivers, lakes) and in tectonic fissured zones of increased groundwater circulation, there are zones composed of thawed sediments for the entire thickness of the permafrost or for part of it, and their number increases from north to south. Such zones are called taliks (through or non-through), which can serve as zones for unloading a gas deposit [8,74,75].

Frozen sediments are widely developed not only on land, but also on the shelf of the Arctic seas [76–83]. However, to date, there are only separate field data on the thickness, distribution, and features of sediments in the permafrost zone of the Arctic shelf of Russia [84,85], as well as mathematical modeling data and individual geophysical surveys. The first data on the existence of the permafrost on the Arctic shelf (when the top of frozen sediments was discovered while drilling) appeared in 1970s [86,87]. But mainly the data on thickness and distribution of permafrost are obtained by the mathematical modeling data.

Figure 3 shows some of the latest data on modeling the propagation of the zero isotherm on the Arctic shelf, which corresponds to the distribution of the permafrost zone there [82]. The depth of underwater permafrost, which was identified earlier (in 2001) on the map of the International Permafrost Association, is indicated by a blue line. In the shaded area, assumed present-day seafloor temperatures result in permafrost formation more than 50 m above the calculated depth [82].

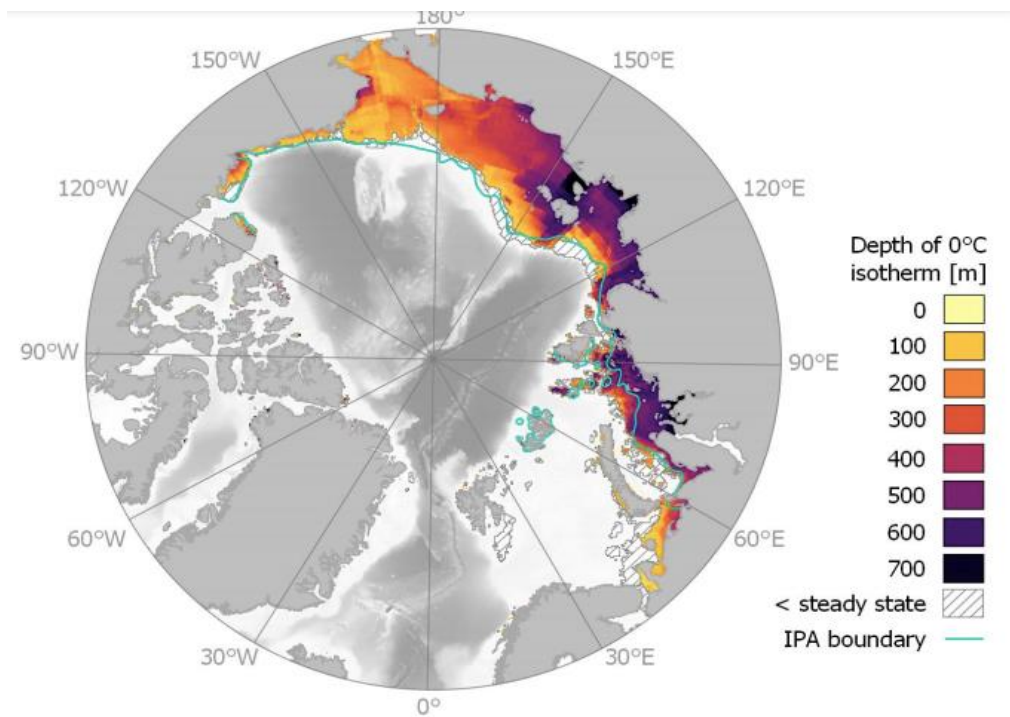


Figure 3. Simulation of the zero isotherm propagation on the Arctic shelf [82].

A distinctive feature of the Arctic shelf is the wide distribution of the subaqueous permafrost zone of complex structure, represented by cooled saline and permafrost sediments [88].

The permafrost zone of the Arctic sea basin was formed as a result of active thermodynamic, chemical and hydrodynamic interaction of the atmosphere, hydrosphere and lithosphere. At the same time, the formation of the submarine permafrost occurred due to freezing from above at the stages of sea regressions; and thawing - mainly from below due to geothermal gradient [76,84,89].

As Yakushev V.S. [8] noted, three main oil and gas provinces are located wholly or partially in the territory of the permafrost zone on the territory of Russia: Timan-Pechora, West Siberian and East Siberian (Table 1).

Table 1. Depth of permafrost bottom on the north of West Siberia gas fields [8].

Field name	Depth of permafrost bottom, m
Bovanenkovo	120-170
Kharasaveyskoe	160-180

South-Soleninskoye	230-260
Yamburg	265-336
South-Pestsovoye	390-460
Zapolyarnoye	420-463
Urengoi	400-480

And depending on the combination of the above-described characteristics of frozen sediments, three categories of section complexity are defined: with especially difficult geocryological conditions, complex and uncomplicated. So, for example, the Nizhnepechorsko-Korotaikhsky, Shapkino-Adzvinisky, Yamalo-Gydansky, Tazovsky North-Siberian, Yenisei-Putoransky, Anabarsky, and Priverkhoyano-Central-Yakutsky districts are especially complex. These areas are described in detail, and the main characteristics of geocryological conditions are given for them [8].

Thus, the major part of energy resources of Russia are located in and under the permafrost. In connection with such a wide distribution of permafrost, significant data has been accumulated in Russia on the properties of frozen sediment, the main parameters, patterns of distribution, and complications associated with the economic development of territories occupied by permafrost. The largest oil and gas provinces are located in the region of the highest values of the geocryological risk index: West Siberian, East Siberian and Arctic shelf [90]. Let us consider the complications arising from the economic development of the Arctic on land and on the shelf.

2.1.2. Peculiarities of hydrocarbon deposits development in areas of permafrost distribution

A number of authors note that at almost all stages of the "life" of hydrocarbon fields in the areas of permafrost, numerous complications can occur associated with negative technogenic effects of various nature (thermal, mechanical, chemical, etc.) on the components of permafrost, primarily such as natural salt solutions (cryopegs), underground ice, gas hydrates [1–3,6,91,92]. In most cases, such

complications are little controlled due to inertia, and therefore dangerous. But so far in Russia there is not a single state program for the comprehensive study of permafrost.

Drilling a well is the first and main step necessary to start developing a hydrocarbon field [3]. At the same time, the process of drilling various wells in the permafrost distribution zone differs significantly from analogues located in areas with a mild climate and positive sediment temperatures. The specificity is due to the complex interaction and influence of mining and geological, mining and technical, permafrost and climatic factors [58,93].

As mentioned earlier, the main cementing component of frozen sediment is ice, therefore, the complicated conditions for the construction of wells in permafrost are based mainly on the temperature factor, which determines, on the one hand, the efficiency of the process of destruction and transportation of frozen sediment to the surface, and on the other hand, the stability of the future wells. And above all, it should be mentioned the destruction and melting of ice occurs due to its thermal, erosive and physico-chemical interaction with the drill bit and the circulating flushing fluid, even if it is pre-cooled [94,95].

Drilling fluid is the first process fluid that interacts with newly opened frozen sediment and, accordingly, has a primary effect on permafrost [94–97]. At the moment, the issue of choosing the appropriate composition of the drilling agent, drilling mode to prevent the degradation of permafrost and secondary ice formation has been worked out in sufficient detail. In the main document regulating well drilling [98] the main recommendations on the choice of the fluid composition are given. It is recommended to use high-viscosity polymer-clay and biopolymer solutions with controlled solids content, bottomhole purge with air or foams. However, most works devoted to drilling fluids do not take into account the hydrate component of frozen sediment, and even more so, this is not mentioned in regulatory documents.

At the same time, it is allowed to use aqueous salt solutions (NaCl, KCl, CaCl₂, MgCl₂) as an additive to drilling fluids, and in some cases as a full-fledged drilling fluid when drilling in permafrost. [97]. Previously, it was found that saline solutions cause thawing of permafrost, as was shown experimentally [49,99], and therefore potentially can also cause destabilization of gas hydrate formations.

The temperature effect of drilling fluid on frozen sediment is difficult to describe. On the one hand, a permafrost system initially in equilibrium is exposed to a drilling fluid with a temperature elevated relative to the formation (this can happen if the solution was not sufficiently cooled initially, or was heated as a result of the mechanical rotation of the drill bit, or the temperature of the overlying warm sediments) [95]. In this case, the equilibrium will be shifted, a temperature gradient will arise, and the pore ice will begin to melt under the influence of a cleaning agent, turning into liquid water. As a result, the sediment will go into a softened state. However, the thermal effect can be partially absorbed by the endothermic process of the ice-liquid water phase transition and, accordingly, somewhat smoothed out. On the other hand, if the treatment agent is at a lower temperature than the host sediment, then the opposite effect may occur. Unfrozen water under the influence of a decrease in temperature will turn into ice with the release of heat. During the transformation of unfrozen water into ice, the salts contained in it can also be squeezed out increasing salt concentration in the remaining pore fluid, therefore increasing its freezing temperature [1,95,100]. A decrease in the freezing temperature of frozen sediments leads to a change in the physical and mechanical properties of sediments: with ice thawing (as far as new freezing temperature has not been reached yet) and consequent liquid water increase their viscosity and plasticity increase, and a tendency to creep appears, up to a complete loss of sediment cohesion [101].

Thus, field experience shows that during the well drilling in the area of permafrost distribution on land, phase transitions are observed in frozen sediments with a change in the strength

characteristics of the sediment as a result of both temperature and chemical effects of technogenic nature [94]. Opening of gas-saturated lenses, opening of cryopegs and saline frozen horizons can also occur, followed by the flow of salts down the section [102,103]. As a result, a number of negative consequences can occur, one of which is hydrate dissociation, accompanied by powerful methane emissions, subsidence of sediment masses around wells, the formation of a deformation field, absorption of drilling fluid, cavern formation, griffon formation, and many others [4,5,10,42,104].

Another important issue is the exploration of deposits on the Arctic shelf. However, in this area, the issues of possible complications have been studied less. Nevertheless, it can be noted that all of the above-mentioned complications typical of land permafrost are possible. In addition to them, salt ions migrate from sea water to sediments on the Arctic shelf, causing degradation of the permafrost zone [76,105] and relic methane hydrate dissociation [31].

The generalization on the complications that arise when drilling wells in the areas of permafrost is carried out on the basis of several publications and is given in Table 2 [1,3,106]. It should be noted that the types of impact of the drilling process on permafrost and its consequences are divided conditionally. Consequences of this or that influence are appearing in nature in a complex.

Table 2. Complications, which can be caused during drilling in the permafrost (modified after [3,49]).

Type of drilling influence	Typical processes	Consequences	Associated phenomena
Thermal	Temperature change, thawing	Change in sediments temperature, sediment thawing (taliks formation), column subduction	Axial deformations of the metal lining, the cause of which is the loss of longitudinal stability of the columns due to stresses arising from the consolidation of frozen sediment thawed in the borehole zone
Mechanical	Visco-plastic deformation; ground discontinuity	Deformation due to porosity change, collapse of the sediments, funnels formation in subsidence sediments	Bending of the above-ground well structure. Threat of deformation fracture of casing pipes and open flowing; inability to maintain the wellhead and perform repair work

Chemical	Dissolution, substitution, redox	Transformation of mineral and chemical composition (with formation of the new one), cavern formation	Collapse of the wellbore walls, formation of cavity widening in the wellbore, mud contamination, sticking, clogging of the wellbore with particles of thawed sediment, decrease in ROP, complications during well cementing, drilling fluid loss
Physical and chemical	Texture transformation, mass transfer, secondary ice formation	Transformation of structure up to sediment damage, change in chemical composition and moisture content of sediment	Loss of cohesion of permafrost sediments with a well walls and poor-quality cementing ring due to repacking of grains, formation of ice plugs in borehole's channel, deformation of the drill string, freezing of the drill pipe

These negative phenomena lead to an increase in the risk of emergencies and negative consequences, leading to an increase in financial costs during the operation of deposits in the Arctic [1,107,108].

In addition to all the above complications of the development and production of hydrocarbon deposits, the environmental component of the potential permafrost thawing and hydrate dissociation is also relevant, which is especially important to take into account for the very vulnerable environmental conditions of the Arctic. As noted above, in addition to changes in the bearing capacity of sediment and the emergence of a number of associated hazardous geocryological processes, there is possibility of gas pockets opening and gas hydrate dissociation. Thus, a number of authors note numerous gas manifestations when drilling wells in areas where the permafrost zone is distributed [36,42,101,109–114]. Some generalization of the recorded cases of gas shows is given in Table 3.

Thus, active methane emission can occur, the transformation of the greenhouse effect, a possible change in climatic conditions, the formation of ozone holes and the so-called "methane catastrophe" [115–120].

Summarizing all of the above, ensuring well stability is one of the most important problems, especially in the permafrost area [36,100,121]. At the same time, a vast area of the main oil and gas provinces in the Arctic is located in an area of very complex and complex geocryological conditions. The existing domestic and foreign experience in the construction of wells in permafrost and their

subsequent operation have shown that insufficient knowledge of permafrost conditions, unreasonable choice of technical, technological and design solutions has a causal relationship with the occurrence of accidents and complications. Such serious problem as wellbore instability can be caused by fluid flow, heat transfer, pressure redistribution, and also hydrate decomposition. The quantitative change in the natural temperature field of the surrounding sediment depends mainly on the temperature of the cleaning agent, the sediment thermal characteristics, the radius of the well, the drilling method, and also on the amount of heat released due to the mechanical destruction (cutting) of sediments.

2.2. Conditions for gas hydrate existence and formation in permafrost

Scientists from various fields of science have been studying gas hydrates for more than 200 years, since the accidental discovery of sulfur oxide (SO₂) hydrate by chemist Joseph Priestley in 1777-1778, and the first mention of the term "hydrate" by Davy in 1811 [15,122]. At the moment, the main issues of consideration of gas hydrates can be divided into two large groups: 1) gas hydrates as one of the promising non-traditional sources of hydrocarbons, the energy capacity of which is comparable to the potential of traditional energy resources [12,123–130]; 2) gas hydrates as a factor complicating the development of hydrocarbon deposits and transforming climatic conditions [10,11,109,131–134].

2.2.1. Characteristics of gas hydrate as a substance

At present, the structure and general characteristics of gas hydrate as a chemical compound are known in sufficient detail thanks to the work of a number of scientists. The clathrate structure of gas hydrate was first suggested by Nikitin in 1935, and a few years later this assumption was confirmed experimentally [135]. A clathrate (from the Latin *clathratus* - “to place in a cage”), or an inclusion

compound, is a compound of the “host-guest” structure. In the case of hydrates, the clathrate structure is described as follows. Water molecules form a polyhedral structure with cavities that represent the “host” structure. These cavities are filled with gas molecules (“guests”) (Figure 4). There is no chemical bond between gas and water molecules, only a weak van der Waals interaction [14,33,117,136–140].

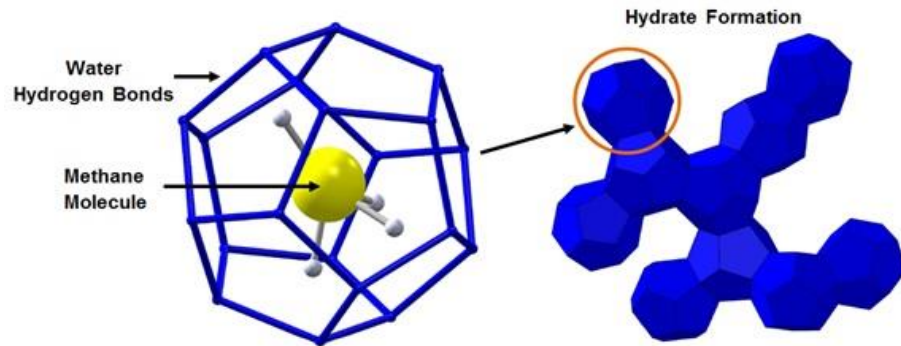


Figure 4. Structure of gas hydrates [141].

Gas hydrates have changing composition (i.e., non-stoichiometric chemical compound). The following chemical formula defines hydrates composition: $M \times nH_2O$ (M – gas, forming hydrate, n – the amount of water molecules per one gas molecule, also named the hydrate number [12,142].

Typically, the hydrate number (n) value determined accordingly to the temperature, pressure, and gas composition, and located in the range from 5.75 to 17. For instance, the hydrate number equals 5.9 in the case of methane hydrates. The hydrate number is of particular importance for all calculations related to the study of gas hydrates [117,143–145].

Figure 5 shows different hydrate structures: (a) cubic structure I, (b) cubic structure II, (c) hexagonal structure H [146].

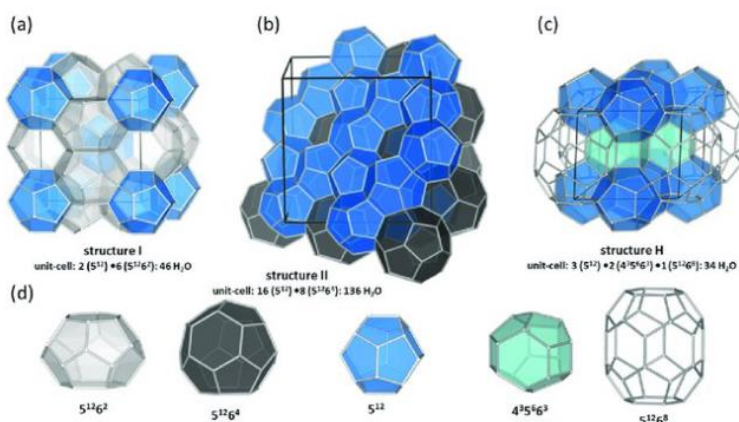


Figure 5. Different crystalline arrangement of hydrates: a – structure I, b – structure II, c – structure H and d – host cages of water. Dense line is the hydrate unit-cell [147].

Structure I is most widespread in nature and it is presented by 2 small dodecahedral voids, 6 large tetradecahedral voids formed by 46 water molecules. Such structure is able to include gases with a molecular size less than 5.2 \AA , particularly CH_4 , CO_2 , C_2H_6 and some other gases [128,148].

Structure II is able to include gas molecules of the size $5.9 - 6.9 \text{ \AA}$ (for example C_3H_8 or C_4H_{10}) and consist of 8 large hexadecahedral and 16 small dodecahedral voids composed of 136 H_2O molecules [122].

Less common structure is H structure, which forms only by gas mixtures (like $CH_3C_6H_{11}$ mixed with H_2S) [15].

Such natural gases as CO_2 , C_2H_6 , C_3H_8 , C_4H_8 , O_2 , N_2 , H_2S , and more often CH_4 , able to form hydrates both separately and in mixtures. Some other gases are able to go into a hydrate form only at the very high pressures (such gases as H_2 , He, Ne) or unable to make a hydrate at all (for example C_5H_{12} et al.) [149]. The composition of natural gas hydrates may include hydrocarbons (methane, ethane, propane, butane), as well as gases such as CO_2 and SO_2 . As shown by the data of chemical analysis of gas from intrapermafrost gas shows, the most common gas that forms natural gas hydrates is methane. However, pure methane is extremely rare. Almost always, nitrogen, carbon dioxide,

hydrocarbon homologues of methane, hydrogen sulfide are present in small amounts in the composition of the gas [12,33,122].

In appearance, gas hydrates mainly resemble ice (Figure 6), which was one of the reasons for the relatively late start of the study of gas hydrates.



Figure 6. Gas hydrate burning (photo by Dinara Davletshina).

Hydrates have been encountered for a long time, but scientists could not explain the cause of many phenomena, such as, for example, the sudden emission of methane, the release of a sediment mass, the formation of plugs that resemble ice in a well, etc. [2,150]. Active exploration of gas hydrates only began in the 1940s and 1960s with the work of Makogon Yu. F., Strizhov I.N., Trofimuk A. A., Mokhnatkin M.P., Chersky N. V., Vasiliev V. G., Trebin F. A., who suggested the hydrate existence in nature in the permafrost area and proved it in the laboratory conditions [142,151].

The external similarity of gas hydrate and ice, due to the framework of water molecules with van der Waals bonds, determines the closeness of the values of their physical properties (density, heat capacity, acoustic properties, Poisson's ratio) [15,142]. At the same time, a number of properties are noted for which there are significant differences: thermal (ice thermal conductivity (λ) equals 2.2 W /

m K, and methane hydrate $\lambda=0.5$ W / m K) and dielectric (dielectric constant of ice - 94, methane hydrate - 58). Also, during hydrate formation, the specific volume can increase by 26%, while when water freezes, the volume increases by 9% [15,140].

Under normal conditions, unit volume of methane hydrate, as mentioned above, contains 160 volumes of gas, which emphasizes its potential use as an energy source, on the one hand, and the danger of dissociation of gas hydrate formations in the sediment, on the other. [33].

Figure 7 shows the phase diagram of the existing conditions of methane hydrate, one of the most common types of gas hydrates in nature. When the thermobaric conditions change, gas hydrates dissociate into water and gas [152].

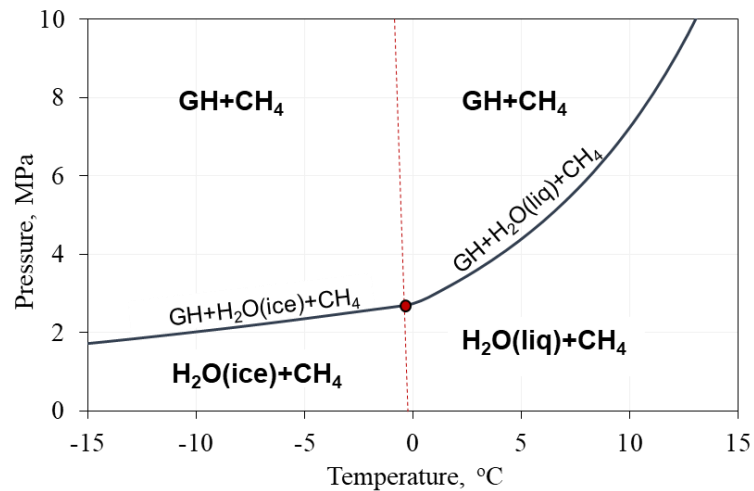


Figure 7. Schematic stability curve for CH_4 hydrate (built in “HydraFlash” software [153]): GH – gas hydrate; liq – liquid water; red dot – quaternary point (four-phase equilibrium "gas – water – ice – hydrate"); red line – line of ice-liquid water phase equilibrium.

There are many works devoted to the study of the p-T shift of the conditions for the existence of hydrate and its dissociation and the influence of various factors on this process (inhibition by various substances, type of gas hydrate, etc.) [33,137,154]. Works on the study of the dissociation of gas hydrates are mainly devoted to their inhibition in the development of hydrocarbon deposits (to

prevent hydrate formation) [155–159], or for the purpose of methane production from hydrate-bearing sediment [55,140,160–164]. Within the framework of this work, it is interesting to review the hydrate dissociation at temperatures below 0 °C.

The dissociation of methane hydrate can occur as a result of a change in thermobaric conditions, when the pressure drops below the stable one or the temperature rises and the conditions go out of equilibrium [129,138,152,165,166]. Also, dissociation can occur when the gas hydrate stability curve shifts as a result of various factors (mainly due to the presence of inhibitors in the system) [14,167]. Figure 8 schematically shows the shift in hydrate stability as a function of various factors.

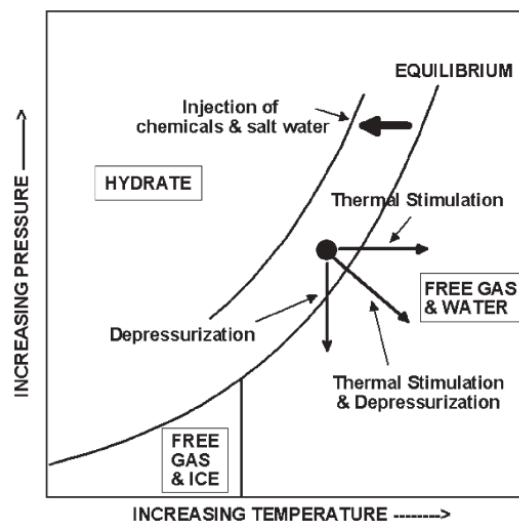
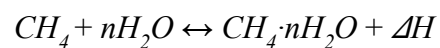


Figure 8. Shift of gas hydrate equilibrium by different methods of methane extraction [146].

Hydrate dissociation is an endothermic process (i.e., it occurs with the absorption of heat) [14,168,169], and the following chemical equation describes that process [138]:



where n - hydrate number, and ΔH - hydrate formation (or dissociation) enthalpy (equals around 52-54 kJ/mol [14,168]).

Most authors distinguish two stages in the process of hydrate decomposition due to pressure reduction at negative temperatures: active hydrate dissociation and then slowing of the hydrate

dissociation. Such a slowdown in the hydrate dissociation can be explained by the self-preservation effect of gas hydrate (Figure 9) [23,25,27]. When the pressure drops below equilibrium and the gas hydrate begins to dissociate, the water formed as a result of the decomposition of the hydrate at a negative temperature turns into a fairly thick and strong ice shell around the crystals or aggregates of gas hydrates, under which there is an excess internal gas pressure that prevents further dissociation of the hydrate [22,170]. Such an ice cover ensures the long-term preservation of gas hydrates even at atmospheric pressure without significant changes in their gas content under conditions of negative temperatures [137].

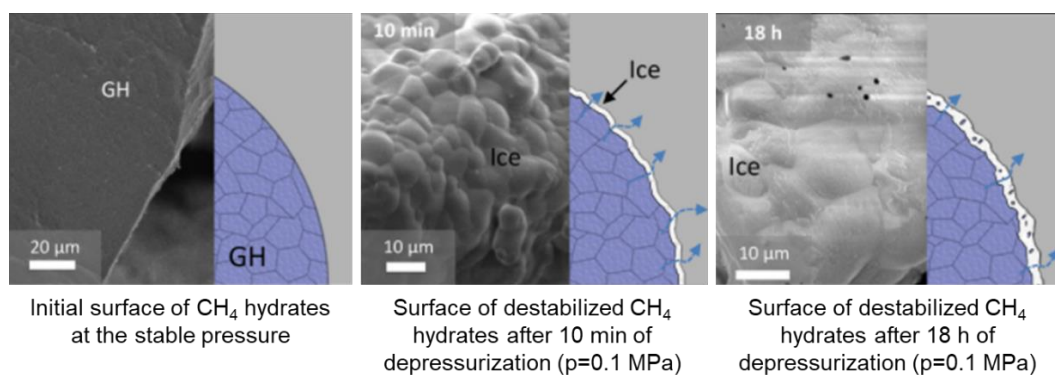


Figure 9. Scheme of bulk hydrate self-preservation at the negative temperature (picture obtained and analyzed through extensive cryo-FE-SEM imaging [171]).

Works devoted to the study of the gas hydrate dissociation as a result of exposure to various chemicals were carried out from the standpoint of hydrate inhibition for the extraction of methane (for example [172]) or to prevent hydrate formation in wells and pipelines (for example [157,158,173]). A hydrate inhibitor is a chemical compound, which shift the hydrate phase equilibrium to the side of lower temperatures and higher pressures (Figure 8). Consequently, the hydrate formation process is slowed down in the reservoir [127,138].

There are organic (methanol, ethylene glycol, etc.) and inorganic (brines, sea water) inhibitors of gas hydrates (Figure 10) [15,147,157].

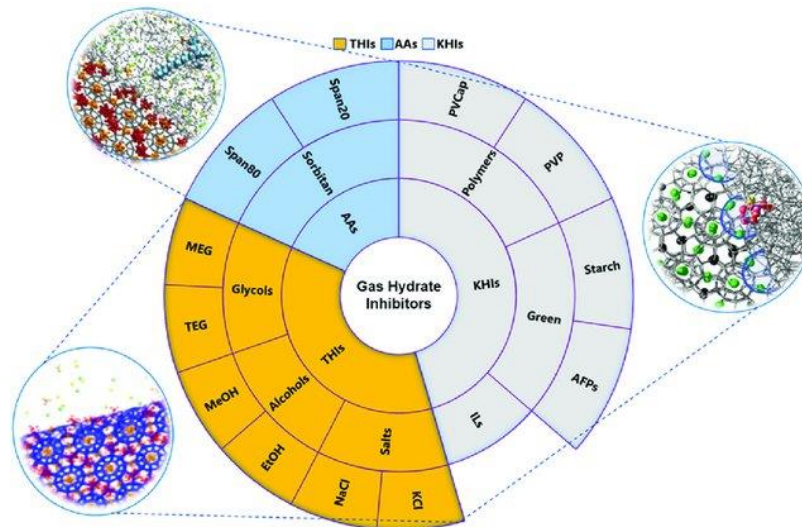


Figure 10. Different hydrate inhibitors and scheme of their work principle [147].

Within the framework of this work, of particular interest are studies devoted to the effect of inorganic inhibitors, particularly salts, on the dissociation of gas hydrate. There are several works devoted to the investigation of hydrate dissociation, mainly from the standpoint of their potential development by the method of inhibition with saline solutions.

First of all, there are a number of works on the thermodynamic study of the effect of salts on the conditions for the gas hydrate existence, which is directly related to their potential destabilization [12,14,179–188,15,189–195,130,142,174–178]. It was found, that an increase in the concentration of chloride salts shifts the equilibrium conditions towards higher pressures and lower temperatures [138,142,194].

In addition, research works [53,54,197–201,56,164,172,182,190,191,193,196] contain studies on the effect of salt solutions of electrolytes of various concentrations and temperatures on the hydrate component. The rate of hydrate dissociation has been shown to depend on brine temperature, brine concentration, hydrate/brine interaction surface area, and pressure. Because of both experimental and mathematical modeling, it was found that the rise in temperature, the salt concentration of the solution, and reduction in pressure contribute to the intensification of the hydrate

dissociation process. An increase in the contact area also contributes to a more intensive decomposition of methane hydrate. Zheng with co-authors [190] also noted a decrease in temperature in the course of experimental modeling of the NaCl influence on the hydrate decomposition, and the higher the concentration of the injected brine, the greater its decrease. However, the paper does not provide an explanation for this temperature effect.

The mechanism of gas hydrate inhibition under the influence of NaCl salts at positive temperatures is described [167,182,201–204]. The authors believe that the mechanism by which the salt solution stimulates the dissociation of hydrates is caused by the interaction between water molecules involved in the structure of the hydrate complex and NaCl ions in an aqueous solution. The salt is ionized in an aqueous solution and interacts with hydrogen-water molecules on a hydrate cell, and its Coulomb bond is much stronger than the hydrogen bond or the Van der Waals force. Consequently, a stronger bond between salt and water ions will lead to the destruction of the initially stable hydrate structure and methane releases (Figure 11).

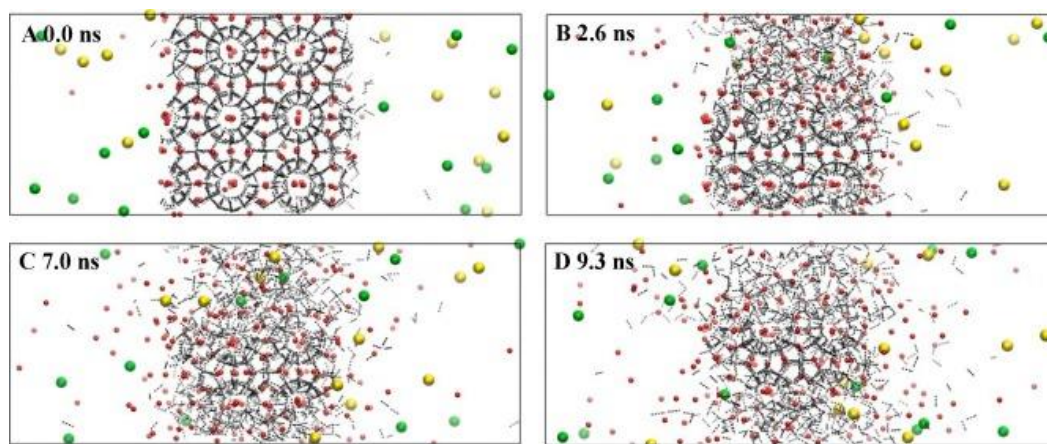


Figure 11. Hydrate decomposition in water by NaCl ions migration in time by mathematical modeling (red – methane, green – Na⁺, yellow – Cl⁻) [204].

Scientists [167,182,207,185,186,189,194,200,203,205,206] conducted experimental studies of the influence of the salts composition of (NaCl, CaCl₂, MgCl₂, KCl) on the processes of hydrate

formation and dissociation in water free volume. An increase in the intensity of dissociation of gas hydrates in the series without saline solution - KCl solution - CaCl₂ solution - NaCl solution - MgCl₂ solution was revealed, however, with a change in concentration, the ratio may change. Additionally, Saw with co-authors (2014) determined the enthalpy of hydrate dissociation depending on the salt composition. So, more heat will be absorbed in the presence of sodium chloride salts in the system, and less heat in the case of calcium chloride salts, which means that secondary ice formation is more likely to be more intense in the system with NaCl [167]. However, it should be noted that the issues of inorganic salts influence on the kinetics of hydrate dissociation are less studied [208].

The conditions for the hydrate formation and dissociation in the sediments pore space is a more complex process. A number of scientists believe that a porous medium contributes to a more intensive process of hydrate formation compared to a free one because more nucleation sites are provided, the energy of the nucleation process is lower, the gas-liquid contact increases and the barrier to hydrate nucleation decreases [174,209–213]. And, there is also an opinion that the pore space can act as an inhibitor of hydrate formation (by reducing the activity of water and improving the dissolution of methane), and at the moment this view is the most common [214–217]. Wu with co-authors suggests that both formation and dissociation of hydrate more actively occurs in a porous medium than in the bulk phase [218].

There is an optimal size of the pore space at which hydrate accumulation occurs faster and the hydrate is subsequently more stable. [213,219–221]. In addition, there is the concept of non-clathrate water - moisture that does not go into a hydrated state and remains in a liquid state in equilibrium with the rest of the system components (ice, hydrate) [64,222].

2.2.2. Conditions for the existence of permafrost associated gas hydrate and possible causes of their destabilization

Methane hydrates are widely distributed throughout the world. To date, more than 200 gas hydrate deposits have been registered [33,140]. The volume of methane contained in the hydrated form in sediment is estimated over a wide range: $3.1 \cdot 10^{13} - 3.4 \cdot 10^{16}$ on land and $2 \cdot 10^{14} \text{ m}^3 - 7.6 \cdot 10^{18} \text{ m}^3$ in marine conditions [2,15,33,140,223,224].

In nature, gas hydrates exist in the layer of the lithosphere, where there is suitable thermobaric and geochemical regime, in so-called hydrate stability zone (HSZ) [33,123,225]. Such conditions for methane hydrate may exist in the permafrost zone (onshore) (Figure 12B) and in the bottom marine sediments (for example, from the depth 200 m in the Arctic seas, Figure 12A) - offshore [15,33,123,152].

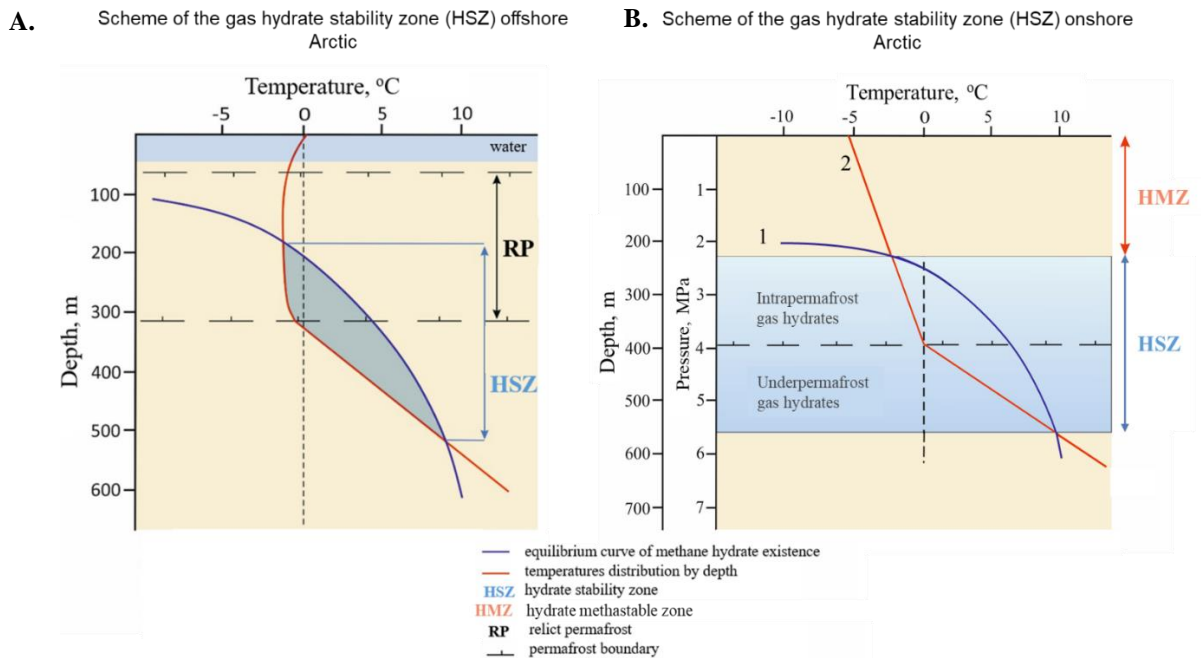


Figure 12. Existence of methane hydrate in natural permafrost conditions (modified from [17,226]).

Estimates of the depth of the upper and lower HSZ boundaries for onshore permafrost conditions have been obtained from field data and through mathematical modeling and vary widely, mainly

depending on the thickness of the permafrost. The upper boundary of HSZ for methane hydrates is located at the depth of about 150-200 m in continental permafrost regions where surface temperatures are maintained at about 0 °C [227]. The lower limit of the existence of methane hydrates can reach a depth of 1000 meters (for example, on the Siberian platform) (Figure 12B).

At the same time, the hydrate existence on the Arctic shelf is a much more complex issue due to less field data. Romanovsky with co-authors obtained some data on the thickness, history of formation and evolution of the permafrost zone and HSZ of the Arctic shelf based on a retrospective analysis, and Malakhova and co-authors made a publication based on mathematical modeling [57,228]. On Russian Arctic shelf the HSZ upper boundary is traced at around 100-145 m beneath the sea bottom, accounting average sea depth of around 50-70 m. The location of the upper boundary will be determined by an additional baric factor due to the weight of the water layer on the outer shelf. The thickness of HSZ increases with decreasing sea depth, which is explained by lower temperatures of sediments in the shallow part of the shelf and the greater permafrost thickness. The current value of the thickness of the stability zone, according to the simulation results, is approximately 700 m for the outer shelf and 1130 m for the inner shelf [84].

However, gas hydrate in the permafrost zone can also exist above the gas hydrate stability zone in the region of relatively low pressures (below equilibrium) at temperatures below 0 °C for a long time, in the so-called hydrate metastability zone (HMZ). It represents the permafrost layers above the HSZ, where relic hydrates exist due to the self-preservation effect [23]. The hydrate metastability zone, in contrast to the zones of stability, is not a thermodynamic, but a geological zone. Relic gas hydrates are not formed in HMZ, but exist in the conserved form under the condition of ice coexistence for a long geological time [23].

There are several scenarios for the history of the formation of intrapermafrost hydrate in the permafrost zone [229]:

- 1) With rapid freezing of closed taliks containing methane, due to the creation of excess pressure;
- 2) During periods of glaciation due to the pressure created by ice on the underlying gas-containing sediments;
- 3) Due to the increased pressure exerted by the water column on gas-containing sediments during transgression.

Due to the creation of increased pressure in gas-containing sediment, the gas hydrate is formed in the gas hydrate stability zone. However, later, during the evolution of the permafrost zone, as a result of changes in thermobaric conditions, part of the relict gas hydrate formations passed into the area of pressures below equilibrium, while maintaining negative temperatures of the host sediment [84].

V.A. Istomin and V. Yakushev (1992) defined three main type of natural hydrate formation depending on their location in permafrost: supraperafrost, intrapermafrost and subpermafrost [15,30,230]. Subpermafrost gas hydrates are currently the most studied due to the many cases of real registered natural core extraction of gas hydrate-bearing sediments (Mallik, Canada [165]; Prudhoe Bay and Mount Elbert, Alaska, USA [13,128,231]; Qilianshan, Tibet, China [35,232–235] etc.).

As mentioned above, the specificity of the hydrocarbon fields development is that many large hydrocarbon fields (Bovanenkovskoye, Yamburgskoye, Zapolyarnoye, Medvezhye, Urengoyskoye, etc.) are located in the permafrost zone. Both exploration and production wells can pass through the gas hydrate stability interval. Consequently, during the development of deposits, destabilization of gas hydrate formations may occur [10,109,236].

Currently, there are only a few areas of permafrost where the natural hydrates existence has been proven by direct data (extraction of hydrate-bearing deposits as a result of drilling). However,

there are many prospects where the presence of hydrate-bearing formations is suspected due to active methane emission, well logging and stability conditions [17].

Purposeful study of gas manifestations in the Arctic regions of Russia began relatively recently (about 60 years ago), which was associated with the discovery of the largest hydrocarbons fields in the North of Western Siberia and their development: Messoyakha (1967), Urengoyskoye (1966), Yamburgskoye (1969), Bovanenkovskoye (1971), etc [8,33,129,237]. When arranging the field infrastructure and laying transport routes, prospectors and builders began to encounter numerous gas emissions from the upper horizons of the permafrost zone, which often accompanied drilling operations. At the same time, both spontaneous short-term gas emissions and long-term gas emissions from engineering and geological wells drilled in monolithic permafrost occurred [42,113,238,239]. At the same time, they began to pay attention to natural gas emissions from the bottom of the Arctic seas and lakes [118,120,240,241].

An analysis of gas manifestations described by researchers shows that they can be conditionally divided according to the place of manifestation - on land and on the Arctic shelf, and according to the conditions of occurrence - into natural (natural) and man-made, associated with anthropogenic impact on the permafrost. Natural gas vents on land are often associated with various natural sources of water (lakes, rivers) and wetlands [239]. In the frame of this work, the gas that is generated in the seasonally thawed layer is not considered. Recently, another natural source of methane emission is gas emission craters, recorded in recent decades during the development of the Arctic zone of Western Siberia [74,108,239,242].

The collection and analysis of available literature data on gas shows in the Russian Arctic made it possible to compile a summary table (Table 3), reflecting the detection area, characteristic features and a possible source of gas, as well as a schematic map of gas shows in the Arctic region of Russia (Figure 13) [239].

Table 3. Registered cases of gas emanations in the Russian Arctic [239].

		No in map	Location	Signatures	Possible gas sources	Reference	
Onshore	Natural	Lakes	1	Yamal Peninsula, Lake Neyto	Gas plumes on water surface, mud flows, holes in ice	Deep gas from Neyto field	[243]
			2	Yamal Peninsula, Crater Lake	Craters and parapets on lake bottom, mud flows	Possibly, deep gas-water fluids	[241,243]
			3	Yamal Peninsula, group of lakes south of Bovanenkovo field	Blue water, holes in ice, mud flows	Active emission, possibly, deep gas	[244]
			4	Gydan Peninsula, a lake on the left bank of Yuribey River	A crater encircled by a parapet	Prolonged ascending flow, possibly, deep gas	[244]
			5	Yamal Peninsula, 54 km northeast of Arctic field, Otkrytie Lake	Large craters (up to 40 m in diameter on lake bottom)	Deep gas, possibly, from Cenomanian gas reservoirs	[112]
		6	Craters	Yamal Peninsula, 30 km south of Bovanenkovo field	A large crater (up to 40 m in diameter and ~70 m deep), encircled with a well-pronounced parapet; ground dispersed to a distance of 120 m	Possibly, intrapermafrost gas	[245–250]
		7		Gydan Peninsula, 100 km northwest of Antipayuta Village	A crater, 10-13 m in diameter and ~15 m deep; no parapet	Possibly, intrapermafrost gas	[251]
		8		Yamal Peninsula, floodplain of Erkuta-Yakha River	A crater, 10-12 m in diameter and ~20 m deep, with a preserved fragment of a 2-3 m high mound and ground dispersed to a distance of 100 m	Biogenic gas in a talik and deep gas	[252]
		9		Yamal Peninsula, 33 km northwest of Seyakha, Myudriyakha River	Fire gas explosion that produced a 50 m deep 50×70 m crater in a river, with dispersed blocks of permafrost and ice-rich soil, up to 150 m ³	Possibly, deep gas	[253,254]
		10		Gydan Peninsula, north of Deryabino field, bank of Mongoche River	Fire gas explosion that produced a 20 m deep crater, with dispersed large fragments of sediment	Possibly, deep gas	[85,244]
	Man-caused	Drilling in permafrost	11	North Yakutia, Anabar—Khatanga interfluve	Gas shows at depths 70-120 m	Intrapermafrost gas	[255]
			12	Yamal Peninsula, Yuribey River	Gas shows at depths 10-50 m	Intrapermafrost gas	[113,256]
			13	Taz Peninsula, Zapolyarny field	Gas shows at depths 50-120 m	Intrapermafrost gas, possibly relict gas hydrates	[33]
			14	Taz Peninsula, Yamburg field	Gas shows at depths 45-55 m	Intrapermafrost gas, possibly relict gas hydrates	[33,257]

		15	Ascending flows and seeps	Yamal Peninsula, Kharasavey field	Gas shows at depths 10-210 m	Intrapermafrost gas, possibly relict gas hydrates	[258,259]
		16		Yamal Peninsula, South-Tambey field	Gas shows at depths 40-60 m	Intrapermafrost gas, possibly relict gas hydrates	[260]
		17		Gydan Peninsula, Pelyatka field	Gas shows at depths 20-30 m	Intrapermafrost gas	[33]
		18		Gydan Peninsula, Salman (Utrenneye) field	Gas shows at depths 50-150 m	Intrapermafrost gas, possibly relict gas hydrates	[23]
		19		Yamal Peninsula, Bovanenkovo field	Gas shows at depths 20-130 m	Intrapermafrost gas, possibly relict gas hydrates	[68,259,261,262]
Offshore	Natural	20	Ascending flows and seeps	Laptev Sea, Yana Delta	Ebullition	Deep gas	[33,263]
		21		East Siberian Sea, Bennett Island	Gas plumes, up to 1000 km long	Possibly, deep gas	[263,264]
		22		Laptev Sea, between Semyonovsky Island and Lena Delta	Gas seeps	Possibly, deep gas	[265]
		23		Laptev Sea, Ivashkina Lagoon	About twenty gas seeps; high concentration of methane in air	Deep gas	[266–268]
		24		Laptev Sea, Kotelny Island	Gas seeps	Possibly, deep gas	[269]
		25		Laptev Sea shelf, New Siberian Islands	A cluster of gas seeps at 50-90 m sea depths	Possibly, deep gas	[270]

Man made	26	Laptev Sea (between 76.5–77.5° N; 121–132° E)	More than 700 gas seeps, up to 1.3 km in diameter	Possibly, deep gas	[268,271]	
	27	Chukchi Sea, Herald Canyon and Wrangel Island	About 90 gas seeps at 50-95 m sea depths	Deep gas	[272]	
	28	Kara Sea, Universitetskaya structure	Gas seeps from a depth of 80 m and pingo-like features	Deep gas	[273,274]	
	29	Drilling in subsea permafrost	Pechora Sea, Kara Gates	10 m high gas fountain from a borehole at subbottom depth 50 m	Deep gas	[113,257]
	30		Pechora Sea, Vaygach Island	10 m high gas fountain from a borehole at subbottom depth 50 m, with a ebullition zone up to 200 m in diameter on the sea surface	Gas from subsea permafrost	[275,276]
	31		Kara Sea, Baydaratskaya Bay	Gas show from subbottom depth 10-50 m	Possibly, deep gas	[254]
	32		Kara Sea, Leningrad field	Gas show from a 200 m deep borehole	Possibly, deep gas	[254]
	33		Laptev Sea, Lena Delta	Gas show from a borehole at 9 m depth	Gas from permafrost	[277]
	34		Laptev Sea, Buor-Khaya Gulf	Gas show from a 13-16 m deep borehole	Gas from permafrost	[277]
	35		Laptev Sea, Mamontov Klyk Cape	Gas show from boreholes up to 80 m deep	Gas from permafrost	[278]

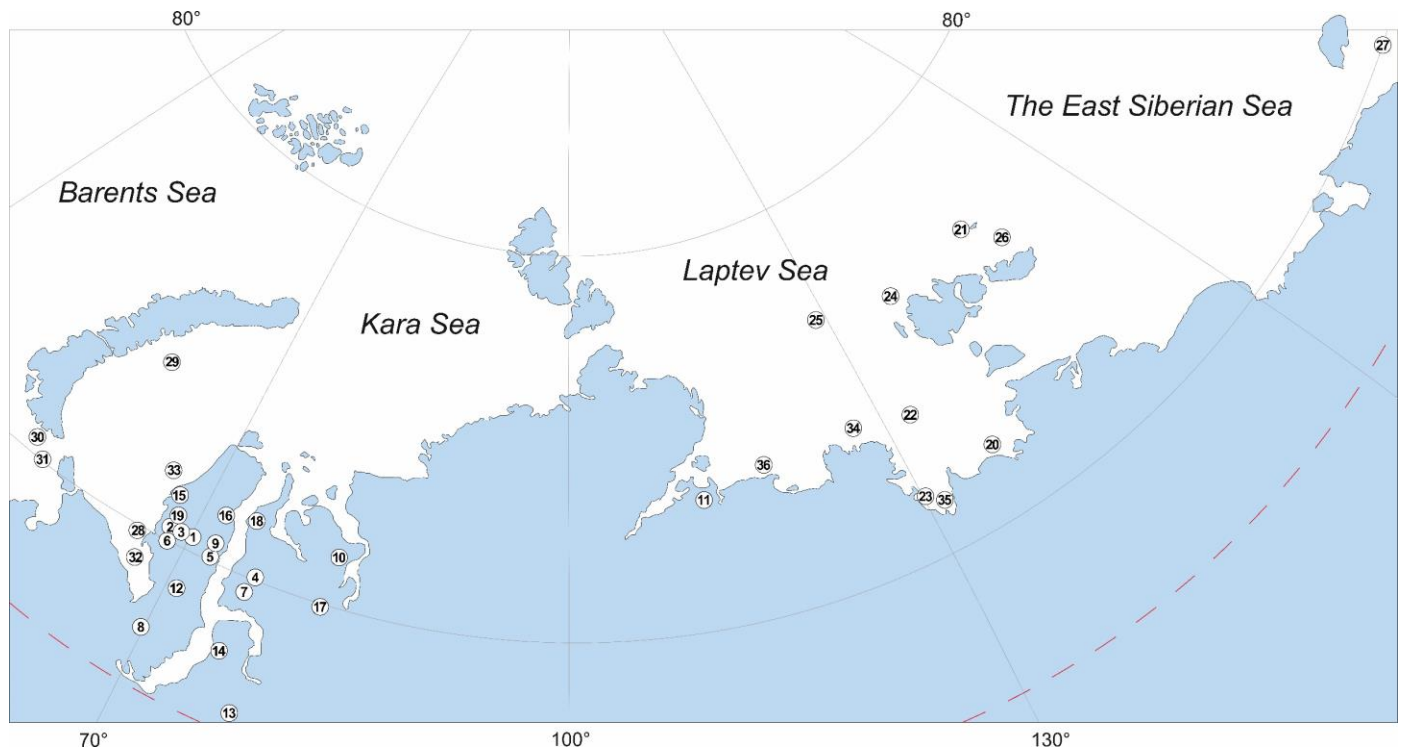


Figure 13. Schematic map of registered gas emanations in the Russian Arctic [239].

Connection of part of the gas manifestation with hydrate formation in permafrost was shown by N.N. Romanovsky et al. (2006), D.Yu. Nikolsky et al. (2012), D. Delisle (2000), N.E. Shakhova et al. (2010), V.I. Bogoyavlensky, O.S. Sizov, I.V. Bogoyavlensky, R.A. Nikonov (2016), Bondur, T.V. Kuznetsova, V.E. Vorobyov, V.V. Zamshin (2014) and other scientists [227,243,253,279–285]. Should be especially noted that shallow gas manifestation (up to 120 m depth) can be associated with relic (metastable) hydrates, which exist in the preserved form and are especially sensitive to the thermobaric and geochemic conditions change.

However, there is an alternative point of view. So, for example, O.A. Anisimov with co-authors conducted research on the Arctic shelf based on mathematical modeling and concluded that deep-seated methane that is not associated with hydrates is biogenic [116,286]. C.D.Ruppel and J.D.Kessler in their studies emphasis as well on still unproven connection of gas manifestations and gas hydrate

destabilization, that methane out of hydrates at all reaches atmosphere. They state, that main part of methane is dissolved in the layer of sea water [287].

Hydrate-bearing sediment in the areas of permafrost distribution can be affected by various technogenic and natural solutions, such as highly mineralized solutions left from the development of deposits and / or buried in permafrost, cryopegs discovered during well drilling, wastewater of various origins (industrial, municipal, etc.), drilling fluids (including salt-containing ones) used in the process of drilling wells, as well as the penetration of sea water into hydrate-bearing sediment on the Arctic shelf [60,74,76,102,105,288]. However, at the moment there is a lack of understanding of the patterns of occurrence of the whole complex of complications during well drilling associated with the dissociation of gas hydrate formations [18].

There are a number of works devoted to the experimental study of the interaction of drilling fluids (including salt-containing ones) [3,95,100] and salt solution [43,45,46,99,289] with frozen sediment, excluding the hydrate component; experimental simulation of drilling fluid interaction [96,110,290–292] and salt solution [201,208,293–295] with hydrate-containing non-frozen sediments; experimental and mathematical modeling of the effect of salts on methane hydrate in free volume at negative temperatures [211]; mathematical modeling of the interaction of salt solutions with thawed and frozen sediment [49]; and only a few works are devoted to mathematical modeling of the interaction of frozen hydrate-bearing sediment with drilling fluids that do not contain salt [131,291,296,297].

Prasad with co-authors (2019) made an investigation of the salt influence on the hydrate stability and their self-preservation. The authors consider salt solutions as a thermodynamic inhibitor of hydrate formations. In this regard, the penetration of salts into the thickness of frozen hydrate-bearing sediment can shift the HSZ deeper to the reservoir, thus reducing the HSZ parameters (length and thickness) [211].

The authors note that in the HMZ permafrost zone, the hydrate exists until the concentration of the pore solution reaches the melting point of ice around the preserved hydrate.

According to the results of experimental studies [211] 3 stages of interaction of salts with sediment containing metastable gas hydrates are distinguished: replacement of the initial fresh pore solution of hydrate-containing sand (no dissociation is observed at this stage), when salinity reaches a certain critical value of ice melting, the metastable hydrate begins to dissociate; the third stage, when there is no hydrate in the system and only heat is absorbed from the environment to return the initial temperature state of the system. By analyzing the change in temperature, the authors traced the dissociation of pore gas hydrate by a sharp decrease in temperature. So, the higher the salt concentration, the more significant was the decrease in temperature, that is, the more intensively the pore hydrate dissociated. It should also be noted that the authors consider concentration diffusion as the main mechanism of salt migration [211].

S. Sun with co-authors (2011) [293] considers the p-T shift of the conditions for the hydrate existence in the pore space due to NaCl ions at positive temperatures based on experimental modeling of the interaction of sea water with hydrate-bearing sediment. The authors note that conditions are shifting towards higher pressures and lower temperatures, and the higher the salt concentration, the greater this shift. The authors attribute the intense dissociation of gas hydrates in the pore space due to the migration of salts to a decrease in the activity of pore moisture during the hydration of salt ions, and also to the fact that weak van der Waals bonds are less preferable than electrostatic ones - therefore, salt ions will also be easier to "pull" water molecules from the crystal lattice of the hydrate, thereby destroying its lattice and facilitating the release of methane [211].

Perlova E.V. et al. (2017) suggest that the destabilization of hydrate-bearing horizons can occur as a result of penetration of drilling fluid, as well as salts from highly mineralized horizons (cryopegs) based on the results of the analysis of the geological section and comparison with the highest production rates

of methane emissions (exactly where cryopegs, the most intense methane emissions were observed) [121].

Another side of the issue is the use of permafrost as a storage of liquid hydrocarbons or oil and gas production waste. The attractiveness of using the permafrost as a storage facility is explained by the almost complete impermeability of permafrost to fluids [49].

In the 1970s, storage facilities for waste from the development of mineral deposits were put into operation in the permafrost zone in the north of the Magadan Region, at Cape Schmidt, in the area of the Leningradskoye and Bovanenkovskoye deposits [49,298–300]. However, cases of dispersion of chemical elements in the frozen sediment around such storages have been recorded. For example, migration of buried drainage fluids was registered in the frozen sediment in Western Yakutia [49,300]. Dissipation halos were found, which led to the conclusion that active migration of chemicals into frozen sediment (for more information on these works and migration processes, see Chapter 2.3) [298,299]. Intense gas manifestation was recorded during the injection of industrial brines into the aquifers of the permafrost zone of Western Siberia, in the Daldynsky district, up to the release of a gas-water mixture and the flowing of gas, which can be connected with the gas hydrate nature of the emission. Later, in this area, two hydrate-bearing intervals were identified in the permafrost strata at depths of 80-100 and 140-190 m, as well as similar signs - subpermafrost, but negative - temperature (within the permafrost zone) hydrate-bearing horizons in the depth range from 330 to 550 m [299].

Then a field experiment was carried out on the injection of brines into the expected hydrate-containing intervals for 3.5 months. During the experiment, consumption of the salt solution, its desalination and cooling by 1.5-2 °C were observed. The volume of released methane amounted to about 50 million m³ [299,300].

Thus, today there is a sufficient amount of information about gas hydrates, the forms and conditions of their existence in nature, as well as the causes of destabilization (pressure decrease, temperature increase, exposure to chemical compounds). However, the effect of salts on gas hydrates is considered mainly from the position of thermodynamics, and rare publications are devoted only to the assumption of a possible destabilization of gas hydrates in frozen sediment as a result of salt migration.

2.3. The study of salt migration processes in frozen sediments

As noted above, one of the reasons for the hydrate dissociation in permafrost zone can be the migration of salts into the strata of frozen sediments containing gas hydrates. At the moment, in literature any special studies on the interaction between frozen hydrate-bearing sediments and salt solution are absent. While these studies are vital for assessing the intensity of methane emission during the permafrost degradation.

However, there are data on the study of salt migration in frozen sediments that do not contain gas hydrates, which is undoubtedly of interest for the problem under consideration, given the similarity of the ice and gas hydrate components of sediment. Before proceeding to the consideration of existing works on the interaction between salt solution and frozen sediments, it should be reviewed the mechanism of ice melting, as one of the most important components of frozen sediment.

Salt ions can cause ice to melt in the pore space of frozen sediments. The melting of ice due to the migration of salt ions is a complex physical and chemical process, the intensity of which is determined by a number of factors. Ice is a crystal lattice composed of dipoles of water molecules. Salt ions, when in contact with ice, pull the dipole of water towards themselves, thus destroying the crystal lattice of ice - i.e. causing it to melt. So, in the case of the action of sodium chloride on ice, a negatively

charged chloride ion attracts the water dipole with a positively charged end, and a positively charged sodium ion - negative (Figure 14). Thus, the salt ions are hydrated, causing the crystal structure of the ice to break down (melting), and hence solution of salts is formed whose freezing point is lower than the freezing point of pure non-salt water [301].

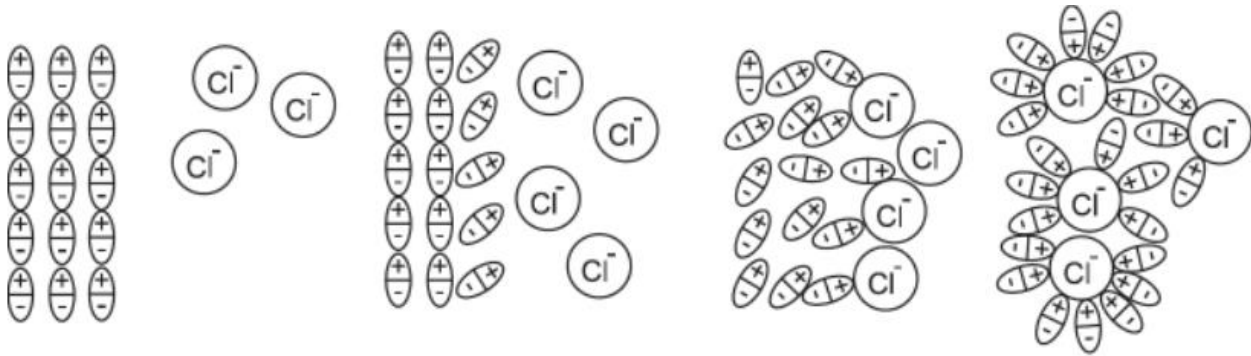


Figure 14. Scheme of solvation of ice due to the action of NaCl ions [301].

When a salt solution interacts with frozen sediment, salt ions migrate from an area of high salt concentration (brine) to an area of low concentration (films of unfrozen water around ice crystals) due to the so-called concentration diffusion. Salt ions cause the ice to melt, and the releasing fresh water lowers the concentration of salts in the solution. An increase in the content of unfrozen water in the contact zone leads to the appearance of density inhomogeneities and a more pronounced convective mass transfer in this area [302–304]. In the case when the amount of the solution becomes large enough compared to the amount of melting ice, the ice regime is considered to be quasi-steady. Ice melts until the salt concentration in the pore solution reaches the equilibrium concentration corresponding to the beginning of the solution freezing. The melting of pore ice is accompanied by a decrease in temperature until the new equilibrium of the ice-water-salt system is reached in porous media [305–307].

At the same time, the temperature effect depends on the composition of the salts. So, when exposed to NaCl ions, the process of ice melting is endothermic (with heat absorption), and in the case

of CaCl_2 , it is exothermic (with heat release). Therefore, the effect of sodium chloride on ice melting is slower than the effect of calcium chloride ions [301].

It should be noted that there is also the concept of the eutectic point for each salt solution. The lowest freezing point and the highest concentration of the solution (brine) corresponding to it is called the eutectic concentration at which solid matter crystallizes. If, as a result of lowering the temperature and increasing the concentration, the eutectic point is reached, then ice and salt crystals exist in the system, and not a liquid salt solution (Figure 15) [306].

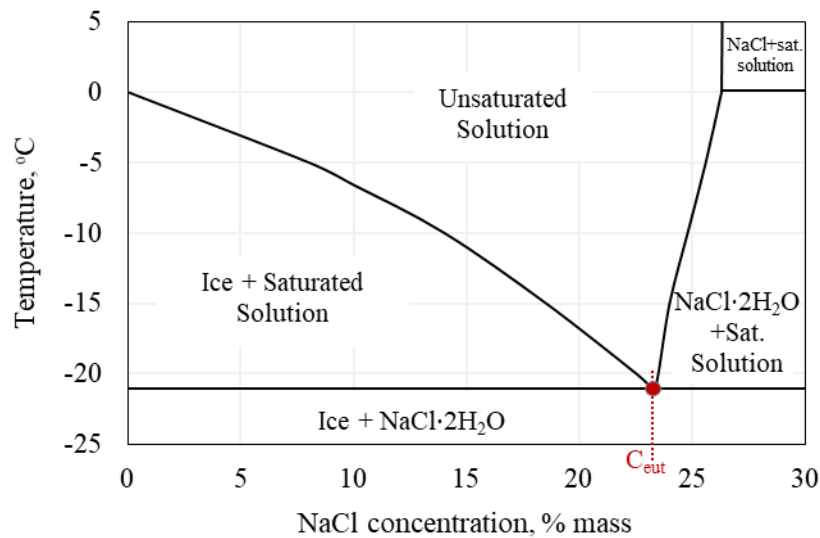


Figure 15. Phase diagram of NaCl aqueous solution (modified after [308]).

It is according to the patterns described above that cryopegs exist in permafrost. Cryopegs do not freeze, since the crystallization of salts dissolved in them requires deeper cooling, for example, to -21.4 °C for sodium chloride, or -55 °C for potassium chloride [103,305]. Such solutions are not in equilibrium with ice and can convert it into a liquid phase, eliminate the fluid resistance of frozen strata and migrate through cryogenic strata, including into horizons containing gas hydrates [41,49,51]. In this regard, special experimental and mathematical studies were carried out on the interaction of frozen sediments with salt solution.

2.3.1. Experimental research of salt migration processes in ice-containing sediments

Until a certain point in the development of geocryology, frozen sediments were considered to be an absolute seal. However, in the 1960s, based on field observations of the haloes of dispersion of chemical elements in frozen sediment in the north of Russia, it was concluded that the permafrost is an active environment where chemical and physicochemical processes take place: water migration, transport of chemical elements, structure and texture formation (ice release, swelling, cracking, etc.). Such field studies were carried out by Safronov N.I., Glazovskaya M.A., Targulyan V.O., Shvartsev S.L., Ivanov A.M., Ivanov O.P., Makarov V.N., Pitulko V.M., Chibisov N .P. Shilo N.A., Vinokurov I.P. and some other scientists. The researchers also noted the particular ecological danger of this phenomenon for an extremely sensitive complex multicomponent system of frozen sediment. In this regard, it became necessary to study and describe the mechanisms and patterns of salt ions migration in frozen sediment and to set up special experimental studies.

Separate experimental studies on the migration of chemical elements were carried out in the 1960-1980s, among which are the works of Murrman, Hoekstra, Nacano (1971), devoted to the study of the migration of sodium ions in frozen bentonite pastes; Nechaev, Kan (1980), Romanov V.P. (1985) on salt migration in frozen sands; Ostroumova V.E. (1989), on the salt migration in frozen sand and loam in a gradient temperature field; as well as in general the work on the study of the migration of ions of various elements by Tyutyunov (1951), Derbenev (1967), Savelyev (1971) and some other scientists. After the 80s, the process of interaction of frozen sediments with salt solutions was studied in sufficient detail thanks to the works of I.A. Tyutyunov, M.A. Derbeneva, V.E. Ostroumova, E.A. Nechaev, E.V. Kan, V.P. Romanov, E.D. Ershov, E.M. Chuvilin, Yu.P. Lebedenko, I.A. Komarov, J.M. Marrion, Xu Xiaozu, B. Hallet, V.N. Makarov, K.V. Biggar, Murrman, Hoekstra, Nacano and other scientists.

In the investigations of E.D. Ershov, E.M. Chuvilin, Yu.P. Lebedenko, N.A. Benediktova, O.G. Smirnova on the basis of an experimental study and previous works, a description of the mechanisms of ion migration in frozen sediment is given. The authors explain the course of such a process as follows. Before the contact, there are two systems - solution and frozen sediment, in each of which the chemical potentials of water are in equilibrium, but not equal to each other. The same should be said about concentrations. After the contact, the sediment and the solution begin to interact as a single system in which the state of equilibrium is disturbed. In connection with the desire of the new system to again achieve a state of equilibrium, a water potential gradient arises in it, causing a fluid flow into the frozen sediment, by direction matching with salt flow. Salt ions capture water in solvate films, i.e. reverse osmosis happens. Over time, the flow of solution into the frozen sediment significantly decreases [43,45,48,289,309].

The main media for ions migration in frozen sediment are films of unfrozen water that exist on the mineral particles surface, as well as between boundaries of pore ice crystals [106]. The thickness of the layer of the liquid phase of water decreases with decreasing temperature up to its complete disappearance at a temperature of about -45°C . Also, the content of the liquid phase is the greater, the higher the sediment dispersion (the size of sediment particles) [310]. So, in clay sediments, the content of unfrozen water can reach 13%, while in sand its content does not exceed 1%.

Depending on the structure of pore ice, gas inclusions, density, size of crystals, presence and composition of impurities, its ion permeability will be determined [48]. Air inclusions in ice (and, accordingly, less dense ice) contribute to a decrease in the flux of salt ions. The main flow of salts is carried out along the contact of ice crystals, respectively, in single-crystal ice, where the flow occurs along structural deformations, dislocations, the migration of ions is lower than with an increase in the number of crystals [99].

As driving forces of mass transfer in frozen sediments Ershov E.D. with co-authors pointed out the electrokinetic potential gradient (due to the difference in ion concentrations on the surface of the mineral particles, in the pore and in the external solution), adsorption forces (due to interaction with the particle surface), and electrostatic forces (due to the distribution of electric charge over the surface of negatively charged minerals and positively charged pore ice). A similar statement, but using a different term, was given in the work of Nechaev, Kan (1980) and Romanov V.P. (1985). They pointed out that the migration of salt ions is influenced by electrostatic properties. The authors attribute the migration of salt ions to the action of electrochemical processes in pore waters. As the driving force of water migration, the magnitude of the gradient of the total thermodynamic potential of ground water or the Gibbs free energy is taken. The thermodynamic potential is the sum of particular values [311,312].

$$\mu_w = \psi_{\text{KK}} + \psi_p + \psi_o + \psi_{es}$$

ψ_{KK} – frame-capillary thermodynamic potential;

ψ_p – hydrostatic thermodynamic potential;

ψ_o – osmotic thermodynamic potential;

ψ_{es} – electrostatic thermodynamic potential.

When the thermodynamic parameters change, the migration of water and chemical elements is possible, since the system comes into non-equilibrium both in terms of the chemical potential and in terms of the general thermodynamic potential. The authors also note that the osmotic potential decreases with increase in salt concentration in pore solution. When the salt concentration drops to a certain minimum value, water transfer in the system may stop due to the equality of the total thermodynamic potential of ground water to the osmotic potential of water in the external solution [311–313].

One of the most difficult questions to study was the question of the mechanisms of migration of salt ions in frozen sediments. Back in 1965, M.M. Derbeneva wrote that the transfer of salt ions occurs

due to moving films of unfrozen water and due to diffusion with an existing difference in concentrations, that is, the presence of a concentration gradient. Later, these two mechanisms were named by E.D. Ershov with co-authors in 1989 advective (convective) and concentration diffusion, respectively, and they also singled out a third mechanism of salt migration, adsorption [289,313].

Concentration diffusion is characteristic of the process of salt migration due to a concentration gradient at high negative temperatures, when the content of unfrozen water is relatively high. In this case, the migration of salt ions occurs along the films of unfrozen water from the region with the highest concentration to the region with a low concentration of salt ions [60,99].

Advective salt migration occurs at high flux densities of salt ions into the frozen sediment and is usually observed at high negative temperatures. At the same time, a feature of this mechanism is the joint water and salt transfer, that is, not only the migration of salt ions takes place, but there is a joint movement of water with salt ions. And due to this mechanism, there is an intensification of mass transfer, structure-forming and physico-chemical processes [60,99].

As the temperature decreases, the convective component of the total ion flux decreases, but rather high values of migration fluxes continue to be observed. This is no longer due to the action of the convective mechanism, but to the activation of other ion transport mechanisms, primarily adsorption [48,60,99,314].

The adsorption mechanism of salt transfer occurs in frozen sediments in the range of low negative temperatures (from -20 to -60 °C) due to the exploit of the ice surface forces. In this case, the thickness of unfrozen water films becomes equal to or close to the size of salt ions and migration almost completely stops [46].

Another important aspect of the interaction between salt solution and frozen sediments is the temperature changes that occur during this process. E.D. Ershov et al. (1993) studied the heat fluxes

arising from the interaction of frozen sediment with salt solutions, which made it possible to interpret the phenomena occurring in the process of migration. Thus, the authors argue that before the start of contact with the solution, a stationary temperature field was observed in the sample, i.e., the temperature in the sediment did not change, and the heat fluxes were constant and close to zero [45]. After the contact of the sediment and the salt solution, phase transitions begin, which, in turn, are associated with thermal effects. In case of thawing, heat is absorbed. However, when secondary ice formation happens (due to the release of fresh water during thawing) the heat flow is observed. Thus, in the interacting “sediment-salt solution” system there is a complex picture of heat flows [45].

As described earlier, the migration of salt ions in frozen sediments occurs due to the difference in chemical potentials. And it, in turn, is determined by the temperature gradient, humidity, dispersion and mineralogical composition of the sediment system [309]. Hence, separate studies are devoted to the influence of various factors (external and internal) on the process of salt migration in frozen sediments. Due to the works of Yu.P. Lebedenko (1989), E.M. Chuvilin (1999), E.D. Ershov et al. (1999, 1998) and others it was revealed that the ions migration is predominantly defined by the features of the frozen sediments: water content, mineral and chemical composition, dispersion, cryogenic structure, and also external parameters: salt solution concentration, interaction temperature, etc. [45,315,316]..

For instance, studies demonstrated, that total ions permeability and accumulation can increase with the rise in the ice and water content in the pore space of frozen sediments [46].

The study of the effect of temperature showed that with increasing temperature, the intensity of salt ion migration and accumulation increases [45,313]. Also, the salt flux in frozen sediment increases with the increase in the salt solution concentration. [99].

Ershov with co-authors (1999), when analyzing the migration of ions of various salts in frozen sediments, found that the activity of ions decreases in the series [313,316]:

$\text{Ca}^{+2} > \text{Na}^+ > \text{Hg}^{+2} > \text{Cu}^{+2} > \text{Pb}^{+2} > \text{K}^+ > \text{Fe}^{+2} > \text{Co}^{+3}$ (at the temperature -6°C).

However, depending on the granulometric composition, the dependence may change. So, for example, in clays, the mobility of Ca^{+2} is much lower, which is due to its adsorption characteristics, that is, the mobility of cations and anions is also determined by their adsorption capacity. Also interesting are the results of an experimental study on ice release depending on the composition of the contacting solution. So in the series KCl, NaCl, MgCl_2 , CaCl_2 , ice release increases [99].

With a decrease in size of sediment particles (decrease of grain fineness), the migration and accumulation of water and ions increases in the sand-clay series. This is explained by the fact that the ion permeability of frozen sediments decreases (that is, salts penetrate a shorter distance) with increasing fineness. At the same time more fine sediment has a greater exchange capacity (sorption), i.e. the ability of the mineral surface to bind salt ions, as a result of which their mobility decreases, and, consequently, the intensity of the salt migration flow decreases [48,316]. At the same time, in a series of clays, the greatest accumulation is observed in kaolinite clay, the smallest in montmorillonite (weak water and ionic conductivity due to the high sorption capacity of montmorillonite) [316].

The main role in coarse-grained sediment is played by concentration diffusion through pore ice, since there is no unfrozen water or its content is extremely low (up to 1%). With an increase in dispersion, the amount of unfrozen water increases, and along with diffusion, advection begins to play a role in the salt ions migration. However, as noted above, sorption is also observed, which reduces the ion permeability in fine-grained sediment [314].

Ershov E.D. with co-authors also showed different migration abilities of cations and anions using the example of the migration of sodium ions and chlorine ions. During the experiment, chloride ions migrate more from solution to frozen sediment than sodium ions, which is due to the greater migration ability of chloride ions [45].

Another study shows, that the increase of gas pressure causes the decrease of salt ions migration in sediments with low dispersion (mainly clay-containing sediments). Thus, in clays there is a certain critical pressure at which the migration of salt ions almost completely stops, since the convective component of the migration flow, which provides the highest values of salt transport, is suppressed. While in the sands such an effect is not observed [314].

2.3.2. Existing physico – chemical models of salt transfer processes in sediment media

To describe the migration processes in frozen sediments, several concepts of mass transfer, the concept of suction forces, the concept of crystallization forces, and the osmotic pressures concept have been proposed to explain experimental results. One of the most widely applicable is the approach based on effective transport equations. This model is established on the laws of energy conservation and mass of pore water, supplemented by water migration under the action of a water gradient, and/or a temperature gradient, and/or any other gradients. However, this model also has its own difficulties, mainly associated with the need for experimental data (obtaining diffusion coefficients), but also with the determination of boundary conditions on the phase transition surfaces. Therefore, this model was partially supplemented by G.G.Tsyarkin in 2009 [317].

In general, the salt migration in thawed sediment is defined by the processes of concentration diffusion. And it, in turn, is described by the Fick's first law, which was formulated back in 1855 and has the form of the following equation:

$$\Phi = -K \frac{\partial C}{\partial x}$$

where Φ – rate of salt ions diffusion; K – salt diffusion coefficient; C – concentration of dissolved components; x – distance of salt ions migration.

However, E.D.Ershov (1999) pointed out the imperfection of the calculation scheme for diffusion coefficients through Fick's law for frozen sediments, since the coefficient of proportionality between the total ion flux and the concentration gradient is calculated and there is no consideration of other mechanisms of salt transfer besides diffusion: advection and adsorption. To obtain the actual parameters of the migration of salt ions, it is necessary to take into account all the components in the total ion flux, and not just diffusion. Nevertheless, on the basis of this law, numerous schemes for calculating diffusion coefficients in thawed soils have been proposed [318,319], and several schemes in frozen and freezing sediments [49,50,320–322], however, no universal one has been singled out. Moreover, there is no such scheme for frozen hydrate-bearing sediments.

The second important part of the mathematical model for describing transport processes with phase transitions, which are undoubtedly observed during the interaction of salt solutions with frozen sediments, is based on the Stefan problem. The classical Stefan problem assumes that the phase transition is localized in a narrow region, modeled by a front, which is the weak discontinuity surface for the temperature function. The position of the phase transition front relative to the medium changes with time and is in the process of solving the problem [317].

The Stefan problem is based on the law of conservation of energy, and heat transfer in a stationary medium is described by the heat equation. In the one-dimensional case, the melting problem has the form:

$$\frac{\partial T_j}{\partial t} = a_j \frac{\partial^2 T_j}{\partial t^2} ,$$

where solid phase takes the area:

$$j = 1, \quad X(t) < x < \infty, \quad t > 0,$$

and liquid phase – area:

$$j = 2, \quad 0 < x < X(t), \quad t > 0$$

The initial and boundary conditions can be described in the following form:

$$X(0) = 0; \quad T_1(x, 0) = T_0 < T_f, \quad t > 0; \quad T_2(0, t) = T^o > T_f, \quad x > 0$$

The salt concentration in the pore solution C during the frozen sediments thawing changes in accordance with the dependence:

$$C = \frac{C_0 W}{W_{\text{unf}}}$$

where W – water content in the frozen sediment; W_{unf} – unfrozen water content in the frozen sediment; C_0 – initial salt concentration in the pore solution.

Salt diffusion coefficient is one of the main parameters of the salt ion migration process in frozen sediments, which depends on various factors. First of all, it is determined by the sediment dispersity, the geometry and relative position of the ice crystals and water films, and the parameters of the water films in the pore space of sediments.

One of the main parameters of the salt migration in frozen sediments is the diffusion coefficient of salt ions, which depends on many parameters, described in chapter 2.3.1. One of the schemes for calculating the diffusion coefficient, which based on the following formula [323]:

$$D = W \cdot D_0$$

where D_0 – diffusion coefficient of salt in free water; for sodium chloride (NaCl) D_0 is approximately $1.1 \cdot 10^{-5}$ – $1.4 \cdot 10^{-5}$ cm^2/c .

Another design scheme was proposed by Ershov E.D., Komarov I.A., Chuvilin E.M. in 1997 [49].

The salt transfer model is presented with the following assumptions:

- convective-diffusion mass transfer of salt ions occurs under isothermal conditions;
- there is no interaction of salt ions with pore solutions with the release (absorption) of heat;
- ion migration occurs in a semi-infinite array evenly along the height of the well;
- one-dimensional process;
- taking into account the pore space characteristics, the fracturing of the host sediments is carried out using the effective porosity parameter n_e , and the sediment horizon is considered as quasi-homogeneous;
- the concentration of salts in the operating brine is taken constant;
- the influence of pressure and the processes of mechanical interaction of brines with the sediment is not taken into account.

The problem of salt transfer is solved in a self-similar approximation, and the problem of mass transfer in a quasi-homogeneous massif and its solution have the form [49]:

$$D \frac{\partial^2 C}{\partial x^2} - v \frac{\partial C}{\partial x} = n_e \frac{\partial C}{\partial \tau}$$

$$C(\infty, \tau) = C(x, 0) = C_f$$

$$C(\infty, \tau) = C_s$$

where C – current salt concentration; D – diffusion coefficient; n_e – porosity; x – current coordinate; v – average volumetric velocity of the filter flow, determined through the flow rate; C_s – ions concentration; C_f – initial concentration of that ions in pore solution of the sediment.

$$\bar{C} = \frac{C - C_\varphi}{C_p - C_\varphi} = 0.5 \left[\operatorname{erfc} \theta + \exp(P_e) \operatorname{erfc}(\theta^2 + P_e)^{\frac{1}{2}} \right]$$

where

$$\theta = \frac{n_e x - v \tau}{2(n D \tau)^{\frac{1}{2}}}, \quad P_e = \frac{v x}{D} - \text{Peclet criterion } \operatorname{erfc}(\cdot) =$$

1 – $\operatorname{erf}(\cdot)$, $\operatorname{erf}(\cdot)$ – Gaussian error function.

The diffusion coefficients of chlorides in frozen sediment obtained using this calculation scheme were $10^{-6} - 10^{-7} \text{ cm}^2/\text{h}$ [49]. While in thawed sediment the diffusion coefficient varies from 10^{-6} to $10^{-10} \text{ cm}^2/\text{sec}$, and in ice, the diffusion coefficient can range from 10^{-7} from $10^{-9} \text{ cm}^2/\text{sec}$ [314].

Recent studies have also considered the migration of sea water on the Arctic shelf and the influence of this process on the evolution of permafrost zone and HSZ.

The authors compared the displacement of the depth of the gas hydrate stability zone with an increase in seawater salinity, and also compared two calculation schemes. Thus, the shift in equilibrium temperature is calculated using the expression [57]:

$$T_D = \frac{T_{D,ref} \cdot \log(1 - x_s)}{\log(1 - x_{s,ref})}$$

$$T_D = T_{D,ref} \cdot \log(1 - x_s) / \log(1 - x_{s,ref})$$

where $T_{D,ref}$ – temperature reference value for hydrate decomposition at the corresponding reference salt content value $x_{s,ref}$ and x_s – mole fraction of salt in pore water.

In the work [185] a method is proposed for predicting the shift in the equilibrium temperature of a hydrate in a free volume based on information on a decrease in the freezing point of aqueous solutions containing various salt concentrations in relation to the freezing point of fresh water (ΔT_F):

$$T_D = 0.6825 \cdot \Delta T_F$$

In the calculations, the authors also used the dependence of the freezing point of water ($^{\circ}\text{C}$) on the salt concentration S (‰) and pressure in bottom sediment P (MPa) is presented in the work [185,324]:

$$T_F = -0.073P - 0.064S$$

Salt diffusion coefficient was taken equal to $10^{-9} \text{ m}^2/\text{sec}$ in accordance with estimates based on drilling data in the Laptev Sea [57,325].

Based on the modeling results, the authors [57,325] argue that an increase in salinity causes degradation of the gas hydrate stability zone and leads to a displacement of the boundary down the section. However, the authors note that due to the great depth of hydrate occurrence on the Arctic shelf, the influence of salts can be not so sufficient. It should be noted that these calculations do not take into account the presence of metastable gas hydrates, which can be affected by salts and which, as noted in Chapter 2.2, are especially sensitive to changes in external conditions, the authors also point out this fact, but without taking it into account in the calculations. In addition, the diffusion parameters of salt ions are not calculated, but are given according to previous calculations, which means that the power of the ion flow and the time factor are not taken into account.

Another study is dedicated to the hydrate decomposition as a result of the migration of salt drilling fluid into hydrate-bearing sediments (in the thawed state) [326]. According to the proposed calculation scheme, the phase equilibrium pressure and phase equilibrium temperature for hydrate-bearing sediments satisfy the exponential function:

$$P_{eq} = e^{AT_{eq}+B}$$

where:

$$A = 0.5212w^2 - 0.0609w + 0.1109$$

$$B = -119.76w^2 + 18.638w - 29.306$$

where w mass fraction of salt.

The authors assume that drilling fluids consisting of sea water and may be comparable to a sodium chloride solution with a mass fraction of 0.03.

Rate of hydrate dissociation connected with hydrate equilibrium pressure in the reservoirs:

$$\frac{dc_H}{dt} = k_d^0 \cdot e^{-\frac{E}{RT}} \cdot A_{hS} \cdot (P_{eq} - P_g) = k_d^0 \cdot e^{-\frac{E}{RT}} \cdot \sqrt{\frac{\varepsilon^3 (S_l + S_g)^3}{2k}} \cdot (P_{eq} - P_g)$$

The porous medium conservation equations describe changes in mass and temperature per unit volume of the formation. Takes into account the porosity and properties of the porous medium:

$$\text{Gas phase} \quad \frac{\partial}{\partial t} (\rho_g S_g \varepsilon) + \nabla \cdot (\rho_g \vec{v}_g) = -x_g \frac{dc_H}{dt}$$

$$\text{Liquid phase} \quad \frac{\partial}{\partial t} (\rho_l S_l \varepsilon) + \nabla \cdot (\rho_l \vec{v}_l) = -x_l \frac{dc_H}{dt}$$

$$\text{Hydrate phase} \quad \frac{\partial}{\partial t} (\rho_H S_H \varepsilon) = \frac{dc_H}{dt}$$

$$\text{Energy} \quad \rho_{eff} c_{eff} \frac{\partial T}{\partial t} + \nabla \cdot (\rho_g \vec{v}_g c_{pg} \Delta T + \rho_l \vec{v}_l c_{pl} \Delta T) = \nabla \cdot (k_{eff} \nabla T) + \dot{q}$$

$$\text{Salts} \quad \frac{\partial}{\partial t} (\rho_S S_S \varepsilon w) + \nabla \cdot (\rho_S \vec{v}_S) = 0$$

Methane is characterized by changing density and follows the equation of state for an ideal gas.

$\nabla \cdot (\rho_g \vec{v}_g c_{pg} \Delta T + \rho_l \vec{v}_l c_{pl} \Delta T)$ - advective energy transfer initiated by gas migration.

Salt migration can be described by the equation:

$$\vec{v}_S = w \vec{v}_l - D_S \nabla w$$

Cohesion determines the hydrate-bearing sediment strength and it is related to hydrate content.

$$C = C_0 (1 + \psi (S_H - S_0))$$

This calculation scheme was proposed with the following assumptions [326]:

- The model is limited to 1 m from the wellbore;
- 2D model;
- External boundary conditions are the initial reservoir parameters;
- Internal boundary conditions are downhole pressure and temperature.

Based on this model, the authors calculated the depth of dissociation of gas hydrate formations from the well during the penetration of salt solution for 1 m in radius [326].

In general, today there are practically no works on experimental modeling of the interaction of salt and drilling fluids with frozen hydrate-bearing sediments, just as there are no attempts to describe the process of such interaction and obtain diffusion characteristics, including through mathematical modeling. In this regard, setting up experimental modeling to study the mechanism and patterns of hydrate dissociation during interaction of frozen sediments and salt solution is of particular interest to ensure the safe and uninterrupted construction of exploration and production wells in the area of permafrost.

Conclusion to the Chapter 2.

Thus, based on literature review, it can be concluded that today there is a lot of information about the processes of mass transfer in frozen sediments during their interaction with salt solutions, which creates good prerequisites for setting up special experimental studies to study the behavior of frozen hydrate-bearing sediments under saline conditions. The specificity of permafrost sediments: the presence of driving forces of water migration. At high negative temperatures, the migration flow of water has a significant effect on ions migration in finely dispersed sediments, which is typical for ions of light elements.

Chapter 3. Method of experimental study of salt ions migration in hydrate-bearing sediments

A series of experiments were conducted in order to study the mechanisms and dependences of methane hydrate dissociation in porous media of frozen sediments during their interaction with salt solutions at the range of negative temperatures (-3 ... -20 °C) in equilibrium (at the pressure >2 MPa) and non-equilibrium (at a pressure from atmospheric - 0.1 MPa to 2 MPa) conditions. The experimental procedure is following:

1. Formation of the laboratory synthesized hydrate bearing specimens;
2. Determination of the initial parameters;
3. Bringing frozen samples, containing methane hydrates, and salt solution into the contact;
4. Assessment of the main characteristics change (changes in water, hydrate content and salt ions concentration) during the interaction between salt solution and hydrate-bearing frozen sediments, and determination of the main interaction parameters.

3.1. Experimental setup and preparation technology of hydrate-bearing sediments

The technique for forming frozen hydrate-bearing media included preparation of sediment samples with given water content, locating samples in the pressure cell, hermetic closure of the pressure cell and the creation of a vacuum, increase of the pressure up to the hydrate equilibrium values by the methane injection of CH₄ [327,328].

The sediments are filled with hydrates using a special technique that allows samples of hydrates evenly distributed in the porous medium of the sediments to be obtained. The initial hydrate saturation of the sediment sample was carried out at a negative temperature of -4...-6°C. In order to increase the hydrate saturation of the sample, a heating-cooling cycle was made with the transition through 0°C. When the gas pressure is higher than the equilibrium pressure, the thawing and freezing of the pore water of the sediment sample leads to the activation of the hydrate formation process and the increase of the overall hydrate saturation. The formation of gas hydrates happens on the pore ice surface, which inhibits the water transfer process and makes the hydrates evenly distributed in the sediment samples [328].

A special pressure cell used for artificial hydrate saturation of sediment media is shown on the Figure 16. Pressure cell volume is 419 cm³ and it was designed for pressures up to 20 MPa.



Figure 16. Equipment (pressure cell) for artificial formation of hydrate in sediment samples.

Initially, sediment used for experimental modeling was filled by the set water content (around 11-12%). Then wet sediment was placed in special perforated plastic containers of cylindrical shape, which height equals to 6-9 cm and diameter - 3 cm. Sediment samples in these plastic containers were then frozen for 1 day at temperatures of -6 ... -8 ° C to limit any potential migration of water, which can lead to the non-uniformed distribution of pore hydrate. No migration of water happen in the sediment due to the fast freezing of them at the temperatures below zero.

Frozen sediments samples in plastic containers were then placed in the pressure cell. The pressure cell was able to fit from 5 to 7 perforated plastic containers with the studied frozen sediment. A steel cover was hermetically fastened to the body of the cell through a teflon gasket with studs, on which a pressure gauge with a division value of 0.05 MPa was used. After the pressure cell was sealed and depressurized, and cooled hydrate-forming gas (methane, volume fraction 99.98%, t=-6...-8°C) was

supplied into the system up to the pressure above equilibrium (4-5 MPa). Then, the pressure cell with samples of frozen sediments is placed in a freezer. First, a cooling cycle ($t = -10\text{ }^{\circ}\text{C}$) is set, lasting about 3-5 days, then a defrosting cycle ($t = 0 \dots +1\text{ }^{\circ}\text{C}$), lasting about 1-2 days. Such a change of cycles is carried out 3-4 times. By transmission of the sediment samples through negative temperature by cycles the bigger amount of the residual ice, which was not transferred in the hydrate form before, was transited to form hydrate afterward. Due to that, sufficient saturation with methane hydrate of the sediment porous media is achieved (up to 60%). Thus, the saturation of the studied frozen sediment samples with hydrate occurs within 2 weeks to a month.

After the hydrate saturation, hydrate-containing samples were cooled to the temperature $-6 \pm 1\text{ }^{\circ}\text{C}$ in the pressure cell. Meanwhile, the residual pore water, which did not transform into hydrate, freezes. This approach makes it possible to obtain sediment samples with a high degree of filling of sediment pore media with hydrates up to 60% or more (calculation of the hydrate saturation and other experiment's characteristics is shown in the section 3.6) [23].

Then, gas pressure was reduced from stable (around 3-4 MPa) to the atmospheric (0.1 MPa) in the pressure cell at the negative temperature ($-6 \pm 1\text{ }^{\circ}\text{C}$). Subsequently, frozen hydrate-bearing samples for testing at the atmospheric conditions were kept in a non-equilibrium state for about a day to stabilize the self-preservation process. Then, specimens were removed from the pressure cell at $-6\text{ }^{\circ}\text{C}$. Due to self-preservation effect at negative temperatures, the porous hydrate formations in a frozen state at a temperature of $-6 \pm 1\text{ }^{\circ}\text{C}$ had good preservation for a long time, during all time of the experiment (1-2 days and longer with decrease in initial hydrate coefficient not more than 0.1-0.2), what was tested on the several hydrate-bearing frozen samples without contact with salt solution by their interval analysis for hydrate coefficient in time.

Before the contact with salt solution, small probe of hydrate-bearing sediment was taken from each sample for gas content evaluation and water content. Several characteristics for frozen hydrate-containing samples, including gravimetric water content (W , %), density (ρ , g/cm^3), porosity (n , %) and hydrate coefficient (K_h , u.f.) were obtained. Detailed description of the parameters calculation is given in Chapter 3.6.

The appearance of frozen hydrate-bearing sediments before the experiment is shown in Figure 17. Subsequently, artificially formed hydrate samples were used in experiments on interaction with salt solutions.

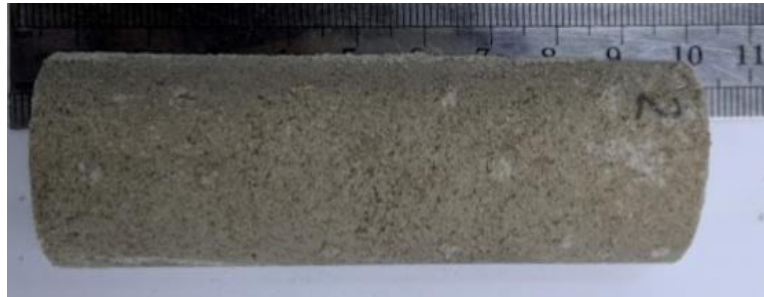


Figure 17. The appearance of frozen sand filled with pore hydrate after extraction from the pressure cell.

All obtained samples had similar characteristics ($W=11-12\%$, $n=35-40\%$, $K_h=0.4-0.6\%$) and were used in the experiment as “twin” samples. Figure 18 shows an example of the distribution of water content, porosity, and amount of water in the hydrate form (hydrate coefficient) by intervals of obtained frozen hydrate-bearing sediment samples. Water content by the length of the samples varies with a difference of around 1-2%, porosity – around 2-5%, and hydrate coefficient 0.05-0.07.

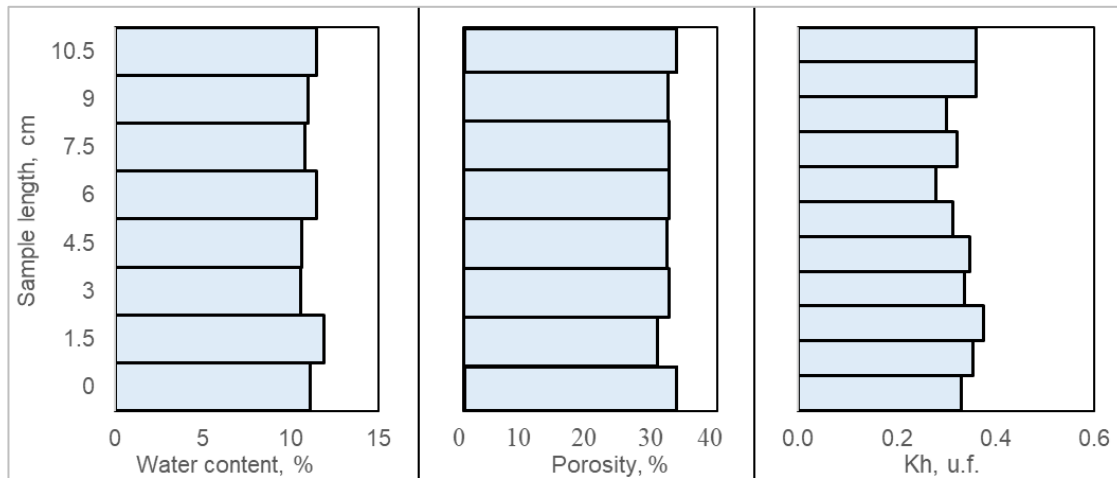


Figure 18. Distribution of water content, porosity, and hydrate coefficient by the length of frozen hydrate-bearing sediment samples.

After measuring the initial parameters, the hydrate-bearing frozen samples were brought into contact with the test saline solution at the end face under different thermobaric conditions.

3.2. Sediment characteristics used in experimental simulation

For the experimental modeling, both model sediments (clean quartz sand and sand with the addition of clay particles of kaolinite or montmorillonite) and natural sediments are taken in the areas of gas manifestations. Parameters of gas emission here indirectly demonstrates their possible connection with natural porous hydrate [115,239]. Sediment characteristics are shown in Table 4.

Table 4. Particle size distribution, mineral composition, and salinity of investigated sediments.

Sample	Place of Sampling	Size of Sediment Particles (mm), %						Mineralogy	Salinity, %
		1 - 0.5	0.5 - 0.25	0.25 - 0.1	0.1 - 0.05	0.05 - 0.001	< 0.001		
Fine sand 1	Moscow region	6	7	80	2	3	2	>98% quartz	0.01
Fine sand 2	Moscow region	0	2	80	17	1	0	>98% quartz	0.01

Medium sand	Moscow region	0	63	25	11	1	0	>98% quartz	0.01
Fine sand 3	South Tambey gas field	0	12	63	22	2	1	>98% quartz	0.11
Sandy loam	Laptev Sea, Buor-Khaya	1	9	52	20	16	2	54% quartz 41% microcline + albite 4% illite	0.4

*The listed mineral phases have percentages > 1%

The determination of the mineral composition was carried out using an X-ray diffractometer (XRD) in the laboratory of sediment science and technical sediment reclamation of the Department of Engineering and Ecological Geology, Faculty of Geology, Lomonosov Moscow State University. The particle size distribution was obtained by the sieve method. While composition and content of water-soluble salts was defined by the method of water extracts on the flame photometer PFP-7 (Jenway) [329,330].

The physical characteristics of the samples were determined according to GOST 5180-84 [331].

Fine sand-1, fine sand-2 and medium sand are represented by homogeneous quartz sand (quartz > 98%) of marine upper Jurassic genesis mJ₃ with the predominance of 0.1-0.2 mm fraction (fine sand-1 and fine sand-2 around 80%), and 0.2-0.5 mm (medium sand 63%). Fine sands have light yellow color, homogeneous, well sorted, non-saline (salinity is 0.01%). The specific active surface is 0.6 g/m². The density of the solid component is 2.65 g/cm³.

In addition, two sediments were obtained during drilling in permafrost area, where by indirect signs hydrate formation may exist, and they represented by:

- Fine sand 4 is a marine deposit from the upper Pleistocene (mQ_{III}²⁻³). The sampling site is a permafrost zone close to the South Tambey gas condensate field at a the depth of 32 - 35 m. Sand is light grey, well-sorted, homogeneous in grains, and composed of quartz

(>98%). Characterized by predominance of 0.1-0.2 mm (63%), and also 0.1-0.05 mm (22%) fraction. The density of the solid component is 2.68 g/cm³. Salinity is 0.11% presented mainly by sodium chloride composition.

- Sandy loam, a polymineral of alluvial genesis from the Neopleistocene (aQ_{II}). It was extracted during drilling of the permafrost zone of the Arctic shelf in the western part of the Buor-Khaya Bay (Laptev Sea), 17 km northeast of the island Muostakh, where parameters of gas emission indirectly demonstrates their possible connection with natural hydrate existence [30,115,267,332,333]. The depth of sediment sampling is 43-45 m. The sandy loam is light gray, and rounded, with the predominance of 0.1-0.2 mm fraction (52%), and 0.1-0.001 (36%). The mineral composition is dominated by quartz – 54%, microcline+albite – 41%, and illite – 4%. The density of the solid component is 2.64 g/cm³. Salinity is 0.4% represented mainly by sodium chloride composition.

Salinity in natural sediments was decreased to 0.1-0.05% by removing salts through washing with distilled water several times.

In addition to the described sediments, special model mixtures were prepared from fine sand-2 and clay. As clay contaminants, kaolinite and montmorillonite were taken in different percentages (up to 15%):

- Montmorillonite clay (eP_{2ogl}) was sampled near the Dzembel train station, in Turkmenistan. It is presented with montmorillonite (94%), andesite (3%) and biotite (3%).
- Kaolinite clay (eP₂) was taken at the town Novokaolinoviy in the Chelyabinsk region. It is presented by kaolinite (92%), quartz (6%), and muscovite (2%).

Described above sediments of disturbed composition were used to form frozen hydrate-bearing sediment samples for the experimental modeling.

3.3. Technique for studying the interaction of frozen hydrate-containing sediments with saline solutions in non-equilibrium and equilibrium conditions

The study of salt migration processes in frozen hydrate-containing sediment was based on the experimental modeling of the interaction between salt solution and frozen hydrate-bearing sediment samples at the fixed temperature below zero and various pressures. The procedure as following:

1) preparation of frozen sediment sample with a given water content (12%) and saturation with methane hydrates in a special pressure cell;

2) hydrate-bearing samples are frozen in a pressure cell and transferred to a metastable state by reducing the pressure to atmospheric pressure at a negative temperature freezing hydrate-bearing samples in a pressure cell and transferring them to the metastable state by reducing the pressure to atmospheric at a negative temperature;

3) frozen samples, containing hydrate, was extracted from the pressure cell, measuring the initial parameters (initial water content, density, initial hydrate coefficient K_h^{in}), and bringing them into the contact with a frozen NaCl solution in the state of salted ice at a constant negative temperature and various pressure conditions (below (<2 MPa) or above (>2 MPa) equilibrium);

4) monitoring the process of interaction between salt ice and frozen hydrate-containing samples in time.

The technique for obtaining frozen hydrate-containing media is described in chapter 3.1. As a result of artificial hydrate dissociation of frozen sediments, 5 to 7 of twin identical samples were obtained with unified water content, porosity, and hydrate distribution.

Afterwards, the gas pressure drops to 0.1 MPa at temperature -6 °C, transferring the frozen hydrate-bearing sediment samples into metastable conditions. Then initial characteristics were determined (water content (W, %), density (ρ , g/cm³), porosity (n, %) and hydrate coefficient (K_h^{in} ,

u.f.)) and samples were brought into the contact with salt solution. Before and after the experiment on the interaction of hydrate-bearing sediment with a saline solution, a sample was photographed.

Experiments on the study of salt transfer in frozen sandy sediments containing porous gas hydrates were carried out at a temperature from -2.5 to -20 °C and pressures from atmospheric to 4 MPa. The contacting solution was a NaCl with a concentration from 0.1 to 0.4N (0.2-2.5%), and also with KCl, Na₂SO₄, CaCl₂, MgCl₂ solution with a concentration of 0.1 N. Usually, around 5-7 samples were brought into the contact at the same time for comparison. Part of samples were used as a repeat of one experiment (at least 3 repeating tests per experiment with the same conditions), other for determination of different factor effect (for example, different pressure when other characteristics are the same). Contact of the hydrate-bearing frozen sample with the salt solution was made in a sealed container to prevent sublimation processes, and the entire setup was placed in a thermal box to maintain a constant negative temperature (Figure 19). During all experimental modeling under atmospheric pressure, the negative temperature was fixed (from -2.5 to -20°C).

When studying the processes of salt transfer in frozen hydrate-bearing sediment under gas pressure, hydrate – bearing frozen samples, after being brought into contact with salt ice, were again placed in a pressure cell. Then the gas pressure of methane increased to values below (from 0.1 to 2.5 MPa) or above equilibrium (from 2.5 to 4 MPa) for a given temperature condition (-4 or -6 °C). Then the installation was also placed in a thermal box (Figure 19).

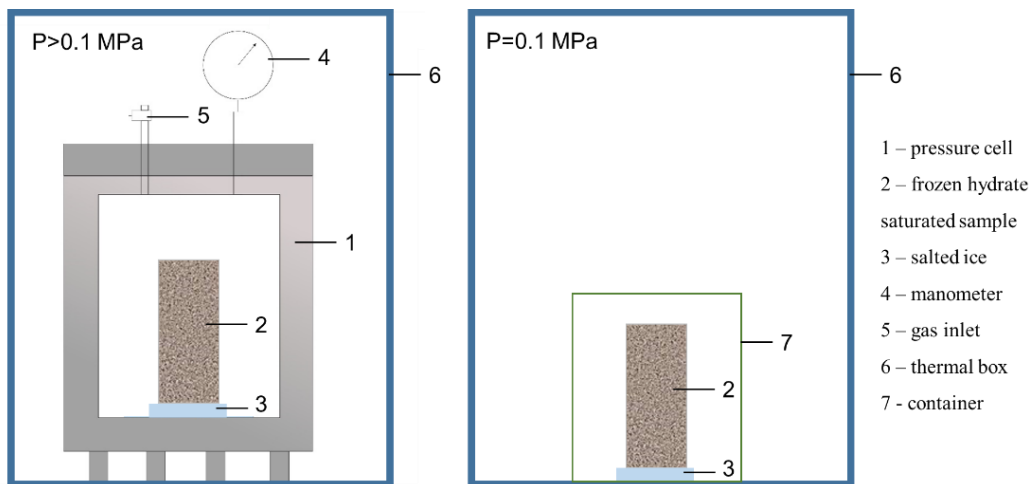


Figure 19. Scheme of the installation for the interaction of frozen hydrate-bearing and non-hydrate-bearing sediments with salt solutions under pressure.

For comparison, experiments were also carried out with frozen samples that did not contain methane hydrates. In experiments with frozen non-hydrate samples under gas pressure, nitrogen was used to prevent hydrate formation processes.

At certain intervals of time from the start of the interaction, one of the hydrate-bearing samples was removed from the contact with salt solution at certain intervals of time from the start of the interaction. In experiments under pressure > 0.1 MPa, for this, the gas pressure was first released in the pressure chamber, after which it was opened, while under the atmospheric conditions this additional step was not required. For each sample, the number of parameters was determined that characterize the content of salts, water content, and gas hydrate (through the hydrate coefficient) along the length separately in 5-8-mm-thick layers of each sample (6-9 cm height). Two probes of sediment were taken from each interval of the sample: for water/salt content and hydrate content (with 2 repetitions). In parallel with frozen hydrate-containing samples, frozen non-hydrate-bearing samples were taken from

the contact with salt solutions under the same experimental conditions, and their interval analysis was made for water and salt content.

Such interval analyses of the samples allows to follow the dynamics of salinization, dissociation of pore gas hydrates, and thawing in frozen sediment samples under various thermobaric conditions, and to study different factors that influence the salt transfer process.

Gas content was assessed (with 2-3 times duplicating) by thawing of sediment probes (weight around 1-2 g) in sodium chloride solution. As a result, the released gas displaces a certain volume of water. A graduated and pre-calibrated glass tube was used to measure changes in water volumes. The glass tube was placed in a vessel filled with warm water. This tube was filled with water using a rubber bulb, after which the valve was closed and the initial level was recorded in the log. Then a probe of the studied hydrate containing sediment was placed under the expanded part of the tube, and the water level change in the tube was registered. For estimation of hydrate content through hydrate coefficient gained gas content values were used [328,334,335]. Detailed description of the calculation is given in the Chapter 3.6.

Also in experiments the thaw front in the samples was fixed by the characteristic color change of the sample (Figure 29), as well as additionally checked by the special probe-needle. For this, after the experiment a frozen hydrate-bearing sample was pierced with a needle. In the place where the sample was thawed, the needle easily entered the sample, since the ice cementing the sediment particles transferred into a liquid state. And where the sample remained frozen, the needle did not enter the sample at all.

Experimental modeling was aimed to study of dynamics of salt migration in frozen hydrate bearing sediments (Chapter 4), and the influence of different factors on that process:

- 1) thermobaric conditions – temperature from -2.5 to -20 °C (Chapter 5.2), pressure from 0.1 to 4 MPa (Chapter 5.1);
- 2) the concentration of the salt solution – from 0.1 to 0.4 N (Chapter 5.3);
- 3) composition of the contact solution – NaCl, KCl, MgCl₂, Na₂SO₄, CaCl₂ (Chapter 5.4);
- 4) sediment composition – model fine sand of 0.1-0.2 mm fraction, model fine sand 0.2-0.5 mm fraction, natural fine sand from South Tambey gas-condensate field, and natural sandy loam from the Arctic shelf, Buor-Khaya (Chapter 5.5).

The list of all experiments are given in the Appendix 1.

3.4. Method of the temperature field change investigation during the contact of frozen hydrate-bearing sediment with salt solution

Method of study of the temperature field change during interaction of frozen hydrate-bearing sediments with salt solution consists of the following steps:

- 1) preparation of the sand sediments with defined water saturation in a special plastic container and freezing it;
- 2) artificial hydrate saturation of frozen sediments in the pressure cell under high pressure and negative temperatures (-4...-6±1 °C);
- 3) the pressure drop in the pressure cell, extraction of the hydrate-bearing frozen sediment samples at negative temperature, and atmospheric pressure;
- 4) measuring initial parameters of the frozen hydrate - bearing samples;
- 5) inserting the temperature sensor into hydrate-bearing sand samples and bringing the samples into contact with the salt solution.

Experimental modeling of the temperature field change during interaction of frozen hydrate bearing sediments with a salt solution at the atmospheric pressure and negative temperature (-6.5°C) was made using special temperature registration Kriolab Tbf system designed at the KrioLab LTD (Russia) equipped with the respective built-in software (Figure 20). It consists of a special thermal box for maintaining negative temperatures, thermal sensors (8 pieces, d=2.5 mm), and an automatic recording system, making temperature records with defined time intervals. In the frame of this work time interval of 10 seconds was chosen for a more precise register of the fast temperature drop during hydrate-bearing sediments interaction with the salt solution. The temperature sensors were calibrated to a precision of ± 0.05 °C alongside a special reference sensor in a liquid thermostat. The temperature in the freezing cell was programmed to a certain value (-6.5 °C) and maintained during whole experiment. Finally, the sensor through the thermistor streamer and multiplexer module was connected to the PC, and the software was set up for continuous acquisition. The measurements in a temperature field change were made whilst the frozen hydrate-bearing sediments interacted with the salt solution. The measurements of the temperature were finished when the recorded sample temperature returned to its initial value and remained stabilized at that value.

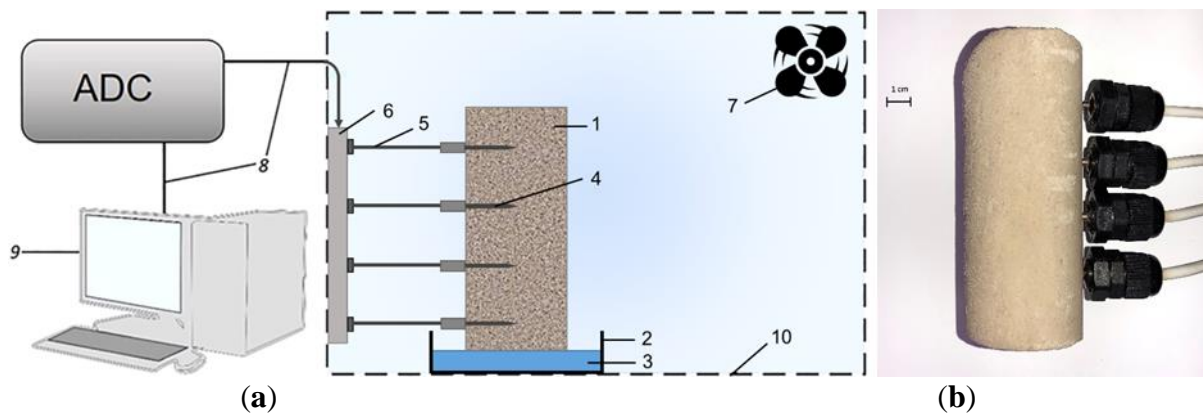


Figure 20. Scheme of Kriolab Tbf system for temperature field change investigation (a) and picture of the frozen hydrate-bearing sand sample with temperature sensors (b). 1 - frozen hydrate-bearing sediment; 2 -

solution container; 3 - frozen NaCl solution; 4 - temperature sensors; 5 - thermistor streamer; 6 - multiplexer module; 7 - fan; 8 - USB cable; 9 - PC with Kriolab Tbf software; 10 - cooling chamber. Modified after [310].

Model fine sand-2 was used for this investigation as an object of research. The studied sediment was filled with distilled water up to 12%, then placed in special plastic perforated tubes of 5 cm diameter and around 8 cm length, and frozen. After, frozen samples were artificially hydrate-saturated by the method described in the Chapter 3.1. Then, 4 holes of 2.5mm diameter were drilled in each sample, up to a depth of 3cm in the direction of the center. The distance between temperature sensors is around 1.5 cm. Thus, sensors are located from the contact zone up to the top of the sample deep in the frozen hydrate-bearing sediment, and register the temperature of the sample whilst the hydrate is dissociating as a result of salt migration.

After placing the sensors, frozen hydrate-bearing sand samples were brought into contact with frozen NaCl salt solution of different concentration (from 0.1 to 1 N) at atmospheric pressure and a fixed negative temperature (-6.5°C).

The specimen temperature was recorded from the beginning of the experiment on the interaction of a frozen sample with a salt solution to the stabilization of temperature conditions in the sample. The average duration of the experiment was about 5-9 hours depending on solution concentration. The further procedure of the experiment is similar to the algorithm described in chapter 3.3.

To compare the results against a baseline, a sample made of non-hydrate-bearing sediment sand was investigated under the same conditions and in the same way ($P=0.1\text{MPa}$, $t=-6.5^\circ\text{C}$, $C_{\text{sol}}=0.1\text{N}$).

In addition to the study of the dynamic of the temperature field change in frozen hydrate-bearing and frozen non-hydrate-bearing sediment as a result of salt migration, different contact solution concentration was tested (from 0.1 to 1 N).

3.5. Method for assessing the salt content in sediment samples

Over the course of the experimental modelling, samples of saline sand were obtained after the interaction of frozen hydrate-bearing sediment with saline solutions. It was necessary to check the salt content to assess dependences of salt migration in frozen hydrate-bearing sediments. Nowadays, there is a problem of a rather high cost of chemical analysis of sediment samples for the content of ions of water-soluble salts, among which one of the most applicable are atomic adsorption and flame photometric methods. In addition, these methods use aqueous extracts of salts, which requires long-term sample preparation, and dilution of concentrations is used, which can lead to inaccurate results and additional errors. In this regard, within the framework of this work, a new method was proposed for determining the concentration of salts in a certain range of water and concentrations through the activity of pore water.

Thus, the measurement of the content of Na^+ cations in the course of experiments during the interaction of frozen hydrate-containing sand with NaCl salt solution was carried out by the method of water extracts using a flame photometer, a conductometer, as well as by a specially developed method for determining the concentration of salts through the activity of pore water (potentiometric method).

The samples on which water content was determined were subsequently (before drying, right after the experiment) used for the interval determination of the salt ions content that migrated from the contact saline solution.

One way the analysis of ion concentration was carried out was using the method of water extraction of water-soluble salts using a MARK 603 conductometer. For that, dry probe of sediment (weight around 2-3 g) was placed in cellulose filter (“Blue ribbon”), and distilled water in the proportion of 1:5 to the weight of the probe was filtered through it. Concentration was measured in the obtained salt water extraction by sensor of the conductometer. The measurement error of the conductometer was

checked on standard solutions of NaCl salts in the water concentration range from 0.02% to 15%, which corresponds to the range of NaCl concentration in the studied water extracts. The accuracy of determining the concentration of Na⁺ ions using a conductometer in the samples under study was 0.1 ± 0.05 mg-EQ/100 g (measuring range 0.1 – 70 mg-EQ/100 g).

Another method, a newly proposed one, was based on the measurement of the water potential (activity). Pore water activity is the ratio of the vapor pressure of water over a given material to the vapor pressure of pure water at the same temperature. Measurements of water activity were conducted with special equipment WP4C by the “Decagon” (“Metro group”) production. Detection of the water potential is based on the chilled mirror method, when mirror in the chamber is cooled down until dew just starts to form on it [310].

First of all, it was found that the water content in a certain range does not affect the activity of pore water (Figure 21).

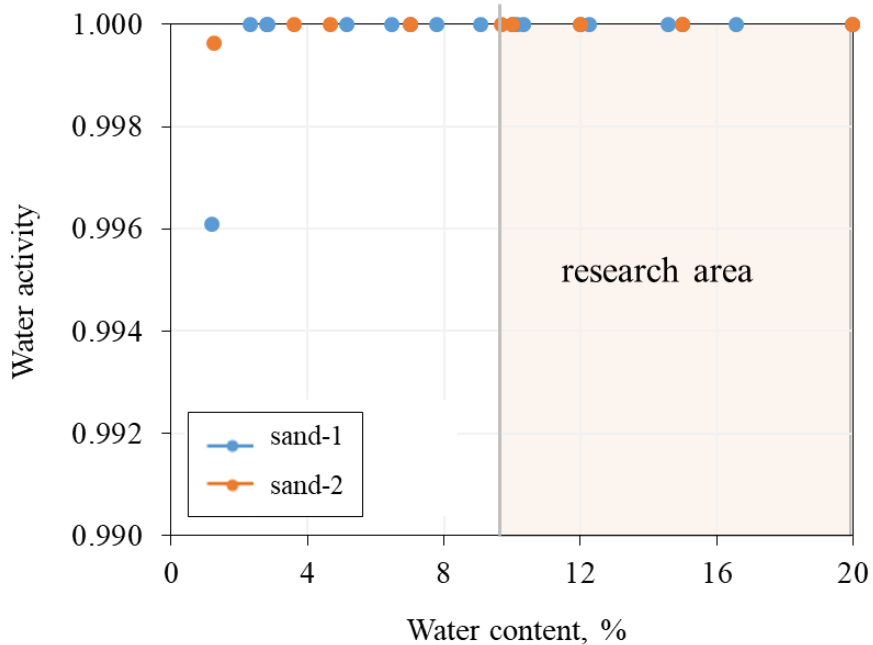


Figure 21. The water activity of non-saline sand at the various water content.

Therefore, any change in the pore water activity value in a given water range will be determined solely by the salt content in the studied sand samples. To further test this theory, and to identify empirical dependencies, sand samples with a given salinity (% of salts to a dry sample of sand by weight) were prepared and their activity was studied depending on water content. Based on the measurement results, graphs of the distribution of pore water activity against salinity for several values of water content (10, 12, 15, and 20%) (Figure 22).

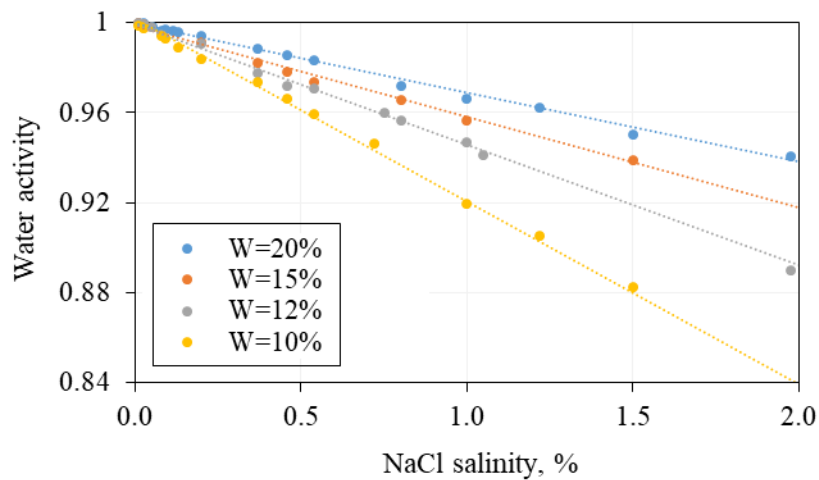


Figure 22. Distribution of water activity from sand salinity.

It should be noted that when recalculating the salt concentration from salinity to concentration per pore water (weight content of salts per content of pore water), all obtained values of the pore water activity gave a linear dependence (Figure 22). The results showed a high correlation between the activity of pore water and the concentration of salts in sand samples. The correlation coefficient was 0.9981.

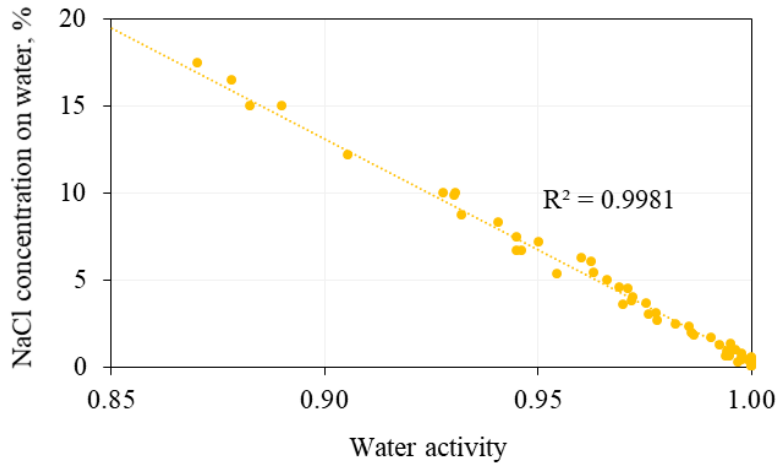


Figure 23. The water activity from NaCl concentration in pore water solution.

To finally confirm the theory and establish the limitations and accuracy of the method, the salt concentration in sand samples was assessed after the contact of frozen hydrate-bearing sediment with saline by two methods through water extracts: conductometric and flame photometric, followed by the comparison of the results with each other (Figure 24).

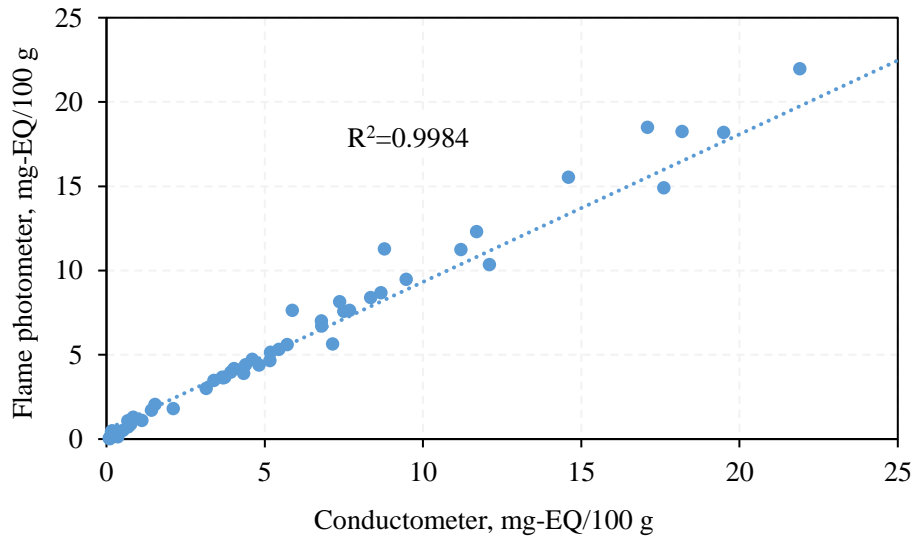


Figure 24. Comparison of the measurement results of the Na⁺ concentration by a flame photometer and a conductometer.

The results showed a high dependence (correlation coefficient 0.9984) between the methods, which makes it possible to compare the proposed potentiometric method with one of the methods of aqueous salt extracts.

To analyze the accuracy and limitations of the potentiometric method, we compared the results of measurements of the activity of pore water on sand samples with a given salinity and samples of saline sand after experimental modeling with data from a conductometer, which made it possible to identify an empirical equation for calculating the salt concentration (mg-EQ/100 g) through activity (Figure 25).

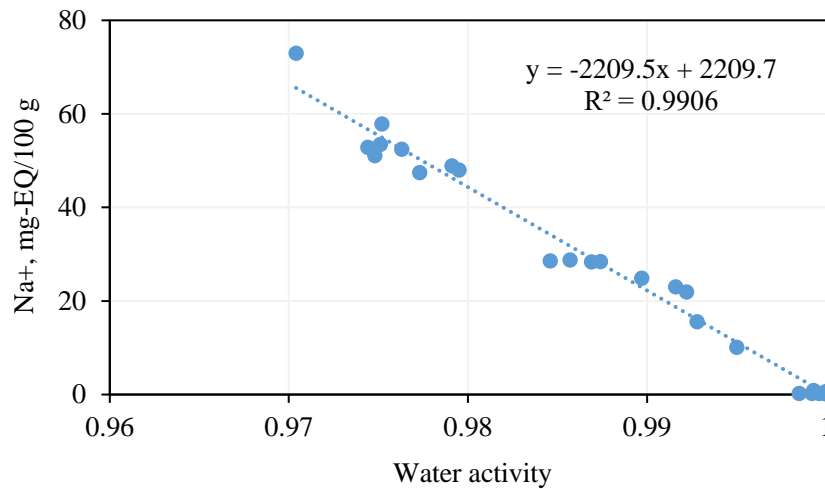


Figure 25. Pore water activity versus Na⁺ ion concentration.

Thus, the procedure for calculating salt concentration through water activity consists of the following steps:

- 1) Obtaining the water activity value of sediment probe on the WP4C device;
- 2) Calculation of salt concentration in pore water through empirical dependence (C, $\frac{mg \cdot EQ}{100 g}$):

$$C = -2209.5 \cdot a + 2209.7$$

where a – water activity, u.f.

The proposed method has several advantages:

- 1) No need for special sample preparation. The WP4C can measure pore water activity even at low sample weights. Only 1-2 g of sample is sufficient for measurements;
- 2) Relatively high measurement accuracy: ± 0.5 mg-EQ/100 g ($\pm 0.01\%$);
- 3) Direct measurement method without dilution. Due to the absence of additional manipulations with the sand sample, the measurement error is reduced solely to the instrumental error of the device measurement of pore water activity, which is ± 0.0004 ;
- 4) Cheapness. The instrument for determining the activity is much cheaper than the equipment used in atomic absorption analysis or flame photometry.

The method has a number of limitations:

- 1) Applicable in the sediment salinity range from 0.01 to 2%. At the higher concentrations instrumental error is increasing and the method is impossible to use accurately;
- 2) Method accuracy $\pm 0.01\%$ of salinity;
- 3) Mainly applicable to sandy sediments, and not to clayey sediments.
- 4) Measurements WP4C are mainly should be done on probes of sandy sediments in the laboratory conditions, and until now not in the field conditions. However, applicable both for natural and for artificial sand with water content from 2% and low salinity (up to 2%).

3.6. Processing of the experimental data

For all samples during processing, initial characteristics (before the start of the experiment) and residual characteristics for the selected intervals (after the experiment) were obtained on probes (weight of around 1-3 g).

Processing of experimental data related to the study of the kinetics of gas release from frozen hydrate-containing sediment samples when interacting with salt solutions was carried out in the following order:

Water content (W , %) of the samples was determined by the gravimetric method [329]:

$$W = \frac{m_{wet\ sed} - m_{dry\ sed}}{m_{dry\ sed}} \cdot 100\%$$

where $m_{wet\ sed}$ – mass of the wet thawed sediment after the experiment (g), $m_{dry\ sed}$ – dry sediment mass (g).

Density (ρ , g/cm³) determined by the method of geometric measurement:

$$\rho = \frac{m_{sample}}{V}$$

where m_{sample} – mass of the frozen hydrate-bearing sediment sample (g), V – volume of the sediment sample (cm³).

Calculation of the density of the sediment skeleton (ρ_d , g/cm³) was made according to the formula:

$$\rho_d = \frac{\rho}{1 + W}$$

where ρ – sediment density (g/cm³), W – gravimetric water content (%).

Defining volume water content (W_{vol} , %):

$$W_{vol} = \rho_d \cdot W$$

where ρ_d – density of sediment skeleton, W – gravimetric water content.

Calculation of porosity (n , %):

$$n = \frac{\rho_s - \rho_d}{\rho_s} \cdot 100\%$$

where ρ_s – density of solid particles of sediment, ρ_d – density of sediment skeleton.

The degree of filling the pores with ice (S_i , %) was calculated by the formula:

$$S_i = \frac{W_{vol}}{0.92 \cdot n} \cdot 100\%$$

where W_{vol} – volume water content, n – porosity. Then, the initial specific gas content (G , $\frac{cm^3}{g}$) of the hydrate-containing sample and the residual specific gas content, both calculated by the formula:

$$G = \frac{(V_2 - V_1) \cdot T}{m_p}$$

where $(V_2 - V_1)$ – change of the water volume in the glass gas collecting tube (cm^3); T – temperature correction; m_p – mass of the sediment probe taken from the frozen hydrate-containing sample (g).

Mass of gas (Δm_{gas} , g) calculated through the specific gas content:

$$\Delta m_{gas} = \frac{M(CH_4) \cdot G \cdot P}{R \cdot T \cdot z}$$

where $M(CH_4)$ – methane molecular weight, P – pressure (in case of metastable conditions equal to the atmosphere, i.e. 0.1 MPa), $R=8.314$ J / mol·K - universal gas constant, $z = 0.95$ - coefficient of methane compressibility.

Mass of hydrate (M_h , g):

$$M_h = 7.64 \cdot \Delta m_{gas}$$

where 7.64 coefficient is obtained from empirical formula of methane hydrate $\text{CH}_4 \cdot n\text{H}_2\text{O}$. To calculate the parameters of the hydrate content of sediment, the coordination number (n) for methane hydrate was used 5.9 [336].

Mass of hydrated water ($m_{gh\ water}, g$) is calculated by the below formula, where 6.47 hydrate coefficient for methane hydrate:

$$m_{gh\ water} = 6.47 \cdot \Delta m_{gas}$$

Amount of water converted to hydrate ($W_h, \%$):

$$W_h = \frac{m_{gh\ water}}{m_p} \cdot 100\%$$

Based on the data obtained, the initial and residual hydrate coefficient (K_h) was calculated for the intervals - the proportion of pore water that passed into hydrate from the total amount of water in the sample.

$$K_h = \frac{W_h}{W}$$

where W_h – the amount of pore water that has passed into the hydrate (% in relation to the mass of the dry sample), W – gravimetric water content of the sample (%).

The proportion of gas hydrate inclusions located in the pore space of frozen samples was quantitatively determined - weight hydrate content ($H, \%$ of sample weight):

$$H = \frac{Mh}{m_p} \cdot 100\%$$

Volumetric hydrate content ($H_v, \%$) was defined by the formula:

$$H_v = \frac{H \cdot \rho}{\rho_H}$$

where ρ – sediment density (g/cm^3), ρ_H – hydrate density (g/cm^3) and methane hydrate density equal 0.9 g/cm^3 .

Knowing the volumetric hydrate content, it is possible to determine the degree of pore filling with hydrate – hydrate saturation (S_h , %):

$$S_h = \frac{H_v}{n}$$

The change in the flow of Na^+ ions through the cross section of a frozen hydrate-containing sample was also calculated (J , $\text{mol/m}^2 \cdot \text{sec}$) based on the measurements of concentration (C , initially in %, then recalculated in $\text{mg - EQ} / 100 \text{ g}$) in each interval of the sample, by conductometer:

$$J = \frac{v}{S \cdot t}$$

where S – sample cross-sectional area (m^2); t is the salt migration time (sec); $v = m/23$, m is the mass of sodium ions obtained through the mass ratio of the sediment probe (g); 23 – atomic mass of sodium (g/mol).

The result of processing the experimental data obtained are graphs of changes in the concentration of salt ions along the height of the sample (C , $\text{mg - EQ} / 100 \text{ g}$) and the hydrate coefficient (K_h , u.f.) which are provided in the Chapters 4 and 5. Considering the results of temperature measurements, graphs of changes in the temperature field over time were plotted. Also, critical salt concentration of complete hydrate dissociation (C_{cr}) was determined by the comparison of the graph of salt ions concentration distribution by the length of the sample and hydrate coefficient distribution. In the sample interval where the hydrate coefficient became lower than 0.05, the corresponding salt concentration in this interval was taken as critical. Thus, determination of the critical concentration for each of the experimental frozen hydrate bearing sample made it possible to follow the change of that parameter

depending on different factors (i.e. pressure, temperature, solution concentration and composition, sediment characteristics).

Chapter 4. Mechanism and dynamics of salt transfer processes in hydrate-bearing sediments

Experimental modeling of the dynamics of hydrate-bearing frozen sediments with the salt solution was carried out on the fine sand-1. The prepared sediment samples had an initial water content of 12%. After hydrate saturation, the frozen samples were removed from the pressure cell at a low negative temperature ($-6 \pm 1^\circ\text{C}$) under the atmospheric pressure. Due to the self-preservation effect, the frozen hydrate-bearing samples were well preserved during the whole experiment (2-3 days). The fraction of pore water converted to hydrate (K_h) was 0.6.

Typical characteristics of frozen samples containing conserved hydrates are presented in Table 5.

Table 5. Main initial characteristics of frozen hydrate-containing sand samples.

Sediment	W, %	ρ , g/cm ³	n, u.f.	S _i , %	K _h
Fine sand-1	12	1.69	0.39	47	0.6

Then the frozen hydrate-containing samples at a negative temperature ($-6 \pm 1^\circ\text{C}$) were brought into contact with a 0.2N NaCl solution previously cooled to the experimental temperature (Figure 19).

At the end of the experiment, for the samples interacting with the salt solution, layer-by-layer determination of the parameters of water content, gas, and salt content was carried out.

4.1. Influence of hydrate presence on the salt migration in frozen sediments

Experimental modeling of the interaction of hydrate-bearing frozen sediment with the cooled (frozen) salt solution shows that active diffusion of salt ions into the sand sample occurs, which resulted in salinization of the frozen sample and dissociation of methane hydrate in porous media.

Two experiments were carried to identify the effect of the hydrate component of frozen sediments on the process of the salt migration under equilibrium pressure (2.5 MPa) and non-equilibrium pressures (0.1 MPa) at the constant negative temperature (-6 ± 1 ° C): with frozen samples, where the hydrate was absent; and with hydrate-containing frozen sediment. Pressure in case of frozen non-hydrate containing samples was created by nitrogen injection in the pressure cell to prevent hydrate formation. It was found that the migration of salt ions into a frozen hydrate-containing sample occurs more intensively than in a sample without hydrates. This dependence is observed both at non – equilibrium pressure under conditions of hydrate self-preservation (0.1 MPa) and at pressures above equilibrium (2.5 MPa) (Figure 26).

As a result, at atmospheric pressure, Na^+ ions penetrated deep into the sample from the contact zone to 5.3 cm in a frozen hydrate-containing sample, whilst the penetration of salts did not exceed 2.6 cm in the frozen non-hydrate-containing sample after 4 hours from the start of interaction with 0.2 N NaCl solution (Figure 26). At the same time, the total accumulation of salts in a frozen sample that did not contain hydrates was significantly lower than in a sample with hydrate. An experiment at a pressure above equilibrium (2.5 MPa) demonstrates a similar dependence but differs in a lower intensity of salt accumulation (Figure 26). Thus, Na^+ ions penetrated to a depth of 3.6 cm in a frozen hydrate-containing sample, while in a frozen non-hydrate-containing sample only by 2.2 cm after 4 hours from the onset of interaction. Also, difference in the level of salt accumulation is observed by the whole length of each sample. This way, in the near contact zone the highest concentration (22 mg-EQ/100 g) was observed

in the hydrate-bearing sample at the atmospheric pressure, while when pressure is increased up to 2.5 MPa concentration was lower (14 mg-EQ/100 g). Lower salt concentration was registered in frozen non-hydrate-containing sample and it equals 10-13 mg-EQ/100 g at pressure 2.5 and 0.1 MPa correspondingly. Such difference in the concentration in the near contact zone (which were measured in the sediment itself) is associated only with pressure factor influence and hydrate component effect, because the rest of factors are the same (solution concentration and composition, temperature conditions and sediment composition).

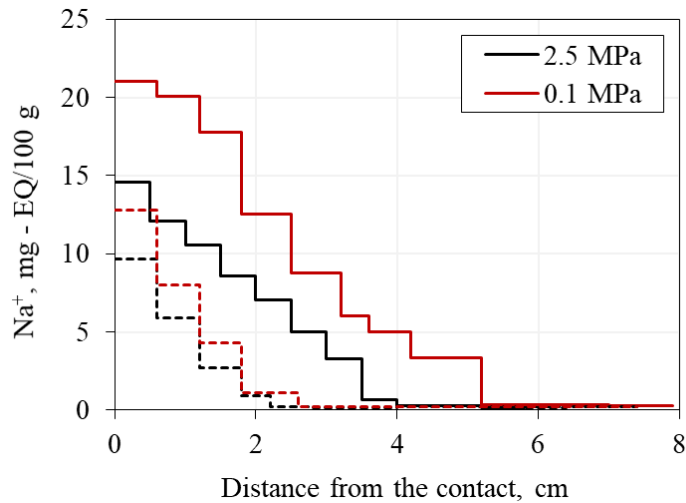


Figure 26. Effect of gas pressure on the accumulation of salt ions (Na^+) in frozen sand (fine sand -1) samples ($W=12\%$) containing (solid line) and not containing (dashed line) gas hydrates 4 hours after interaction with 0.2 N NaCl solution ($t=-6\text{ }^\circ\text{C}$).

Thus, it can be observed, that gas pressure has a strong influence on the salt migration in hydrate-bearing frozen sediments, while in frozen non-hydrate-bearing sediments pressure almost does not affect salt accumulation.

For the studied samples, the average Na^+ flux (J , $\text{mol}/\text{cm}^2\cdot\text{sec}$) was calculated for different gas pressure conditions and fixed temperature ($-6\text{ }^\circ\text{C}$) (Table 6). Results of calculation demonstrate that salt

flow is less in non-hydrate samples and barely depends on pressure (equals $1.2-1.7 \cdot 10^{-10}$ mol/cm²). While the flow in hydrate-bearing samples under atmospheric pressure is more than twice higher and reaches $5 \cdot 10^{-10}$ mol/cm²·sec. However, at the stable pressure (2.5 MPa) average Na⁺ flux is just slightly higher than flow in the frozen non-hydrate bearing sediments and equals $1.9 \cdot 10^{-10}$ mol/cm² at a pressure 2.5 MPa.

Table 6. Average Na⁺ flux in frozen hydrate-containing and non-hydrate-containing sand (fine sand-1) under the equilibrium (2.5 MPa) and non-equilibrium (0.1 MPa) pressure (4 hours of interaction with 0.2N NaCl solution at -6 °C).

Pressure	Sample	Average Na ⁺ flux J·10 ⁻¹⁰ , mol/cm ² ·sec
0.1 MPa	non-hydrate	1.2
	hydrate	5
2.5 MPa	non-hydrate	1.7
	hydrate	1.9

The specificity of salt migration in frozen hydrate-containing sediments is due to the presence of not only the process of ice melting but also the dissociation of pore gas hydrate with the formation of a liquid phase of water and the release of large volumes of methane (which is state based on the residual hydrate determination in the experiment). When gas is released, the structure of gas hydrate formations also loosens, and formed water becomes gas-saturated. The greater the content of the liquid phase – the more active the salt migration, therefore, the higher the diffusion coefficient. In addition, the absorption of ions through gas-saturated pore water also promotes higher salt flow to pass through hydrate-bearing frozen sediment.

Therefore, salt migration is more active in hydrate - containing sediments at atmospheric pressure. Moreover, if salt migration in frozen non-hydrate-containing sediments does not depends on the pressure, in the case of frozen hydrate containing sediment there is a much higher flow of salts at the non-equilibrium pressure. When pressure is changed from equilibrium to non-equilibrium the average density flow rises more than 2 times.

4.2. The interaction of frozen hydrate-bearing sediments with salt solutions in time

Interaction of hydrate-bearing sediments with NaCl (concentration 0.1N) was studied during different time period (3.9, 17.5, 25.5 and 28.8 hours after the start of interaction) at a constant negative temperature ($-6 \pm 1^\circ\text{C}$) and pressure (0.1 MPa). It was observed that there is a direct dependence between salts accumulation and hydrate dissociation. So, when salts migrate from the zone of contact, hydrate start to dissociate in the same direction – from the zone of contact (Figure 27).

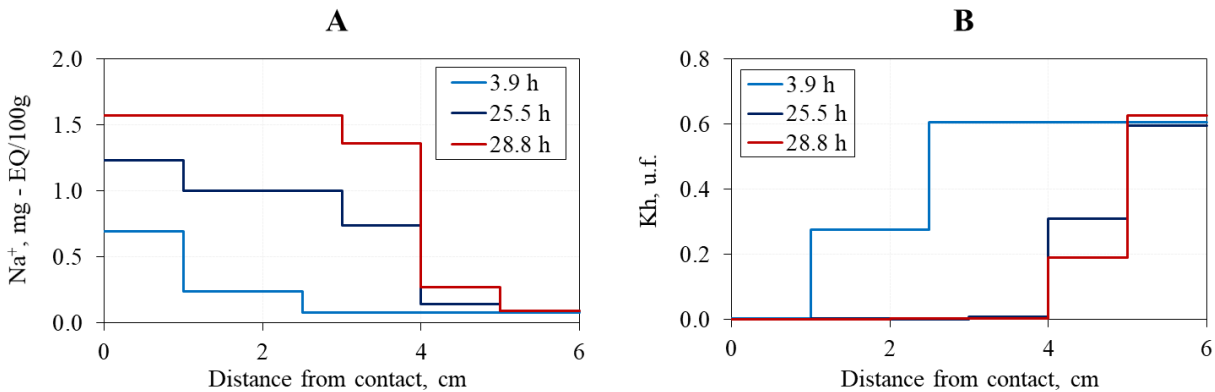


Figure 27. Accumulation of Na⁺ ions (A) and changes in the hydrate coefficient (B) in samples of frozen hydrate-containing sand-1 ($K_h^{in} = 0.6$, $W=12\%$) at different times after interaction with NaCl solution 0.1 N ($P=0.1$ MPa, $t=-6$ °C).

Figure 27 shows the accumulation of Na^+ ions (A) and the amount of pore water in hydrate form (hydrate coefficient) (B) in frozen samples containing preserved (metastable) hydrate at atmospheric pressure after contact with a frozen NaCl solution with a concentration of 0.1N at different times. After 4 hours, the salts penetrated to a depth of 2.3 cm, and the maximum concentration increased from 0.1 to 0.7 mg-EQ/100 g in the contact zone. After 29 hours, the accumulation of salts was recorded at a distance of 5 cm from the contact area with maximum value of concentration 1.6 mg-EQ/100 g.

Joint analyses of the salt distribution (Figure 27A) and hydrate coefficient (K_h) by the height of the sample (Figure 27B) shows, that the salinity value determines the residual content of methane hydrate in porous media. In the initial state (before the contact with the solution) for sand samples (fine sand-1), about 60% of the pore water was in the hydrate form initially. In the process of salinization, there was a decrease in the proportion of pore water in the hydrate form (K_h), and the appearance of a front of complete hydrate decomposition (Figure 27B). This way, after 4 hours of interaction hydrate completely decomposed within 1 cm from the contact with salt solution, while after 29 hours no residual hydrate was observed within 4 cm.

In this case, it is possible to distinguish a certain critical content of salt ions in sand samples, which causes complete gas hydrate decomposition in the sediments (C_{cr} , mg-EQ/100 g). Under given conditions (temperature -6°C and concentration of NaCl contact solution 0.1 N) in sediment samples (fine sand 1), the critical value of salt accumulation was about 0.7-0.8 mg-EQ/100 g.

During the process of salt migration in a frozen hydrate-containing sample, a thawing front can also occur in addition to the decomposition front of pore hydrates, when the accumulated salt ions completely transfer the pore ice into water. In Figure 28 the movement of two fronts is shown: hydrate decomposition and thawing boundary. Each point of the graph represent one sample-twin which was

analysed by intervals for the residual hydrate content and location of the thawing boundary. Detailed description of the procedure of interval analysis is given in the Chapter 3.3.

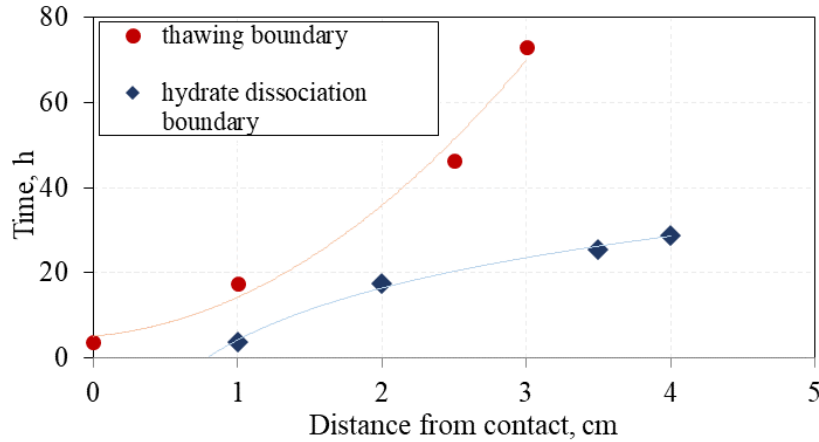


Figure 28. Experimental evaluation of the decomposition front of porous gas hydrates and the thawing front in frozen hydrate-containing sand samples (sand-1, $W = 12\%$) when interacting with 0.1 N NaCl salt solution at a temperature -6°C and pressure 0.1 MPa.

The pore hydrate decomposition front is ahead of the thawing front since thawing requires a higher value of salt accumulation in the frozen sample. This way, after 4 hours of interaction hydrate dissociation reached 1 cm from the contact with salt solution, while the thawing boundary was not registered at all. Only after 17.5 hours thawing front reached 1 cm, while the hydrate dissociation front at that time was already 2 cm from the contact with 0.1 NaCl solution at -6°C and pressure 0.1 MPa. Moreover, with time the difference between fronts became bigger. That is, the critical concentration of pore hydrate dissociation is lower than the critical concentration of thawing and is about 0.7 mg-EQ/100 g and 1.5 mg-EQ/100 g, respectively. Thus, the thawing critical concentration is 2 times higher than hydrate dissociation C_{cr} in the porous media of the studied model sand.

The thaw front in the sample is well fixed by the characteristic dark color distribution of the sample (Figure 29). Additionally, it was evaluated using a special probe-needle method, which described in the Chapter 3.3.

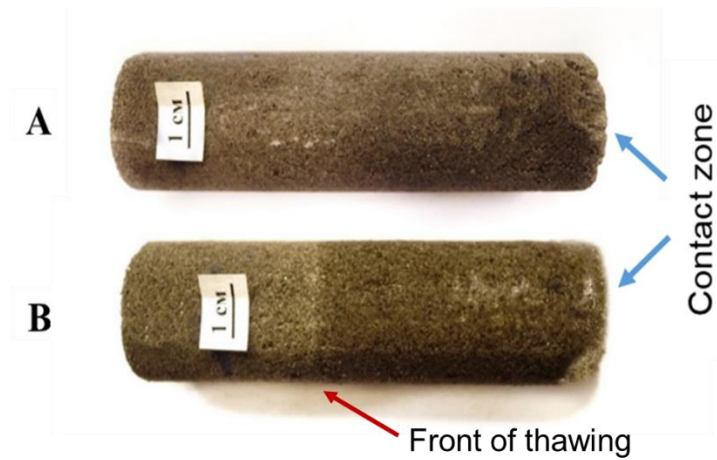


Figure 29. The appearance of frozen sand samples (fine sand 4, W=12%) before (A) and after interaction (B) with 0.1 NaCl solution at -6°C .

In addition, the average Na^+ flux was calculated in time based on the data of salt ions concentration in the frozen hydrate saturated samples (fine sand-4) (Figure 30). The Na^+ flux in the first 5 hours is $2 \cdot 10^{-10} \text{ mol/cm}^2 \cdot \text{s}$, with time the flux decreases, and after 30 hours it decreases to values of about $0.2 \cdot 10^{-10} \text{ mol/cm}^2 \cdot \text{s}$, so 10 times less than at the beginning of the interaction.

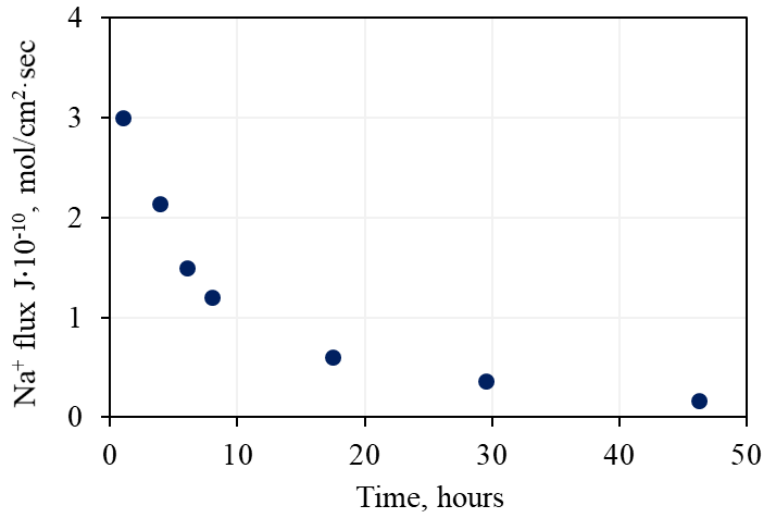


Figure 30. Average Na⁺ flux change in time during interaction of frozen hydrate-bearing sediment (fine sand-1) with NaCl solution of 0.1N at -6 °C and 0.1 MPa.

The presented experimental data on the interaction of frozen hydrate-containing sediments with salt solutions showed that the processes of salt ions migration in frozen hydrate-bearing sediment can occur more quickly compared to frozen sediments that do not contain hydrates. That is apparently associated with the processes of dissociation of hydrate in porous media and the appearance of a liquid phase of water. Accumulation of salts causes active hydrate dissociation in porous media, so the concentration of ions defines residual hydrate content and it is possible to define the critical concentration of complete hydrate dissociation (C_{cr}). Salt migration contributes to the formation of two fronts: the gas hydrate dissociation front and the thawing front, while the dissociation front is ahead of the thawing front of a frozen hydrate-containing sample.

4.3. Temperature changes as a result of salt migration in frozen hydrate-bearing sediments

As shown earlier, when frozen hydrate-bearing sediments interact with a cooled (frozen) saline solution, active diffusion of salt ions occurs into these samples, resulting in salinization of the frozen sample. When a certain critical value of salt concentration in a frozen hydrate-containing sample was reached, the hydrate dissociation front was formed.

The process of salinization of a frozen hydrate-containing sample, as well as a frozen non-hydrate-bearing sample, is associated with a temperature decrease since the methane hydrate dissociation and the ice melting under the influence of salts is an endothermic process. Given that the enthalpy of hydrate dissociation is 1.5 times higher than the amount of heat required to melt ice, a more significant decrease in temperature can be expected in a hydrate-containing sample compared to non-hydrate-containing one during their interaction with a salt solution. Experimental data on the dynamics of temperature change over time close to the contact area (2.5 cm from contact with NaCl 0.4N saline solution) in frozen sand samples (fine sand-2), containing and not containing hydrates, confirm this (Figure 31) (at 0.1 MPa).

In these experiments, samples (fine sand-2) were used, which had an initial water content of 12%, and porosity of the order of 38-40%. At the same time, the saturation of the pore space with ice in a non-hydrate-containing frozen sample was 50%, and in a hydrate-containing one with a total degree of pore filling of 53%, the saturation with hydrate was 35% (Table 7). All experiments on the temperature change investigation were conducted at the atmospheric pressure (0.1 MPa).

Table 7. Frozen non-hydrate-bearing (sample 1) and hydrate-bearing (sample 2) fine sand -2 initial characteristics.

Sample	Water content, %	Density, g/cm ³	Porosity, %	Degree of pore filling with ice, %	Degree of pore filling with hydrate, %
1	12	1.80	40	50	0

2	12	1.85	38	18	35
---	----	------	----	----	----

As follows from Figure 31, a decrease in temperature in the samples (fine sand-2) is recorded almost immediately after being brought into contact with a saline solution at the atmospheric pressure. However, the temperature reaches its minimum value at a distance of 2.5 cm from the contact area in a frozen sample after 0.7 h, and in a hydrate-containing sample only after 1 h. At the same time, the value of temperature decrease in the hydrate-containing sample is 0.6°C and only 0.2 °C in the frozen one. The rate of temperature decrease after bringing a frozen non-hydrate-containing sample into contact with a saline solution was 0.4 °C/h; for hydrate samples, 0.6 °C/h. After the temperature decrease in the samples, its gradual increase to the initial value of -6.5°C is observed, which is achieved in the hydrate-containing sand sample after 5 hours, and in the frozen one - after 3.7 hours.

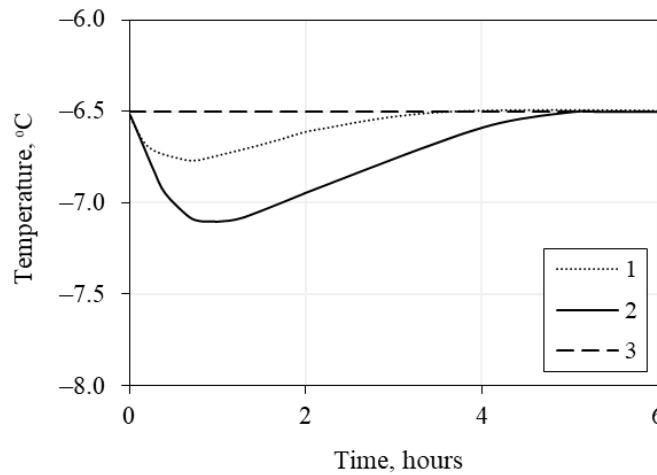


Figure 31. Dynamics of temperature change in time in the near-contact area (2.5 cm from the contact) in frozen sand samples (fine sand-2) interacting with 0.4 N saline solution at atmospheric pressure: 1 – non-hydrate-containing frozen sample (dotted line); 2 - hydrate-containing (solid line); 3 - initial temperature (tin) - 6.5 °C (dashed line).

The temperature distribution along the length of a frozen sample containing and not containing pore hydrates at a fixed point in time (0.6 h after the start of contact with the salt solution) can be traced in Figure 32. As follows from the obtained data, at the time point of 0.6 hours after the start of the interaction of fine sand-2 with 0.4N NaCl solution at an initial temperature of -6.5°C , a regular decrease in the temperature deviation from the initial value is observed with distance from the contact area. This deviation in frozen non-hydrate bearing sand is much less than in frozen hydrate-bearing sample. For a sample containing hydrates, a temperature deviation is registered along the entire length of the hydrate-bearing frozen sample in contrast to a non-hydrate-containing sample, where temperature decrease was observed only in the area closest to the contact with salt solution (fine sand-2).

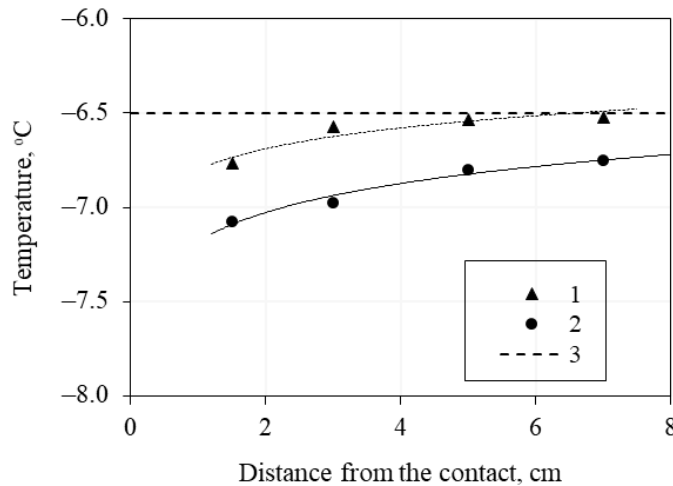


Figure 32. Temperature distribution along the length of a frozen sample (fine sand-2), not containing (1) and containing gas hydrate (2) after 0.6 h of interaction with 0.4 N. NaCl solution at atmospheric pressure. The dotted line - 3 shows the initial temperature $t_{in} = -6.5^{\circ}\text{C}$.

Figure 33 demonstrates the temperature dynamics of a frozen hydrate-containing sample (fine sand-2) overtime at different distances from the area of contact with 1N NaCl solution. In the initial state, both the frozen hydrate-containing sample and the solution had a temperature of -6.5°C . After bringing them

into contact, a regular decrease in temperature in the sample was observed. This was fixed at different distances from the contact area. The temperature decrease in the sample relative to the initial value (-6.5 °C) reached 1.9 °C. At the same time, at different distances from the contact area, this decrease shifted in time. So, at a distance of 2.5 cm from the contact (value for 1 sensor), the minimum temperature (-8.3 °C) was reached 20 minutes after contact with saline solution, and at a distance of 7 cm, this temperature decrease was recorded after 35 minutes. At the same time, there was some delay in the start of sample cooling depending on the distance from the contact area, while the general cooling rate at different intervals remained almost the same (0.08-0.1 degrees per minute). After reaching the minimum temperature value in each interval, a gradual increase in temperature to the initial values (-6.5°C) was observed. Moreover, after 3 hours after the start of the interaction, the difference in temperature between the intervals was practically not observed, although later in the sample a gradual increase in temperature continued.

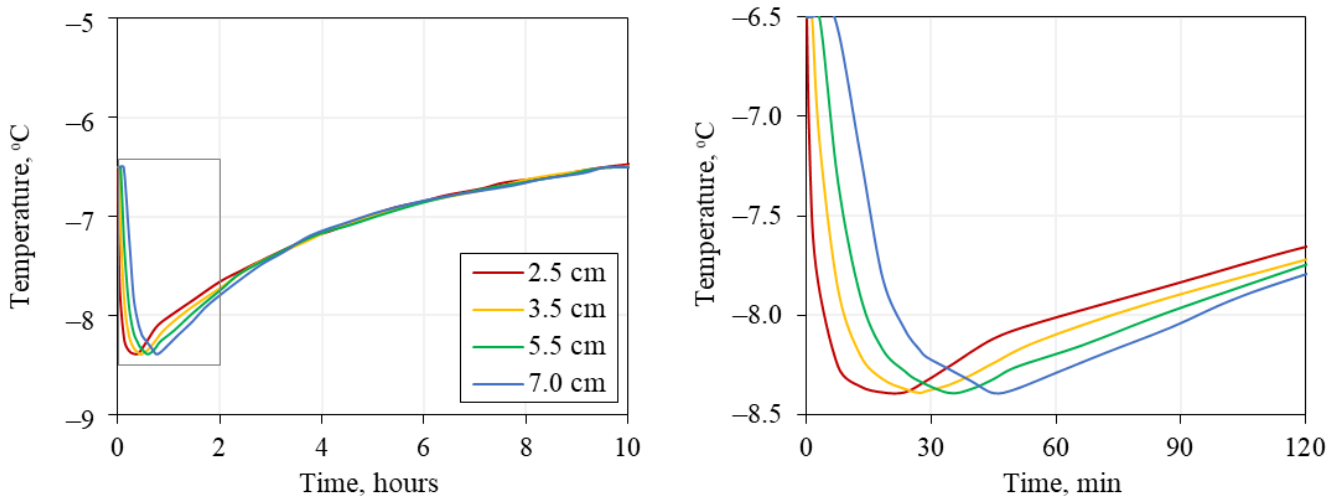


Figure 33. Dynamics of temperature change in time in a frozen hydrate-containing samples (fine sand-2, $S_h^{in}=38\%$, $S_i^{in}=15\%$) on the distance 2.5; 3.5; 5.5 and 7.0 cm from the contact zone with 1 N NaCl solution ($t_{in}=-6.5$ °C, $P=0.1$ MPa).

The temperature distribution along the height of a frozen hydrate-containing sample (fine sand-2) at various times after the start of the contact of a frozen hydrate-containing sample with NaCl (1 N) salt solution at the cooling stage can be seen on Figure 34. Prior to contact with the saline solution, the temperature of the sample practically did not change and was equal to -6.5°C . After the frozen sample was brought into contact with saline solution, a decrease in temperature was observed within a minute at a distance of 2.5 cm from the contact with the saline solution ($\Delta t=1^{\circ}\text{C}$). At the same time, at a distance of 3.5 cm or more, the temperature remained the same (-6.5°C). After 4 min, a decrease in temperature was recorded to a depth of 5.5 cm from the contact area, and after 8 min, a change in temperature was observed throughout the whole sample. At the same time, at a depth of 2.5 cm, the temperature reduced by 1.8°C , and the temperature gradient along the length of the sample reached $0.4^{\circ}\text{C}/\text{cm}$. Subsequently, the temperature in the sample was equalized (fine sand-2) by stabilizing the temperature near the contact and lowering the temperature away from the contact area. As a result, after 30 min, the temperature distribution in the observed region (from 2.5 to 7 cm) was almost linear. The temperature of the sample varied within $-8.2\text{...}-8.4^{\circ}\text{C}$. Then, a gradual increase in the temperature of the sample was observed, primarily from the side of the area adjacent to the contact with the salt solution. So, one hour after the interaction of a frozen hydrate-bearing sample (fine sand-2) with a saline solution, the temperature at a depth of 2.5 cm increased by 0.3°C from the minimum value (at a time point of 30 min), and at a depth of 7 cm it practically did not change (Figure 34).

Thus, when a cooled salt solution interacts with a frozen hydrate-containing sample (fine sand-2), a cold wave arises due to the dissociation of pore gas hydrate caused by salt migration. As a result, a decrease in temperature along the length of the sample (by 1.8°C) can be observed. After completion of the hydrate dissociation process, a gradual increase in temperature takes place, which begins primarily in the interval of the sample adjacent to the area of contact with the salt solution.

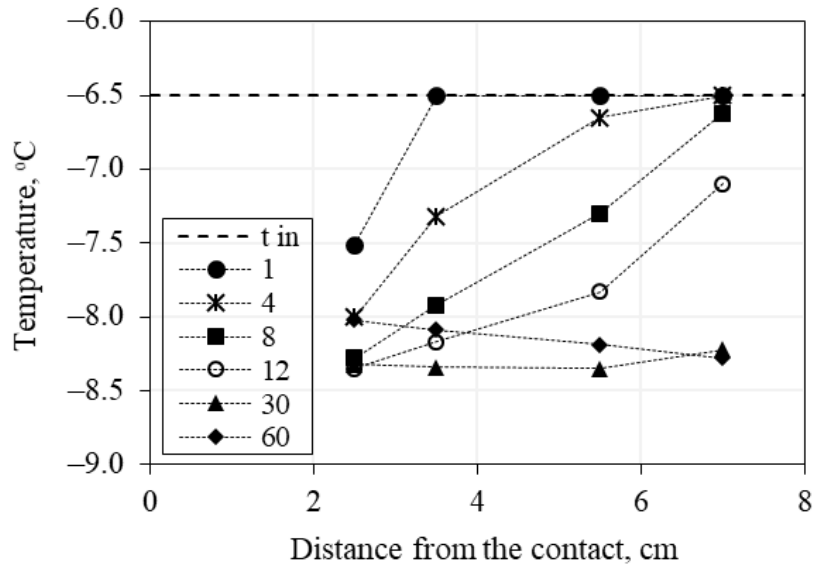


Figure 34. Change in the temperature distribution along the length of the frozen hydrate-bearing sample fine sand-2 ($S_h^{in}=41\%$, $S_i^{in}=12\%$) at the stage of cooling in the first hour (time on the legend is in minutes) of interaction with 1 N NaCl solution ($t_{in}=-6.5\text{ }^\circ\text{C}$, $P=0.1\text{MPa}$).

The intensity of the temperature decrease of a frozen hydrate-bearing sample (fine sand-2) upon contact with a saline solution strongly depends on the concentration of the contact solution. In the course of the experiments, the influence of various NaCl solution concentrations (0.2, 0.4, 0.6, 1 N) on the temperature change of frozen hydrate-bearing fine sand-2 dynamics was studied. Table 8 shows the initial characteristics of the studied samples, which were used to assess the effect of contact solutions. The saturation of the pore space of frozen samples with gas hydrate ranged from 35 to 41% and saturation with ice from 11 to 18%.

Table 8. Initial characteristics of the frozen hydrate-bearing fine sand-2 samples before the contact with NaCl solution of different concentrations.

Solution, N	Sample	Water content, %	Density, g/cm ³	Porosity, %	Ice saturation, %	Hydrate saturation, %
0.2	1	12	1.8	40	12	41
0.4	2	12	1.85	38	18	35
0.6	3	12	1.79	39	11	40
1	4	12	1.83	38	15	38

A plot of experimental data illustrating the temperature change of frozen hydrate-bearing sand in time when it comes into the contact with a NaCl solution of various concentrations are shown in Figure 35.

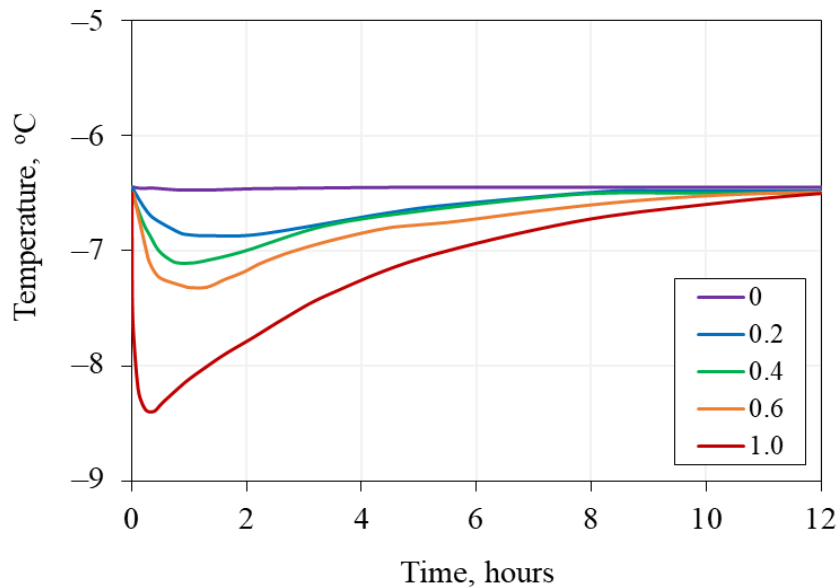


Figure 35. Dynamics of temperature changes in time of frozen hydrate-containing samples (fine sand-2) in the near-contact area (2.5 cm from the contact) interacting with NaCl solution of various concentrations (0.2-1N) ($t_{in} = -6.5^{\circ}\text{C}$, $P = 0.1 \text{ MPa}$).

As follows from the obtained data, the magnitude of the decrease in temperature in the studied samples (fine sand-2) depends on the concentration of the contact solution. With an increase in the concentration of the contact solution from 0.1 to 1 N, the temperature decrease in the near-contact region (2.5 cm) changed from 0.3°C to 1.9°C. In addition, the time to reach the minimum temperature was reduced from 1 hour to 15 minutes (Figure 35).

A more significant decrease in the temperature of a frozen hydrate-containing sample (fine sand-2) with an increase in the concentration of the interacting solution is associated with an increase in the rate of gas hydrate dissociation in the pore space of sediments. Dependence of the maximum decrease in temperature during the interaction of a frozen hydrate-containing sample (fine sand-2) with a saline solution (Δt) on the concentration of the contact solution ($t_{in}=-6.5^\circ\text{C}$, $p=0.1\text{MPa}$) is presented on Figure 36.

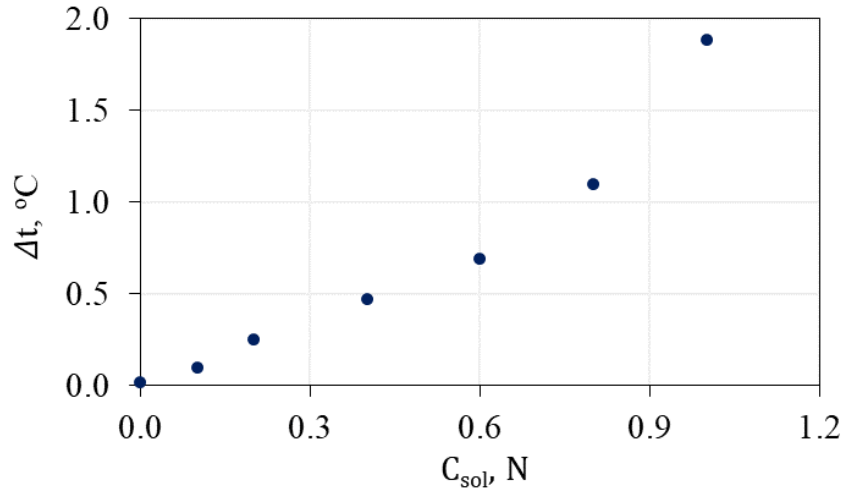


Figure 36. Influence of the contact solution concentration on the maximum temperature drop ($\Delta t=t_{in}-t_{min}$) in frozen hydrate-bearing fine sand-2 (C_{sol} from 0.1 to 1 N, $t_{in}=-6.5^\circ\text{C}$, $P=0.1\text{MPa}$).

At a concentration of NaCl contact solution of 0.1 N, the decrease in temperature was only 0.1 °C. In addition, with an increase in the concentration of the solution to 1 N, the decrease in the temperature

reached 2 °C. Thus, with an increase in the concentration of the contact solution from 0.1 to 1 N, the decrease in the temperature of a frozen hydrate-bearing sand sample increases by a factor of 20.

It should be noted that with an increase in the concentration of the contact solution, there is a significant increase in the rate of temperature decrease (V_t , °C/hour) (Figure 37). Thus, at a contact solution concentration of 0.1 N, the rate of temperature decrease in a frozen hydrate-containing sample (fine sand-2) caused by salinity was 0.4 °C/h, and at a contact solution concentration of 1 N it increased to 4.7 °C/h, which is more than 10 times higher than in contact with 0.1 N solution.

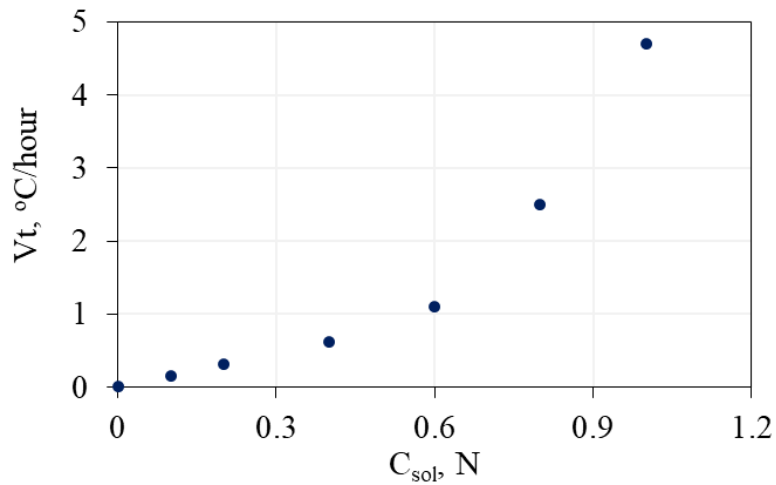


Figure 37. Influence of contact solution concentration on the rate of temperature decrease (V_t) of frozen hydrate-bearing fine sand-2 (C_{sol} from 0.1 to 1 N, $t_{in} = -6.5^\circ\text{C}$, $P = 0.1$ MPa).

The time of the sample temperature recovery to its original value (back to the surrounding temperature -6.5°C) after the initial period of cooling, caused by the interaction of hydrated frozen fine sand-2 with saline solution, also depends on the concentration of the contact solution (Figure 38).

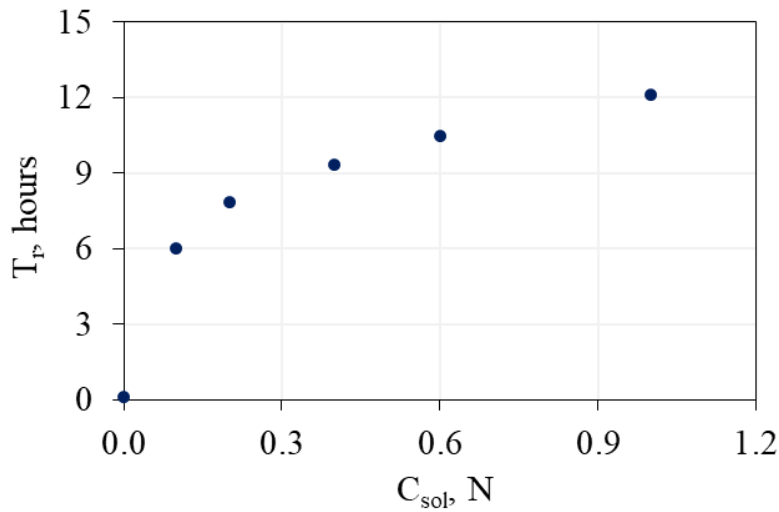


Figure 38. Influence of concentration on the time taken for the temperature of the sample to return to the initial value (T_r) after the cooling period caused by the interaction of hydrate-containing frozen sand with saline solution ($t_{in} = -6.5^\circ\text{C}$, $P = 0.1 \text{ MPa}$).

Thus, it takes about 8 hours for the sample temperature to return to its original state value (-6.5°C) when a frozen hydrate-bearing sample (fine sand-2) interacts with a saline solution with a concentration of 0.2 N, and about 12 hours are required at a concentration of 1N.

Thus, based on experimental studies, it can be inferred that when samples containing ice and pore hydrate interact with a salt solution, a change in the temperature field in the sample was observed, caused by the processes of salt migration, pore hydrate dissociation and ice melting. The amount of cooling of the sample due to the dissociation of the pore gas hydrate significantly exceeds the effect of cooling from the melting of the pore ice interacting with the salt solution. At the same time, the concentration of the contact solution has a great influence on the intensity of temperature changes.

4.4. Mechanisms of salt migration in frozen hydrate-containing sediments

The experimental data make it possible to represent the dynamics of the interaction of frozen hydrate-containing sediments with saline solution in the following way. When a hydrate-containing sample is brought into contact with a saline solution, salt ions penetrate deep into the sample, which causes ice melting and hydrate dissociation in porous media. As a result, a porous hydrate dissociation front appears, which expands from the area of contact with the salt solution. At the same time as the dissociation front is expanding, a thawing front forms at the same time with a more significant accumulation of salt ions.

As the gas pressure increases, the stability of the gas hydrate component increases because a higher concentration of salts in the pore space is needed to cause the pore hydrates to dissociate in accordance with the phase diagram (Figure 51).

In this regard, with an increase in gas pressure in the saline solution-sample system, the flow of salt ions decreases, as well as the amount of liquid water in the sample, which is formed due to the dissociation of pore hydrate, decreases. In frozen sediments that do not contain gas hydrates, gas pressure in the studied pressure range (up to 4.0 MPa) practically does not have a significant effect on the phase composition of water, which is not noticeably reflected in the accumulation of salts in frozen sandy sediments in the absence of water migration.

Analysis of experimental modeling data on the interaction of frozen hydrate-bearing sediments with NaCl salt solution and existing knowledge of hydrate and ice in porous media allows us to suppose phase changes in frozen hydrate-containing sand in equilibrium and non-equilibrium (with self-preservation) pressure and negative temperature (-6°C) as follows (Figure 39). At gas pressure values below equilibrium (<2.4 MPa), the pore hydrate in frozen sand exists in a metastable state due to the manifestation of the self-preservation effect (Figure 39a). Residual gas hydrate accumulations are

located under the ice shell, which was formed during the crystallization of water released during the partial dissociation of the pore gas hydrate. Migration and accumulation of salt ions in frozen hydrate-bearing sediment when interacting with a salt solution occurs primarily along films of unfrozen water on the surface of sand particles, as well as along the boundaries of ice crystals. This is accompanied by an increase in the thickness of unfrozen water films due to melting of pore ice. With the disappearance of the ice film on the surface of the hydrate, its active dissociation begins with the release of gas and water, which, under conditions of negative temperature and the endothermic effect of dissociation, partially freezes with the formation of ice (Figure 39a).

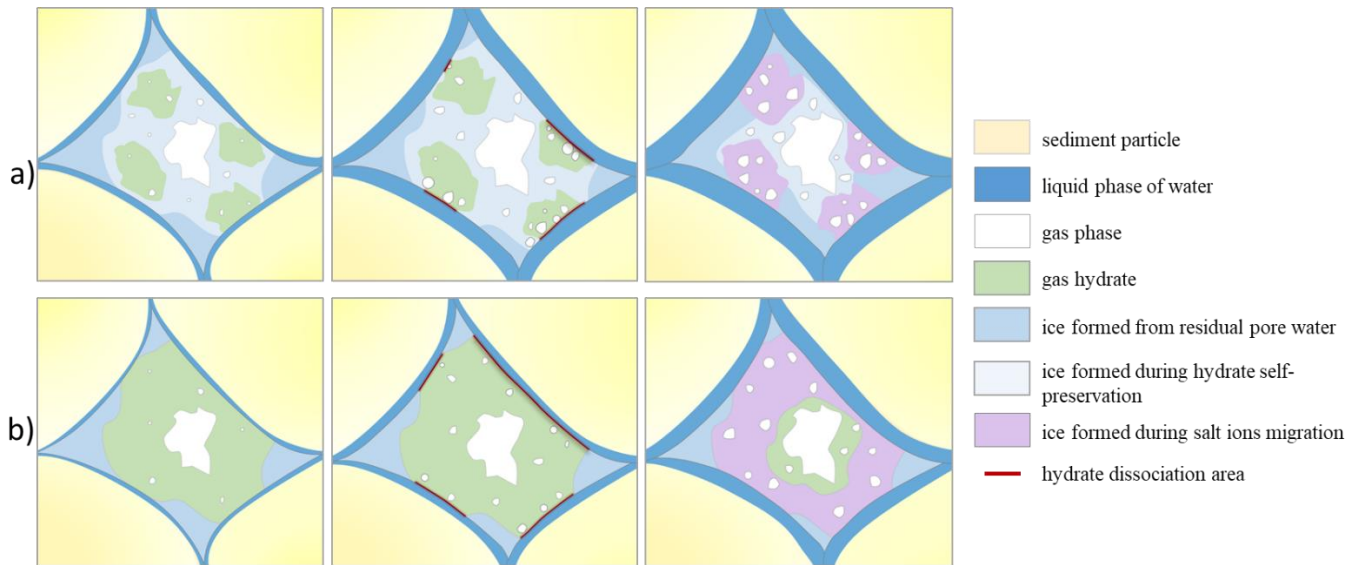


Figure 39. Scheme of phase-transformation of frozen hydrate-bearing sediments during salt migration:

(a) metastable conditions (experimental pressure $P_{exp} < P_{eq}$); (b) stable conditions

$$(P_{exp} \geq P_{eq}).$$

At an initial pressure above equilibrium (2.4 MPa and above), the pore methane hydrate in non-saline frozen sand is in stable conditions (Figure 39b). The equilibrium content of the liquid phase of water under these conditions should be less than in the sample containing preserved gas hydrate.

Considering that the process of salt ions migration occurs primarily through films of unfrozen water in a hydrate-containing frozen sample, at pressures above equilibrium the migration of ions occurs more slowly than at gas pressure below equilibrium. In addition, it can be assumed that the intergranular permeability of the gas hydrate is much lower than the permeability of ice. Under these conditions, taking into account a significant shift in pressure (ΔP) relative to the equilibrium value, when the salt solution interacts with a frozen hydrate-containing sediment sample, higher critical salt ion concentrations are required to destabilize the pore hydrate, which are achieved over a longer time. When critical concentrations are exceeded, gas hydrate dissociation is observed. However, unlike metastable conditions, this process is less active and the process of formation of pore ice is slower. The gas formed during the dissociation of the pore hydrate can later concentrate in the void space with an incomplete degree of filling of the pores, and also be in the form of separate gas inclusions in the ice that was formed during the dissociation of the hydrate. In this case, part of the gas can dissolve in unfrozen water, but this will be limited by the concentration of salts in the liquid phase (Figure 39b). However, this description of phase transformation require additional research on mirco-scale level.

Phase transitions that occur during the salts migration and accumulation in ice- and hydrate-bearing sediments are accompanied by temperature effects associated with the salt migration, melting of pore ice and the dissociation of pore gas hydrate. Given that these processes are endothermic, a decrease in the temperature of saline sediment samples is observed. The effect of temperature decrease is most pronounced in frozen hydrate-bearing sediment, since the enthalpy of dissociation of pore gas hydrate is 1.5 times higher than during ice melting.

A decrease in the temperature of the frozen sediment when interacting with a salt solution is associated with a shift of the thermodynamic equilibrium that exists in frozen sediment at a fixed negative temperature. As a result of salt transfer in frozen sediment, the content of salt ions in films of

unfrozen water increases. This disturbs the existing phase equilibrium and causes the melting of pore ice, which is accompanied by a decrease in temperature. As the salts continue to accumulate, additional melting of pore ice and a further decrease in temperature occur. This decrease will continue until an equilibrium occurs between the sediment temperature, pore solution concentration and ice. This can be clearly seen in the phase diagram for the NaCl solution (Figure 15), where at a given concentration of the salt solution, there is an equilibrium temperature corresponding to the freezing point of this solution. So, the change of temperature stops, when there is an equilibrium between the solution and ice at a fixed negative temperature. Based on this, the maximum decrease in temperature will correspond to the equilibrium temperature formed during the interaction of the salt solution with the pore ice of the concentration of the salt solution.

Taking into account that in the process of salt migration, the salinization front in the sediment sample shifts, the area of temperature decrease will also shift, which is clearly seen from the data obtained (Figure 33). The maximum decrease in sample temperature, while ambient temperature is constant over the experiments, corresponds to the maximum rate of ice melting and hydrate dissociation. Subsequently, when the melting of the pore ice and the dissociation of the gas hydrate dies out, or when the pore ice turns into liquid water and the gas hydrate inclusions completely decompose, a gradual increase in the sample temperature to ambient temperature is observed. In hydrate-containing samples, this process is longer than in frozen ones, which is due to deeper cooling and the formation of additional ice during the dissociation of porous gas hydrate.

The temperature effect in frozen hydrate-containing sediment caused by salt transfer can be schematically represented as follows (Figure 40). Initially, before bringing the sediment into contact with the salt solution, a uniform temperature field (Figure 40a) is observed in the sample at a fixed negative ambient temperature. The temperature of the frozen hydrate-containing sample corresponds to

the ambient temperature. After bringing the sample into contact with the salt solution under isothermal conditions, the temperature decreases in the near-contact region of the sample due to the migration and accumulation of salt ions, which causes the melting of ice and the dissociation of the pore gas hydrate (Figure 40b). With the accumulation of salt ions, the process of dissociation of the pore gas hydrate increases, which contributes to the continuation of the process of lowering the temperature (Figure 40c). Subsequently, the process of temperature decreases in this interval decays and shifts into the depth of the sample, where the salinization front moves (Figure 40d). Depending on the intensity of salinity, which is determined by the concentration of the contact solution, partial or complete decomposition of gas hydrates is possible. In the latter case, along with the salinization front, a porous gas hydrate dissociation front appears and even a porous ice thaw front, if there is a significant accumulation of salts.

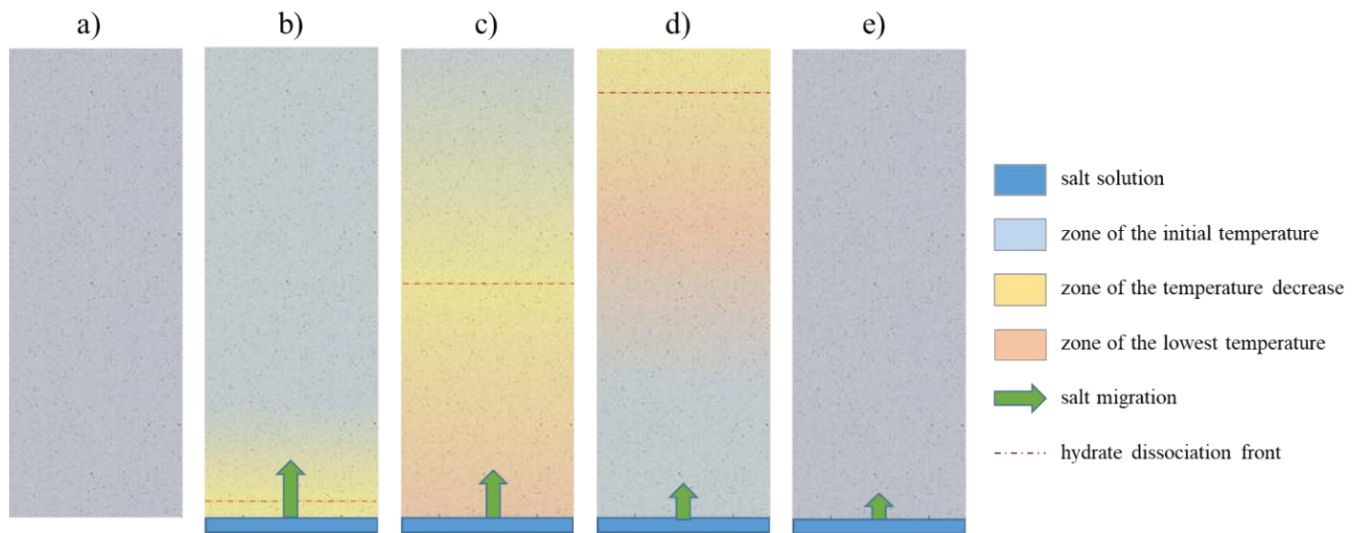


Figure 40. Scheme of temperature changes during the interaction of a frozen hydrate-containing sample with saline solution.

The displacement of the cooling wave to the end of the sample opposite from the contact during salt transfer is replaced by a gradual increase in the temperature of the sample to the ambient

temperature. That is due to the damping of phase transitions along the sample and the establishment of a new thermodynamic equilibrium between the pore ice and the salt solution (Figure 40e).

A more detailed scheme of changes occurring in frozen samples containing a metastable hydrate in the contact with saline solution can be seen in Figure 41.

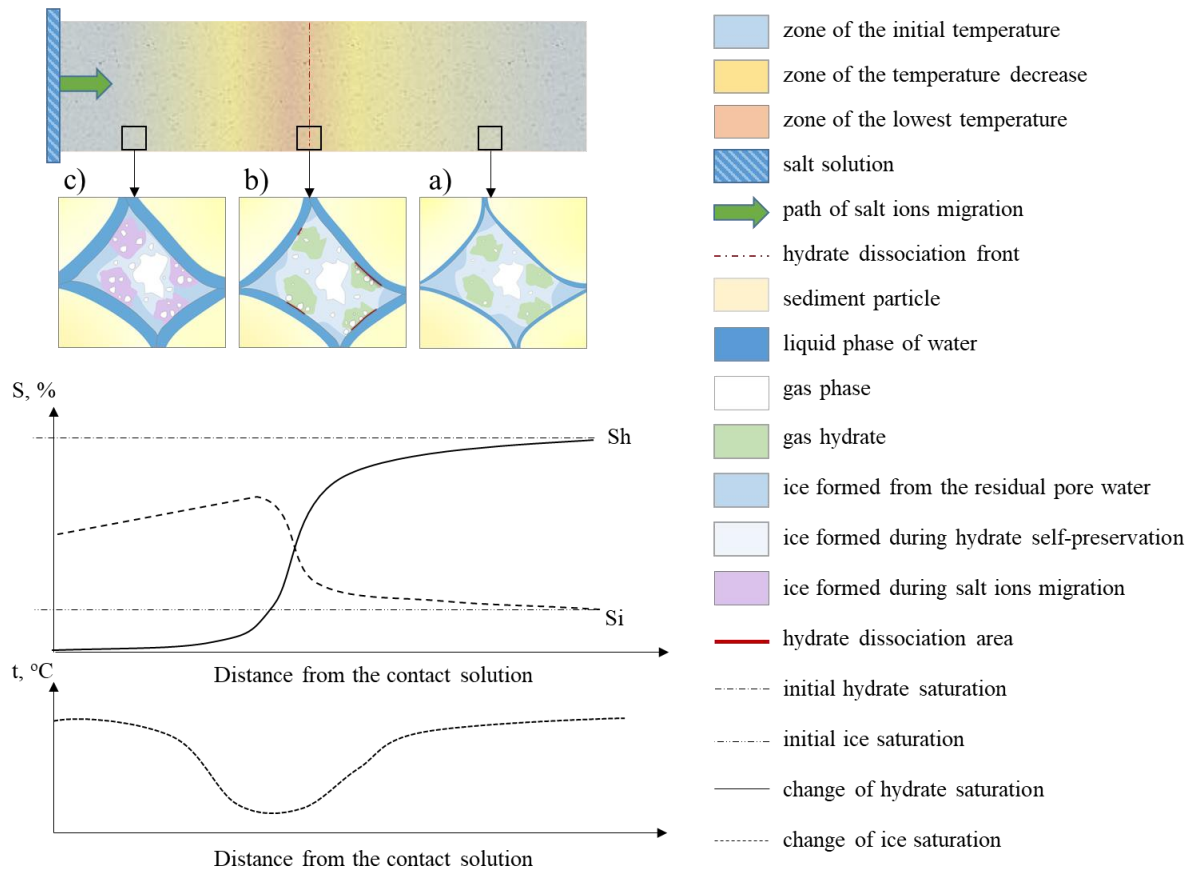


Figure 41. Scheme of temperature changes in a frozen hydrate-containing sample in the process of salt transfer, phase transformations, and changes in ice and hydrate saturation along the height of the investigated sample.

At some point in time after the start of the interaction with the salt solution, a cooling zone is clearly visible in the sample, caused by the dissociation of the pore gas hydrate and the melting of ice due to the migration and accumulation of salt ions. An analysis of phase transformations in the pore

space of sediment at a given point in time shows that in the region far from the contact, to where salt ions have not yet penetrated, the frozen hydrate-bearing sample has an initial temperature equal to the ambient temperature and initial values of ice and hydrate content. Under these conditions, the hydrate continues to exist in a preserved state without phase transitions (Figure 41a).

In the middle part of the sample, where the minimum temperature values are fixed, there is a dissociation front of the porous gas hydrate, which causes a local decrease in temperature (Figure 41b). In this region, a sharp decrease in hydrate saturation is observed due to the decomposition of pore hydrate. The water formed during the dissociation of the pore gas hydrate reduces the concentration of salts in the liquid phase. This, occurring under lower temperatures, contributes to its freezing, as a result of which an increased ice content is observed in the near-contact zone compared to the initial value, despite an increase in salt accumulation and an increase in the content of unfrozen water (Figure 41c). As a result, the temperature of the sample in the contact zone rises to the initial values, both due to the release of heat during freezing of water, and due to the temperature equalizing with the ambient temperature. In addition, in the near-contact area, when approaching the contact solution, ice saturation can decrease due to the high accumulation of salts, and, accordingly, the high content of unfrozen water.

Thus, salt migrates in frozen hydrate-bearing sediments more actively than in frozen non-hydrate-bearing frozen sediment and with greater temperature effect. That is due to a higher amount of potential paths for salt ions migration (mainly by the borders of ice crystals and unfrozen water). And the lower the pressure, the more active the hydrate dissociation due to higher unfrozen content and more intensive salt migration.

Conclusion to the Chapter 4.

Salt migration and accumulation has high influence on the process of hydrate decomposition, and decrease in temperature corresponds to the process of hydrate dissociation in the porous space, when

certain salt concentration is reached. The temperature reaching its minimum values indicates a decrease in the rate of decomposition of the gas hydrate and the beginning of the attenuation of this process. Then the temperature of the cooled zone of the sample begins to rise gradually and comes into equilibrium with the ambient temperature. This occurs both due to heat exchange with the environment, and due to the heat released during freezing of the water formed during the dissociation of the hydrate.

Chapter 5. Influence of the different factors on the process of salt migration in frozen hydrate-bearing sediments

During experimental modelling of the interactions of saline solution with methane hydrate-bearing frozen sediments the following factors were investigated: pressure, temperature, contact solution concentration and composition, and dispersity of the sediment.

5.1. Salt and mass transfer in sediment containing gas hydrate as a function of pressure

Earlier in Chapter 4.1, an analysis of the influence of pressure on interactions between saline solution and both hydrate-bearing and non-hydrate-bearing frozen sediments was made (Figure 26). And it was shown that the process of salt migration in frozen hydrate-containing samples strongly depends on pressure conditions, which determine gas hydrate stability in frozen sediments.

Figure 42 shows the thermobaric conditions for the existence of bulk methane hydrates, obtained by a computer simulation using the “HydraFlash” software [153]. In this case, points (T1-T6) show the P-T conditions of the aforementioned experiments investigating the interaction of frozen fine sand-2 containing methane hydrates with saline solution. As a part of the investigation, a series of 6 experiments

were devised, which were carried at a constant negative temperature of -6°C and at pressures ranging from atmospheric (0.1MPa) to 6.0 MPa. Two series of experiments were carried out at a pressure below equilibrium (under self-preservation conditions) (T1 - 0.1 MPa, T2 - 1.8 MPa), and the other three were carried out above equilibrium conditions (T4 - 3.5 MPa, T5 - 4.0 MPa, T6 – 6.0 MPa). In addition, P-T conditions of one series of experiment were close to the hydrate stability limit (T3 – 2.5 MPa at $P_{\text{eq}}=2.4$ MPa).

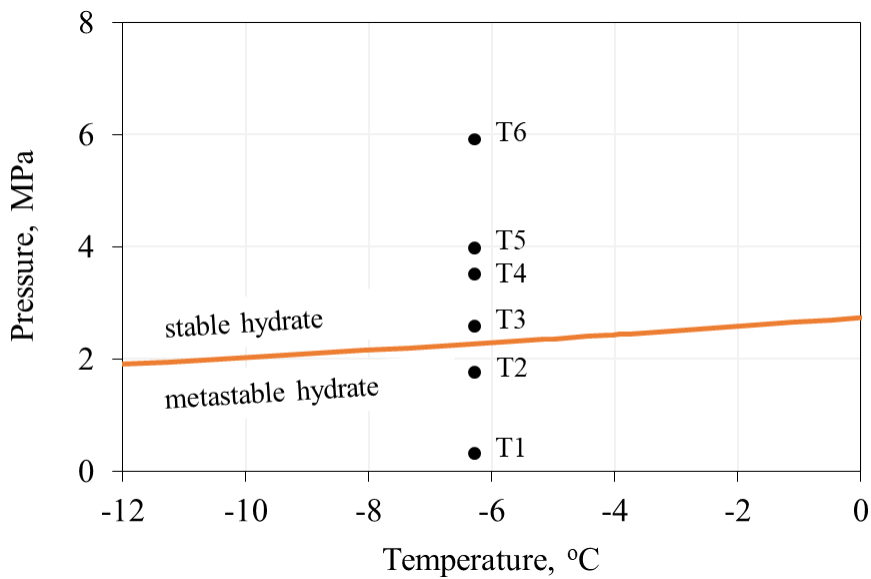


Figure 42. Modeling P-T conditions of methane hydrate stability in the HydraFlash program [153] and thermobaric conditions for conducting experiments on the migration of salt ions in frozen hydrate-bearing sediments (T1-T6).

A comparison of experimental data on the interaction of frozen hydrate-bearing sediments with salt solutions at a fixed negative temperature (-6°C) and pressures ranging from 0.1 MPa to 4.0 MPa demonstrates that with increasing pressure, the intensity of accumulation of salt ions (Na^+) decreases, as shown in Figure 43. A particularly significant reduction in the accumulation of salt ions was observed at gas pressures above equilibrium. The decrease in the intensity of accumulation of salt ions with

increasing pressure is reflected in the increase in the pore hydrate preservation at a fixed time of interaction.

Thus, in a frozen hydrate-containing sample (fine sand-2) 4 hours after interaction with a 0.1 N NaCl solution, Na⁺ ions penetrated 5.2 cm deep into the sample at a pressure of 0.1 MPa, and at a pressure of 4.0 MPa the penetration depth was only 3.4 cm. At the same time, the salt content in the contact zone decreased from 22 mg-EQ/100 g to 7 mg-EQ/100 g (Figure 43).

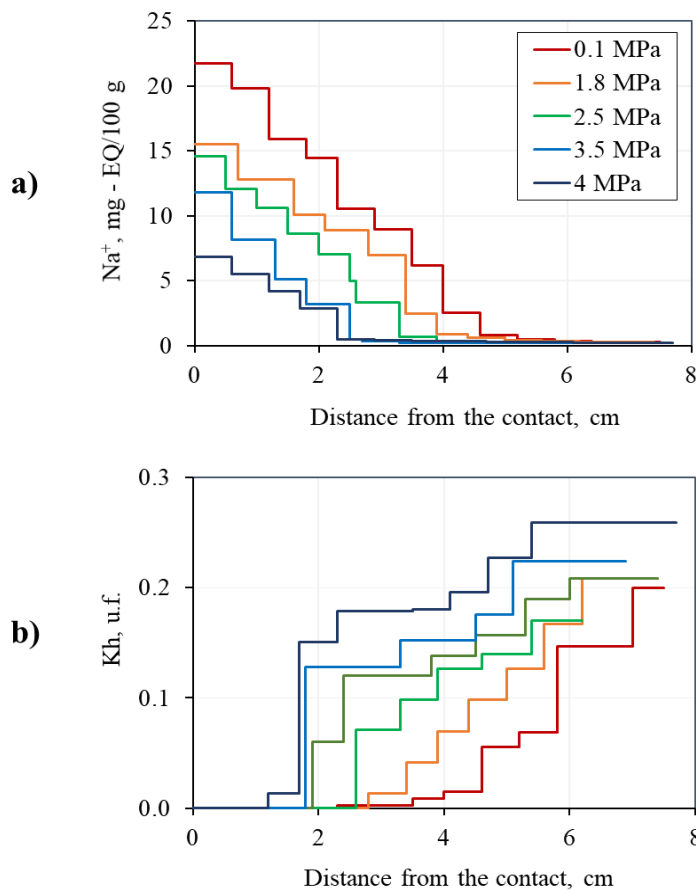


Figure 43. The effect of pressure on the accumulation of salt ions (Na⁺) (a) and the decrease in the hydrate coefficient (K_h) (b) in samples of frozen hydrate-bearing fine sand-2 ($K_h^{in} \sim 0.3$, W=12%) at non-equilibrium and equilibrium pressure 4 hours after the start of interaction with a frozen NaCl solution 0.1 N (t= -6°C).

The amount of salt ions accumulated in the studied samples determines the hydrate content. In the initial state (before the contact with the NaCl solution) for fine sand-2 samples, about 25% of the pore water was in the hydrate form. During one-sided salinization of the sample, a regular decrease in hydrate content was observed from the side of the contact zone. The hydrate coefficient decreases when moving from a pressure above equilibrium (4.0 MPa) to non-equilibrium (0.1 MPa), while the areas where there is a sharp decrease in hydrate content expand, as shown in Figure 43 b). So, 4 hours after the start of the interaction of hydrate-containing samples with a solution of 0.1 NaCl, the area of complete decomposition of the gas hydrate due to salinization changed from 1.8 cm at a pressure of 4.0 MPa to 3.4 cm at a pressure of 0.1 MPa (Figure 43b). Thus, it is possible to trace the presence of a gas hydrate decomposition front in the porous media of a frozen sample, the position of which depends on the pressure at fixed values of temperature and concentration of the contact salt solution.

The calculation of the average migration flow of salt through the frozen hydrate-bearing sample of sand for the described experiments shows that its value sharply decreases from $38 \cdot 10^{-10}$ to $0.5 \cdot 10^{-10}$ mol/(cm²·s) with an increase in pressure from 0.1 MPa to 6.0 MPa (Figure 44).

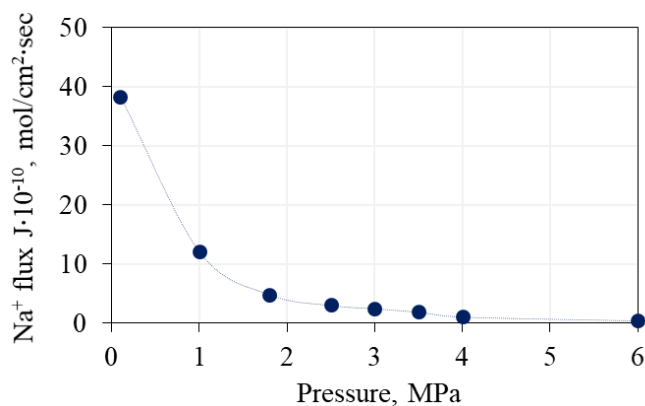


Figure 44. Influence of gas pressure on the flux density of Na⁺ ions through the cross section of a frozen hydrate-containing sample 4 hours after the start of interaction with a frozen salt solution 0.1 N NaCl (t = – 6°C).

Analysis of the salt accumulation in the studied samples and the change in hydrate content in the process of salt transfer made it possible to reveal the dependence of the critical concentration of salts in the sample (C_{cr}), which causes the complete decomposition of pore gas hydrates, on gas pressure at a fixed negative temperature (-6°C) and the concentration of the contact solution (0.1 N) (Figure 45). The detailed description of the process of critical concentration determination is given in the Chapter 3.6.

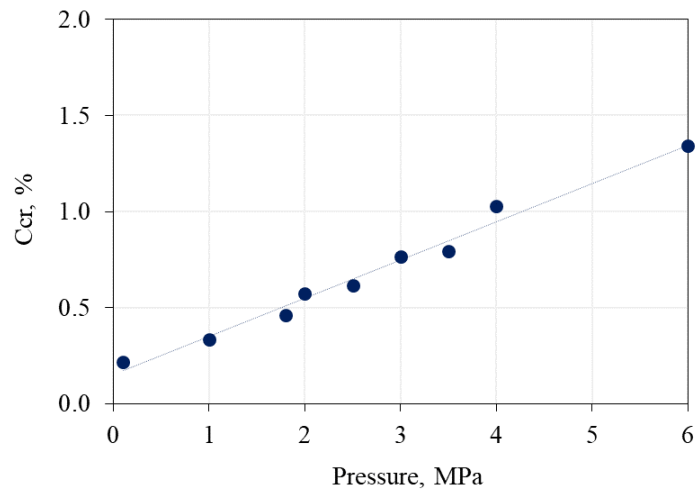


Figure 45. Dependence of the critical concentration (C_{cr}) causing decomposition of pore hydrate in a frozen sand sample on gas pressure ($t = -6^{\circ}\text{C}$, $C_{sol} = 0.1 \text{ N}$).

Studies show that the value of the critical concentration (C_{cr}) increases almost linearly ($R = 0.9672$) with increasing gas pressure at a fixed negative temperature. When the pressure rises from 0.1 to 6.0 MPa, the value of (C_{cr}) at -6°C increases nearly a factor of 7. Thus, at atmospheric pressure, the critical concentration of salts causing complete gas hydrate dissociation is 0.2% NaCl, and at 6.0 MPa it reaches 1.3% NaCl.

The empirical dependence of the critical salt concentration on pressure (Figure 46) obtained on the basis of experimental studies made it possible to calculate, for the interval values of the salt ion

concentration in the sample, the critical pressure values below which complete decomposition of the pore gas hydrate occurs.

The critical pressure values were compared with the gas pressure specified in the experiment. As a result, a salinization interval was identified along the length of the sample, where the calculated critical pressures corresponding to the values of salt accumulation exceed the gas pressures specified in the experiment. At a critical pressure below the experimental pressure, a residual content of pore hydrate is observed. In this case, the lower the concentration of salts, and, accordingly, the lower the critical pressure, the greater the residual content of hydrate. This made it possible to explain the nature of the distribution of salts and pore hydrate along the length of the sample and to find their relationship with the value of the gas pressure specified in the experiment. This pattern can be traced in Figure 46, which shows the distribution of sodium ion concentration and hydrate content along the height of a frozen hydrate-containing sample after interaction with NaCl salt solution at a fixed negative temperature (-6°C) and a given gas pressure (2.5 MPa).

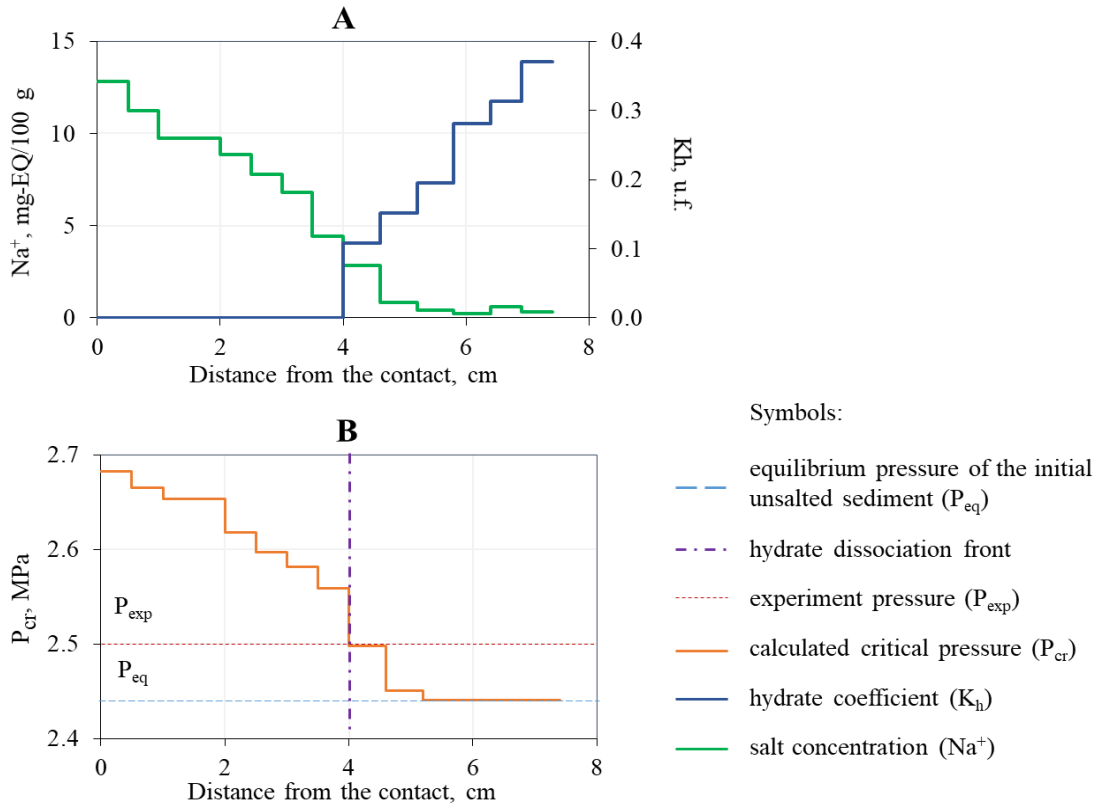


Figure 46. Altitude distribution of a frozen hydrate-containing sample (fine sand-2): (A) salt concentrations and hydration coefficient; (B) – critical pressure of dissociation of methane hydrate (concentration of contacting NaCl solution 0.1 N, $t = -6^\circ C$).

So, at the distance of 4 cm from the point of contact with a saline solution, no hydrate was recorded, but at the distances greater than 4cm, a residual hydrate content was observed. Figure 46B shows the critical pressure of pore gas hydrate decomposition calculated from the salt concentration for each interval of a frozen hydrate-containing sample and the given gas pressure of the experiment, as well as the equilibrium pressure characteristic of the initial non-saline sample. At distances up to 4 cm from the contact, the critical pressure of hydrate dissociation was higher than the given gas pressure, so the hydrate in this region completely dissociated. Thus, in few centimeters of the sample (from the contact area), as a result of the accumulation of salts, the critical pressure was 2.68 MPa, which is 0.18

MPa higher than the specified gas pressure in the experiment (2.5 MPa). And at a distance of more than 4 cm, the given gas pressure exceeds the critical pressure and therefore residual hydrate content is observed. Thus, in the range from 4.5 to 5 cm, the critical pressure is 2.45 MPa, which is 0.05 lower than the experimental pressure.

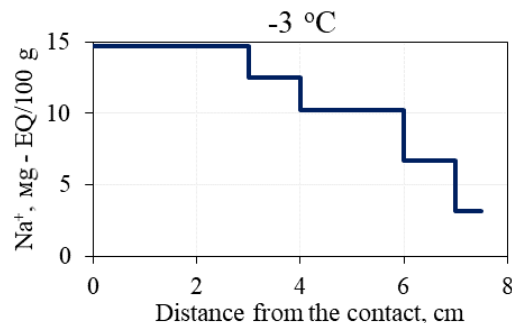
Also, thermodynamic modeling was carried out using software “HydraFlash” software [153] to assess the equilibrium values of salt concentration for methane hydrate for given thermobaric conditions. According to “HydraFlash” calculations, the equilibrium values of salt concentrations for the considered pressures turned out to be higher than the critical concentrations obtained in the experiments. So, at a temperature of -6°C and a pressure of 4.0 MPa, the equilibrium concentration defined in software for methane hydrate is 15%, and at 2.5 MPa it is 0.8% (1% and 0.6% according to the experimental investigations). Such a difference between them is primarily due to the fact that in calculations of the equilibrium concentration of salts, its value is considered in relation to the volume of bulk hydrate. And in the experiment, there was a local non-equilibrium accumulation of salt ions at the boundary with hydrate particles, as well as strong influence of sediment pore media.

So, during the experiments, it was revealed that in frozen hydrate-containing sediment samples, when the pressure decreases from values above equilibrium (>2.4 MPa) to pressures below equilibrium (up to 0.1 MPa), the flow of salts into the sample increases significantly. When the pressure drops from 6.0 MPa to 0.1 MPa at a fixed negative temperature (-6°C), the salt flux into a frozen hydrate-containing sample increases by a factor of 40.

5.2. Temperature influence on the process of hydrate-bearing sediment interaction with saline solutions

As is well known, from the thermobaric point of view an increase in temperature shifts the conditions for the stability of gas hydrates towards higher pressures. The study of the temperature influence on the dissociation of gas hydrate in porous media was considered on the frozen fine sand-2 containing methane hydrate. Samples in the initial state had a uniform distribution of methane hydrate ($K_h=0.4$) in porous media, and water content equal to 12%.

The temperature influence on the processes of salt transfer in frozen hydrate-containing sandy sediments was considered in the range from -2°C to -20°C at the pressure 0.1 and 4 MPa. During the experiments, it was found that with an increase in the ambient temperature, salinization processes are intensified, which accelerates the hydrate decomposition in the porous space of frozen hydrate-containing sediments. At a higher negative temperature (-3°C), during the experiment of 2 hours, NaCl ions, unlike other temperature conditions (-6°C and -20°C), penetrate almost the entire depth (8 cm) of a frozen hydrate-containing sample of fine sand-2 (Figure 47). At the same time, in a sample with a lower temperature (-6°C), salt ions migrated to a depth of up to 6 cm from contact, and at -20°C only up to 2.2 cm from contact with a salt solution ($C_{\text{sol}}=0.2\text{N NaCl}$).



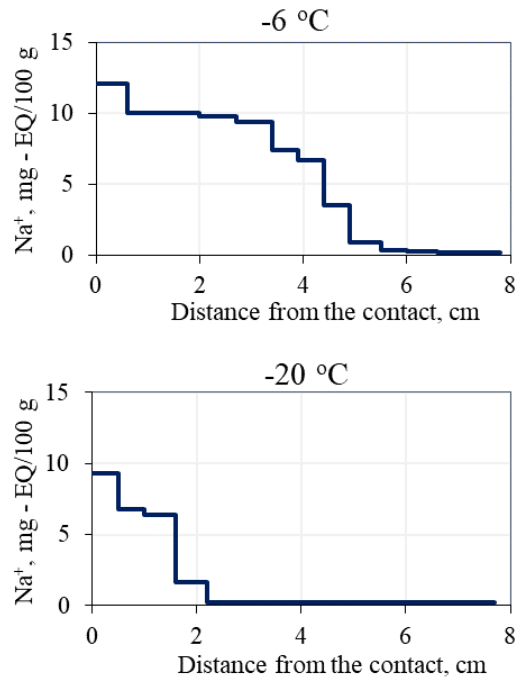


Figure 47. Effect of temperature on the accumulation of salt ions (Na^+) in frozen hydrate-containing samples (fine sand-2) after 2 hours of interaction with 0.2 N NaCl solution ($P=0.1$ MPa).

As a result of migration and accumulation of salts in frozen hydrate-bearing samples (fine sand-2), interacting for 2 hours with a salt solution (0.2 N NaCl), methane hydrate completely decomposed to a depth of 7 cm from contact at a temperature of -3°C . In addition, the residual hydrate content ($K_h=0.22$ in comparison with the initial value equals $K_h^{\text{in}}=0.4$) was observed only in the top part of the sample, as shown in Figure 48. In the experiment at an ambient temperature of -6°C , the porous gas hydrate completely decomposed in the region of 3.5 cm from the contact. Although at a lower negative temperature (-20°C), partial decomposition of the hydrate was recorded only in the near-contact region (1 cm from the contact), where the hydrate coefficient decreased from the initial 0.37 to 0.1 (Figure 48).

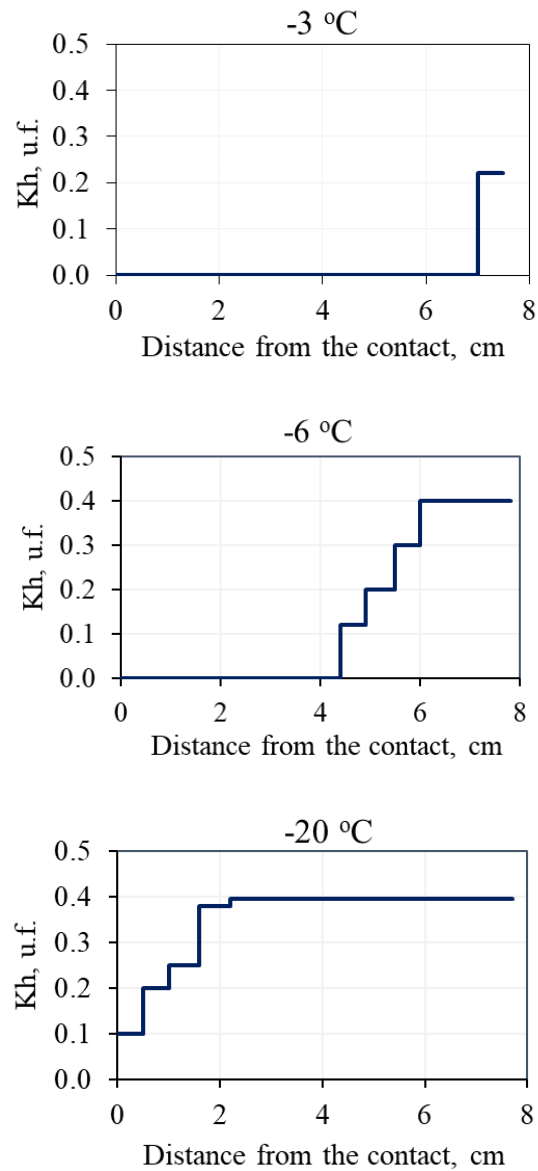


Figure 48. The effect of temperature (-3, -6, -20°C) on the decrease in the hydration coefficient (K_h) in samples of frozen hydrate-containing fine sand-2 ($K_h^{in} \sim 0.4$, $W=12\%$) 2 hours after the start of interaction with frozen 0.2 N NaCl salt solution.

The calculation of the average migration flow of salt for the described experiments shows that its value decreases with decreasing temperature (Figure 49). So, at -2°C the salt flux was $70 \cdot 10^{-10}$ mol/cm²·s,

at -6°C the Na^+ flux decreased more than 3 times to $20 \cdot 10^{-10} \text{ mol/cm}^2 \cdot \text{s}$, and at -20°C Na^+ flux did not exceed $4.2 \cdot 10^{-10} \text{ mol/cm}^2 \cdot \text{s}$ (Figure 49).

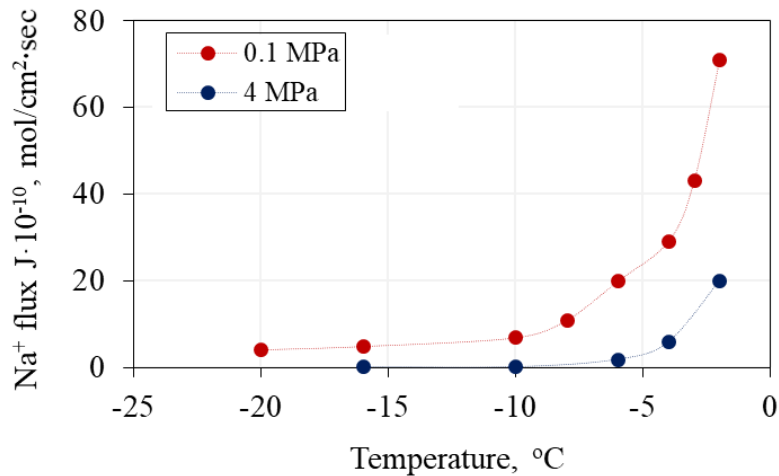


Figure 49. Effect of temperature on the average Na^+ flux into a frozen hydrate-containing sample (fine sand-2) for 4 hours of interaction with a frozen salt solution of 0.1N NaCl (P=0.1 and 0.4 MPa).

When study of the temperature influence on salt migration in hydrate-bearing frozen sediment (fine sand-2) at the pressure above equilibrium (4 MPa), the same general dependence was obtained: decrease of temperature lowering the Na^+ flux. However, the values of average salt flow is lower at the gas pressure 4 MPa, than at the atmospheric pressure. Thus, Na^+ flux was equal to $20 \cdot 10^{-10} \text{ mol/cm}^2 \cdot \text{s}$ at gas pressure 4 MPa and temperature -2°C , what is more than 3 times lower, than at the atmospheric pressure. And at the pressure 4 MPa and -6°C Na^+ flux was equal to $2 \cdot 10^{-10} \text{ mol/cm}^2 \cdot \text{s}$ – by factor 10 lower, than at the pressure 0.1 MPa (Figure 49).

The analysis of salt accumulation in the studied samples and the change in hydrate content in the process of salt transfer made it possible to reveal the dependence of the critical salt concentration in the sample (C_{cr}), which causes complete decomposition of metastable (self-preserved) porous gas hydrates

(at P=0.1 and 4 MPa), on temperature during the interaction of frozen hydrate-containing sediments (fine sand-2) with NaCl solution (0.1N) (Figure 50).

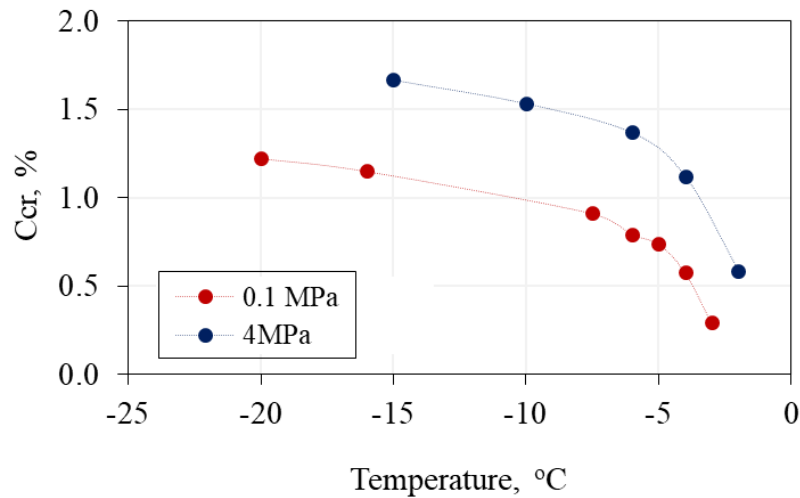


Figure 50. Effect of temperature on the critical concentration (Ccr) causing decomposition of pore hydrate in a frozen sand sample (fine sand-2, P=0.1 and 4MPa, $C_{sol}=0.1N$).

Experimental data show that the critical concentration (Ccr) increases with decreasing ambient temperature (Figure 50). So, at atmospheric pressure and a temperature of $-3^{\circ}C$, the critical concentration (Ccr) was 0.3% NaCl for pore water, at a temperature of $-10^{\circ}C$ - 1%, and at $-16^{\circ}C$ - it reached 1.2%, which is actually 4 times exceeds the critical concentration at $-3^{\circ}C$.

With an increase in pressure and the transition of a hydrate-containing system to an equilibrium state, the value of the critical concentration at a fixed negative temperature increases. But general dependence of the critical concentration increase with temperature decrease was observed as well. Hence, critical concentration increases from 1.1 to 1.4% NaCl in pore water at gas pressure 4MPa with temperature decrease from -4 to $-6^{\circ}C$, while at 0.1MPa Ccr change in this temperature range 0.6 to 0.8%.

Such obtained dependence can be explained the following way. Under conditions of increasing experimental (ambient) temperature, the process of migration of salts from the contact solution into the frozen hydrate-containing sample increases, which leads to faster dissociation of the porous gas hydrate due to an increase in the accumulation of salt ions and a decrease in the critical concentration required for the complete decomposition of the porous gas hydrate, as in conditions of initially equilibrium pressure, and under conditions of self-preservation.

Thus, the influence of temperature on the intensity of mass transfer in frozen hydrate-containing sediments and the intensity of hydrate dissociation during interaction with salt solutions have been experimentally obtained. It is noted that with a decrease in temperature, the preservation of methane hydrate in porous media of frozen sediment increases, due to the slowing down of the processes of migration of salt ions. The critical concentration of Na^+ ions in frozen hydrate-containing sediment samples increases by a factor of 8 with a decrease in negative temperature from -3 to -16°C . Finally, the average Na^+ flux decreases exponentially (by a factor 10) when temperature decreases from -3 to -20°C .

5.3. Influence of salt solution concentration on the intensity of salt migration and hydrate dissociation in hydrate-bearing sediments

Before the start of the experimental modeling on the interaction of frozen hydrate-bearing sediments with salt solution of different concentration, computer simulation of thermobaric conditions for the stability of methane hydrate in salt solution system were calculated depending on the concentration of NaCl in “HydraFlash” software [153] (Figure 51).

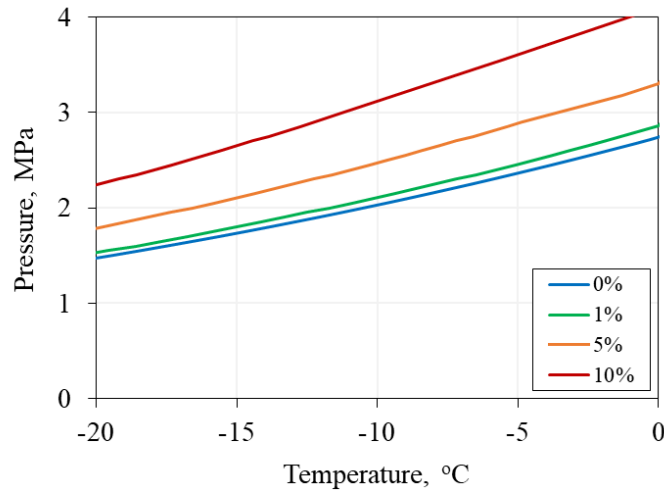


Figure 51. Thermobaric conditions of hydrate stability in the water-NaCl solution of different concentration simulated in “HydraFlash” software [153].

The results of thermodynamic modeling showed that the presence of salts shifts the stability conditions of methane hydrate towards higher pressures and lower temperatures from a thermodynamic point of view. This shift depends on the concentration of salts. So, at a fixed pressure of 2.5 MPa, with an increase in NaCl concentration from 1 to 5%, the equilibrium temperature decreases from -5 to -10°C.

It can be assumed that for metastable hydrates in the pore space of frozen sediment, the concentration of salts (NaCl) will also have a significant impact on their preservation at a fixed negative temperature.

As part of the experimental simulation, two series of experiments were carried out. The first series was aimed at studying the influence of the concentration of the contacting NaCl solution on the processes of dissociation of pore gas hydrate in frozen sediment (fine sand-2) under non-equilibrium (metastable) conditions ($P=0.1$ MPa), when the dissociation of pore gas hydrate is determined mainly by the kinetics of salt transfer. The second series of experiments is devoted to studying the influence of

the concentration of the contacting NaCl solution on the processes of hydrate dissociation under stable conditions ($P=4$ MPa), when the dissociation of pore gas hydrate is determined by thermodynamic and kinetic factors.

An increase in the concentration of a salt solution in contact with frozen hydrate-bearing fine sand-2 at a fixed negative temperature (-6°C) and atmospheric pressure (i.e. below equilibrium) leads to more intensive migration and accumulation of salt ions in the sample. Thus, at a contact solution concentration of 0.1N at a fixed interaction time (4 hours), salt ions (Na^+) migrated to a depth of 4.5 cm from the contact into hydrate-bearing frozen sand (Figure 52). With an increase in the concentration of the contact solution to 0.2N, the salinization zone of the frozen hydrated sample increased to 5.2 cm (Figure 52), and at a concentration of 0.4N, salt ions penetrated almost the entire depth of the sample (7 cm) (Figure 52).

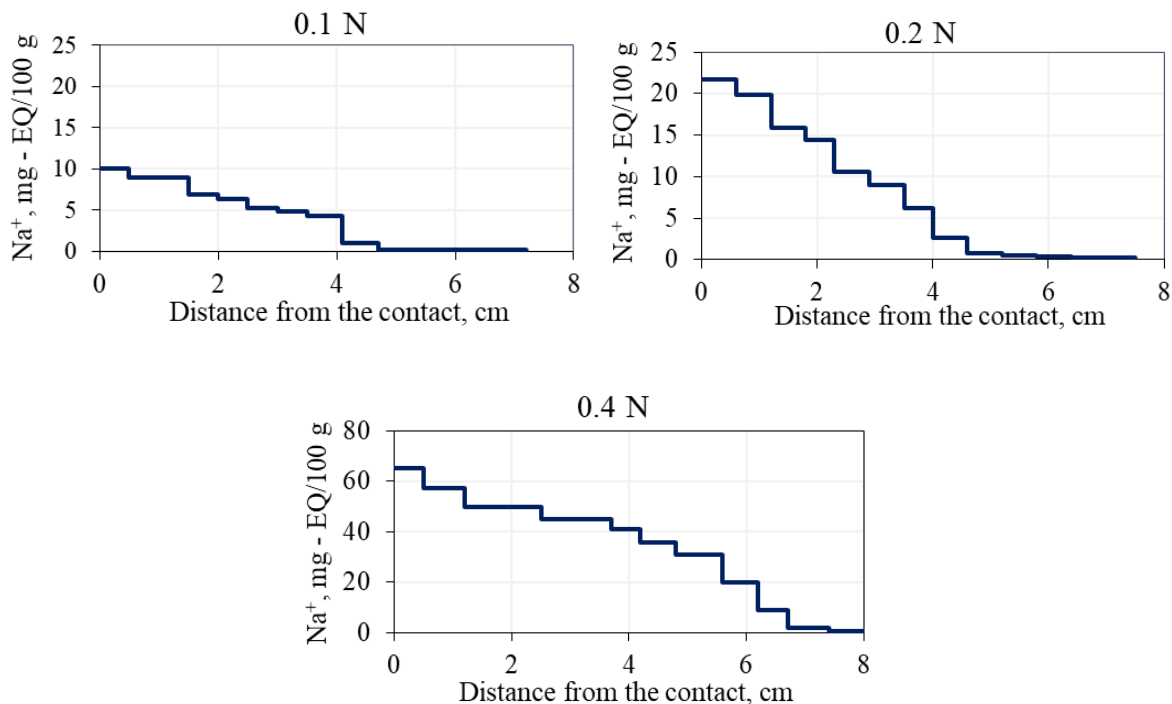


Figure 52. Effect of contact solution concentration on the accumulation of salt ions (Na^+) in frozen hydrate-containing samples (fine sand-2) after 4 hours of interaction with NaCl solution ($t=-6^{\circ}\text{C}$, $P=0.1$ MPa).

The amount of salt ions accumulation in the studied sand samples determines the distribution of hydrate over the sample. In the initial state (before contact with the solution), about 40% of the pore water in the sand samples (fine sand-2) was in the hydrate form. In the course of one-sided salinization of the sample, a regular decrease in hydrate content was observed from the side of the contact zone. With an increase in the concentration of the NaCl contact solution from 0.1 to 0.4N at a fixed interaction time (4 hours) and a temperature (-6°C), the area of a sharp decrease in the hydrate coefficient expands significantly, as shown in Figure 53.

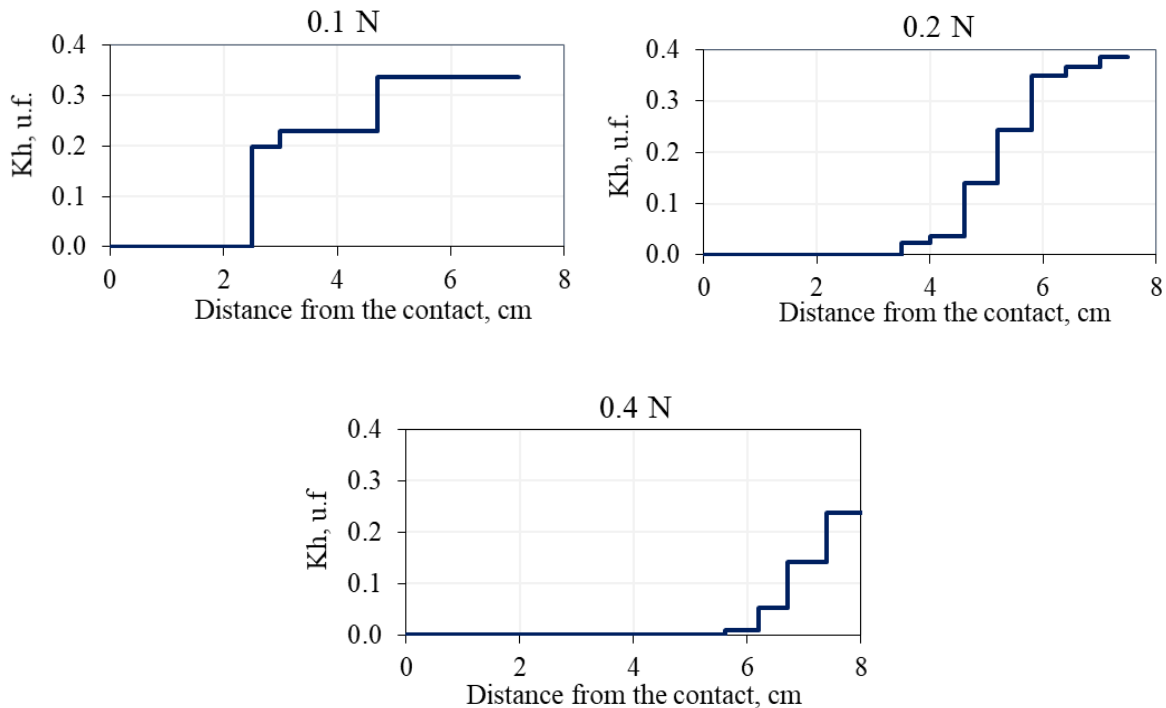


Figure 53. Influence of NaCl contact solution concentration on the distribution of hydrate coefficient (K_h) along the length of frozen hydrate-containing samples (fine sand-2) ($K_h^{\text{in}} \sim 0.4$, $W=12\%$) after 4 hours of interaction ($t=-6^{\circ}\text{C}$, $P=0.1 \text{ MPa}$).

Thus, with an increase in the concentration of the contact solution from 0.1 to 0.4 N, the area of complete decomposition of the gas hydrate due to salinity changed from 2.5 cm to 5.6 cm (Figure 53).

At the same time, a decrease in the hydrate coefficient (K_h) was also observed in the interval of the sample (fine sand-2), where residual hydrate was fixed.

Thus, it is possible to trace the shift of the decomposition front of porous gas hydrate in frozen samples depending on the concentration of the contact salt solution.

In the experiment with a frozen hydrate-containing sample (fine sand-2) interacting with a NaCl solution at a pressure above equilibrium (4.0 MPa), similar dependence was obtained, which indicate a more active accumulation of salt ions and dissociation of pore methane hydrate with an increase in the concentration of the contact NaCl solution, as shown in Figure 54. At this pressure, after 4 hours salt ions (Na^+) migrated into hydrate-bearing frozen fine sand-2 to a depth of 3.4 cm from contact with a 0.1N NaCl solution. And with an increase in the concentration of the solution to 0.2N, salt ions were fixed at a depth of 6 cm (Figure 54).

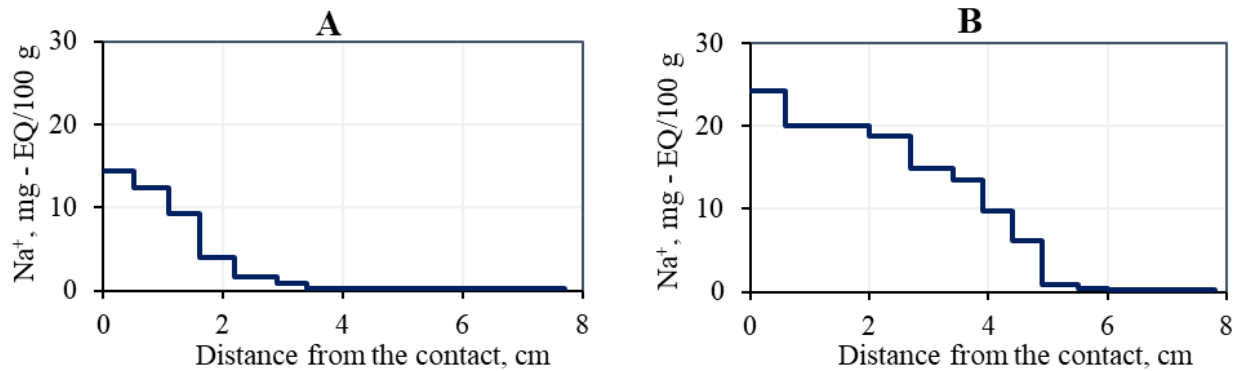


Figure 54. Influence of the contact solution concentration on the accumulation of salt ions (Na^+) in frozen hydrate-containing samples (fine sand-2) interacting for 4 hours under a pressure of 4.0 MPa with a NaCl solution ($t=-6^\circ\text{C}$): A – 0.1N; B – 0.2N.

An increase in the intensity of salt ions migration and accumulation in frozen hydrate-bearing sediments interacting with a NaCl solution at a pressure above equilibrium (4.0 MPa) with an increase in the concentration of the contact solution was also accompanied by a more active hydrate

decomposition. Thus, in the initial state (before contact with saline solution) in frozen hydrate-containing samples, about 40% of pore water was in the gas hydrate form. After 4 hours of the contact of the frozen hydrate-containing sample (fine sand-2) with saline solution at -6°C , the pore hydrate completely decomposed at a distance of 1.6 cm from the contact area with 0.1N NaCl solution, and at a distance of 4.4 cm from the contact area with 0.2N NaCl solution (Figure 55).

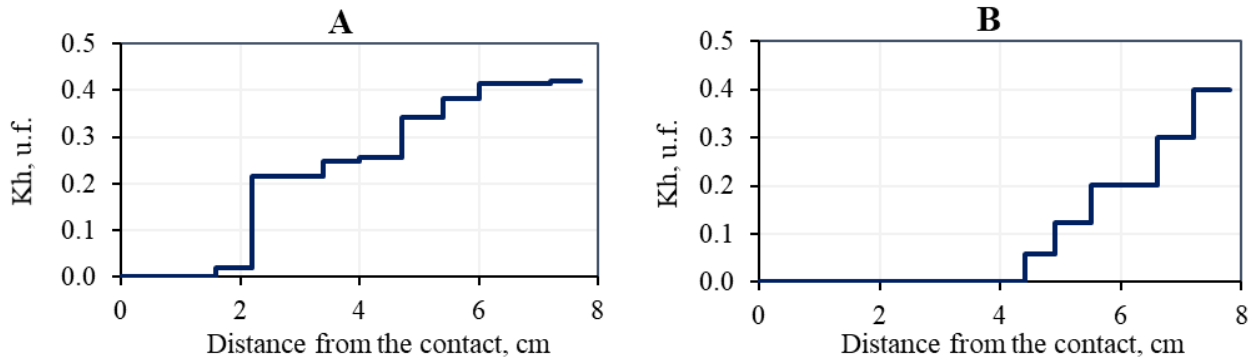


Figure 55. Effect of contact solution concentration on distribution of hydrate coefficient (K_h) along the height of frozen hydrate-containing sample (fine sand-2, $K_h^{\text{in}} \sim 0.4$, $W=12\%$) after 4 hours of the interaction with frozen NaCl salt solution ($t=-6^{\circ}\text{C}$, $P=4.0$ MPa): A – 0.1N; B – 0.2N.

With an increase in the concentration of the contact solution, the average Na^+ flux into the frozen hydrate-containing sample increases. Thus, when frozen hydrate-bearing fine sand-2 interacted with a 0.1N NaCl solution at atmospheric pressure, the Na^+ flux was $1 \cdot 10^{-10}$ mol/cm²·s, and with an increase in concentration to 0.4 N, the Na^+ flux increased to $8.2 \cdot 10^{-10}$ mol/cm²·s (Figure 56). A similar dependence was also observed in experiments at a pressure above equilibrium (4.0 MPa): with an increase in the concentration of the NaCl contact solution from 0.1 to 0.4 N, the average Na^+ flux in them increased from 0.4 to $4.6 \cdot 10^{-10}$ mol/cm²·s, however these values were lower than the salt fluxes in frozen hydrate-bearing fine sand-2 under atmospheric pressure conditions (Figure 56).

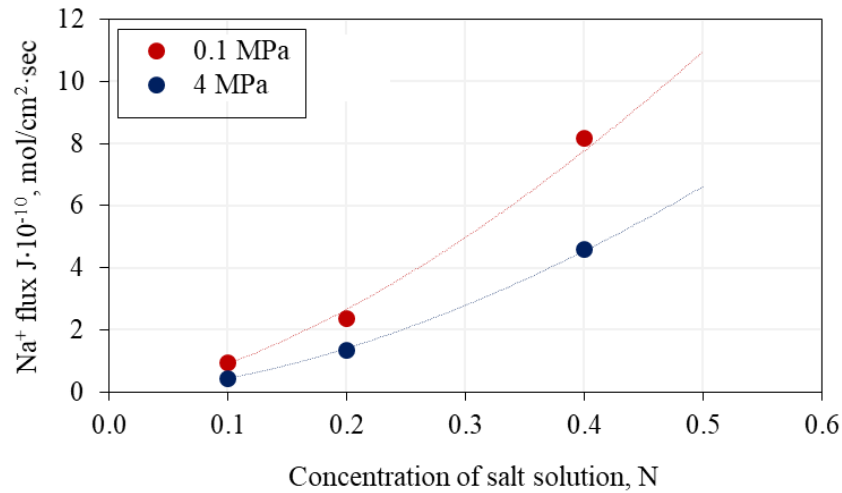
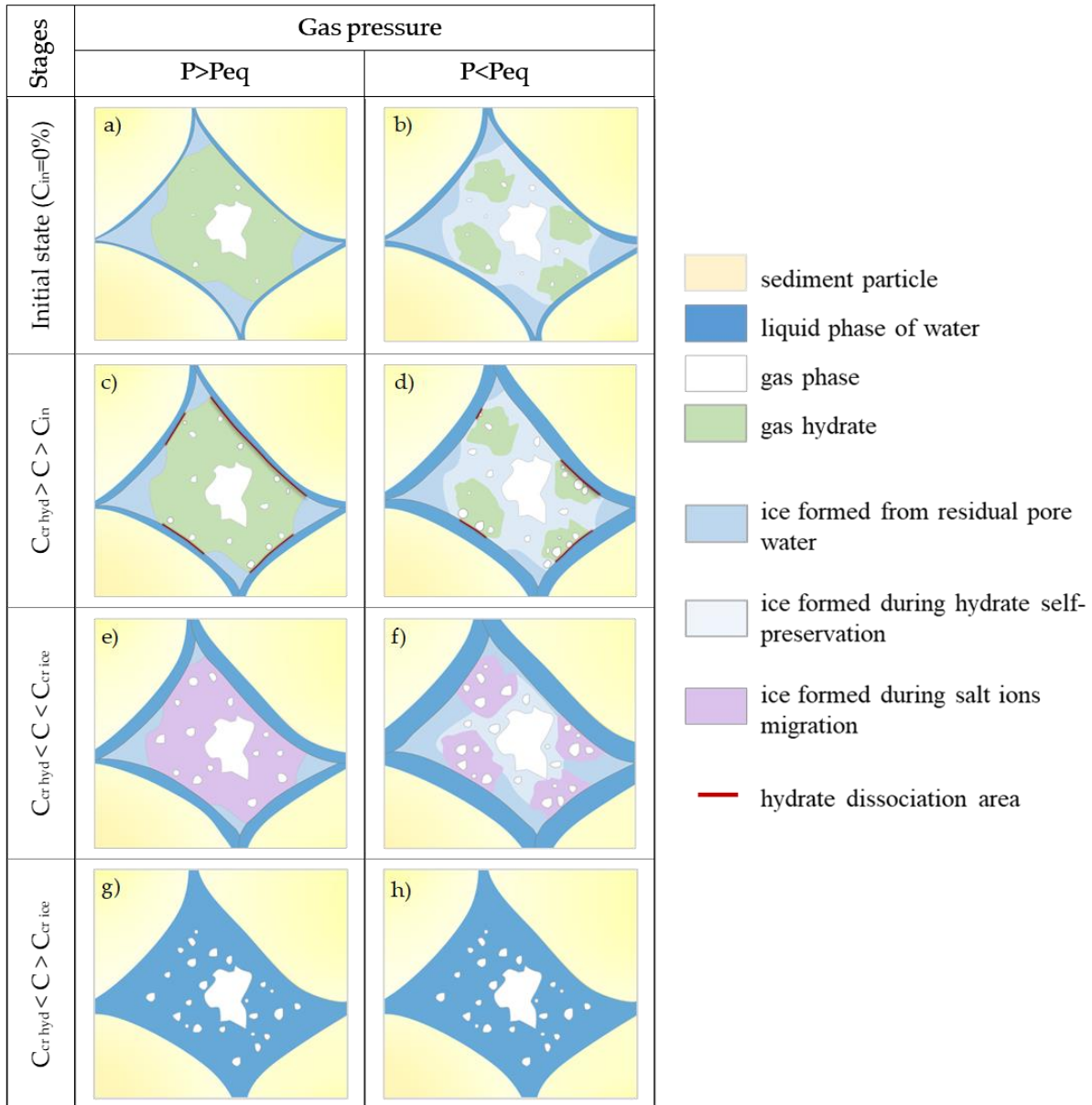


Figure 56. Influence of contact solution concentration on the average Na⁺ flux in frozen hydrate-bearing sample (fine sand-2) after 4 hours of the interaction ($t = -6^{\circ}\text{C}$, $P = 0.1$ MPa and 4.0 MPa).

An analysis of the experimental modeling data and previous data on hydrate and ice in porous media makes it possible to assume phase changes in frozen hydrate-containing sediment in the process of salt migration at equilibrium and non-equilibrium (with self-preservation) gas pressure under the influence of different concentration (Table 9). In the initial state before the start of the experiment, the concentration of salts in the pore solution of the sample is close to zero. At the same time, under conditions of a fixed negative temperature (-6°C) and a pressure above equilibrium (4 MPa), the pore methane hydrate in the initially non-saline frozen sand was in stable conditions (Table 9a).

After contact with a saline solution at a temperature of -6°C in a frozen sample, an increase in the concentration of salts in the pore space occurs as a result of their migration and accumulation. The migration of salt ions from the contact solution occurs primarily along the films of unfrozen water on the surface of sediment particles, as well as along the boundaries of ice crystals. This is accompanied by an increase in the thickness of unfrozen water films due to partial dissociation of the hydrate and melting of pore ice (Table 9c).

Table 9. Scheme of phase-transformation in the pore space of the frozen hydrate-bearing sediments during increase of salt solution concentration at stable conditions (experimental pressure $P_{exp} \geq$ equilibrium pressure P_{eq}) and metastable conditions ($P_{exp} < P_{eq}$).



Upon reaching a certain critical salt concentration ($C > C_{cr\ hydr}$) there is a sharp increase in the rate of hydrate dissociation, which leads to its complete decomposition. The water formed in this case under

conditions of negative temperature and the endothermic effect of dissociation is supercooled and then frozen (Table 9e).

A further increase in salt concentration to values above the critical concentration of pore ice melting ($C > C_{cr \text{ ice}}$), which can be observed when a frozen hydrate-containing sample comes into the contact with a high-concentration salt solution (non-freezing at a given negative temperature), will be accompanied by complete thawing of the sample (Table 9g).

With a decrease in gas pressure below the equilibrium, the pore hydrate in frozen sediment can pass in a metastable state due to the manifestation of the self-preservation effect (Table 9b). Under these conditions, the residual gas hydrate inclusions in frozen sediment will be under the ice cover, which was formed due to the crystallization of water released during the partial dissociation of the pore gas hydrate at a negative temperature.

Under these conditions, the interaction of a salt solution with frozen sediments containing porous gas hydrate under metastable conditions is also accompanied by the migration and accumulation of salt ions. However, this process is more active, and the critical concentration causing the decomposition of pore methane hydrate will be lower than when interacting under stable conditions ($P > P_{eq}$) (Table 9d).

Studies [217] show that the equilibrium content of the liquid phase of water at a pressure above equilibrium ($P > P_{eq}$) is less than in a hydrate-containing sample in a metastable state ($P < P_{eq}$). Taking into account that the migration of salt ions occurs mainly through films of unfrozen water, the process of salt ions migration in frozen sediments containing metastable gas hydrate will occur more intensively than at pressures above equilibrium.

In addition, the role of intergranular (along crystal boundaries) permeability of pore hydrate and ice in the migration of salt ions in frozen hydrate-bearing sediment should be noted. From the literature [316] it is known that the intergranular (ionic) permeability of pore ice contributes significantly to salt

transport in frozen sediment. It can be assumed that the intergranular permeability of the hydrate is much lower than the permeability of ice. Thus, in frozen hydrate-containing sediment under non-equilibrium conditions, which are usually characterized by an increased ice content compared to stable conditions, the critical concentration of pore gas hydrate dissociation is reached faster (Table 9f). However, this description of phase transformation require additional research on mirco-scale level.

Thus, the experimental data show that an increase in the concentration of the contact solution (NaCl) increases the accumulation of salt ions in frozen hydrate-bearing sediments and activates the dissociation of pore gas hydrate. This is observed both at pressures below equilibrium, when the porous gas hydrate is in the metastable conditions, and at pressures above equilibrium (4.0 MPa). However, in the latter case, the intensity of these processes decreases.

5.4. The process of interaction of hydrate-containing sediments with salt solutions of various chemical compositions

Thermodynamic modeling of the conditions of P-T stability of methane hydrate in the bulk volume for negative temperatures (from 0 to -20°C) for the most widespread salts in the permafrost (NaCl, CaCl₂, MgCl₂, KCl and Na₂SO₄) in the "HydraFlash" software [153], carried out before the start of the experiments. It demonstrated a significant shift in the stability conditions of methane hydrate, depending on the chemical composition of the studied salts. It was found that the value of the equilibrium conditions for hydrate stability shifts to lower temperatures and pressures in the following series of salts of 5wt% concentration: Na₂SO₄ - KCl - CaCl₂ - NaCl - MgCl₂. Thus, for a temperature of -5°C, the pressure shift for Na₂SO₄ was 2.8 MPa, and for MgCl₂ it was 3.8 MPa compared to a non-saline gas-water system (Figure 57).

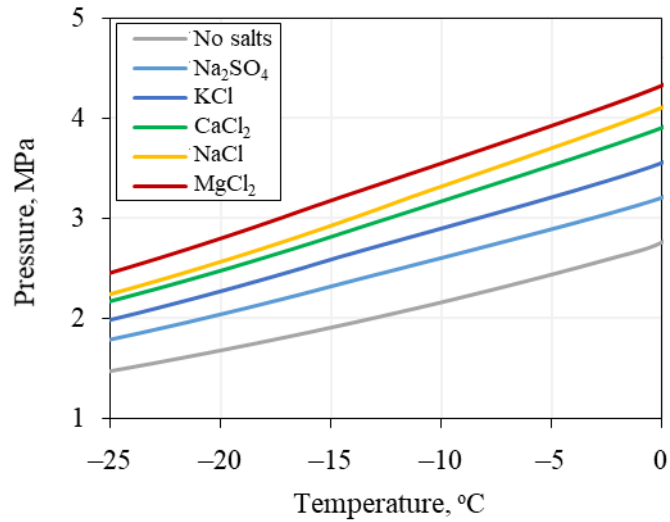


Figure 57. Influence of a chemical composition of salt solution (Na_2SO_4 , KCl , CaCl_2 , NaCl , MgCl_2) with a concentration of 5wt% on the conditions of methane hydrate stability in the range of negative temperatures from 0 to -20°C (calculations were made in the “HydraFlash” software [153]).

The obtained results of thermodynamic modeling generally coincide with the existing data presented by other researchers [183,192,200].

For salts of various chemical compositions used in the calculations, special experiments were carried out on their interaction with samples of frozen hydrate-bearing sand (fine sand-2). The experiments were carried out at a fixed temperature (-6°C), atmospheric pressure and salt concentration (0.1N). For the comparison of the experimental results equivalent concentration was used (mg-EQ/100 g) for each salt, and in addition it was recalculated in weight percent (wt%) for the critical concentration determination.

Figure 58 shows the accumulation of salt ions in samples of frozen hydrate-bearing sand interacting with salt solutions of various chemical compositions (NaCl , CaCl_2 , MgCl_2 , KCl and Na_2SO_4). The obtained experimental data demonstrate that the intensity of migration and accumulation of salts increases in the series $\text{Na}_2\text{SO}_4 - \text{KCl} - \text{CaCl}_2 - \text{NaCl} - \text{MgCl}_2$ (Figure 58).

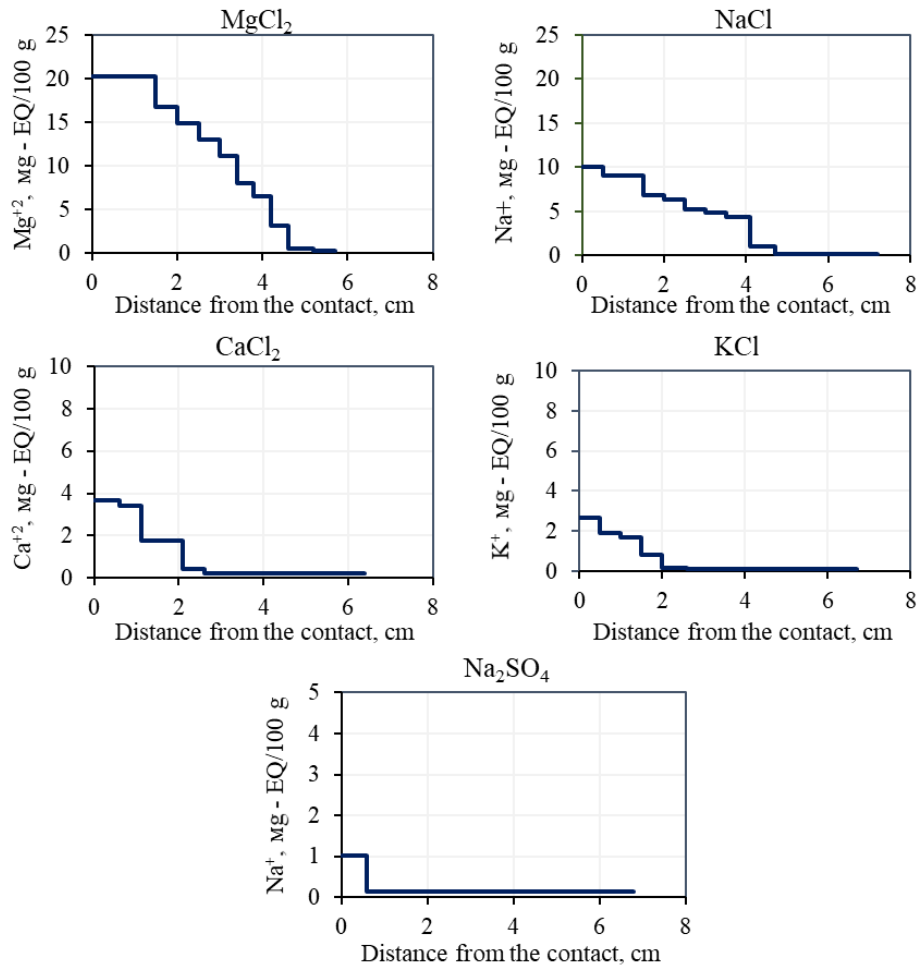


Figure 58. Accumulation of Na⁺ ions in samples of frozen hydrate-bearing sand (fine sand-2, W=12%) after 4 hours of contact with 0.1N NaCl solution of different composition ($t = -6^{\circ}\text{C}$, $P = 0.1\text{MPa}$).

Thus, 4 hours after the start of the interaction, the maximum penetration of salt ions (up to 5 cm) was recorded in the sample in contact with the MgCl₂ solution. For the NaCl solution, this value did not exceed 4.6 cm, while for the CaCl₂ and KCl solutions it was 2.8 and 2 cm, respectively. The smallest depth of salt accumulations was observed in the sample interacting with the Na₂SO₄ solution (about 0.6 cm).

The distribution of the residual content of hydrates in samples of frozen hydrate-bearing sand after 4 hours of their interaction with salt solution of various chemical composition confirms the revealed

pattern in the described series: $\text{Na}_2\text{SO}_4 - \text{KCl} - \text{CaCl}_2 - \text{NaCl} - \text{MgCl}_2$, which is determined by the intensity and magnitude of the salt accumulations and hydrate dissociation. In this series, there is a regular decrease in the residual content of gas hydrate in the pore space of sand (fine sand-2). So, if in the initial (before contact) state, about 40-50% of the pore water was in the hydrate form, then after 4 hours of interaction with the MgCl_2 solution, the pore hydrate completely dissociated in the range up to 4.5 cm from the contact (Figure 59).

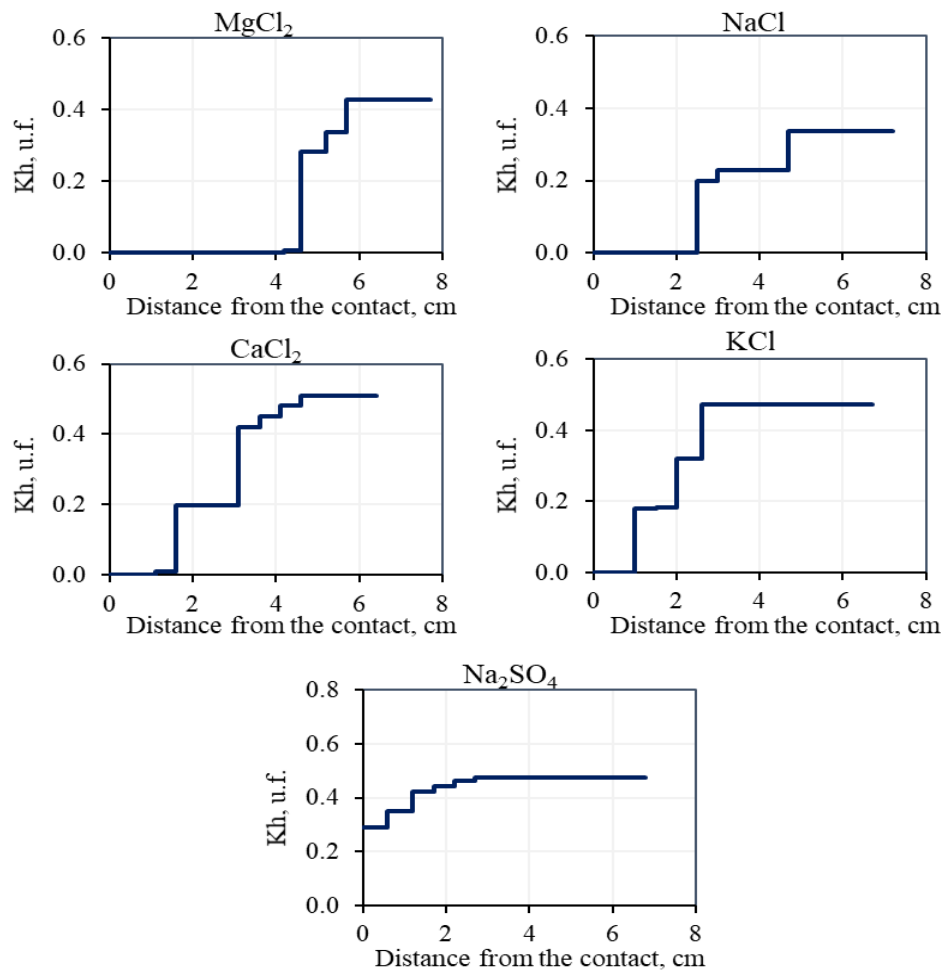


Figure 59. The influence of the chemical composition of the contact salt solution on the decrease in the hydrate coefficient (K_h) in frozen hydrate-containing samples (fine sand-2, $K_h^{\text{in}} \sim 0.5$, $W=12\%$) after 4 hours of interaction with the frozen salt solution ($t=-6.5^\circ\text{C}$, $C_{\text{sol}}=0.1\text{N}$, $P=0.1\text{MPa}$).

In the case of the NaCl solution hydrate dissociate up to 3.4 cm, and in the case of CaCl₂ and KCl, this interval did not exceed 2 cm and 1 cm, respectively. In the experiment with a solution of Na₂SO₄, in contrast to the solutions described above, only a partial decrease in the hydrate coefficient in the contact zone was noted. In the range up to 0.5 cm, this decrease was twofold (from the initial 0.5 to 0.25), and the decrease in the hydrate coefficient was generally recorded only at a distance of 3 cm from the contact of the sample with the saline solution (Figure 59).

For each contact solution of different chemical composition, the average salt flux into a frozen hydrate-bearing fine sand-2 sample was calculated (Figure 60). The highest value of salt ions flux was obtained upon the contact of frozen hydrate-bearing fine sand-2 with MgCl₂ solution (5.4·10⁻⁶ 100g)/cm²·sec. At the same time, in the series MgCl₂ - NaCl - CaCl₂ - KCl - Na₂SO₄, the salt flux decreases by almost 5 times.

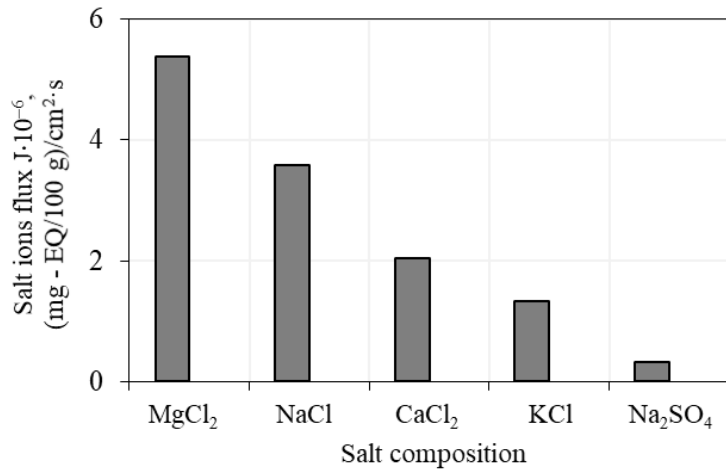


Figure 60. The influence of the chemical composition of the salt contact solution on the salt flux into frozen hydrate-containing sample (fine sand-2) after 4 hours of interaction with a frozen salt solution (t=-6°C, Csol=0.1N, P=0.1MPa).

The critical concentration of pore hydrate decomposition was calculated for the studied salts during their interaction with frozen hydrate-bearing sand at a fixed negative temperature (-6°C) and atmospheric pressure. This concentration (C_{cr}) varied from 3.23 mg - EQ/100 g (0.08%) for $MgCl_2$ solution to 3.5 mg - EQ/100 g (0.16%) for Na_2SO_4 . In the described series ($MgCl_2 - NaCl - CaCl_2 - KCl - Na_2SO_4$), the critical concentration of complete hydrate dissociation increased almost 2 times (Table 10).

Table 10. Dependence of the critical concentration (C_{cr}) causing the decomposition of pore hydrate in a frozen fine sand-2 sample on the chemical composition of the contacting solution ($t=-6^\circ C$, $P=0.1MPa$, $C_{sol}=0.1N$).

Salt	C_{cr} , mg - EQ/100 g	C_{cr} , % of weigh
$MgCl_2$	3.23	0.08
$NaCl$	4.89	0.11
$CaCl_2$	3.29	0.13
KCl	3.90	0.15
Na_2SO_4	3.50	0.16

The influence of the chemical composition of the contacting solution at a fixed concentration is primarily associated with the migration ability of salt ions. Thus, chloride salts have a greater migration capacity in frozen sediments compared to sulfates [46]. The results of experimental studies are consistent with this relationship: chloride salts, compared with sulfates, more actively penetrate into frozen hydrate-bearing sediment and cause more intense hydrate dissociation. In this case, in a series of cations, the mobility of ions is determined by their radius [99,313]. Thus, among the chloride salts used in the experiments, the cation radii increase in the series: $Mg^{2+} < Na^+ < Ca^{2+} < K^+$. In the same series, a decrease

in the salt ions migration intensity into frozen hydrate-containing sediments was experimentally obtained, which was reflected in a decrease in the activity of hydrate dissociation in porous media of frozen sediment.

Therefore, in the frame of the experimental modeling influence of different compositions of the contact solution on the process of salt migration in frozen hydrate-bearing sediments was tested. It was found, that in the raw $\text{MgCl}_2\text{-NaCl-CaCl}_2\text{-KCl-Na}_2\text{SO}_4$ accumulation of salts in frozen hydrate-bearing sand decreases, and as a result, less active hydrate dissociation is observed. Less accumulation of salts can be explained by the decrease in the average density flow by 5 times, and the increase in the critical concentration by 2 times in the described raw.

5.5. Sediment grain size influences the process of salt migration in hydrate-bearing sediments

To reveal the role of the finess (sediment particle size) of the sediment medium and various clay minerals, special studies were carried out on the interaction of frozen hydrate-bearing sediments of various compositions with a 0.1 N NaCl salt solution at a fixed negative temperature (-6°C) and atmospheric pressure.

Several series of experiments were performed at the atmospheric pressure (0.1 MPa). First of all, an assessment was made of the influence of the content of clay particles and their mineral composition on salt transfer in frozen hydrate-bearing sand samples.

Samples were prepared using quartz sand with a fraction of 0.1–0.2 mm (fine sand-2) to which kaolinite particles (up to 15% to the total mass) were added. The initial characteristics of frozen hydrate-bearing samples are presented in Table 11.

Table 11. Properties of hydrate-bearing frozen sand with different amount of kaolinite.

Sample	Kaolinite, %	Water content, %	Density, g/cm ³	Porosity, %	Ice saturation, %	Hydrate saturation, %
1	0	12	1.8	39	14	50
2	5	12	1.8	38	14	50
3	7	12	1.82	37	12	49
4	10	12	1.86	35	15	52
5	15	12	1.85	34	18	51

In the course of experiments on the interaction of frozen hydrate-containing samples with saline solution (NaCl), it was found that with an increase in the content of kaolinite particles, the intensity of salt transfer decreases. So, 3 hours after the interaction of a frozen hydrate-containing sample with a NaCl 0.1N solution, the depth of penetration of Na⁺ ions into a frozen hydrate-containing sand sample decreases from 5.3 cm to 2.6 cm with an increase in the number of clay particles from 0 to 10% (Figure 61).

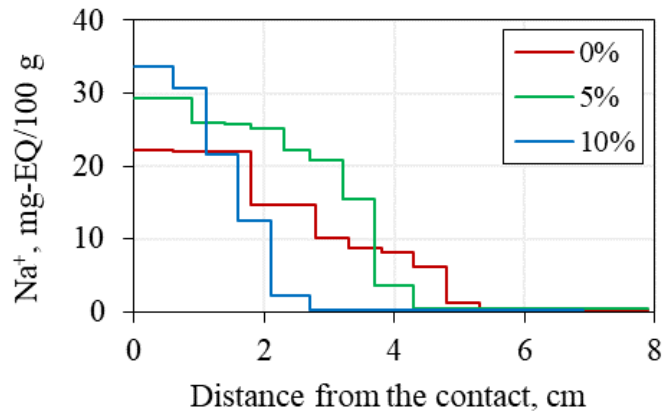


Figure 61. Influence of kaolinite content in fine-grained sand (fine sand-2) on the accumulation of Na⁺ ions in frozen hydrate-bearing samples 3 hours after interaction with 0.1 N NaCl solution at -6 °C and p=0.1 MPa.

A decrease in the intensity of salt accumulation with an increase in the amount of kaolinite particles leads to a decrease in the dissociation of pore gas hydrate. Thus, 3 hours after the contact of frozen hydrate-containing samples with 0.1N NaCl solution, the area of complete decomposition of pore hydrate decreased from 4.8 cm in sand without clay particles to 1.6 cm in a sample with 10% kaolinite (Figure 62).

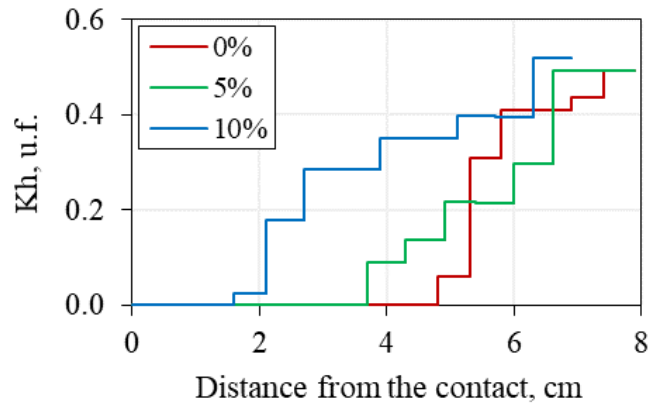


Figure 62. Effect of kaolinite content in fine sand-2 on hydrate dissociation in a frozen hydrate-bearing sample ($K_h^{in} \sim 0.5$, $W=12\%$) 3 hours after the start of interaction with a frozen salt solution of 0.1 N NaCl at $-6\text{ }^\circ\text{C}$.

With an increase in the amount of clay particles in frozen hydrate-bearing sand in the process of interaction with a saline solution, the accumulation of water increases. Thus, in frozen hydrate-bearing sand without clay additives, only little water accumulation was observed, ΔW in the near-contact area (about 2.5 cm) did not exceed 1.5% (Figure 63). With an increase in the amount of clay particles to 5%, an increase in water content in the near-contact area up to 7% was recorded, and in a sample of frozen hydrate-containing sand with 10% kaolinite, the increase in water content reached almost 8% (Figure 63).

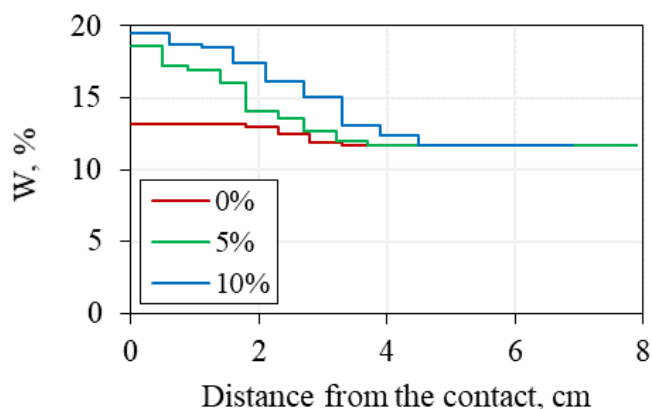


Figure 63. Influence of kaolinite content in sand (fine sand-2) on water accumulation in a frozen hydrate-bearing sample ($W=12\%$) after 3 hours of interaction with frozen salt solution of 0.1 N NaCl at $-6\text{ }^{\circ}\text{C}$.

Thus, an increase in the amount of clay particles in sandy hydrate-containing frozen samples led to an increase in the water flux from the frozen salt solution. So, with an increase in the number of kaolinite particles from 0 to 15%, the average water flux increased by more than 6 times (from 1.5 to $6.8 \cdot 10^{-7}$ g/sec) (Figure 64).

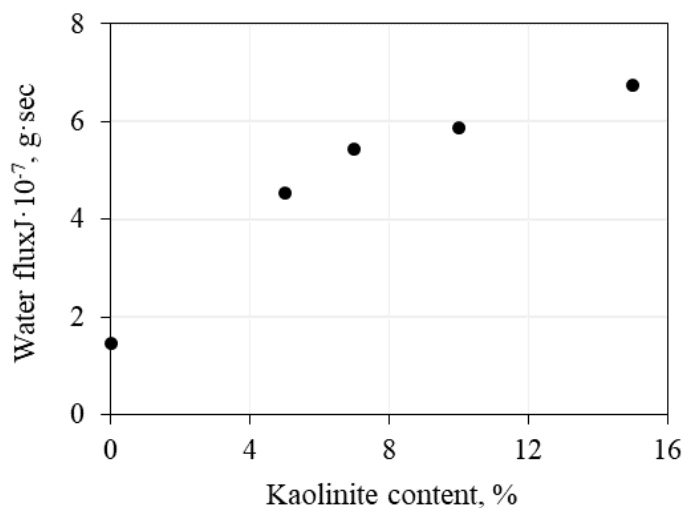


Figure 64. Effect of kaolinite content in sand (fine sand-2) on the average water flux through a frozen hydrate-bearing sample ($W=12\%$) after 4 h of interaction with a frozen salt solution of 0.1 N NaCl at $-6\text{ }^{\circ}\text{C}$.

An experimental study of the influence of clay mineralogy on the process of interaction of frozen hydrate-bearing samples with saline solution was carried out by adding 5% kaolinite or montmorillonite to quartz sand (fine sand-2). The initial characteristics of frozen hydrate-bearing samples are presented in Table 12.

Table 12. Properties of hydrate-bearing frozen sand with different composition of clay (5% additives).

Sample	Type of clay	Water Content, %	Density, g/cm ³	Porosity, %	Ice Saturation, %	Hydrate Saturation, %
1	kaolinite	12	1.8	38	15	47
2	montmorillonite	12	1.81	36	18	47

An analysis of the distribution of Na⁺ ions along the height of a frozen hydrate-containing sandy sample demonstrates that less accumulation of salt ions is typical for a sediment mixture with montmorillonite than with the addition of kaolinite particles. So, after 4 hours of interaction, Na⁺ ions migrated to a depth of up to 6 cm with the addition of kaolinite particles, and with the use of montmorillonite particles only up to 4 cm (Figure 65).

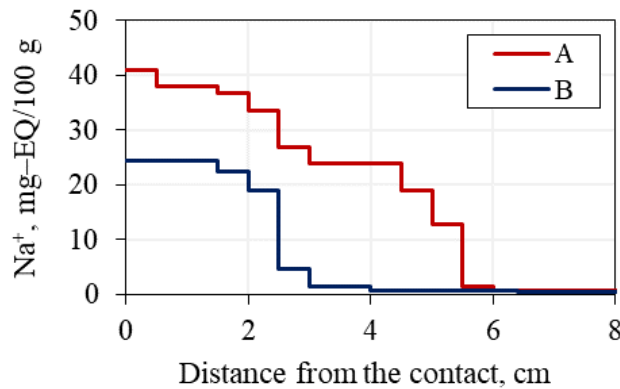


Figure 65. Influence of the mineralogical composition of clay in quartz sand (fine sand-2 with 5% additives) on the accumulation of Na⁺ ions in frozen hydrate-bearing samples after 4 hours of interaction with 0.1 N NaCl solution at t=-6°C: A – kaolinite; B – montmorillonite.

As a result of the migration and accumulation of salt ions in frozen hydrate-bearing sand samples containing 5% clay particles of various mineral composition, the pore methane hydrate completely decomposed to a depth of 5 cm from the contact area with the frozen salt solution in the sample with kaolinite particles and only 2 cm in the sample with 5% montmorillonite (Figure 66).

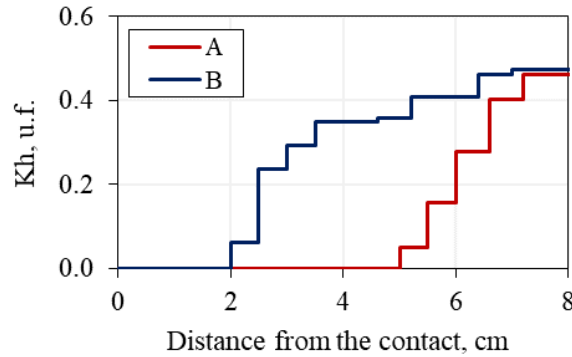


Figure 66. Influence of the mineralogical composition of clay in quartz sand (fine sand-2) on the decrease in the hydration coefficient (K_h) in frozen hydrate-containing samples ($K_h^{in} \sim 0.4$, $W=12\%$) 4 hours after the start of interaction with frozen salt solution 0.1 N NaCl at $t=-6^\circ\text{C}$: A – kaolinite; B, montmorillonite.

Figure 67 shows that hydrate-bearing sand with kaolinite particles accumulates more water compared to the sample containing kaolinite particles.

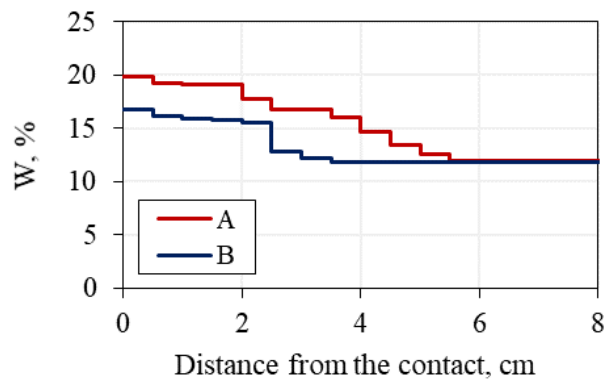


Figure 67. Influence of the mineralogical composition of clay in quartz sand (fine sand-1) on the accumulation of water in a frozen hydrate-bearing sample ($W=12\%$) after 4 hours of interaction with a frozen salt solution of 0.1 N NaCl at -6°C : A - kaolinite; B - montmorillonite.

Thus, in the contact area in a sample of frozen hydrate-containing sand with kaolinite particles, water content increased from the initial 12% to 20%, and in a sample with a montmorillonite additive, only up to 16.8% (Figure 67).

The calculation of the average migration flow of salt for the described experiments shows that its value decreases with an increase in the amount of clay particles (Figure 68).

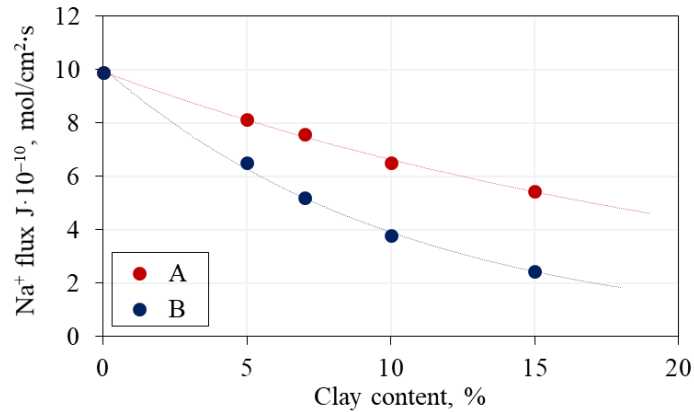


Figure 68. Influence of the content of clay particles of various compositions (kaolinite and montmorillonite) in quartz sand (fine sand-2) on the average flux density of Na⁺ ions into a frozen hydrate-containing sample over 4 hours of interaction with a frozen salt solution of 0.1N NaCl (p=0.1MPa, t= -6°C): A – kaolinite; B – montmorillonite.

Thus, at a temperature of -6°C, the average flux density of salt ions in frozen hydrate-bearing fine sand-2 without impurities was $10 \cdot 10^{-10}$ mol/cm²·s, and with the addition of 15% kaolinite, the flux decreased almost 2 times (to $5.5 \cdot 10^{-10}$ mol/cm²·s). At the same time, when clay particles of montmorillonite composition were added to quartz sand in an amount of 15%, the value of the average migration flow decreased even more (almost 4 times) and amounted to $2.5 \cdot 10^{-10}$ mol/cm²·s (Figure 68).

Analysis of the accumulation of salts in the studied samples and the change in hydrate content in the process of salt transfer made it possible to reveal the dependence of the critical concentration of salts in

the samples (C_{cr}), which causes the complete decomposition of metastable pore gas hydrates (at $P=0.1$ MPa), on the content of clay particles of various mineral composition in quartz sand (Figure 69).

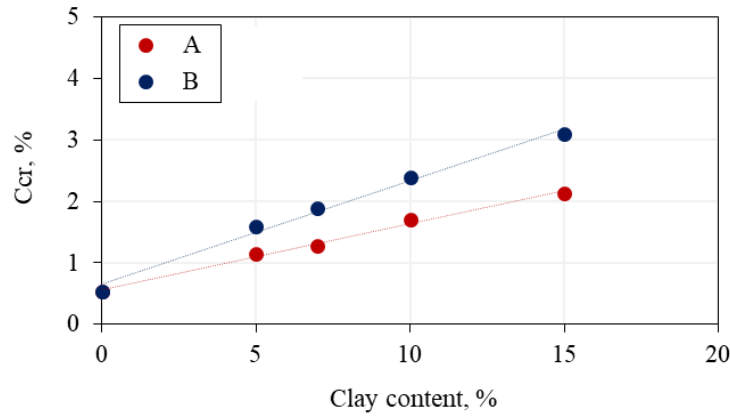


Figure 69. Influence of the content of clay particles of different mineral composition in quartz sand (fine sand-2) on the critical concentration (C_{cr}) causing the decomposition of pore hydrate in a frozen sand sample ($t = -6^{\circ}\text{C}$, $p = 0.1\text{MPa}$, $C_{sol} = 0.1\text{N}$): A – kaolinite; B – montmorillonite.

As experimental data show, the critical concentration (C_{cr}) increases with the increase in the content of clay particles in quartz sand (Figure 69). Thus, with an increase in the content of kaolinite to 15%, the critical concentration (C_{cr}) increased 4 times (from 0.5% to 2.1%), and with an increase in the content of montmorillonite particles, the critical concentration increased almost 6 times (from 0.5 to 3.1%).

Less intense salt migration in sand with montmorillonite particles, than with kaolinite particles connected with the different sorption ability of clay minerals. Thus, montmorillonite has the higher sorption ability, than kaolinite, therefore more actively adsorb salt ions and decrease their migration through the frozen hydrate-bearing sample.

An experimental study of the influence of the particle size of the studied quartz sand on salt transfer in frozen hydrate-containing sediment showed that with an increase in the size of the predominant sand fraction from 0.1-0.2 (fine sand-2) to 0.2-0.5 mm (medium sand), the intensity of accumulation of salt

ions increases, which accompanied by an increase in the dissociation of pore methane hydrate. Thus, at a fixed negative temperature (-6°C), 4 hours after the interaction of frozen hydrate-bearing fine sand-2 with NaCl 0.1N salt solution, Na^+ ions penetrated 5.4 cm into the depth of the sample, and 7.2 cm into medium sand (Figure 70).

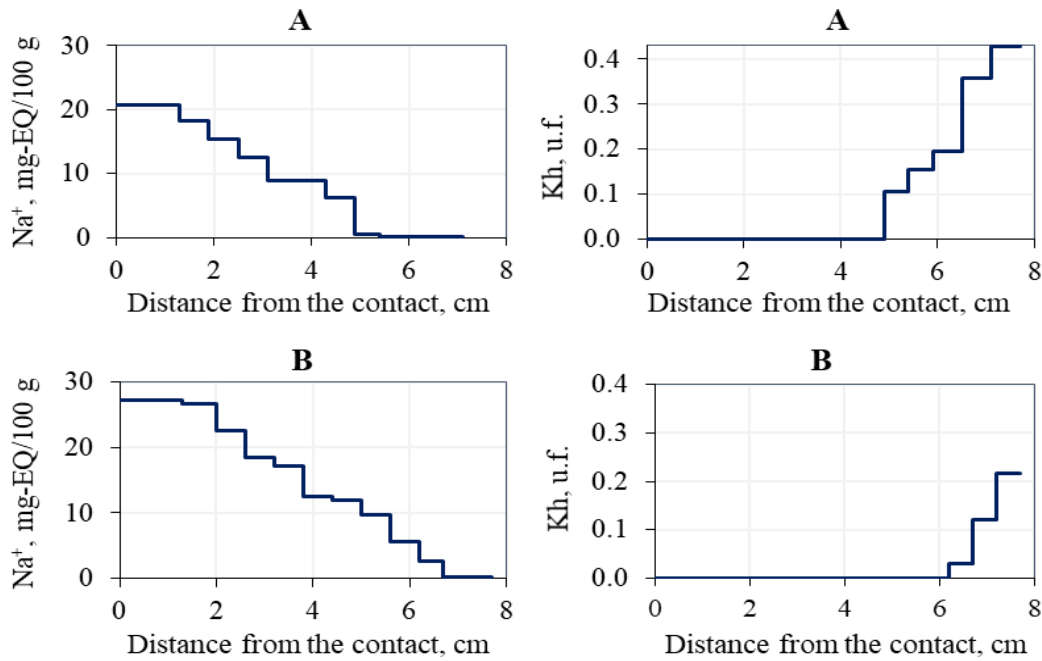


Figure 70. Influence of the size of sand particles on the accumulation of salt ions (Na^+) and the decrease in the hydrate coefficient (K_h) in frozen hydrate-containing samples ($K_h^{\text{in}} \sim 0.4$, $W=12\%$, $t = -6^{\circ}\text{C}$) 4 hours after the start of interaction with frozen salt solution 0.1 N NaCl: A - fine sand-2 (0.1-0.2 mm $\sim 80\%$); B – medium sand (0.2-0.5 mm $\sim 60\%$).

An increase in the intensity of migration and accumulation of salt ions in frozen hydrate-bearing sand interacting with a NaCl solution at a fixed negative temperature (-6°C), with an increase in the predominant size of sand particles (from 0.1-0.2 to 0.2-0.5 mm) is accompanied by a more active decomposition of the pore hydrate. Thus, 4 hours after the contact of a frozen hydrate-containing fine sand-2 sample (0.1–0.2 cm) with a 0.1N NaCl solution at -6°C , the pore hydrate completely decomposed

at a distance of 5 cm from the contact area. In a frozen hydrate-bearing sample with a predominance of a coarser fraction (medium sand), complete decomposition of the hydrate was recorded to a depth of 6.2 cm. At the same time, K_h , in the area far from the contact, decreased significantly (from 0.4 to 0.2) (Figure 70).

A special series of experiments was devoted to the analysis of the migration of salt ions in frozen hydrate-bearing sediment with different content of particles less than 0.05 mm (silt): fine sand-2 (~1% silt), fine sand-3 (~5% silt) and sandy loam (~ 18% silt). The initial characteristics of frozen hydrate-bearing samples are presented in Table 13.

Table 13. Properties of hydrate-bearing frozen sand with different amount of silt.

Sample	Type of sediment	Amount of silt, %	Water content, %	Density, g/cm ³	Porosity, %	Ice saturation, %	Hydrate saturation, %
1	Fine sand-2	1	12	1.8	38	15	44
2	Fine sand-3	5	12	1.83	37	16	37
3	Sandy loam	18	12	1.86	35	18	37

In the course of experimental modeling, it was found that with an increase in the content of silt, the migration and accumulation of salt ions in frozen hydrate-containing samples decreases. So, after 4 hours of interaction with NaCl 0.1 N salt solution at a fixed negative temperature of -6 °C, with an increase in the amount of silt from 1% to 18%, the penetration depth of ions in the samples decreased from 5.8 cm to 4.6 cm (Figure 71).

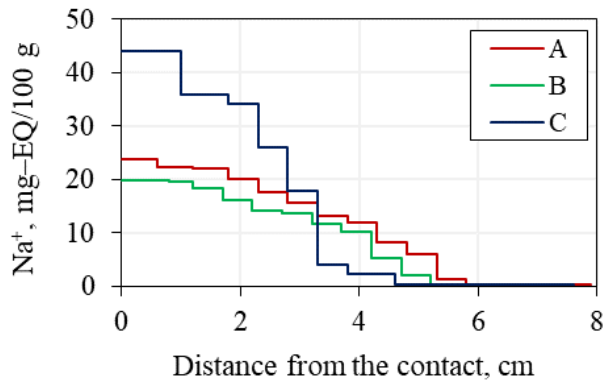


Figure 71. Influence of silt content on the accumulation of salt ions in frozen hydrate-containing samples 4 hours after interaction with 0.1 N NaCl solution at $t = -6^{\circ}\text{C}$: A – fine sand-2 (silt ~ 1%); B – fine sand-3 (silt ~ 5%); C – sandy loam (silt ~ 18%).

A decrease in the migration and accumulation of salts with an increase in the content of silt is accompanied by a decrease in the dissociation of pore gas hydrate. For example, in frozen hydrate-bearing fine sand-2, where the silt content did not exceed 1%, the hydrate completely dissociated in a region of 4.8 cm from the contact. And in the frozen hydrate-containing fine sand-3 sample with a silt content of about 5%, the pore hydrate dissociated to a depth of 4.2 cm. In the sandy loam sample with a silt content of 18%, the pore hydrate decomposition area was only 3.3 cm (Figure 72).

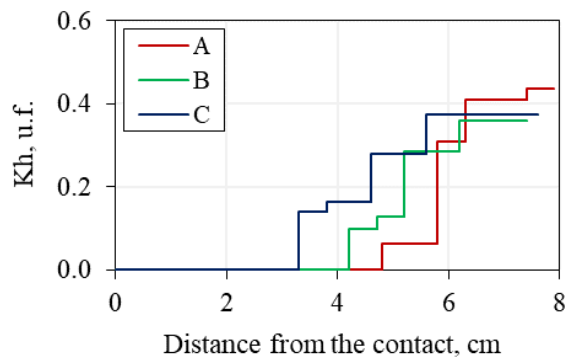


Figure 72. Influence of silt content on the hydrate coefficient (K_h) of frozen hydrate-containing samples ($K_h^{\text{in}} \sim 0.4-0.5$, $W=12\%$) 4 hours after interaction with 0.1 N NaCl solution at $t = -6^{\circ}\text{C}$: A – fine sand-2 (silt ~ 1%); B – fine sand-3 (silt ~ 5%); C – sandy loam (silt ~ 18%).

The different content of silt in frozen hydrate-bearing samples interacting with salt solution is also reflected in water accumulation during salt migration. With an increase in the content of silt in frozen hydrate-bearing samples, an increase in water content was recorded in the near-contact area. So, in a sample with a silt content of 5%, the increase in water content was up to 5%, and in a sample with a silt content of 18%, water content increased by more than 2 times (from 12 to 28%) (Figure 73).

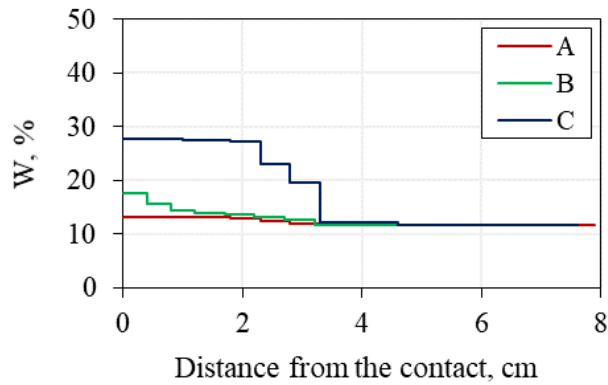


Figure 73. Influence of silt content on water accumulation in a frozen hydrate-bearing sample ($W=12\%$) after 4 hours of interaction with a frozen salt solution of 0.1 N NaCl at $-6\text{ }^{\circ}\text{C}$: A – fine sand-2 (silt $\sim 1\%$); B – fine sand-3 (silt $\sim 5\%$); C – sandy loam (silt $\sim 18\%$).

An increase in the average water flux in frozen hydrate-bearing samples was also recorded with an increase in the content of silt (from 1 to 18%): from $1.5 \cdot 10^{-7}\text{ g}\cdot\text{s}$ to $22.8 \cdot 10^{-7}\text{ g}\cdot\text{s}$.

For the described samples, the critical concentrations of the decomposition of the pore hydrate during their interaction with the NaCl salt solution were also calculated. This concentration (C_{cr}) increased from 0.05% to 0.19% as silt increased from 1% to 18% (Table 14).

Table 14. Dependence of the critical NaCl concentration on the amount of silt in frozen hydrate-bearing sandy sediment at the temperature -6°C .

Sediment	C_{cr} , mg - EQ/100 g	C_{cr} , %
Medium sand (silt $\sim 1\%$)	2.0	0.05

Fine sand-1 (silt ~1%)	3.4	0.13
Fine sand-2 (silt ~5%)	7.5	0.18
Sandy loam (silt~18%)	7.9	0.19

For the studied frozen hydrate-containing samples of different particle size, the average salt flux was calculated during their interaction with 0.1N NaCl solution at a temperature of $-6\text{ }^{\circ}\text{C}$ and $p=0.1\text{MPa}$ (Figure 74). It was found that in sandy-loamy and sandy sediments with an increase in the content of silt from 1 to 18%, represented mainly by quartz-feldspar particles, the flux of Na^+ ions increases from $6.2 \cdot 10^{-10}\text{ mol/cm}^2\cdot\text{s}$ to $16.3 \cdot 10^{-10}\text{ mol/cm}^2\cdot\text{s}$. This is due to the increase in the paths for migration with a decrease in particle size without a noticeable increase in their sorption capacity.

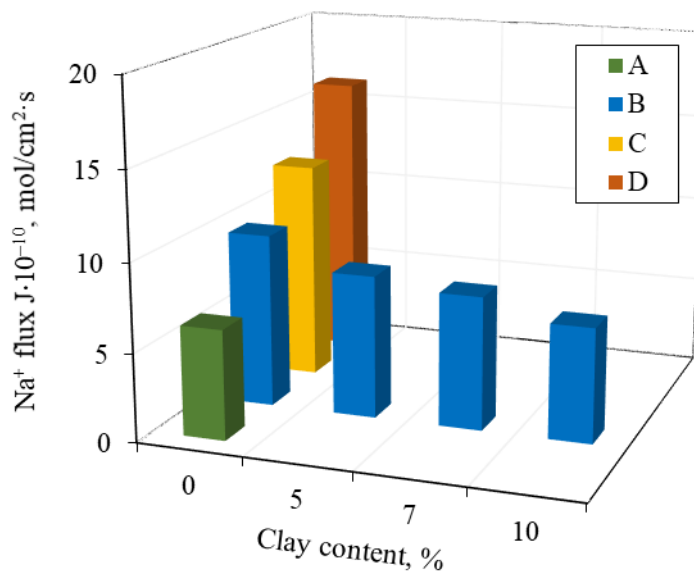


Figure 74. Influence of fineness and amount of clay particles (kaolinite) on the average migration flow of Na^+ in frozen hydrate-bearing samples interacting with NaCl solution 0.1 N for 4 hours at $t= -6^{\circ}\text{C}$: A – fine sand-3; B – fine sand-2 with kaolinite (from 0 to 10%); C – medium sand; D – sandy loam.

When finely dispersed clay particles (kaolinite composition) are added to quartz sand (fine sand-2), on the contrary, the density of the ion migration flux decreases, almost 2 times (from 9.9 to $6.5 \cdot 10^{-10}$

10^{-10} mol/cm²·s) (Figure 74). This behavior is associated with sorption processes that occur on the surface of clay particles during their interaction with salt ions [337]. This is confirmed by the addition of clay particles of montmorillonite composition (having a high sorption capacity) to the sand, where a 4-fold decrease in the salt flux density is observed (Figure 68).

Thus, with an increase in the content of silt in frozen hydrate-containing sand samples interacting with a salt solution, the intensity of the accumulation of salt ions and the dissociation of pore hydrate increases. That is due to the increase of water migration, which leads to an increase in the gradient of the water potential and the content of unfrozen water. Salt ions are also transferred with migrating water, as a result, the total flow of ions and the accumulation of salts as a whole increases. This happens despite the fact that the diffusion component can decrease due to the appearance of the sorption effect. When more finely dispersed clay particles (kaolinite and montmorillonite) are added, on the contrary, the accumulation of salt ions and the dissociation of the hydrate decreases, despite the increase in water migration, which is due to an increase in the sorption activity of the sediment.

Conclusion to the Chapter 5.

The experimental results demonstrate the active migration and accumulation of salts in frozen hydrate-bearing sediments, what causes active hydrate dissociation in pore space. Salt transfer and hydrate dissociation during interaction between frozen hydrate-bearing sediments and salt solution depends on many factors, such as pressure, temperature, sediments (dispersion, clay content) and contact solution (concentration, chemical composition) characteristics. Experimental data demonstrates, that migration of salt solution may lead to the destruction of intrapermafrost and subpermafrost gas hydrate formations, permafrost thawing, and methane emissions.

Chapter 6. Concept models of hydrate interaction with natural and technical salt solution in hydrate-bearing collectors in permafrost

As confirmed by the results of experimental modeling on the interaction between frozen hydrate-bearing sediments and salt solutions, salt ions can migrate from natural and technogenic solutions to frozen horizons containing gas hydrates and can cause intrapermafrost hydrate decomposition in the Arctic region. This is possible when salt ions penetrate from sea water on the Arctic shelf into underwater permafrost containing gas hydrates, and when intrapermafrost saline water (cryopegs) flows down the frozen section as a result of the evolution of the permafrost zone (during temperature increase), as well as during technogenic impact (for example, when drilling wells in frozen strata containing hydrates). And the intensity of mass transfer processes is defined by internal (sediments characteristics) and external factors (ambient temperature, pressure, salt concentration and composition). These issues have not been sufficiently studied until recently.

The obtained experimental data allow us to present some model-scheme of destabilization of intrapermafrost hydrate during salt migration in frozen hydrate-bearing sediments in continental conditions (Figure 75) and on the shelf (Figure 76).

In continental conditions, initially, intrapermafrost gas hydrates exist both in stable and metastable conditions. At the same time, there are cryopegs around which there is a certain salinity halo (Figure 75a). This salinity halo very slowly spread over time, without significant influence of salt solution on the surrounding frozen sediments. However, during the evolution of the permafrost zone (i.e. degradation with an increase in the sediment temperature) or under technogenic impact (for example, during drilling), the migration of salts from cryopegs proceed faster down the section, and a salinization front is formed (Figure 75b). Salt ions, when reach hydrate-bearing frozen horizon, destabilized hydrates and at a certain critical concentration causes their complete dissociation. Since the critical concentration of hydrate

dissociation in frozen sediment at a gas pressure below equilibrium is lower than at the pressure above equilibrium, the destabilization of metastable gas hydrate deposits occurs first (Figure 75c), as does the thawing of host frozen sediments. And the diffusion of salts into the frozen horizons, which contain gas hydrates under stable conditions, proceeds much more slowly. When the metastable gas hydrate reservoir had already dissociated, the salt front only partially destabilized gas hydrates at the higher pressure (Figure 75d).

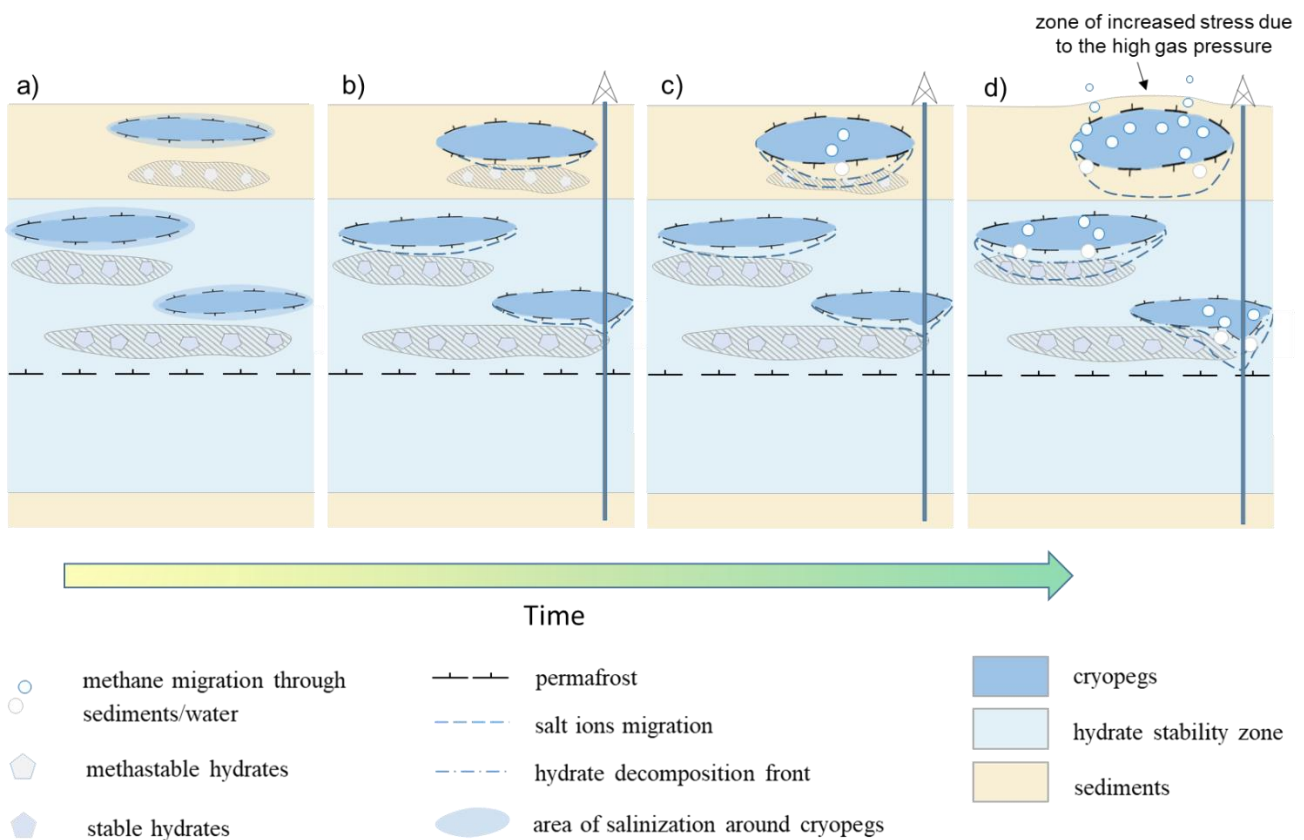


Figure 75. Proposed model of interaction between saline horizons and frozen deposits containing gas hydrates: a) initial state; b) start of salt migration from cryopegs due to ambient temperature increase; c) dissociation of metastable hydrates occurs; d) dissociation of stable hydrates occurs.

The methane released during the dissociation of gas hydrates migrates through permeable areas of frozen horizons (along taliks), and only part of it enters the atmosphere. The main mass of methane accumulates under less permeable frozen horizons, forming a gas deposit and creating zone of increased pressure. And when gas pressure of this gas deposit exceed the critical gas pressure, an explosion and the formation of a crater can happen [108,251,252,338].

Based on the experimental results some recommendations can be created for hydrocarbon production in the area of permafrost distribution. Firstly, careful investigation of the sediment cross-section is needed, possibility of hydrate existence, their location in relation to the cryopegs, and possibility of cryopeg opening by the drilling rig. As well as assessment of possible salt solutions (either technical or natural) penetration path and salt migration diffusion characteristics. In addition, special attention should be paid to the composition of the drilling fluid. Salt concentration in it should not exceed critical concentration of hydrate dissociation in the condition of each drilled horizon or better to use alternative non-salt-containing fluid (for example polymer based).

On the Arctic shelf in the conditions of submarine permafrost bottom sediments (in frozen and thawed state), including hydrate containing, are in the contact with sea water. Consequently, salt migration down by the cross-section occur, what can play crucial role in the hydrate destabilization in the submarine permafrost (Figure 76).

Initially (Figure 76A), during sea regression gas hydrates exist in the stable and metastable state without significant change. Then sea transgression occurs (Figure 76 B) and frozen hydrate-containing sediments start to interact with salted sea water, sediments temperature rises, and thawing front is formed (Figure 76 B. 1) [281,332,339]. Over time, the rate of thawing of underwater permafrost decreases. In this case, the penetration of sea water into the thawing zone is observed (Figure 76 B. 2).

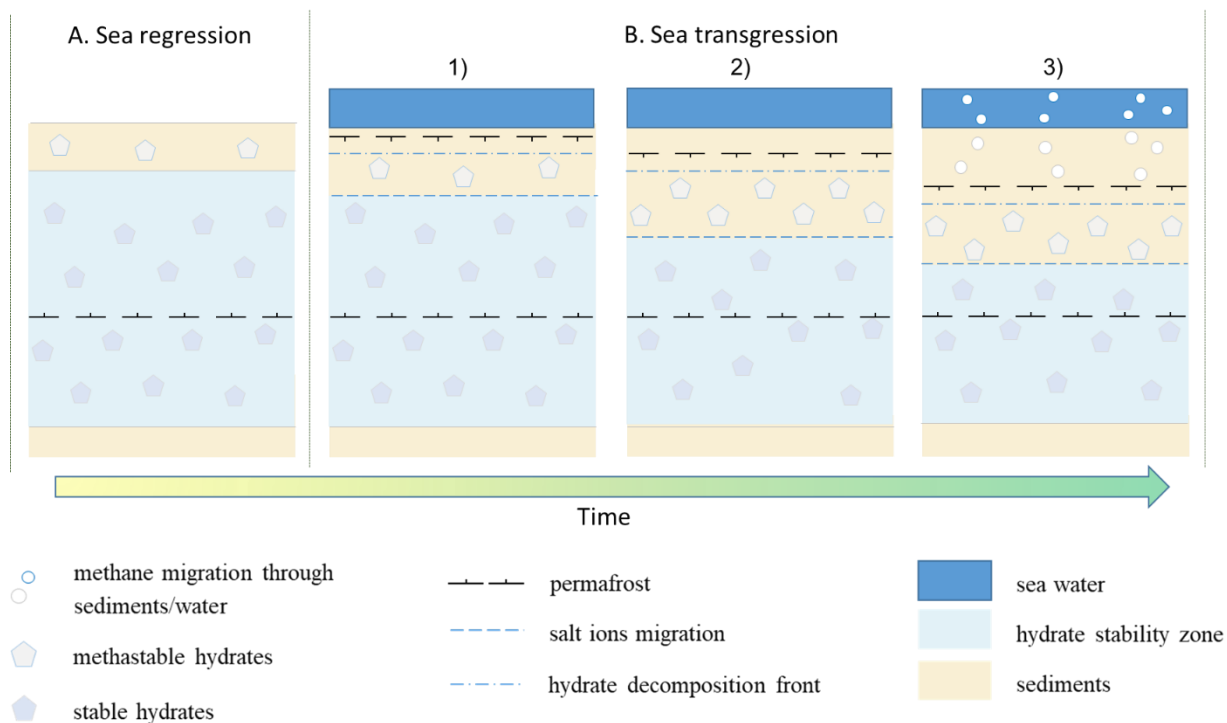


Figure 76. The proposed conceptual model on the interaction between frozen hydrate-containing sediments and sea water: A) preliminary state – sea regression; B. 1) after sea transgression – start of interaction between frozen sediments and sea water; B. 2) migration of salt into permafrost sediments (development of salinity and thawing fronts); B. 3) propagation salt front into sediments, containing intrapermafrost gas hydrate followed by hydrate decomposition and active methane emission.

Since frozen sediments are permeable to salt ions, there is an advancing movement of salt ions from sea water relative to the thawing front. During the migration and accumulation of salt ions in frozen deposits, the temperature of phase transitions decreases and the content of the liquid phase in sediment increases. As a result, the deceleration of the thawing front decreases. Salt ions migrating in frozen deposits, upon reaching horizons containing relict hydrates, will destabilize them and contribute to their active dissociation and methane release (Figure 76 B. 3), thus forming the second front of phase transitions - the dissociation front of gas hydrates. It occurs when a certain critical salt concentration is

reached in the frozen hydrate-containing sediment. This concentration, as shown by experimental studies, depends on the composition of hydrate-containing deposits and thermobaric conditions. During phase transitions ice-water / hydrate-water (ice), gas caused by salt transfer, the permeability of saline permafrost increases [340]. Methane formed during the dissociation of gas hydrates subsequently migrates to the bottom surface and enters the sea water, where it partially dissolves, oxidizes, and also diffuses through the water column and escapes into the atmosphere (Figure 76 B. 3).

This scheme makes it possible to explain the possible cause of numerous gas manifestations recorded on the Arctic shelf in areas of submarine permafrost distribution as a result of destabilization of intrapermafrost gas hydrate formations due to heat and mass transfer processes associated with the migration of salt ions from sea water.

Chapter 7. Conclusion

An analysis of the natural conditions of occurrence of frozen hydrate-bearing sediment indicates the possibility of their interaction with salt solutions. This is possible when salt ions penetrate from sea water on the Arctic shelf into submarine permafrost containing gas hydrates, when intrapermafrost saline water (cryopegs) flows down the frozen section as a result of the evolution of the permafrost zone (temperature increase), as well as during technogenic impact (for example, when drilling wells in frozen strata containing hydrates). Salt migration causes thawing of frozen sediment and destabilization of intrapermafrost gas hydrates, which leads to the emission of methane into the atmosphere. Thus, the transformation of climatic conditions can occur, as well as the emergence of technological complications during the development of Arctic deposits of hydrocarbons. However, literature analysis has shown that

the issue of interaction between frozen hydrate-bearing sediment and salt solutions has not been studied enough so far.

The conducted experimental studies allow us to draw the following conclusions:

1) The new method for determination of water dissolving salt concentration in sandy sediments through water activity was proposed (water extraction for instance). The method allows to obtain values of salt ions concentration without special probe preparation. It is fast, cheap and has high accuracy ($\pm 0.2\%$), but applicable only to the low concentration of salts (up to 5%);

2) The new method was created for investigating of hydrate-bearing frozen sediments interaction with salt solution under the pressure higher than 0.1 MPa in the pressure cell;

3) The method for temperature change investigation during interaction of frozen hydrate-bearing sediments with salt solution was developed. The method allows to register temperature change in time with using of special equipment with high precision of temperature sensors ($\pm 0.05^\circ\text{C}$). All external temperature influence in that method is limited, i.e., ambient temperature is fixed at one value. So, only internal temperature changes in the frozen hydrate-bearing sample is observed;

4) Mechanism and dynamics of hydrate-bearing frozen sediments interaction with salt solution were experimentally investigated:

- during the interaction of frozen hydrate-bearing sediments with salt solutions, not only active processes of salt migration are observed, which are accompanied by the accumulation of salt ions in the pore space, but also phase transitions of pore ice and dissociation of gas hydrates in the pore space, accompanied by anomalous temperature drops;
- the migration of salt ions into a frozen hydrate-containing sample occurs more intensively than into a sample without hydrates (due to the higher content of liquid water films), and with

deeper temperature decrease (temperature decrease was 3 times lower in hydrate-containing sand, than in non-hydrate-containing);

- in the process of salts migration and accumulation, two fronts are formed: thawing of frozen sediments and gas hydrate decomposition. It is noted that the front of decomposition of gas hydrate is ahead of the front of thawing, because critical concentration of hydrate dissociation is lower than critical concentration of thawing;
- Na^+ flux is decreasing with time of interaction between frozen hydrate-bearing and salt solution. After 30 hours of contact between hydrate-bearing sand and NaCl solution salt flux decreased by 6 times.
- based on the experimental data scheme of water phase transition in frozen sand containing stable and metastable hydrate is proposed, furthermore according temperature effect during that process is analysed.

5) Experimental investigation of different factors influence on the process of hydrate-bearing frozen sediments and salt solution interaction was conducted. The following results was obtained:

- the rate of salt penetration in frozen sediments and the rate of hydrate dissociation is increasing when the experimental conditions are transferred from stable to metastable state (from 6 MPa to 0.1 MPa by 2 times both), as well as Na^+ flux from 1 to $38 \cdot 10^{-10}$ mol/cm²·sec. As it was assumed, such dependence connected with decrease in liquid water amount in hydrate-bearing frozen sediments with increasing gas pressure;
- higher temperature leads to more active decomposition of the hydrate in frozen sediments as a result of salt penetration. The dissociation rate is more than 4 times higher when the temperature of interaction rises 3 times from -20 to -6.5 °C. Salt critical concentration of hydrate

decomposition in porous media of frozen sediment vary from 3.4% to 0.6% when temperature of interaction increase from -16 to -2.5 °C;

- higher concentration of the contact solution leads to more active hydrate decomposition in frozen hydrate-bearing sediments interacting with salt solution. The penetration of Na⁺ is 3 times greater with an increase in concentration of the contact solution by 2 times. The rate of hydrate dissociation is 6 times faster in the case of contact with a 0.4N solution than in contact with a 0.2N solution. The higher the concentration of the contacting solution, the more significant the decrease in temperature associated with the more intense dissociation of the hydrate, and the longer the time required for the temperature to reach equilibrium (up to the initial temperature values);
- hydrate stability in porous media of frozen sediments increases in the series MgCl₂-NaCl-CaCl₂-KCl-Na₂SO₄. The intensity of pore hydrate dissociation is 3 times higher upon contact with a NaCl solution than upon contact with Na₂SO₄ solution, and 2 times higher than upon contact with CaCl₂ solution. Data confirmed by computer simulations in “HydraFlash”;
- rise of clay content in sand decreases intensity of salt accumulation and hydrate dissociation: critical concentration increases by 4 times and the average salt flux decreases by 2 times when clay content change from 0 to 15%;
- more active salt accumulation and hydrate dissociation happen in the sand with kaolinite particles, than in the sand with montmorillonite;
- salt accumulation is more active and hydrate decomposes more rapidly when amount of silt with low sorption ability increases. Thus, more active salt migration and hydrate dissociation was observed in sand than in sandy loam.

6) On the basis of experimental data, a conceptual scheme for the destabilization of intrapermafrost formations in the areas of permafrost distribution in continental conditions and on the Arctic shelf is proposed. This scheme makes it possible to explain the possible cause of numerous gas manifestations recorded in the Arctic area of permafrost distribution as a result of destabilization of intrapermafrost gas hydrate formations due to heat and mass transfer processes associated with the migration of salt ions.

The results of experimental modeling on the interaction of salt solutions with frozen hydrate-containing sediments indicate the active migration of salt ions at negative temperatures into sediment media containing ice and gas hydrates. Thus in permafrost area, salt migration can lead to the melting of ice in porous media of sediment, the destruction of intrapermafrost gas hydrate formations, and the active emission of methane. The intensity of salt migration in frozen hydrate-bearing sediments depends on a number of factors (ambient temperature, pressure, composition and concentration of salt contact solutions, sediment dispersity) and is followed by the complex picture of heat flows due to the phase transitions.

The conducted experimental studies allow us to take a newly look at the mechanism and patterns of migration of salt ions in frozen hydrate-bearing sediment during their contact. Experimental data demonstrate the potential danger of destabilization of gas hydrate formations in the Arctic as a result of exposure to natural and artificial solutions, especially for the oil and gas industry.

Also, this research contains the important basis for future mathematical model development of hydrate destabilization due to salt solution penetration and allows to create a scheme for main salt diffusion characteristics calculation (particularly diffusion coefficient – the measure of salt migration rate). With use of diffusion coefficient it will be possible to predict how fast salts can reach hydrate horizon in permafrost, and when critical concentration of hydrate dissociation will be reached. In addition

special tests need to be done on salt migration in frozen-hydrate bearing sediments under NMR and X-ray computed tomography investigations. Such investigation will help to understand internal processes happen during salt migration, the role of frozen hydrate bearing components in that process etc. That is the point for further investigation and continue of this research.

Bibliography

1. Kudryashov, B.; Yakovlev, A. *Well Drilling in Permafrost (Published in Russian)*; Nedra: Moscow, Russia, 1983; p. 283.
2. Lu, S. M. A Global Survey of Gas Hydrate Development and Reserves: Specifically in the Marine Field. *Renew. Sustain. Energy Rev.* **2015**, *41*, 884–900.
<https://doi.org/10.1016/j.rser.2014.08.063>.
3. Timofeev, N. G.; Skryabin, R. M.; Atlasov, R. A. Wells Drilling Temperature Regime under the Cryolithozone Conditions (Published in Russian). *Sci. Educ.* **2017**, No. 3, 51–56.
4. Ma, Y.; Yang, J.; Feng, P.; Zhang, C. The Challenges and Key Technology of Drilling Safety in the Area of the Arctic. In *Springer Series in Geomechanics and Geoengineering*; Springer, 2020; pp 522–532. https://doi.org/10.1007/978-981-13-7127-1_48.
5. Yakushev, V. S.; Collett, T. S. Gas Hydrates in Arctic Regions: Risk to Drilling and Production. In *Proceedings of the Second International Offshore and Polar Engineering Conference*; San Francisco, 1992; Vol. 1, pp 669–673. <https://doi.org/10.1016/j.jaad.2006.01.013>.
6. Medvedsky, R. I. *Construction and Operation of Oil and Gas Wells in Permafrost (Published in Russian)*; Nedra: Moscow, Russia, 1987; p. 127.
7. Kontorovich, A. E.; Epov, M. I.; Burshtein, L. M.; Kaminskii, V. D.; Kurchikov, A. R.; Malyshev, N. A.; Prischepa, O. M.; Safronov, A. F.; Stupakova, A. V.; Suprunenko, O. I. Geology and Hydrocarbon Resources of the Continental Shelf in Russian Arctic Seas and the Prospects of Their Development. *Russ. Geol. Geophys.* **2010**, *51*, 1, 3–11.
<https://doi.org/10.1016/j.rgg.2009.12.003>.
8. Yakushev, V. S. *Gas and Gas Condensate Fields Development at Complicated Geocryological Conditions (Published in Russian)*; Gubkin Russian State University: Moscow, Russia, 2014; p.

188, ISBN 978-5-91961-114-1.

9. Wegner, S. A.; Campbell, K. J. Drilling Hazard Assessment for Hydrate Bearing Sediments Including Drilling through the Bottom-Simulating Reflectors. *Mar. Pet. Geol.* **2014**, *58*, PA, 382–405. <https://doi.org/10.1016/j.marpetgeo.2014.08.007>.
10. Nimblett, J. N.; Shipp, R. C.; Strijbos, F. Gas Hydrate as a Drilling Hazard: Examples from Global Deepwater Settings. In *Proceedings of the Annual Offshore Technology Conference*; 2005; Vol. 2005-May, pp 1429–1435. <https://doi.org/10.4043/17476-ms>.
11. McConnell, D. R.; Zhang, Z.; Boswell, R. Review of Progress in Evaluating Gas Hydrate Drilling Hazards. *Mar. Pet. Geol.* **2012**. <https://doi.org/10.1016/j.marpetgeo.2012.02.010>.
12. Max, M. *Natural Gas Hydrate In Oceanic and Permafrost Environments*; Kluwer Academic Publishers: Washington, 2000; p. 419, ISBN 978-1-4020-1362-1. <https://doi.org/10.1007/978-94-011-4387-5>.
13. Collett, T. S.; Dallimore, S. R.; Max, M. D. Natural Gas Hydrate in Oceanic and Permafrost Environments. In *v. 5, chapter 5*; Springer Science & Business Media, 2003; Vol. 5.
14. Sloan Jr., E. D.; Koh, C. A. *Clathrate Hydrates of Natural Gases*; CRC Press: Boca Raton, FL, USA, 2007; p. 752, ISBN 9780429129148. <https://doi.org/10.1201/9781420008494>.
15. Istomin, V. A.; Yakushev, V. S. *Gas Hydrates in Nature (Published in Russian)*; Nedra: Moscow, 1992; p. 235.
16. Boswell, R.; Hancock, S.; Yamamoto, K.; Collett, T.; Pratap, M.; Lee, S.-R. Natural Gas Hydrates. In *Future Energy*; Elsevier, 2020; pp 111–131. <https://doi.org/10.1016/B978-0-08-102886-5.00006-2>.
17. Chuvilin, E.; Davletshina, D. Formation and Accumulation of Pore Methane Hydrates in Permafrost: Experimental Modeling. *Geosciences* **2018**, *8*, *12*, 467.

<https://doi.org/10.3390/geosciences8120467>.

18. Collett, T.; Bahk, J.-J.; Baker, R.; Boswell, R.; Divins, D.; Frye, M.; Goldberg, D.; Husebø, J.; Koh, C.; Malone, M.; et al. Methane Hydrates in Nature—Current Knowledge and Challenges. *J. Chem. Eng. Data* **2015**, *60*, 2, 319–329. <https://doi.org/10.1021/je500604h>.
19. Ruppel, C. Permafrost-Associated Gas Hydrate: Is It Really Approximately 1 % of the Global System? *J. Chem. Eng. Data* **2015**, *60*, 2, 429–436. <https://doi.org/10.1021/je500770m>.
20. Waite, W. F.; Ruppel, C. D.; Boze, L.-G.; Lorenson, T. D.; Buczkowski, B. J.; McMullen, K. Y.; Kvenvolden, K. A. Preliminary Global Database of Known and Inferred Gas Hydrate Locations. *U.S. Geol. Surv. data release* **2020**. <https://doi.org/10.5066/P9LLFVJM>.
21. Ruppel, C. D. Gas Hydrate in Nature. *U.S. Geol. Surv.* **2018**, *Fact Sheet*, 4. <https://doi.org/https://doi.org/10.3133/fs20173080>.
22. Ershov, E. D.; Lebedenko, Y. P.; Chuvilin, E. M.; Istomin, V. A.; Yakushev, V. S. Features of the Existence of Gas Hydrates in the Cryolithozone (Published in Russian). *Rep. Acad. Sci. USSR* **1991**, *321*, 788–791.
23. Chuvilin, E.; Bukhanov, B.; Davletshina, D.; Grebenkin, S.; Istomin, V. Dissociation and Self-Preservation of Gas Hydrates in Permafrost. *Geosciences* **2018**, *8*, *12*, 431:1-431:12. <https://doi.org/10.3390/geosciences8120431>.
24. Hachikubo, A.; Takeya, S.; Chuvilin, E.; Istomin, V. Preservation Phenomena of Methane Hydrate in Pore Spaces. *Phys. Chem. Chem. Phys.* **2011**, *13*, 39, 17449–17452. <https://doi.org/10.1039/c1cp22353d>.
25. Takeya, S.; Ebinuma, T.; Uchida, T.; Nagao, J.; Narita, H. Self-Preservation Effect and Dissociation Rates of CH₄ Hydrate. *J. Cryst. Growth* **2002**, *237*, 379–382. [https://doi.org/10.1016/S0022-0248\(01\)01946-7](https://doi.org/10.1016/S0022-0248(01)01946-7).

26. Stern, L. A.; Circone, S.; Kirby, S. H.; Durham, W. B. Anomalous Preservation of Pure Methane Hydrate at 1 Atm. *J. Phys. Chem. B* **2001**, *105*, 9, 1756–1762.
<https://doi.org/10.1021/jp003061s>.
27. Kuhs, W. F.; Genov, G.; Staykova, D. K.; Hansen, T. Ice Perfection and Onset of Anomalous Preservation of Gas Hydrates. *Phys. Chem. Chem. Phys.* **2004**, *6*, 21, 4917–4920.
<https://doi.org/10.1039/B412866D>.
28. Istomin, V. A.; Yakushev, V. S. Makhonina, N. A.; Kwon, V. G.; Chuvilin, E. M. Self-Preservation Phenomenon of Gas Hydrate. *Gas Ind. Russ.* **2006**, *4*, 16–27.
29. Istomin, V. A.; Yakushev, V. S. Gas-Hydrates Self-Preservation Effect. *Phys. Chem. Ice* **1992**, 136–140.
30. Chuvilin, E. M.; Tumskey, V. E.; Tipenko, G. S.; Gavrilov, A. V.; Bukhanov, B. A.; Tkacheva, E. V.; Audibert-Hayet, A.; Cauquil, E. Relic Gas Hydrate and Possibility of Their Existence in Permafrost Within the South-Tambey Gas Field. *SPE Arct. Extrem. Environ. Tech. Conf. Exhib. Soc. Pet. Eng.* **2013**, 166925:1-166925:9.
31. Chuvilin, E.; Ekimova, V.; Bukhanov, B.; Grebenkin, S.; Shakhova, N.; Semiletov, I. Role of Salt Migration in Destabilization of Intra Permafrost Hydrates in the Arctic Shelf: Experimental Modeling. *Geosciences* **2019**, *9*, 4, 188:1-188:18. <https://doi.org/10.3390/geosciences9040188>.
32. Chuvilin, E.; Davletshina, D.; Ekimova, V.; Bukhanov, B.; Shakhova, N.; Semiletov, I. Role of Warming in Destabilization of Intrapermafrost Gas Hydrates in the Arctic Shelf: Experimental Modeling. *Geosciences* **2019**, *9*, 407:1-407:12. <https://doi.org/10.3390/geosciences9100407>.
33. Yakushev, V. S. *Natural Gas and Gas Hydrates in the Permafrost (Published in Russian)*; Gazprom VNIIGAZ: Moscow, 2009; p. 192.
34. Yamamoto, K.; Boswell, R.; Collett, T. S.; Dallimore, S. R.; Lu, H. Review of Past Gas

Production Attempts from Subsurface Gas Hydrate Deposits and Necessity of Long-Term Production Testing. *Energy & Fuels* **2022**, *36*, 10, 5047–5062.

<https://doi.org/10.1021/acs.energyfuels.1c04119>.

35. Zhao, R.; Chang, H. J.; Chen, K. L. Environmental Risk of Gas Hydrates Exploitation in Tibetan Plateau Permafrost. *Adv. Mater. Res.* **2014**, *955–959*, 2114–2117.

<https://doi.org/10.4028/www.scientific.net/AMR.955-959.2114>.

36. Yakushev, V. Natural Gas Liberations around Production Wells at Russian Arctic Gas Fields. *Geosciences* **2020**, *10*, 5, 184:1-184:6. <https://doi.org/10.3390/geosciences10050184>.

37. Max, M. D.; Johnson, A. H.; Dillon, W. P. *Natural Gas Hydrate - Arctic Ocean Deepwater Resource Potential*; Springer, Cham: Dordrecht, Netherlands, 2013; p. 113 p., ISBN 9783319025070. <https://doi.org/https://doi.org/10.1007/978-3-319-02508-7>.

38. Chuvilin, E.; Tipenko, G.; Bukhanov, B.; Istomin, V.; Pissarenko, D. Simulating Thermal Interaction of Gas Production Wells with Relict Gas Hydrate-Bearing Permafrost. *Geosciences* **2022**, *12*, 3, 115. <https://doi.org/10.3390/geosciences12030115>.

39. Chuvilin, E.; Ekimova, V.; Davletshina, D.; Krivokhat, E.; Shilenkov, V.; Bukhanov, B. Pressure Influence on Salt Migration in Frozen Hydrate-Saturated Sediments: Experimental Modeling. *Energy & Fuels* **2022**, *12*, 7, 261. <https://doi.org/10.1021/acs.energyfuels.2c01282>.

40. Chuvilin, E.; Ekimova, V.; Davletshina, D.; Bukhanov, B.; Krivokhat, E.; Shilenkov, V. Migration of Salt Ions in Frozen Hydrate-Saturated Sediments: Temperature and Chemistry Constraints. *Geosciences* **2022**, *12*, 7, 276. <https://doi.org/10.3390/geosciences12070276>.

41. Chuvilin, E.; Bukhanov, B.; Istomin, V. Cryopegs as Destabilization Factor of Intra-Permafrost Gas Hydrates. In *EGU General Assembly Conference*; 2016; Vol. 18, pp EPSC2016-3509.

42. Yakushev, V. S.; Istomin, V. A. Causes of Gas Emissions in Frozen Rocks of the Yamburg Gas

- Condensate Field (Published in Russian). In *Features of gas well development in difficult geocryological conditions*; VNIIGAZ: Moscow, Russia, 1987; pp 119–127.
43. Bing, H.; He, P.; Zhang, Y. Cyclic Freeze–Thaw as a Mechanism for Water and Salt Migration in Soil. *Environ. Earth Sci.* **2015**, *74*, *1*, 675–681. <https://doi.org/10.1007/s12665-015-4072-9>.
 44. Maksimov, A. M.; Tsyarkin, G. G. Formation of a Two-Phase Zone in the Interaction of Wet Rocks with Cooled Salt Solution. *J. Eng. Phys.* **1988**, *55*, *3*, 1014–1019. <https://doi.org/10.1007/BF00870486>.
 45. Ershov, E. D.; She, Z. S.; Lebedenko, Y.; Chuvilin, E. M.; Kryuchkov, K. Y. Mass Transfer and Deformation Processes in Frozen Rocks Interacting with Aqueous Salt Solutions (Published in Russian). In *Engineering-geological study and evaluation of frozen, freezing and thawing soils (IGK-92). Materials of the III Scientific and Technical Workshop*; Russian State Scientific Research Institute of Hydraulic Engineering: St Petersburg, 1993; pp 67–77.
 46. Lebedenko, Y. P. Cryogenic Migration of Ions and Bound Moisture in Ice-Saturated Frozen Rocks (Published in Russian). *Eng. Geol.* **1989**, No. 4, 21–30.
 47. Ershov, E. D.; Lebedenko, Y. P.; Chuvilin, E. M.; Ganova, S. D. Features of Moisture Migration in Frozen Fine Soils under the Action of Osmotic Forces (Published in Russian). In *Geocryological research*; MSU: Moscow, Russia, 1987; pp 150–157.
 48. Chuvilin, E. M.; Ershov, E. D.; Smirnova, O. G. Ionic Migration in Frozen Soils and Ice. In *Proceedings of the 7th International Permafrost Conference*; Yellowknife, Canada, 1998; pp 167–171.
 49. Ershov, E. D.; Komarov, I. A.; Chuvilin, E. M. Forecast of Processes of Interaction of Liquid Technogenic Brines Buried in the Frozen Sediment Massif (Published in Russian). *Geoecology. Eng. Geol. Hydrogeol. Geocryol.* **1997**, No. 2, 19–29.

50. Vasiliev, V. I.; Maksimov, A. M.; Petrov, E. E.; Tsyarkin, G. G. *Heat and Mass Transfer in Freezing and Thawing Soils (Published in Russian)*; Nauka: Moscow, Russia, 1996; p. 224.
51. Permyakov, P. P. Mathematical Modeling of Technogenic Pollution in Frozen Soils (Published in Russian). *Bull. Tomsk Polytech. Univ. Georesource Eng.* **2004**, *307*, *5*, 63–68.
52. Permyakov, P. P.; Ammosov, A. P.; Popov, G. G.; Khokholova, S. T. Mathematical Models in Predicting Man-Caused Pollution of the Permafrost Zone (Published in Russian). In *VIII Russian conference “Modern methods of mathematical modeling of natural and man-made disasters” October 26 - 28; Kemerovo, 2005*; pp 1–11.
53. Feng, J.-C.; Wang, Y.; Li, X.-S. Hydrate Dissociation Induced by Depressurization in Conjunction with Warm Brine Stimulation in Cubic Hydrate Simulator with Silica Sand. *Appl. Energy* **2016**, *174*, 181–191. <https://doi.org/10.1016/j.apenergy.2016.04.090>.
54. Li, S.; Wang, Z.; Xu, X.; Zheng, R.; Hou, J. Experimental Study on Dissociation of Hydrate Reservoirs with Different Saturations by Hot Brine Injection. *J. Nat. Gas Sci. Eng.* **2017**, *46*, 555–562. <https://doi.org/10.1016/j.jngse.2017.07.032>.
55. Kamath, V. A.; Mutalik, P. N.; Sira, J. H.; Patil, S. L. Experimental Study of Brine Injection Depressurization of Gas Hydrates Dissociation of Gas Hydrates. *SPE Form. Eval.* **1991**, *6*, *04*, 477–484. <https://doi.org/10.2118/19810-PA>.
56. Kamath, V. A.; Godbole, S. P. Evaluation of Hot-Brine Stimulation Technique for Gas Production From Natural Gas Hydrates. *J. Pet. Technol.* **1987**, *39*, *11*, 1379–1388. <https://doi.org/10.2118/13596-PA>.
57. Malakhova, V. V.; Eliseev, A. V. Salt Diffusion Effect on the Submarine Permafrost State and Distribution as Well as on the Stability Zone of Methane Hydrates on the Laptev Sea Shelf (Published in Russian). *Ice Snow* **2020**, *60*, *4*, 533–546.

58. Polozkov, K.A., Basniev, K.S., Gaftunyak, P. I. Complications Arising from the Construction and Operation of Wells in Permafrost Zones, and Measures to Prevent Them (Published in Russian). *Constr. oil gas wells L. sea* **2010**, *1*, 6–10.
59. Fjellanger, E.; Kontorovich, A. E.; Barboza, S. A.; Burshtein, L. M.; Hardy, M. J.; Livshits, V. R. Charging the Giant Gas Fields of the NW Siberia Basin. In *Petroleum Geology Conference Proceedings*; Geological Society of London, 2010; Vol. 7, pp 659–668.
<https://doi.org/10.1144/0070659>.
60. Ershov, E. D. *General Geocryology (Published in Russian)*; Moscow University Press: Moscow, Russia, 2002; p. 682.
61. Harris, S. A.; Brouckov, A.; Guodong, C. *Geocryology: Characteristics and Use of Frozen Ground and Permafrost Landforms*; CRC Press, 2017; p. 765, ISBN 9781351681629.
<https://doi.org/10.4324/978135166988>.
62. Kudryavtsev, V. A.; Dostovalov, B. N.; Romanovsky, N. N.; Kondratieva, K. A.; Melamed, V. G. *General Permafrost (Geocryology) (Published in Russian)*; MSU: Moscow, Russia, 1978; p. 464.
63. Chuvilin, E. M.; Perlova, E. V.; Yakushev, V. S. Classification of the Intrapermafrost Sediment Gas Component (Published in Russian). *Cryosph. Earth* **2005**, *9*, 3, 73–76.
64. Istomin, V.; Chuvilin, E.; Bukhanov, B.; Uchida, T. Pore Water Content in Equilibrium with Ice or Gas Hydrate in Sediments. *Cold Reg. Sci. Technol.* **2017**, *137*, 60–67.
<https://doi.org/10.1016/j.coldregions.2017.02.005>.
65. Akagawa, S.; Iwahana, G.; Watanabe, K.; Chuvilin, E. M.; Istomin, V. A.; Hinkel, K. M. Improvement of Pulse NMR Technology for Determination of Unfrozen Water Content in Frozen Soils. In *the Tenth International Conference on Permafrost, June*; Salekhard, Russia,

2012; pp 21–26.

66. Miyata, Y.; Akagawa, S. An Experimental Study of Dynamic Solid-Liquid Phase Equilibrium in a Porous Medium. *JSME Int. Journal, Ser. B Fluids Therm. Eng.* **1998**, *41*, 3, 590–600. <https://doi.org/10.1299/jsmeb.41.590>.
67. Kruse, A. M.; Darrow, M. M.; Akagawa, S. Improvements in Measuring Unfrozen Water in Frozen Soils Using the Pulsed Nuclear Magnetic Resonance Method. *J. Cold Reg. Eng.* **2018**, *32*, 1. [https://doi.org/10.1061/\(asce\)cr.1943-5495.0000141](https://doi.org/10.1061/(asce)cr.1943-5495.0000141).
68. Chuvilin, E. M.; Yakushev, V. S.; Perlova, E. V. Gas and Possible Gas Hydrates in the Permafrost of Bovanenkovo Gas Field, Yamal Peninsula, West Siberia. *Polarforschung* **2000**, *68*, 1–3, 215–219.
69. Hornum, M. T. Postglacial Rebound, Permafrost Growth and Its Impact on Groundwater Flow and Pingo Formation - An Investigation Combining Electrical Resistivity Tomography, Hydrogeochemistry and Decoupled Heat and Groundwater Transport Modelling, Adventdalen, Svalbard., 2018.
70. Obu, J.; Westermann, S.; Bartsch, A.; Berdnikov, N.; Christiansen, H. H.; Dashtseren, A.; Delaloye, R.; Elberling, B.; Etzelmüller, B.; Kholodov, A.; et al. Northern Hemisphere Permafrost Map Based on TTOP Modelling for 2000–2016 at 1 Km² Scale. *Earth-Science Rev.* **2019**, *193*, 299–316. <https://doi.org/10.1016/j.earscirev.2019.04.023>.
71. Vasiliev, A. A.; Gravis, A. G.; Gubarkov, A. A.; Drozdov, D. S.; Korostelev, Y. V.; Malkova, G. V.; Oblogov, G. E.; Ponomareva, O. E.; Sadurtdinov, M.R. Streletskaya, I.D. Streletsky, D. A.; Ustinova, E. V.; et al. Permafrost Degradation: Results of the Long-Term Geocryological Monitoring in the Western Sector of Russian Arctic (Published in Russian). *Kriosf. Zemli* **2020**, *XXIV*, 2, 15–30. [https://doi.org/10.21782/KZ1560-7496-2020-2\(15-30\)](https://doi.org/10.21782/KZ1560-7496-2020-2(15-30)).

72. HydroSpetsGeologiya. *Information Note with an Assessment of the Current State of the Subsoil in Significant and Man-Made Disturbed Conditions of the Territory of the Arctic Zone of the Russian Federation, Incl. at Geocryological Polygons Marre-Sale and Vorkuta in 2020* (Publis; 2021; p. 149.
73. Brown, J.; Ferrians Jr, O. J.; Heginbottom, J. A.; Melnikov, E. S. Circum-Arctic Map of Permafrost and Ground-Ice Conditions (Revised February 2001). *US Geological Survey*. Boulder, CO: National Snow and Ice Data Center/World Data Center for Glaciology. Digital media. 1998.
74. Misyurkeeva, N.; Buddo, I.; Kraev, G.; Smirnov, A.; Nezhdanov, A.; Shelokhov, I.; Kurchatova, A.; Belonosov, A. Periglacial Landforms and Fluid Dynamics in the Permafrost Domain: A Case from the Taz Peninsula, West Siberia. *Energies* **2022**, *15*, 8, 2794. <https://doi.org/10.3390/en15082794>.
75. Shakhova, N.; Semiletov, I.; Leifer, I.; Salyuk, A.; Rekant, P.; Kosmach, D. Geochemical and Geophysical Evidence of Methane Release over the East Siberian Arctic Shelf. *J. Geophys. Res. Ocean.* **2010**, *115*, 8, C08007:1-C08007:14. <https://doi.org/10.1029/2009JC005602>.
76. Harrison, W. D.; Osterkamp, T. E. Heat and Mass Transport Processes in Subsea Permafrost 1. An Analysis of Molecular Diffusion and Its Consequences. *J. Geophys. Res.* **1978**, *83*, C9, 4707. <https://doi.org/10.1029/JC083iC09p04707>.
77. Angelopoulos, M.; Overduin, P. P.; Miesner, F.; Grigoriev, M. N.; Vasiliev, A. A. Recent Advances in the Study of Arctic Submarine Permafrost. *Permafrost Periglacial Processes*. **2020**, *31*, 3, 442–453. <https://doi.org/10.1002/PPP.2061>.
78. Matveeva, T.; Savvichev, A. S.; Semenova, A.; Logvina, E.; Kolesnik, A. N.; Bosin, A. A. Source, Origin, and Spatial Distribution of Shallow Sediment Methane in the Chukchi Sea.

- Oceanography* **2015**, 28, 3, 202–217. <https://doi.org/10.5670/oceanog.2015.66>.
79. Lobkovskiy, L. I.; Nikiforov, S. L.; Dmitrevskiy, N. N.; Libina, N. V.; Semiletov, I. P.; Ananiev, R. A.; Meluzov, A. A.; Roslyakov, A. G. Gas Extraction and Degradation of the Submarine Permafrost Rocks on the Laptev Sea Shelf. *Oceanology* **2015**, 55, 2, 283–290. <https://doi.org/10.1134/s0001437015010129>.
80. Nicolsky, D.; Shakhova, N. Modeling Sub-Sea Permafrost in the East Siberian Arctic Shelf: The Dmitry Laptev Strait. *Environ. Res. Lett.* **2010**, 5, 1, 015006:1-015006:9. <https://doi.org/10.1088/1748-9326/5/1/015006>.
81. Portnov, A.; Mienert, J.; Serov, P. Modeling the Evolution of Climate-Sensitive Arctic Subsea Permafrost in Regions of Extensive Gas Expulsion at the West Yamal Shelf. *J. Geophys. Res. G Biogeosciences* **2014**, 119, 11, 2082–2094. <https://doi.org/10.1002/2014JG002685>.
82. Overduin, P. P.; Schneider von Deimling, T.; Miesner, F.; Grigoriev, M. N.; Ruppel, C.; Vasiliev, A.; Lantuit, H.; Juhls, B.; Westermann, S. Submarine Permafrost Map in the Arctic Modeled Using 1-D Transient Heat Flux (SuPerMAP). *J. Geophys. Res. Ocean.* **2019**, 124, 6, 3490–3507. <https://doi.org/10.1029/2018JC014675>.
83. Romanovskii, N. N.; Hubberten, H.-W.; Gavrilov, A. V.; Eliseeva, A. A.; Tipenko, G. S. Offshore Permafrost and Gas Hydrate Stability Zone on the Shelf of East Siberian Seas. *Geo-Marine Lett.* **2005**, 25, 2–3, 167–182. <https://doi.org/10.1007/s00367-004-0198-6>.
84. Romanovskii, N. N.; Tumskoi, V. E. Retrospective Approach to the Estimation of the Contemporary Extension and Structure of the Shelf Cryolithozone in East Arctic (Published in Russian). *Earth's Cryosph.* **2011**, 15, 1, 3–14.
85. Perlshtein, G. Z.; Sergeev, D. O.; Tipenko, G. S.; Tumskoy, V. E.; Khimenkov, A. N.; Vlasov, A. N.; Merzlyakov, V. P.; Stanilovskaya, Y. V. Hydrocarbon Gases and Permafrost Zone of the

- Arctic Shelf (Published in Russian). *Arct. Ecol. Econ.* **2015**, 2, 18, 35–44.
86. Fartyshev, A. I. *Features of the Coastal-Shelf Cryolithozone of the Laptev Sea (Published in Russian)*; Nauka: Novosibirsk, 1993; p. 135.
87. Grigoriev, N. F. *Permafrost in the Seaside Zone of Yakutia (Published in Russian)*; Nauka: Moscow, Russia, 1966; p. 180.
88. Melnikov, V. P.; Spesivtsev, V. I. *Engineering-Geological and Geocryological Conditions of the Shelf of the Barents and Kara Seas (Published in Russian)*; Nauka: Novosibirsk, 1995; p. 195.
89. Zhigarev, L. A. *Oceanic Permafrost (Published in Russian)*; MSU: Moscow, Russia, 1997; p. 318.
90. Anisimov, O. A.; Streletsky, D. A. Geocryological Hazards of Thawing Permafrost (Published in Russian). *Arct. XXI century. Nat. Sci.* **2015**, 2, 3, 60–74.
91. Li, L.; Yang, J.; Zou, X.; Yan, L.; Zhang, C.; Yang, P.; Ling, T.; Li, S. Monitoring Technology of Gas Hydrate in Polar Drilling. In *The 31st International Ocean and Polar Engineering Conference*; Rhodes, Greece, 2021.
92. Sergeev, D. Permafrost-Related Geohazards in Cold Russian Regions. *Oxford Res. Encycl. Nat. Hazard Sci.* **2018**. <https://doi.org/10.1093/ACREFORE/9780199389407.013.291>.
93. Kamenskikh, S. V. Logachev, Y. L.; Nor, A. V.; Ulyasheva, N. M.; Fomin, A. S. *Complications and Accidents during the Construction of Oil and Gas Wells (Published in Russian)*; USTU: Ukhta, Russia, 2014; p. 231.
94. Kamel, A. H. A Novel Mud Formulation for Drilling Operations in the Permafrost. In *SPE Western Regional Meeting Proceedings*; 2013; pp 252–261. <https://doi.org/10.2118/165335-ms>.
95. Avetisyan, N. G. *The Choice of the Type of Drilling Fluid for Drilling in Unstable Rocks. Overview (Published in Russian)*; VNIIOENG: Moscow, Russia, 1983; p. 30.

96. Dong, L.; Wan, Y.; Li, Y.; Liao, H.; Wu, N.; Leonenko, Y. 3d Numerical Simulation on Drilling Fluid Invasion into Natural Gas Hydrate Reservoirs. *SSRN Electron. J.* **2021**.
<https://doi.org/10.2139/ssrn.3898481>.
97. Aksenova, N. A.; Rozhkova, O. V. *Drilling Fluids and Well Flushing (Published in Russian)*; Tyumen Industrial University: Tyumen, 2016; p. 168.
98. RosTechNadzor. *On Approval of Federal Norms and Rules in the Field of Industrial Safety "Safety Rules in the Oil and Gas Industry (Published in Russian)*; 2020; Vol. Order №34.
99. Smirnova, O. G. Migration of Ions of Chemical Elements in Frozen Rocks and Ice (Published in Russian), Moscow State University, 1997.
100. Maramzin, A. V.; Ryazanov, A. A. *Drilling Exploratory Wells in Areas with Permafrost Distribution (Published in Russian)*; Nedra: Moscow, Russia, 1971; p. 145–163.
101. Avetov, N. R.; Krasnova, E. A.; Yakushev, V. S. About Possible Causes and Nature of Gas Showing around Gas and Gas-Condensate Wells at the Territory of Yamburg Oil-and-Gas-Condensate Field (Published in Russian). *News gas Sci.* **2018**, *1*, 33, 33–40.
102. Streletskii, D. A.; Streletskaya, I. D. Redistribution of Ions within the Active Layer and Upper Permafrost, Yamal, Russia. In *8th International Conference on Permafrost, 21-25 July*; Balkema: Zurich, Switzerland, 2003; pp 1117–1122.
103. Streletskaya, I. D. Cryopeg Responses To Periodic Climate Fluctuations. In *Permafrost - Seventh International Conference, June*; Yellowknife, Canada, 1998; pp 1021–1025.
104. Zhang, Q.; Wang, Z.; Fan, X.; Wei, N.; Zhao, J.; Lu, X.; Yao, B. A Novel Mathematical Method for Evaluating the Wellbore Deformation of a Diagenetic Natural Gas Hydrate Reservoir Considering the Effect of Natural Gas Hydrate Decomposition. *Nat. Gas Ind. B* **2021**.
<https://doi.org/10.1016/j.ngib.2021.04.009>.

105. Ulyantsev, A.; Polyakova, N.; Trukhin, I.; Parotkina, Y.; Dudarev, O.; Semiletov, I. Peculiarities of Pore Water Ionic Composition in the Bottom Sediments and Subsea Permafrost: A Case Study in the Buor-Khaya Bay. *Geosciences* **2022**, *12*, 2, 1–49.
<https://doi.org/10.3390/geosciences12020049>.
106. Chuvilin, E. M.; Ershov, E. D.; Naletova, N. S. Mass Transfer and Structure Formation in Freezing Saline Soils. In *7th International Conference on Permafrost*; Yellowknife, Canada, 1998; pp 173–179.
107. Iakovlev, A. A.; Turitsyna, M. V.; Mogil'nikov, E. V. Analysis and Justification of Selecting Cleaning Agents and Technology of Their Application in Permafrost Well Drilling (Published in Russian). *Bull. PNIPU. Geol. Oil gas Min.* **2014**, *12*, 22–32. <https://doi.org/10.15593/2224-9923/2014.12.3>.
108. Khimenkov, A. N.; Sergeev, D. O.; Vlasov, A. N.; Volkov-Bogorodsky, D. B.; Tipenko, G. S.; Merzlyakov, V. P.; Stanilovskaya, Y. V. Explosive Processes in Permafrost Areas – New Type of Geocryological Hazard. In *Innovation and Discovery in Russian Science and Engineering*; Springer, Cham, 2021; pp 83–99. https://doi.org/10.1007/978-3-030-63571-8_5.
109. Merey, Ş. Drilling of Gas Hydrate Reservoirs. *Journal of Natural Gas Science and Engineering*. 2016, pp 1167–1179. <https://doi.org/10.1016/j.jngse.2016.09.058>.
110. Ning, F.; Zhang, K.; Wu, N.; Zhang, L.; Li, G.; Jiang, G.; Yu, Y.; Liu, L.; Qin, Y. Invasion of Drilling Mud into Gas-Hydrate-Bearing Sediments. Part i: Effect of Drilling Mud Properties. *Geophys. J. Int.* **2013**, *193*, 3, 1370–1384. <https://doi.org/10.1093/gji/ggt015>.
111. Yakutseni, V. P. Gas Hydrates - Unconventional Gas Raw Materials, Their Formation, Properties, Distribution and Geological Resources (Published in Russian). *Oil gas Geol. Theory Pract.* **2013**, *8*, 4.

112. Bogoyavlensky, V. I. Natural and Technogenic Threats in Fossil Fuels Production in the Earth Cryolithosphere (Published in Russian). *Min. Ind. J. (Gornay Promishlennost)* **2020**, *1*, 97–118.
<https://doi.org/10.30686/1609-9192-2020-1-97-118>.
113. Are, F. E. Problem of Deep Gas Emission into the Atmosphere (Published in Russian). *Kriosf. Zemli* **1998**, *2*, *4*, 42–50.
114. Rivkin, F. M. Methane in Frozen Rocks and the Forecast of Its Release during Climate Warming and Technogenic Surface Disturbances (Published in Russian). *Proc. Russ. Acad. Sci. Geogr. Ser. Sci. J.* **1998**, *2*, 64–75.
115. Sergienko, V. I.; Lobkovskii, L. I.; Semiletov, I. P.; Dudarev, O. V.; Dmitrievskii, N. N.; Shakhova, N. E.; Romanovskii, N. N.; Kosmach, D. A.; Nikol'skii, D. N.; Nikiforov, S. L.; et al. The Degradation of Submarine Permafrost and the Destruction of Hydrates on the Shelf of East Arctic Seas as a Potential Cause of the Methane Catastrophe: Some Results of Integrated Studies in 2011. *Dokl. Earth Sci.* **2012**, *446*, *1*, 1132–1137.
<https://doi.org/10.1134/S1028334X12080144>.
116. Anisimov, O. A.; Zaboikina, Y. G.; Kokorev, V. A.; Yurganov, L. N. Possible Causes of Methane Release from the East Arctic Seas Shelf (Published in Russian). *Ice Snow* **2014**, *2*, *126*, 69–81.
117. Dyadin, Y. A.; Gushchin, A. L. Gas Hydrates (Published in Russian). *Soros Educ. J.* **1998**, *3*, 55–64.
118. Anisimov, O. A.; Lavrov, S. A.; Reneva, S. A. Methane Emission from Permafrost Swamps in Russia under Climate Change (Published in Russian). In *Problems of Ecological Modeling and Monitoring of Ecosystems*; Israel, S. A., Ed.; Gidrometeoizdat: Saint Petersburg, Russia, 2005; pp 124–142.

119. Bazhin, N. M. Emission of Methane from Sedimentary Layers (Published in Russian). In *Reducing Methane Emissions*; 2000; pp 239–244.
120. Sergienko, V. I.; Semiletov, I. P.; Shakhova, N. E. Emission of Methane and Carbon Dioxide on the East Siberian Shelf Is a Factor of Global Climate Change (Published in Russian). In *Proceedings of the meeting of the Scientific Council of the Russian Academy of Sciences for the Study of the Arctic and Antarctic, 31 March - 2 April*; Arkhangelsk, Russia, 2010; pp 117–136.
121. Perlova, E. V.; Miklyaeva, E. S.; Leonov, S. A.; Tkacheva, E. V.; Ukhova, Y. A. Gas Hydrates within the Yamal Peninsular and Adjoining Kara Sea Continental Shelf as a Negative Factor of the Yamal Region Exploration (Published in Russian). *News gas Sci.* **2017**, *3*, *31*, 255–262.
122. Collett, T. S.; Johnson, A. H.; Knapp, C. C.; Boswell, R. Natural Gas Hydrates: A Review. *AAPG Mem.* **2009**, *89*, 146–219. <https://doi.org/10.1306/13201101M891602>.
123. Kvenvolden, K. A. Gas Hydrates-Geological Perspective and Global Change. *Rev. Geophys.* **1993**, *31*, *2*, 173–187. <https://doi.org/10.1029/93RG00268>.
124. Moridis, G.; Collett, T. Strategies for Gas Production from Hydrate Accumulations under Various Geologic Conditions. *Proc. TOUGH Symp. Lawrence Berkeley Natl. Lab. Berkeley, California, May 12–14* **2003**.
125. Makogon, Y. F.; Holditch, S. A.; Makogon, T. Y. Natural Gas-Hydrates - A Potential Energy Source for the 21st Century. *J. Pet. Sci. Eng.* **2007**, *56*, *1–3*, 14–31. <https://doi.org/10.1016/j.petrol.2005.10.009>.
126. Liang, Y.; Tan, Y.; Luo, Y.; Zhang, Y.; Li, B. Progress and Challenges on Gas Production from Natural Gas Hydrate-Bearing Sediment. *J. Clean. Prod.* **2020**, *261*, 261:1-261:23. <https://doi.org/10.1016/j.jclepro.2020.121061>.
127. Nair, V. C.; Gupta, P.; Sangwai, J. S. Gas Hydrates as a Potential Energy Resource for Energy

- Sustainability; 2018; pp 265–287. https://doi.org/10.1007/978-981-10-7188-1_12.
128. Koh, D. Y.; Kang, H.; Lee, J. W.; Park, Y.; Kim, S. J.; Lee, J.; Lee, J. Y.; Lee, H. Energy-Efficient Natural Gas Hydrate Production Using Gas Exchange. *Appl. Energy* **2016**, *162*, 114–130. <https://doi.org/10.1016/j.apenergy.2015.10.082>.
 129. Makogon, Y. F.; Omelchenko, R. Y. Commercial Gas Production from Messoyakha Deposit in Hydrate Conditions. *J. Nat. Gas Sci. Eng.* **2013**, *11*, 1–6. <https://doi.org/10.1016/j.jngse.2012.08.002>.
 130. Choi, W.; Mok, J.; Lee, Y.; Lee, J.; Seo, Y. Optimal Driving Force for the Dissociation of CH₄ Hydrates in Hydrate-Bearing Sediments Using Depressurization. *Energy* **2021**, *223*,. <https://doi.org/10.1016/J.ENERGY.2021.120047>.
 131. Fereidounpour, A.; Vatani, A. An Investigation of Interaction of Drilling Fluids with Gas Hydrates Indrilling Hydrate Bearing Sediments. *J. Nat. Gas Sci. Eng.* **2014**, *20*, 422–427. <https://doi.org/10.1016/j.jngse.2014.07.006>.
 132. Huang, T.-J.; Zhang, Y.; Wang, Y.; Li, X.-S.; Chen, Z.-Y. An Experimental Drilling Apparatus Used for Evaluating Drilling Risks Related to Natural Gas Hydrate. *MethodsX* **2020**, *7*, 101019. <https://doi.org/10.1016/j.mex.2020.101019>.
 133. Barker, J. W.; Gomez, R. K. *Formation of Hydrates during Deepwater Drilling Operations*; 1996; p. 105–109. <https://doi.org/10.2118/16130-pa>.
 134. Priest, J. A.; Grozic, J. L. H. Stability of Fine-Grained Sediments Subject to Gas Hydrate Dissociation in the Arctic Continental Margin. In *Advances in Natural and Technological Hazards Research*; Springer Netherlands, 2016; Vol. 41, pp 427–436. https://doi.org/10.1007/978-3-319-20979-1_43.
 135. Stackelberg, M. V.; Müller, H. R. On the Structure of Gas Hydrates. *The Journal of Chemical*

- Physics*. 1951, pp 1319–1320. <https://doi.org/10.1063/1.1748038>.
136. Carroll, J. *Natural Gas Hydrates - A Guide for Engineers (3rd Edition)*; 2014; ISBN 978-0-12-800074-8.
 137. Istomin, V.; Yakushev, V.; Makhonina, N. Self-Preservation Phenomenon of Gas Hydrate (Published in Russian). *Gas Ind.* **2006**, *4*, 36–46.
 138. Koh, C. A.; Sloan, E. D. Natural Gas Hydrates: Recent Advances and Challenges in Energy and Environmental Applications. *AIChE J.* **2007**, *53*, 7, 1636–1643.
<https://doi.org/10.1002/aic.11219>.
 139. Koh, C. A.; Sum, A. K.; Sloan, E. D. State of the Art: Natural Gas Hydrates as a Natural Resource. *J. Nat. Gas Sci. Eng.* **2012**, *8*, 132–138. <https://doi.org/10.1016/j.jngse.2012.01.005>.
 140. Makogon, Y. F. Natural Gas Hydrates - A Promising Source of Energy. *Journal of Natural Gas Science and Engineering*. 2010, pp 49–59. <https://doi.org/10.1016/j.jngse.2009.12.004>.
 141. Supak, K. R.; George, D. L. Best Practices for Mitigating Flow Measurement Errors Associated with Hydrate Formation. *Pipeline&Gas J.* **2015**, *242*, 7.
 142. Makogon, Y. F. *Hydrates of Natural Gas (Published in Russian)*; Nedra: Moscow, Russia, 1974; p. 208, ISBN 978-364-214-233-8.
 143. Galloway, T. J.; Ruska, W.; Chappellear, P. S.; Kobayashi, R. Experimental Measurement of Hydrate Numbers for Methane and Ethane and Comparison with Theoretical Values. *Ind. Eng. Chem. Fundam.* **1970**, *9*, 2, 237–243. <https://doi.org/10.1021/i160034a008>.
 144. Sum, A. K.; Burruss, R. C.; Sloan, E. D. Measurement of Clathrate Hydrates via Raman Spectroscopy. *J. Phys. Chem. B* **1997**, *101*, 38, 7371–7377. <https://doi.org/10.1021/jp970768e>.
 145. Groysman, A. G. *Thermophysical Properties of Gas Hydrates*; Nauka: Novosibirsk, 1985; p. 94.
 146. Chong, Z. R.; Yang, S. H. B.; Babu, P.; Linga, P.; Li, X. Sen. Review of Natural Gas Hydrates

as an Energy Resource: Prospects and Challenges. *Appl. Energy* **2016**, *162*, 1633–1652.

<https://doi.org/10.1016/j.apenergy.2014.12.061>.

147. Hassanpouryouzband, A.; Joonaki, E.; Vasheghani Farahani, M.; Takeya, S.; Ruppel, C.; Yang, J.; English, N. J.; Schicks, J. M.; Edlmann, K.; Mehrabian, H.; et al. Gas Hydrates in Sustainable Chemistry. *Chem. Soc. Rev.* **2020**, *49*, *15*, 5225–5309. <https://doi.org/10.1039/C8CS00989A>.
148. Collett, T. S.; Ginsburg, G. D. Gas Hydrates in the Messoyakha Gas Field of the West Siberian Basin - A Re-Examination of the Geologic Evidence. *Int. J. Offshore Polar Eng.* **1998**, *8*, *1*, 22–29.
149. Wang, X. H.; Sun, C. Y.; Chen, G. J.; He, Y. N.; Sun, Y. F.; Wang, Y. F.; Li, N.; Zhang, X. X.; Liu, B.; Yang, L. Y. Influence of Gas Sweep on Methane Recovery from Hydrate-Bearing Sediments. *Chem. Eng. Sci.* **2015**, *134*, 727–736. <https://doi.org/10.1016/j.ces.2015.05.043>.
150. Boswell, R.; Bünz, S.; Collett, T. S.; Frye, M.; Fujii, T.; McConnell, D.; Mienert, J.; Pecher, I.; Reichel, T.; Ryu, B.-J.; et al. Introduction to Special Section: Exploration and Characterization of Gas Hydrates. *Interpretation* **2016**, *4*, *1*, 2. <https://doi.org/10.1190/int-2016-0103-spseintro.1>.
151. Vasiliev, V. G.; Makogon, Y. F.; Trebin, F. A.; Trofimuk, A. A.; Chersky, N. V. The Property of Natural Gases to Be in a Solid State in the Earth's Crust (Published in Russian), 1970.
152. Johnson, A.; Max, M. Technology Options to Enable Low Environmental Risk Production of Natural Gas Hydrate. *9th Int. Conf. Gas Hydrates* **2017**.
153. Hydrafact Ltd., H.-W. U. HydraFlash Software
[Http://Www.Hydrafact.Com/Index.Php?Page=software](http://www.hydrafact.com/index.php?page=software). Heriot-Watt Hydrate and Reservoir Fluids research group: Edinburg, UK.
154. Stern, L. A.; Kirby, S. H.; Circone, S.; Durham, W. B. Scanning Electron Microscopy Investigations of Laboratory-Grown Gas Clathrate Hydrates Formed from Melting Ice, and

Comparison to Natural Hydrates Stern et Al. *Am. Mineral.* **2004**, 89, 8–9, 1162–1175.

<https://doi.org/10.2138/am-2004-8-902>.

155. Kawamura, T.; Ohtake, M.; Yamamoto, Y.; Haneda, H.; Sakamoto, Y.; Komai, T.; Higuchi, S. Investigation For High Concentration Inhibitor Injection Into Artificial Methane Hydrate Bearing Sediment. **2009**, 119–123.
156. Zhao, X.; Qiu, Z.; Zhao, C.; Xu, J.; Zhang, Y. Inhibitory Effect of Water-Based Drilling Fluid on Methane Hydrate Dissociation. *Chem. Eng. Sci.* **2019**. <https://doi.org/10.1016/j.ces.2018.12.057>.
157. Khan, M. S.; Lal, B.; Bustam, M. A. Gas Hydrate Inhibitors. In *Green Energy and Technology*; 2020; pp 27–46. https://doi.org/10.1007/978-3-030-30750-9_2.
158. Sira, J.; Patil, S.; Kamath, V. A. Study of Hydrate Dissociation by Methanol and Glycol Injection. In *Proceedings - SPE Annual Technical Conference and Exhibition*; 1990; Vol. Pi. <https://doi.org/10.2118/20770-MS>.
159. Halliday, W.; Clapper, D. K.; Smalling, M. New Gas Hydrate Inhibitors for Deepwater Drilling Fluids. In *Proceedings of the IADC/SPE Asia Pacific Drilling Technology Conference, APDT*; 1998; pp 201–211. <https://doi.org/10.2118/1198-0052-jpt>.
160. Chong, Z. R.; Yin, Z.; Tan, J. H. C.; Linga, P. Experimental Investigations on Energy Recovery from Water-Saturated Hydrate Bearing Sediments via Depressurization Approach. *Appl. Energy* **2017**, 204, 1513–1525. <https://doi.org/10.1016/j.apenergy.2017.04.031>.
161. Zhao, J.; Zhu, Z.; Song, Y.; Liu, W.; Zhang, Y.; Wang, D. Analyzing the Process of Gas Production for Natural Gas Hydrate Using Depressurization. *Appl. Energy* **2015**, 142, 125–134. <https://doi.org/10.1016/j.apenergy.2014.12.071>.
162. Yang, X.; Sun, C. Y.; Su, K. H.; Yuan, Q.; Li, Q. P.; Chen, G. J. A Three-Dimensional Study on the Formation and Dissociation of Methane Hydrate in Porous Sediment by Depressurization.

- Energy Convers. Manag.* **2012**, *56*, 1–7. <https://doi.org/10.1016/j.enconman.2011.11.006>.
163. Heeschen, K. U.; Abendroth, S.; Priegnitz, M.; Spangenberg, E.; Thaler, J.; Schicks, J. M. Gas Production from Methane Hydrate: A Laboratory Simulation of the Multistage Depressurization Test in Mallik, Northwest Territories, Canada. *Energy and Fuels* **2016**, *30*, 8, 6210–6219. <https://doi.org/10.1021/acs.energyfuels.6b00297>.
164. Duan, Z.; Li, D.; Chen, Y.; Sun, R. The Influence of Temperature, Pressure, Salinity and Capillary Force on the Formation of Methane Hydrate. *Geosci. Front.* **2011**, *2*, 2, 125–135. <https://doi.org/10.1016/j.gsf.2011.03.009>.
165. Dallimore, S. R.; Collett, T. S. Scientific Results from the Mallik 2002 Gas Hydrate Production Research Well Program Mackenzie Delta, Northwest Territories, Canada. **2002**, 1–36.
166. Yang, J.; Okwananke, A.; Tohidi, B.; Chuvilin, E.; Maerle, K.; Istomin, V.; Bukhanov, B.; Cheremisin, A. Flue Gas Injection into Gas Hydrate Reservoirs for Methane Recovery and Carbon Dioxide Sequestration. *Energy Convers. Manag.* **2017**, *136*, 431–438. <https://doi.org/10.1016/j.enconman.2017.01.043>.
167. Saw, V. K.; Das, B. B.; Ahmad, I.; Mandal, A.; Laik, S. Influence of Electrolytes on Methane Hydrate Formation and Dissociation. *Energy Sources, Part A Recover. Util. Environ. Eff.* **2014**, *36*, *15*, 1659–1669. <https://doi.org/10.1080/15567036.2011.557695>.
168. Cherskiy, N. V.; Groysman, A. G.; Nikitina, L. M.; Tserev, V. P. First Experimental Determination of Heats of Decomposition of Natural-Gas Hydrates. *Dokl. Acad. Sci. USSR, Earth Sci. Sect.* **1984**, *265*, 163–167.
169. Handa, P. Y. A Calorimetric Study of Naturally Occurring Gas Hydrates. *Ind. Eng. Chem. Res.* **1988**, *27*, *5*, 872–874. <https://doi.org/10.1021/ie00077a026>.
170. Misyura, S. Y. The Influence of Porosity and Structural Parameters on Different Kinds of Gas

- Hydrate Dissociation. *Sci. Rep.* **2016**, *6*, *1*, 30324. <https://doi.org/10.1038/srep30324>.
171. Rehder, G.; Eckl, R.; Elfgen, M.; Falenty, A.; Hamann, R.; Kähler, N.; Kuhs, W. F.; Osterkamp, H.; Windmeier, C. Methane Hydrate Pellet Transport Using the Self-Preservation Effect: A Techno-Economic Analysis. *Energies* **2012**, *5*, *7*, 2499–2523. <https://doi.org/10.3390/EN5072499>.
172. Feng, J.-C.; Li, G.; Li, X.-S.; Li, B.; Chen, Z.-Y. Evolution of Hydrate Dissociation by Warm Brine Stimulation Combined Depressurization in the South China Sea. *Energies* **2013**, *6*, *10*, 5402–5425. <https://doi.org/10.3390/en6105402>.
173. Grigg, R. B.; Lynes, G. L. Oil-Based Drilling Mud as a Gas-Hydrates Inhibitor. *SPE Drill. Eng.* **1992**, *7*, *1*, 32–38. <https://doi.org/10.2118/19560-PA>.
174. Clennell, M. Ben; Hovland, M.; Booth, J. S.; Henry, P.; Winters, W. J. Formation of Natural Gas Hydrates in Marine Sediments: 1. Conceptual Model of Gas Hydrate Growth Conditioned by Host Sediment Properties. *J. Geophys. Res. Solid Earth* **1999**, *104*, *B10*, 22985–23003. <https://doi.org/10.1029/1999JB900175>.
175. Kumar, N.; Chowdhury, N. B.; Beltran, J. G. A 3-In-1 Approach to Evaluate Gas Hydrate Inhibitors. *Energies* **2019**, *12*, *15*, 2921. <https://doi.org/10.3390/en12152921>.
176. Englezos, P.; Bishnoi, P. R. Prediction of Gas Hydrate Formation Conditions in Aqueous Electrolyte Solutions. *AIChE J.* **1988**, *34*, *10*, 1718–1721. <https://doi.org/10.1002/aic.690341017>.
177. Maekawa, T.; Itoh, S.; Sakata, S.; Igari, S. I.; Imai, N. Pressure and Temperature Conditions for Methane Hydrate Dissociation in Sodium Chloride Solutions. *Geochem. J.* **1995**, *29*, *5*, 325–329.
178. Li, S.; Wang, J.; Lv, X.; Ge, K.; Jiang, Z.; Li, Y. Experimental Measurement and Thermodynamic Modeling of Methane Hydrate Phase Equilibria in the Presence of Chloride

- Salts. *Chem. Eng. J.* **2020**, *395*, 125126. <https://doi.org/10.1016/j.cej.2020.125126>.
179. Dickens, G. R.; Quinby-Hunt, M. S. Methane Hydrate Stability in Seawater. *Geophys. Res. Lett.* **1994**, *21*, *19*, 2115–2118. <https://doi.org/10.1029/94GL01858>.
180. Dholabhai, P. D.; Englezos, P.; Kalogerakis, N.; Bishnoi, P. R. Equilibrium Conditions for Methane Hydrate Formation in Aqueous Mixed Electrolyte Solutions. *Can. J. Chem. Eng.* **1991**, *69*, *3*, 800–805. <https://doi.org/10.1002/CJCE.5450690324>.
181. Qi, Y.; Wu, W.; Liu, Y.; Xie, Y.; Chen, X. The Influence of NaCl Ions on Hydrate Structure and Thermodynamic Equilibrium Conditions of Gas Hydrates. *Fluid Phase Equilib.* **2012**, *325*, 6–10. <https://doi.org/10.1016/J.FLUID.2012.04.009>.
182. Sun, S. C.; Kong, Y. Y.; Zhang, Y.; Liu, C. L. Phase Equilibrium of Methane Hydrate in Silica Sand Containing Chloride Salt Solution. *J. Chem. Thermodyn.* **2015**, *90*, 116–121. <https://doi.org/10.1016/j.jct.2015.06.030>.
183. Masoudi, R.; Tohidi, B. On Modelling Gas Hydrate Inhibition by Salts and Organic Inhibitors. *J. Pet. Sci. Eng.* **2010**, *74*, *3–4*, 132–137. <https://doi.org/10.1016/J.PETROL.2010.08.010>.
184. Zatsepina, O. Y.; Buffett, B. A. Thermodynamic Conditions for the Stability of Gas Hydrate in the Seafloor. *J. Geophys. Res. Solid Earth* **1998**, *103*, *10*, 24127–24139. <https://doi.org/10.1029/98jb02137>.
185. Najibi, H.; Mohammadi, A. H.; Tohidi, B. Estimating the Hydrate Safety Margin in the Presence of Salt and/or Organic Inhibitor Using Freezing Point Depression Data of Aqueous Solutions. *Ind. Eng. Chem. Res.* **2006**, *45*, *12*, 4441–4446. <https://doi.org/10.1021/ie051265v>.
186. Cha, M.; Hu, Y.; Sum, A. K. Methane Hydrate Phase Equilibria for Systems Containing NaCl, KCl, and NH₄Cl. *Fluid Phase Equilib.* **2016**, *413*, 2–9. <https://doi.org/10.1016/j.fluid.2015.08.010>.

187. Kharrat, M.; Dalmazzone, D. Experimental Determination of Stability Conditions of Methane Hydrate in Aqueous Calcium Chloride Solutions Using High Pressure Differential Scanning Calorimetry. *J. Chem. Thermodyn.* **2003**, *35*, 9, 1489–1505. [https://doi.org/10.1016/S0021-9614\(03\)00121-6](https://doi.org/10.1016/S0021-9614(03)00121-6).
188. De Roo, J. L.; Peters, C. J.; Lichtenthaler, R. N.; Diepen, G. A. M. Occurrence of Methane Hydrate in Saturated and Unsaturated Solutions of Sodium Chloride and Water in Dependence of Temperature and Pressure. *AIChE J.* **1983**, *29*, 4, 651–657. <https://doi.org/10.1002/aic.690290420>.
189. Hu, Y.; Lee, B. R.; Sum, A. K. Universal Correlation for Gas Hydrates Suppression Temperature of Inhibited Systems: I. Single Salts. *AIChE J.* **2017**, *63*, 11, 5111–5124. <https://doi.org/10.1002/aic.15846>.
190. Zeng, H.; Zhang, Y.; Li, X.; Chen, C.; Zhang, L.; Chen, Z. Experimental Study on the Influence of Brine Concentration on the Dissociation Characteristics of Methane Hydrate. *J. Nat. Gas Sci. Eng.* **2022**, *100*, 104492. <https://doi.org/10.1016/J.JNGSE.2022.104492>.
191. Jager, M. D.; Sloan, E. D. The Effect of Pressure on Methane Hydration in Pure Water and Sodium Chloride Solutions. *Fluid Phase Equilib.* **2001**, *185*, 1–2, 89–99. [https://doi.org/10.1016/S0378-3812\(01\)00459-9](https://doi.org/10.1016/S0378-3812(01)00459-9).
192. Zheng, R.; Li, X.; Negahban, S. Phase Boundary of Gas Hydrates in Single and Mixed Electrolyte Solutions: Using a Novel Unified Equation of State. *J. Mol. Liq.* **2022**, *345*, 117825:1-117825:13. <https://doi.org/10.1016/j.molliq.2021.117825>.
193. Seo, Y.; Lee, H. Hydrate Phase Equilibria of the Ternary CH₄ + NaCl + Water, CO₂ + NaCl + Water and CH₄ + CO₂ + Water Mixtures in Silica Gel Pores. *J. Phys. Chem. B* **2003**, *107*, 3, 889–894. <https://doi.org/10.1021/jp026776z>.

194. Semenov, A. P.; Stoporev, A. S.; Mendgaziev, R. I.; Gushchin, P. A.; Khlebnikov, V. N.; Yakushev, V. S.; Istomin, V. A.; Sergeeva, D. V.; Vinokurov, V. A. Synergistic Effect of Salts and Methanol in Thermodynamic Inhibition of SII Gas Hydrates. *J. Chem. Thermodyn.* **2019**, *137*, 119–130. <https://doi.org/10.1016/j.jct.2019.05.013>.
195. Choi, W.; Lee, J.; Kim, Y.-G.; Kim, H.; Rhee, T. S.; Jin, Y. K.; Kim, J.-H.; Seo, Y. The Impact of the Abnormal Salinity Enrichment in Pore Water on the Thermodynamic Stability of Marine Natural Gas Hydrates in the Arctic Region. *Sci. Total Environ.* **2021**, *799*, 149357:1-149357:9. <https://doi.org/10.1016/j.scitotenv.2021.149357>.
196. Sung, W.; Kang, H. Experimental Investigation of Production Behaviors of Methane Hydrate Saturated in Porous Rock. *Energy Sources* **2003**, *25*, 8, 845–856. <https://doi.org/10.1080/00908310390207873>.
197. Li, S.; Zheng, R.; Xu, X.; Chen, Y. Dissociation of Methane Hydrate by Hot Brine. *Pet. Sci. Technol.* **2015**, *33*, 6, 671–677. <https://doi.org/10.1080/10916466.2015.1005845>.
198. Ahn, T.; Park, C.; Lee, J.; Kang, J. M.; Nguyen, H. T. Experimental Characterization of Production Behaviour Accompanying the Hydrate Reformation in Methane-Hydrate-Bearing Sediments. *J. Can. Pet. Technol.* **2012**, *51*, 01, 14–19. <https://doi.org/10.2118/136737-PA>.
199. Jin, Y.; Li, S.; Yang, D.; Jiang, X. Determination of Dissociation Front and Operational Optimization for Hydrate Development by Combining Depressurization and Hot Brine Stimulation. *J. Nat. Gas Sci. Eng.* **2018**, *50*, 215–230. <https://doi.org/10.1016/j.jngse.2017.12.009>.
200. Xu, J.; Chen, Z.; Liu, J.; Sun, Z.; Wang, X.; Zhang, J. A Molecular Dynamic Study on the Dissociation Mechanism of SI Methane Hydrate in Inorganic Salt Aqueous Solutions. *J. Mol. Graph. Model.* **2017**, *75*, 403–412. <https://doi.org/10.1016/j.jmgm.2017.03.022>.

201. Ding, T.; Wang, R.; Xu, J.; Camara, M.; Zhou, W.; Zhang, J. Dissociation Mechanism of Methane Hydrate by CaCl₂: An Experimental and Molecular Dynamics Study. *J. Mol. Model.* **2022**, *28*, 4, 109. <https://doi.org/10.1007/s00894-022-05070-6>.
202. Li, X.-S.; Wan, L.-H.; Li, G.; Li, Q.-P.; Chen, Z.-Y.; Yan, K.-F. Experimental Investigation into the Production Behavior of Methane Hydrate in Porous Sediment with Hot Brine Stimulation. *Ind. Eng. Chem. Res.* **2008**, *47*, 23, 9696–9702. <https://doi.org/10.1021/ie8009582>.
203. Xu, J.; Gu, T.; Sun, Z.; Li, X.; Wang, X. Molecular Dynamics Study on the Dissociation of Methane Hydrate via Inorganic Salts. *Mol. Phys.* **2016**, *114*, 1, 34–43. <https://doi.org/10.1080/00268976.2015.1081708>.
204. Chen, J.; Liu, C.; Zhang, Z.; Wu, N.; Liu, C.; Ning, F.; Fang, B.; Wan, Y.; Bu, Q.; Hu, G. Molecular Study on the Behavior of Methane Hydrate Decomposition Induced by Ions Electrophoresis. *Fuel* **2022**, *307*, 121866:1-121866:7. <https://doi.org/10.1016/j.fuel.2021.121866>.
205. Mohammadi, A. H.; Afzal, W.; Richon, D. Gas Hydrates of Methane, Ethane, Propane, and Carbon Dioxide in the Presence of Single NaCl, KCl, and CaCl₂ Aqueous Solutions: Experimental Measurements and Predictions of Dissociation Conditions. *J. Chem. Thermodyn.* **2008**, *40*, 12, 1693–1697. <https://doi.org/10.1016/j.jct.2008.06.015>.
206. Aregbe, A.; Sun, B.; Engineering, L. C.-J. of C. &; 2019, undefined. Methane Hydrate Dissociation Conditions in High-Concentration NaCl/KCl/CaCl₂ Aqueous Solution: Experiment and Correlation. *ACS Publ.* **2019**, *64*, 7, 2929–2939. <https://doi.org/10.1021/acs.jced.8b01173>.
207. Atik, Z.; Windmeier, C.; Oellrich, L. R. Experimental Gas Hydrate Dissociation Pressures for Pure Methane in Aqueous Solutions of MgCl₂ and CaCl₂ and for a (Methane + Ethane) Gas Mixture in an Aqueous Solution of (NaCl + MgCl₂). *J. Chem. Eng. Data* **2006**, *51*, 5, 1862–

1867. <https://doi.org/10.1021/je060225a>.
208. Chong, Z. R.; Chan, A. H. M.; Babu, P.; Yang, M.; Linga, P. Effect of NaCl on Methane Hydrate Formation and Dissociation in Porous Media. *J. Nat. Gas Sci. Eng.* **2015**, *27*, 178–189. <https://doi.org/10.1016/J.JNGSE.2015.08.055>.
209. Stoporev, A. S.; Semenov, A. P.; Medvedev, V. I.; Kidyarov, B. I.; Manakov, A. Y.; Vinokurov, V. A. Nucleation of Gas Hydrates in Multiphase Systems with Several Types of Interfaces. *J. Therm. Anal. Calorim.* **2018**, *134*, *1*, 783–795. <https://doi.org/10.1007/s10973-018-7352-2>.
210. Li, H.; Wang, L. Hydrophobized Particles Can Accelerate Nucleation of Clathrate Hydrates. *Fuel* **2015**, *140*, 440–445. <https://doi.org/10.1016/j.fuel.2014.10.005>.
211. Prasad, P. S. R.; Kiran, B. S. Self-Preservation and Stability of Methane Hydrates in the Presence of NaCl. *Sci. Rep.* **2019**, *9*, *1*, 5860. <https://doi.org/10.1038/s41598-019-42336-1>.
212. Henry, P.; Thomas, M.; Clennell, M. Ben. Formation of Natural Gas Hydrates in Marine Sediments: 2. Thermodynamic Calculations of Stability Conditions in Porous Sediments. *J. Geophys. Res. Solid Earth* **1999**, *104*, *B10*, 23005–23022. <https://doi.org/10.1029/1999JB900167>.
213. Zaripova, Y.; Yarkovoi, V.; Varfolomeev, M.; Kadyrov, R.; Stoporev, A. Influence of Water Saturation, Grain Size of Quartz Sand and Hydrate-Former on the Gas Hydrate Formation. *Energies* **2021**, *14*, *5*, 1272. <https://doi.org/10.3390/en14051272>.
214. Daigle, H.; Dugan, B. Capillary Controls on Methane Hydrate Distribution and Fracturing in Advective Systems. *Geochemistry, Geophys. Geosystems* **2011**, *12*, *1*, Q01003:1–Q01003:18. <https://doi.org/10.1029/2010GC003392>.
215. Smith, D. H.; Wilder, J. W.; Seshadri, K. Methane Hydrate Equilibria in Silica Gels with Broad Pore-Size Distributions. *AIChE J.* **2002**, *48*, *2*, 393–400. <https://doi.org/10.1002/aic.690480222>.

216. Anderson, R.; Llamedo, M.; Tohidi, B.; Burgass, R. W. Characteristics of Clathrate Hydrate Equilibria in Mesopores and Interpretation of Experimental Data. *J. Phys. Chem. B* **2003**, *107*, *15*, 3500–3506. <https://doi.org/10.1021/jp0263368>.
217. Sergeeva, D.; Istomin, V.; Chuvilin, E.; Bukhanov, B.; Sokolova, N. Influence of Hydrate-Forming Gas Pressure on Equilibrium Pore Water Content in Soils. *Energies* **2021**, *Vol. 14*, *Page 1841* **2021**, *14*, *7*, 1841. <https://doi.org/10.3390/EN14071841>.
218. Wu, G.; Ji, H.; Tian, L.; Chen, D. Effects of Salt Ions on the Methane Hydrate Formation and Dissociation in the Clay Pore Water and Bulk Water. *Energy & Fuels* **2018**, *32*, *12*, 12486–12494. <https://doi.org/10.1021/acs.energyfuels.8b03486>.
219. Bello-Palacios, A.; Almenningen, S.; Fotland, P.; Ersland, G. Experimental and Numerical Analysis of the Effects of Clay Content on CH₄ Hydrate Formation in Sand. *Energy & Fuels* **2021**, *acs.energyfuels.1c00549*. <https://doi.org/10.1021/acs.energyfuels.1c00549>.
220. Qin, Y.; Pan, Z.; Liu, Z.; Shang, L.; Zhou, L. Influence of the Particle Size of Porous Media on the Formation of Natural Gas Hydrate: A Review. *Energy & Fuels* **2021**, *35*, *15*, 11640–11664. <https://doi.org/10.1021/acs.energyfuels.1c00936>.
221. Kang, S.; Ryu, H.; Seo, Y. Phase Behavior of CO₂ and CH₄ Hydrate in Porous Media. *World Acad. Sci. Eng. Technol.* **2007**, *33*, 183–188.
222. Istomin, V.; Chuvilin, E.; Makhonina, N.; Kvon, V.; Safonov, S. Description of Gas Hydrates Equilibria in Sediments Using Experimental Data of Soil Water Potential. In *ICGH-2008, July 6-10*; Vancouver, Canada, 2008; pp 1–12.
223. Johnson, A. H. Global Resource Potential of Gas Hydrate – a New Calculation. *Nat. Gas Oil* **2011**, *304*, 285–4541.
224. Solov'yev, V. A.; Ginsburg, G. D. Formation of Submarine Gas Hydrates. *Bull. Geol. Soc.*

Denmark **1994**, 41, 86–94.

225. Okwananke, A.; Yang, J.; Tohidi, B.; Chuvilin, E.; Istomin, V.; Cheremisin, A. Compressed Air Injection for Methane Recovery from Gas Hydrate-Bearing Sediments. *Ninth Int. Conf. Gas Hydrates* **2017**.
226. Davletshina, D. A. Regularities of Formation and Dissociation of Gas Hydrates in Frozen Sediments (Published in Russian), Institute of permafrost, Yakutsk, 2021.
227. Romanovskii, N. N.; Hubberten, H. W.; Gavrilov, A. V.; Eliseeva, A. A.; Tipenko, G. S.; Kholodov, A. L.; Romanovsky, V. E. Permafrost and Gas Hydrate Stability Zone Evolution on the Eastern Part of the Eurasia Arctic Sea Shelf in the Middle Pleistocene-Holocene (Published in Russian). *Earth's Cryosph.* **2003**, 7, 4, 51–64.
228. Malakhova, V.; Golubeva, E. Model Study of the Effects of Climate Change on the Methane Emissions on the Arctic Shelves. *Atmosphere (Basel)*. **2022**, 13, 2, 274:1-274:21.
<https://doi.org/10.3390/atmos13020274>.
229. Chuvilin, E.; Davletshina, D. A.; Lupachik, M. Hydrate Formation in Frozen and Thawing Methane Saturated Sediments (Published in Russian). *Earth's Cryosph.* **2019**, 23, 2, 50–61.
230. Kvenvolden, K. A. Natural Gas Hydrate Occurrence and Issues. *Ann. N. Y. Acad. Sci.* **1994**, 715, 1, 232–246. <https://doi.org/10.1111/j.1749-6632.1994.tb38838.x>.
231. Sun, Y.; Goldberg, D.; Collett, T.; Hunter, R. High-Resolution Well-Log Derived Dielectric Properties of Gas-Hydrate-Bearing Sediments, Mount Elbert Gas Hydrate Stratigraphic Test Well, Alaska North Slope. *Mar. Pet. Geol.* **2011**, 28, 2, 450–459.
<https://doi.org/10.1016/j.marpetgeo.2010.03.001>.
232. Zhu, Y.; Zhang, Y.; Wen, H.; Lu, Z.; Jia, Z.; Li, Y.; Li, Q.; Liu, C.; Wang, P.; Guo, X. Gas Hydrates in the Qilian Mountain Permafrost, Qinghai, Northwest China. *Acta Geol. Sin.* -

- English Ed.* **2010**, *84*, *1*, 1–10. <https://doi.org/10.1111/j.1755-6724.2010.00164.x>.
233. Liu, C.; Meng, Q.; He, X.; Li, C.; Ye, Y.; Lu, Z.; Zhu, Y.; Li, Y.; Liang, J. Comparison of the Characteristics for Natural Gas Hydrate Recovered from Marine and Terrestrial Areas in China. *J. Geochemical Explor.* **2015**, *152*, 67–74. <https://doi.org/10.1016/j.gexplo.2015.02.002>.
234. Lu, Z.; Zhu, Y.; Zhang, Y.; Wen, H.; Li, Y.; Liu, C. Gas Hydrate Occurrences in the Qilian Mountain Permafrost, Qinghai Province, China. *Cold Reg. Sci. Technol.* **2011**, *66*, 2–3, 93–104. <https://doi.org/10.1016/j.coldregions.2011.01.008>.
235. Lu, Z.; Zhu, Y.; Liu, H.; Zhang, Y.; Jin, C.; Huang, X.; Wang, P. Gas Source for Gas Hydrate and Its Significance in the Qilian Mountain Permafrost, Qinghai. *Mar. Pet. Geol.* **2013**, *43*, 341–348. <https://doi.org/10.1016/j.marpetgeo.2013.01.003>.
236. Golmohammadi, S. M.; Nakhaee, A. A Cylindrical Model for Hydrate Dissociation near Wellbore during Drilling Operations. *J. Nat. Gas Sci. Eng.* **2015**, *27*, 1641–1648. <https://doi.org/10.1016/j.jngse.2015.10.032>.
237. Agalakov, S. E.; Kurchikov, A. R.; Baburin, A. N. Geological and Geophysical Background the Existence of Gas Hydrates in the Turonian Deposits of the East Messoyakha Deposits (Published in Russian). *Geol. Geophys.* **2001**, *42*, 11–12, 1785–1791.
238. Andreassen, K.; Hubbard, A.; Winsborrow, M.; Patton, H.; Vadakkepuliambatta, S.; Plaza-faverola, A.; Deryabin, A.; Mattingsdal, R.; Mienert, J. Gas Hydrate Regulate Methane Emissions from Arctic Petroleum Basins. In *Proceeding of the 9th International Conference on Gas Hydrates (ICGH9)*; 2017; p 2.
239. Chuvilin, E.; Ekimova, V.; Davletshina, D.; Sokolova, N.; Bukhanov, B. Evidence of Gas Emissions from Permafrost in the Russian Arctic. *Geosciences* **2020**, *10*, 10, 383:1-383:23. <https://doi.org/10.3390/geosciences10100383>.

240. Anisimov, O. A.; Kokorev, V. A. Comparative Analysis of Land, Marine, and Satellite Observations of Methane in the Lower Atmosphere in the Russian Arctic under Conditions of Climate Change. *Izv. Atmos. Ocean. Phys.* **2015**, *51*, 9, 979–991.
<https://doi.org/10.1134/s0001433815090030>.
241. Bogoyavlensky, V. I. Prospects and Problems of the Arctic Shelf Oil and Gas Fields Development (Published in Russian). *Drill. Oil* **2012**, *11*, 4–9.
242. Bogoyavlensky, V. I. Gas-Hydrodynamics in the Arctic Craters of Gas Blowout (Published in Russia). *Arct. Ecol. Econ.* **2018**, No. 1(29), 48–55. <https://doi.org/10.25283/2223-4594-2018-1-48-55>.
243. Bogoyavlensky, V. I.; Sizov, O. S.; Bogoyavlensky, I. V.; Nikonov, R. A. Remote Detection of Areas of Surface Gas Manifestations and Gas Emissions in the Arctic: The Yamal Peninsula (Published in Russian). *Arct. Ecol. Econ.* **2016**, *3*, 23, 4–15.
244. Sizov, O. S. Remote Analysis of the Consequences of Surface Gas Show in the North of Western Siberia (Published in Russian). *Geomatics* **2015**, *21*, 1, 53–68.
245. Buldovicz, S. N.; Khilimonyuk, V. Z.; Bychkov, A. Y.; Ospennikov, E. N.; Vorobyev, S. A.; Gunar, A. Y.; Gorshkov, E. I.; Chuvilin, E. M.; Cherbunina, M. Y.; Kotov, P. I.; et al. Cryovolcanism on the Earth: Origin of a Spectacular Crater in the Yamal Peninsula (Russia). *Sci. Rep.* **2018**, *8*, 1, 13534. <https://doi.org/10.1038/s41598-018-31858-9>.
246. Bogoyavlensky, V. I. Oil and Gas Emissions on Land and Offshore Areas of the Arctic and World Ocean (Published in Russian). *Drill. oil* **2015**, No. 6, 4–10.
247. Leibman, M. O.; Plekhanov, A. V. Yamal Gas Emission Crater: Results of Preliminary Survey (Published in Russian). *KholodOk* **2014**, *2*, 9–15.
248. Leibman, M. O.; Kizyakov, A. I.; Plekhanov, A. V; Streletskaya, I. D. New Permafrost Feature –

Deep Crater in Central Yamal (West Siberia, Russia) as a Response to Local Climate

Fluctuations. *Geogr. Environ. Sustain.* **2014**, *7*, *4*, 68–79. <https://doi.org/10.24057/2071-9388-2014-7-4-68-79>.

249. Olenchenko, V. V.; Sinitsky, A. I.; Antonov, E. Y.; Eltsov, I. N.; Kushnarenko, O. N.; Plotnikov, A. E.; Potapov, V. V.; Epov, M. I. Results of Geophysical Researches of the Area of New Geological Formation “Yamal Crater” (Published in Russian). *Kriosf. Zemli* **2015**, *19*, *4*, 94–106.
250. Kizyakov, A. I.; Sonyushkin, A. V.; Leibman, M. O.; Zimin, M. V. Geomorphological Conditions of the Gas-Emission Crater and Its Dynamics in Central Yamal (In Russian). *Kriosf. Zemli* **2015**, *19*, *2*, 13–23.
251. Kizyakov, A.; Zimin, M.; Sonyushkin, A.; Dvornikov, Y.; Khomutov, A.; Leibman, M. Comparison of Gas Emission Crater Geomorphodynamics on Yamal and Gydan Peninsulas (Russia), Based on Repeat Very-High-Resolution Stereopairs. *Remote Sens.* **2017**, *9*, *10*, 1023. <https://doi.org/10.3390/rs9101023>.
252. Chuvilin, E.; Stanilovskaya, J.; Titovsky, A.; Sinitsky, A.; Sokolova, N.; Bukhanov, B.; Spasennykh, M.; Cheremisin, A.; Grebenkin, S.; Davletshina, D.; et al. A Gas-Emission Crater in the Erkuta River Valley, Yamal Peninsula: Characteristics and Potential Formation Model. *Geosciences* **2020**, *10*, *5*, 170. <https://doi.org/10.3390/geosciences10050170>.
253. Bogoyavlensky, V. I.; Bogoyavlensky, I. V.; Sizov, O. S.; Nikonov, R. A.; Kargina, T. N. Earth Degassing in the Arctic: Remote and Field Studies of the Thermokarst Lakes Gas Eruption (Published in Russian). *Arct. Ecol. Econ.* **2019**, No. 2(34), 31–47. <https://doi.org/10.25283/2223-4594-2019-2-31-47>.
254. Bogoyavlensky, V. I.; Erokhin, G. N.; Nikonov, R. A.; Bogoyavlensky, I. V.; Bryksin, V. M.

- Study of Catastrophic Gas Blowout Zones in the Arctic Based on Passive Microseismic Monitoring (on the Example of Lake Otkrytiye) (Published in Russian). *Arct. Ecol. Econ.* **2020**, *1*, 37, 93–104. <https://doi.org/doi: 10.25283/2223-4594-2020-1-93-104>.
255. Kalinko, M. K. *History of Geological Development and Oil and Gas Potential of the Khataigekoy Depression (Published in Russian)*; Gostoptekhizdat: Leningrad, 1959; p. 358.
256. Mamzelev, A. P.; Are, F. E. Geological-Engineering Conditions of Yamal Peninsula along Designing Railroad. In *6th International Conference on Permafrost 5-9 July*; South China University of Technology Press: Beijing, China, 1993; pp 436–442.
257. Melnikov, P. I.; Melnikov, V. P.; Tsarev, V. P. On Generation of Hydrocarbons in the Thicknesses of the Permafrost Rocks (Published in Russian). *Izv. AN SSSR. Seriya Geol.* **1989**, *2*, 118–128.
258. Badu, Y. B. The Cryolithic Structure of the Ground. In *The cryosphere of oil and gas condensate fields, Yamal Peninsula*; Nedra: Saint Petersburg, Russia, 2006; pp 85–111.
259. Chuvilin, E. M.; Perlova, E. V.; Baranov, Y. B.; Kondakov, V. V.; Osokin, A. B.; Yakushev, V. S. *Structure and Properties of Rocks in Cryolithozone of the Southern Part of Bovanenkovo Gas-Condensate Deposit (Published in Russian)*; GEOS: Moscow, Russia, 2007; p. 137.
260. Kondakov, V. V.; Kusova, O. F.; Kondakov, M. V. Geocryological Conditions of the North-Eastern Part of the Yamal Peninsula (Published in Russian). In *The fourth conference of geocryologists of Russia*; University book: Moscow, Russia, 2011; pp 89–94.
261. Bolshakov, Yu.Ya. Kultikov, A. M. *Analysis of Gas Showings during Drilling on the Territory of Bovanenkovo and Kharasavey Fields (Published in Russian): Report of the Institute of North Development Problems of the Siberian Branch of the USSR Academy of Sciences. N2 1*; Tyumen, 1989; p. 74.

262. Kondakov, V. V.; Galyavich, A. S. Comprehensive Studies of Permafrost Sediments with an Assessment of Their Water and Gas Saturation (Published in Russian). In *Problems of cryology of the Earth: abstracts. report conferences, 20-24 April*; Pushchino, Russia, 1998; p 105.
263. Ivanov, M. S. Modern Permafrost Coastal Deltaic Sediments of the Yansky Seaside (Published in Russian). *Quest. Geogr. Yakutia* **1969**, 5, 138–147.
264. Masurenkov, Y. P.; Slezin, Y. B.; Sobisevich, A. L. Gas Plumes off Bennett’s Island (Published in Russian). *Bull. Russ. Acad. Sci. Geogr. Ser.* **2015**, 3, 86–95.
265. Rekant, P. V.; Tumskoy, V. E.; Gusev, E. A.; Schwenk, T.; Spiess, F.; Cherkashev, G. A.; Kassens, H. Distribution and Features of Occurrence of the Subaqueous Cryolithozone in the Area of the Semenovskaya and Vasilievskaya Banks (the Laptev Sea) According to Seismoacoustic Profiling (Published in Russian). In *System of the Laptev Sea and Adjacent Seas of the Arctic: Current State and History of development*; Moscow State University: Moscow, Russia, 2009; pp 292–308.
266. Shakhova, N. E.; Semiletov, I. P.; Salyuk, A. N.; Belcheva, N. N.; Kosmach, D. A. Anomalies of Methane in the Water Layer of the Atmosphere on the Shelf of the East Siberian Arctic (Published in Russian). *Reports Acad. Sci.* **2007**, 414, 6, 819–823.
267. Shakhova, N.; Semiletov, I.; Leifer, I.; Sergienko, V.; Salyuk, A.; Kosmach, D.; Chernykh, D.; Stubbs, C.; Nicolisky, D.; Tumskoy, V.; et al. Ebullition and Storm-Induced Methane Release from the East Siberian Arctic Shelf. *Nat. Geosci.* **2014**, 7, 1, 64–70.
<https://doi.org/10.1038/ngeo2007>.
268. Shakhova, N.; Semiletov, I.; Sergienko, V.; Lobkovsky, L.; Yusupov, V.; Salyuk, A.; Salomatin, A.; Chernykh, D.; Kosmach, D.; Panteleev, G.; et al. The East Siberian Arctic Shelf: Towards Further Assessment of Permafrost-Related Methane Fluxes and Role of Sea Ice. *Philos. Trans.*

R. Soc. A Math. Phys. Eng. Sci. **2015**, 373, 2052:1-2052:13.

<https://doi.org/10.1098/rsta.2014.0451>.

269. Shakhova, N. E.; Sergienko, V. I.; Semiletov, I. P. The Contribution of the East Siberian Shelf to the Modern Methane Cycle. *Her. Russ. Acad. Sci.* **2009**, 79, 3, 237–246.
<https://doi.org/10.1134/S101933160903006X>.
270. Baranov, B.; Galkin, S.; Vedenin, A.; Dozorova, K.; Gebruk, A.; Flint, M. Methane Seeps on the Outer Shelf of the Laptev Sea: Characteristic Features, Structural Control, and Benthic Fauna. *Geo-Marine Lett.* **2020**. <https://doi.org/10.1007/s00367-020-00655-7>.
271. Samarkin, V.; Semiletov, I. P.; Finke, N.; Shakhova, N. E.; Joye, S. B. Methane Carbon Stable Isotope Signatures in Waters and Sediments of the Laptev Sea Shelf. In *American Geophysical Union, 3-7 December*; San Francisco, USA, 2012; pp B21D-0411.
272. Weidner, E.; Weber, T. C.; Mayer, L.; Jakobsson, M.; Chernykh, D.; Semiletov, I. A Wideband Acoustic Method for Direct Assessment of Bubble-Mediated Methane Flux. *Cont. Shelf Res.* **2019**, 173, 104–115. <https://doi.org/10.1016/j.csr.2018.12.005>.
273. Firsov, Y. G.; Ivanov, M. V.; Koloskov, E. N. A New Stage in Bathymetric Studies of the Northern Waters of Russia on the Example of the Kara Sea (Published in Russian). *Bull. State Univ. Mar. River Fleet Admiral Makarov* **2014**, 6, 28, 115–124.
274. Koloskov, E. N.; Firsov, Y. G. The Use of Modern Hydrographic Technologies for the Study of Topography and Bottom Gas Occurrence in the Northern Seas of Russia (Published in Russian). *Bull. State Univ. Marit. River Fleet Admiral SB Makarov* **2015**, 3, 31, 54–62.
275. Bondarev, V. N.; Rokos, S. I.; Kostin, D. A.; Dlugach, A. G.; Polyakova, N. A. Underpermafrost Accumulations of Gas in the Upper Part of the Sedimentary Cover of the Pechora Sea (Published in Russian). *Geol. Geophys.* **2002**, 43, 7, 587–598.

276. Rokos, S. I. Engineering and Geological Features of Near-Surface Zones of Anomalously High Reservoir Pressure on the Shelf of the Pechora and Southern Kara Seas (Published in Russian). *Eng. Geol.* **2008**, *4*, 22–28.
277. Grigoriev, M. N. Studies of the Degradation of Permafrost Rocks in the Seas of Eastern Siberia (Based on the Results of Expeditions in 2014–2016) (Published in Russian). *Arct. Antarct. Probl.* **2018**, *1*, 89–96.
278. Safronov, A. F.; Shits, E. Y.; Grigor'ev, M. N.; Semenov, M. E. Formation of Gas Hydrate Deposits in the Siberian Arctic Shelf (Published in Russian). *Russ. Geol. Geophys.* **2010**, *51*, *1*, 83–87. <https://doi.org/10.1016/j.rgg.2009.12.006>.
279. Delisle, G. Temporal Variability of Subsea Permafrost and Gas Hydrate Occurrences as Function of Climate Change in the Laptev Sea, Siberia. *Polarforschung* **2000**, *68*, *1–3*, 221–225.
280. Shakhova, N.; Semiletov, I.; Salyuk, A.; Yusupov, V.; Kosmach, D.; Gustafsson, Ö. Extensive Methane Venting to the Atmosphere from Sediments of the East Siberian Arctic Shelf. *Science* (80-.). **2010**, *327*, *5970*, 1246–1250. <https://doi.org/10.1126/science.1182221>.
281. Nicolsky, D. J.; Romanovsky, V. E.; Romanovskii, N. N.; Kholodov, A. L.; Shakhova, N. E.; Semiletov, I. P. Modeling Sub-Sea Permafrost in the East Siberian Arctic Shelf: The Laptev Sea Region. *J. Geophys. Res. Earth Surf.* **2012**, *117*, *3*, F03028:1-F03028:22. <https://doi.org/10.1029/2012JF002358>.
282. Bondur, V. G.; Kuznetsova, T. V.; Vorobyev, V. E.; Zamshin, V. Detection of Gas Shows (Gas Seeps) on the Russian Shelf Using Satellite Data (Published in Russian). *Georesources. Geoenergy. Geopolit.* **2014**, *1*, *9*, 1–23.
283. Bondur, V. G.; Kuznetsova, T. V. Detecting Gas Seeps in Arctic Water Areas Using Remote Sensing Data. *Izv. Atmos. Ocean. Phys.* **2015**, *51*, *9*, 1060–1072.

<https://doi.org/10.1134/S0001433815090066>.

284. Ananiev, R. A.; Dmitrevsky, N. N.; Roslyakov, A. G.; Chernykh, D. V.; Moroz, E. A.; Zarayskaya, Y. A.; Semiletov, I. P. Acoustic Monitoring of Gas Emission Processes in the Arctic Shelf Seas. *Oceanol.* 2022 621 **2022**, 62, 1, 127–132.
<https://doi.org/10.1134/S0001437022010015>.
285. Bogoyavlensky, V.; Kishankov, A.; Kazanin, A.; Kazanin, G. Distribution of Permafrost and Gas Hydrates in Relation to Intensive Gas Emission in the Central Part of the Laptev Sea (Russian Arctic). *Mar. Pet. Geol.* **2022**, 138, 105527.
<https://doi.org/10.1016/J.MARPETGEO.2022.105527>.
286. Anisimov, O. A.; Borzenkova, I. I.; Lavrov, S. A.; Strelchenko, Y. G. Modern Dynamics of Underwater Permafrost and Methane Emission on the Shelf of the Seas of the Eastern Arctic (Published in Russian). *Ice snow* **2012**, 2, 97–105.
287. Ruppel, C. D.; Kessler, J. D. The Interaction of Climate Change and Methane Hydrates. *Rev. Geophys.* **2017**, 55, 1, 126–168. <https://doi.org/10.1002/2016RG000534>.
288. Fedoseev, S. M. Gas Hydrates of Permafrost (Published in Russian). *Nat. Resour. Arct. Subarct.* **2006**, 1, 22–27.
289. Ershov, E. D.; Lebedenko, Y. P.; Chuvilin, E. M.; Benediktova, N. A. Migration of Chemical Elements and Related Environmental Problems (Published in Russian). In *the III Republican scientific and technical seminar “Modern methods of exploration and development of minerals in the Far North”*; Syktyvkar, Russia, 1989; pp 26–30.
290. Hao, S. A Study to Optimize Drilling Fluids to Improve Borehole Stability in Natural Gas Hydrate Frozen Ground. *J. Pet. Sci. Eng.* **2011**, 76, 3–4, 109–115.
<https://doi.org/10.1016/j.petrol.2011.01.014>.

291. Srungavarapu, M.; Patidar, K. K.; Pathak, A. K.; Mandal, A. Performance Studies of Water-Based Drilling Fluid for Drilling through Hydrate Bearing Sediments. *Appl. Clay Sci.* **2018**.
<https://doi.org/10.1016/j.clay.2017.11.014>.
292. Li, Q.; Liu, L.; Yu, B.; Guo, L.; Shi, S.; Miao, L. Borehole Enlargement Rate as a Measure of Borehole Instability in Hydrate Reservoir and Its Relationship with Drilling Mud Density. *J. Pet. Explor. Prod.* **2021**, *11*, 3, 1185–1198. <https://doi.org/10.1007/s13202-021-01097-2>.
293. Sun, S.; Ye, Y.; Liu, C.; Xiang, F.; Ma, Y. P-T Stability Conditions of Methane Hydrate in Sediment from South China Sea. *J. Nat. Gas Chem.* **2011**, *20*, 5, 531–536.
[https://doi.org/10.1016/S1003-9953\(10\)60224-1](https://doi.org/10.1016/S1003-9953(10)60224-1).
294. Lee, J. Experimental Study on the Dissociation Behavior and Productivity of Gas Hydrate by Brine Injection Scheme in Porous Rock. *Energy & Fuels* **2010**, *24*, 1, 456–463.
<https://doi.org/10.1021/ef900791r>.
295. Chong, Z. R.; Koh, J. W.; Linga, P. Effect of KCl and MgCl₂ on the Kinetics of Methane Hydrate Formation and Dissociation in Sandy Sediments. *Energy* **2017**, *137*, 518–529.
<https://doi.org/10.1016/j.energy.2017.01.154>.
296. Zheng, M.; Liu, T.; Jiang, G.; Wei, M.; Huo, Y.; Liu, L. Large-Scale and High-Similarity Experimental Study of the Effect of Drilling Fluid Penetration on Physical Properties of Gas Hydrate-Bearing Sediments in the Gulf of Mexico. *J. Pet. Sci. Eng.* **2020**, *187*,.
<https://doi.org/10.1016/j.petrol.2019.106832>.
297. Huang, T.; Zhang, Y.; Li, G.; Li, X.; Chen, Z. Numerical Modeling for Drilling Fluid Invasion into Hydrate-Bearing Sediments and Effects of Permeability. *J. Nat. Gas Sci. Eng.* **2020**, *77*,.
<https://doi.org/10.1016/j.jngse.2020.103239>.
298. Zuev, V. M.; Porokhnyak, A. M.; Drozdov, A. V.; Sergievsky, V. V. Zaborovsky, V. V. Method

- of Storing Toxic Brines in Permafrost Environment (Published in Russian), 1988.
299. Porokhniak, A. M. *Gas Hydrates of the Permafrost Zone in Western Yakutia (Published in Russian)*; Publishing house of TsNIITsvetmet: Moscow, Russia, 1988; p. 30.
300. Porokhnyak, A. M.; Rassudov, A. V. *Disposal of Liquid Waste in Permafrost (Published in Russian)*; Nedra: Moscow, Russia, 1993; p. 111.
301. The process of melting ice with chemical reagents (published in Russian)
https://bstudy.net/645082/tehnika/protsess_plavleniya_lda_himicheskimi_reagentami (accessed Mar 22, 2022).
302. Gaidenko, E. P. Solubility of Ice in Frozen Soils under the Influence of Saline Solutions (Published in Russian). In *Problems of engineering glaciology*; Nauka: Novosibirsk, Russia, 1986; pp 32–36.
303. Pekhovich, A. I.; Shatalina, I. N. Experimental Studies of Ice Melting in Aqueous Solution (Published in Russian). In *Heat and mass transfer (volume 2)*; Minsk, 1968; pp 98–104.
304. Fedorov, A. M. Laboratory Studies of the Destruction of Ice and Ice-Rock Monoliths by Brines (Published in Russian). In *Conditions and processes of cryogenic migration of matter*; Yakutsk, Russia, 1989; pp 83–96.
305. Alekseev, S. *Cryogenesis of Groundwater and Rocks (on the Example of the Daldino-Alakitsky Region of Western Yakutia) (Published in Russian)*; SRC OIGGM SO: Novosibirsk, Russia, 2000; p. 119.
306. Borisov, V.; Alekseev, S. Factors of Interaction of Brines with Ice (Frozen Rock) at a Negative Temperature (Published in Russian). In *Fundamental problems of water and water resources at the turn of the III millennium*; NTL: Tomsk, Russia, 2000; pp 584–589.
307. Volkov, N. G.; Komarov, I. A.; Mironenko, M. V.; Fotiev, S. M. Methods for Assessing the

- Formation Temperature of the Ion-Salt Composition of Cryopegs (Published in Russian). *Kriosf. Zemli* **2005**, 9, 4, 54–61.
308. Farnam, Y.; Bentz, D.; Sakulich, A.; Flynn, D.; Weiss, J. Measuring Freeze and Thaw Damage in Mortars Containing Deicing Salt Using a Low-Temperature Longitudinal Guarded Comparative Calorimeter and Acoustic Emission. *Adv. Civ. Eng. Mater.* **2014**, 3, 1, 20130095:1-20130095:27. <https://doi.org/10.1520/acem20130095>.
309. Tyutyunov, I. A. *Introduction to the Theory of Permafrost Formation (Published in Russian)*; Academy of Science USSR: Moscow, Russia, 1960; p. 144.
310. Chuvilin, E. M.; Bukhanov, B. A.; Mukhametdinova, A. Z.; Grechishcheva, E. S.; Sokolova, N. S.; Alekseev, A. G.; Istomin, V. A. Freezing Point and Unfrozen Water Contents of Permafrost Soils: Estimation by the Water Potential Method. *Cold Reg. Sci. Technol.* **2022**, 196, 103488. <https://doi.org/10.1016/j.coldregions.2022.103488>.
311. Nechaev, E. A.; Kahn, E. V. Migration of Salts in Water-Saturated Sands at Negative Temperatures (Published in Russian). *Geochemistry* **1980**, 7,.
312. Romanov, V. P. Investigation of the Connection between Electrical Surface Properties and Ion Transport in Frozen Rocks (Published in Russian). In *Migration of chemical elements in permafrost*; Nauka: Novosibirsk, Russia, 1985.
313. Benediktova, N. A. Physical and Chemical Processes in Frozen Rocks during Their Interaction with Saline Solutions (Published in Russian), Moscow State University, 1992.
314. Chuvilin, E. M.; Smirnova, O. G. Migration of Chemical Elements in Frozen Rocks (Published in Russian). In *Proceedings of the First Conference of Geocryologists of Russia*; Moscow State University Publishing House: Moscow, Russia, 1996; pp 116–129.
315. Andersland, O. B.; Biggar, K. W. Site Investigations of Fuel Spill Migration into Permafrost. *J.*

- Cold Reg. Eng.* **2002**, *13*, 3, 165–166. [https://doi.org/10.1061/\(asce\)0887-381x\(1999\)13:3\(165\)](https://doi.org/10.1061/(asce)0887-381x(1999)13:3(165)).
316. Ershov, E. D.; Chuvilin, E. N.; Smirnova, O. G. Mobility of Ions of Chemical Elements in Ice and Frozen Rocks (Published in Russian). *Dokl. Akad. Nauk* **1999**, *367*, 6, 796–798.
317. Tsypkin, G. G. *Flows with Phase Transitions in Porous Media (Published in Russian)*; Fizmatlit: Moscow, Russia, 2009; p. 232, ISBN 978-5-9221-1102-7.
318. Lekhov, V. A.; Sokolov, V. N. Experimental Determination of the Hydraulic Conductivity and Diffusion Coefficient in Low Permeable Deposits (Published in Russian). *Geoecology. Eng. Geol. Hydrogeol. Geocryol.* **2017**, *3*, 67–75.
319. Belousova, A. P. Preliminary Predictive Assessment of the Conditions of Pollution of the Unsaturated Zone by Oilfield Brines (Published in Russian). *Geoecology. Eng. Geol. Hydrogeol. Geocryol.* **1998**, *1*, 75–89.
320. Malakhova, V. V. Mathematical Modeling of the Long-Term Dynamics of the Submarine Permafrost of the Arctic Shelf (Published in Russian). *Interexpo Geo-Siberia* **2014**, *4*, 1, 1:1-1:5.
321. Tsypkin, G. G. Effect of Liquid Phase Mobility on Gas Hydrate Dissociation in Reservoirs. *Fluid Dyn.* **1992**, *26*, 4, 564–572. <https://doi.org/10.1007/BF01050319>.
322. Vasiliev, V. I.; Danilov, Y. G.; Ereemeev, I. S.; Popov, V. V.; Tsypkin, G. G.; Yuzhui, S.; Yandong, C. Comparison of Mathematical Models of Heat and Mass Transfer in Soils (Published in Russian). *Bull. North-Eastern Fed. Univ.* **2013**, *10*, 4, 5–10.
323. Aksenov, V. I.; Bubnov, N. G.; Klinova, G. I.; Iospa, A. V.; Gevorkyan, S. G. Phase Transformations of Water in Frozen Soils under the Cryopeg Influence (Published in Russian). *Geoecology. Eng. Geol. Hydrogeol. Geocryol.* **2010**, *1*, 40–51.
324. Galushkin, Y. I.; Sitar, K. A.; Frolov, S. V. Permafrost Formation and Degradation in the Urengoy and Kuyumbinskaya Areas of the Siberia. Part 1. Application of Basin Modeling

- System (Published in Russian). *Kriosf. Zemli* **2012**, *16*, *1*, 3–11.
325. Razumov, S. O.; Spektor, V. B.; Grigoriev, M. N. Model of the Post-Cenozoic Evolution of the Cryolithozone of the Shelf of the Western Part of the Laptev Sea (Published in Russian). *Oceanology* **2014**, *54*, *5*, 637–649.
326. Wei, J.; Cheng, Y.; Yan, C.; Li, Q.; Han, S.; Ansari, U. Decomposition Prevention through Thermal Sensitivity of Hydrate Formations around Wellbore. *Appl. Therm. Eng.* **2019**, *159*, 113921. <https://doi.org/10.1016/j.applthermaleng.2019.113921>.
327. Chuvilin, E. M.; Kozlova, E. V. Experimental Estimation of Hydrate-Containing Sediments Stability. In *5th International Conference on Gas Hydrates*; 2005.
328. Chuvilin, E. M.; Guryeva, O. M. Experimental Study of Self-Preservation Effect of Gas Hydrates in Frozen Sediments. In *Proceedings of the 9th International Conference on Permafrost, Fairbanks, AK, USA*; 2008; Vol. 28.
329. Trofimov, V. T.; Korolev, V. A. *Workshop on Soil Science (Published in Russian)*; Moscow State University: Moscow, Russia, 1993; p. 390.
330. *GOST 12536-2014. Soils. Laboratory Determination of the Grain (Grain-Size) and Microaggregate Composition (Published in Russian)*; Standartinform: Moscow, Russia, 2014.
331. 5180-84, G. *Soils. Methods for Laboratory Determination of Physical Characteristics / GOST of October 24, No. 5180-84*; 1984.
332. Shakhova, N.; Semiletov, I.; Gustafsson, O.; Sergienko, V.; Lobkovsky, L.; Dudarev, O.; Tumskoy, V.; Grigoriev, M.; Chernykh, D.; Koshurnikov, A.; et al. Current Rates and Mechanisms of Subsea Permafrost Degradation in the East Siberian Arctic Shelf. *Nat. Commun.* **2017**, *8*, 15872:1-15872:13. <https://doi.org/10.1038/ncomms15872>.
333. Chuvilin, E.; Bukhanov, B.; Grebenkin, S.; Tymskoy, V.; Shakhova, N.; Dudarev, O.;

- Semiletov, I. Thermal Conductivity of Bottom Sediments in the East Siberian Arctic Seas: A Case Study in the Buor-Khaya Bay. In *Proceedings of the 7th Canadian Permafrost Conference; Québec City, Québec, Canada*; 2015; p ABS557:1-ABS557:6.
334. Chuvilin, E.; Kozlova, E.; Makhonina, N. Experimental Investigation of Gas Hydrate and Ice Formation in Methane-Saturated Sediments. In *Proceedings of 8th International Conference on Permafrost*; 2003; pp 145–150.
335. Chuvilin, E.; Istomin, V.; Ekimova, V.; Bukhanov, B.; Hassanpouryouzband, A.; Yang, J.; Tohidi, B. Experimental Modeling of Methane Recovery by Flue Gas Injection Into Frozen Hydrate-Bearing Reservoir. *Geomodel* **2018**.
336. Chuvilin, E. M.; Kozlova, E. V.; Skolotneva, T. S. Experimental Simulation of Frozen Hydrate-Containing Sediments Formation. In *Proceedings of the Fifth International Conference on Gas Hydrates*; Trondheim, Norway, 2005; pp 1561–1567.
337. Ershov, E. D.; Lebedenko, Y. P.; Chuvilin, E. M. Processes in Frozen Rocks Interacting with Salt Solutions (Published in Russian). In *Fundamentals of geocryology. Part 1. Physical and chemical foundations of geocryology.*; MSU: Moscow, Russia, 1995; pp 181–214.
338. Andreassen, K.; Hubbard, A.; Winsborrow, M.; Patton, H.; Vadakkepuliambatta, S.; Plaza-Faverola, A.; Gudlaugsson, E.; Serov, P.; Deryabin, A.; Mattingsdal, R.; et al. Massive Blow-out Craters Formed by Hydrate-Controlled Methane Expulsion from the Arctic Seafloor. *Science* (80-.). **2017**, *356*, 6341, 948–953. <https://doi.org/10.1126/science.aal4500>.
339. Overduin, P.; Liebner, S.; Knoblauch, C.; Kneier, F. Subsea Permafrost Degradation and Inferred Methane Release in Shallow Coastal Water of the Central Laptev Sea. **2013**.
340. Chuvilin, E. M.; Grebenkin, S. I.; Sacleux, M. Influence of Moisture Content on Permeability of Frozen and Unfrozen Soils. *Kriosf. Zemli* **2016**, *20*, 3, 66–72.

Appendix 1. Table of the conducted experiments on the interaction of frozen-hydrate bearing sediments with salt solution

Below there is the table with the list of the experiments, conducted in the frame of this research, with description of experiments condition (temperature, pressure, salt solution characteristics) and main initial characteristics (porosity, ice saturation, hydrate coefficient). It worth to mention, that each experiment include several tests with the use of twin samples. At least 3 tests were run in each experiment for repetition and obtaining reproducible results. Thus, for each experiment the average initial values of frozen hydrate containing samples characteristics are shown.

Table 15. The list of experiments conducted on the interaction of frozen hydrate-bearing sediments with salt solution.

Experiment number	Sediment	t, °C	P, MPa	Salt composition	Csol, N	n, %	Si, %	Kh, u.f.
1	Fine sand-1	-6	0.1	NaCl	0.1	38	18	0.60
2	Fine sand-1	-6	0.1	NaCl	0.1	40	50	0.00
3	Fine sand-2	-6	0.1	NaCl	0.1	38	15	0.43
4	Fine sand-3	-6	0.1	NaCl	0.1	37	16	0.38
5	Sandy loam	-6	0.1	NaCl	0.1	35	18	0.37
6	Fine sand-2+ 5% montmorillonite	-6	0.1	NaCl	0.1	36	18	0.45
7	Fine sand-2+ 5% kaolinite	-6	0.1	NaCl	0.1	38	15	0.48
8	Fine sand-2+ 7% kaolinite	-6	0.1	NaCl	0.1	37	12	0.50
9	Fine sand-2+ 10% kaolinite	-6	0.1	NaCl	0.1	35	15	0.52
10	Fine sand-2+ 15% kaolinite	-6	0.1	NaCl	0.1	34	18	0.48
11	Fine sand-2	-6	0.1	MgCl ₂	0.1	39	18	0.43

12	Fine sand-2	-6	0.1	CaCl ₂	0.1	37	16	0.53
13	Fine sand-2	-6	0.1	KCl	0.1	38	17	0.49
14	Fine sand-2	-6	0.1	Na ₂ SO ₄	0.1	38	16	0.47
15	Fine sand-2	-2	0.1	NaCl	0.1	39	18	0.43
16	Fine sand-2	-3	0.1	NaCl	0.1	37	15	0.40
17	Fine sand-2	-4	0.1	NaCl	0.1	37	16	0.46
18	Fine sand-2	-8	0.1	NaCl	0.1	38	18	0.44
19	Fine sand-2	-10	0.1	NaCl	0.1	38	17	0.40
20	Fine sand-2	-16	0.1	NaCl	0.1	39	18	0.42
21	Fine sand-2	-20	0.1	NaCl	0.1	37	16	0.40
22	Fine sand-2	-3	4	NaCl	0.1	39	17	0.45
23	Fine sand-2	-4	4	NaCl	0.1	39	17	0.43
24	Fine sand-2	-10	4	NaCl	0.1	38	18	0.41
25	Fine sand-2	-16	4	NaCl	0.1	39	18	0.40
26	Fine sand-2	-6	0.1	NaCl	0.2	37	17	0.40
27	Fine sand-2	-6	0.1	NaCl	0.4	39	16	0.42
28	Fine sand-2	-6	4	NaCl	0.2	37	18	0.41
29	Fine sand-2	-6	4	NaCl	0.4	37	16	0.43
30	Fine sand-2	-6	1	NaCl	0.1	39	19	0.35
31	Fine sand-2	-6	1.8	NaCl	0.1	40	18	0.38
32	Fine sand-2	-6	2.5	NaCl	0.1	38	19	0.33
33	Fine sand-2	-6	3	NaCl	0.1	38	17	0.31
34	Fine sand-2	-6	3.5	NaCl	0.1	39	17	0.38
35	Fine sand-2	-6	6	NaCl	0.1	39	18	0.35
36	Fine sand-2	-6	0.1	NaCl	0.1	38	15	0.43
37	Fine sand-2	-6	0.1	NaCl	0.2	40	12	0.45
38	Fine sand-2	-6	0.1	NaCl	0.4	38	18	0.39
39	Fine sand-2	-6	0.1	NaCl	0.6	39	11	0.44
40	Fine sand-2	-6	0.1	NaCl	1	38	15	0.43
41	Fine sand-2	-6	0.1	NaCl	0.4	40	50	0.00